Conducting polymers for micro and nano electrodes. Application to biomolecule sensing and release

Teresa Galán Cascales

Tesi doctoral

Conducting polymers for micro and nano electrodes. Application to biomolecule sensing and release

Memòria presentada per

Teresa Galán Cascales

Per optar al grau de **Doctor en Nanociències**

Universitat de Barcelona

Departament d'Electrònica

Programa de doctorat en Nanociències

Tesi doctoral dirigida per

Prof. Josep Samitier

Barcelona, 2015

CONTENTS

ACRONYMS

2BM-target Two base mismatch target

A Adenine

ABTS 2,2'-Azinobis(3-ethylbenzothiazoline-6-sulfonate)

ACN Acetonitrile

AFM Atomic Force Microscopy

APTES (3-Aminopropyl)triethoxysilane

Azide-EDOT Azidomethyl-modified 3,4 - Ethylenedioxythiophene

Azide-PEDOT Azidomethyl-modified Poly(3,4 - Ethylenedioxythiophene)

Cu(I) Copper iodide

CV Cyclic Voltammetry

CVD Chemical Vapour Deposition

DCM Dichloromethane

DIPEA N,N-diisopropylethylamine

DMSO Dimetyl sulfoxide

DNA Deoxyribonucleic acid

DPN Dip-Pen Nanolithography

DPV Differential Pulse Voltammetry

DWL Direct Write Laser lithography

EBL Electron Beam Lithography

EDOT 3,4 - Ethylenedioxythiophene

EDTA Ethylenediaminetetraacetic acid

Fc/Fc^+ Ferrocene-Ferrocenium

FDTES Trichloro (1H,1H,2H,2H-perfluorooctyl)silane

FET Field Effect Transistor

FIB Focused Ion Beam

G Guanine

HCV-probe Acetylene-terminated "Hepatitis C" virus probe

HCV-target "Hepatitis C" virus target

HPLC-MS High-Performance Liquid Chromatography Mass Spectrometry

HRP Horseradish peroxidase

IJP Ink-Jet Printing

IPA Isopropanol

IR spectroscopy Infrared Spectroscopy

ITO Indium tin oxide

LED Light Emitting Diode

LFM Lateral Force Microscopy

LOD Limit Of Detection

MIBK Methyl isobutyl ketone

MVA MutiVariate Analysis

Nc1-target Non-complementary target 1

Nc2-target Non-complementary target 2

PBS Phosphate buffered saline

PCA Principal Component Analysis

PCs Principal Components

PDMS Polydimethylsiloxane

PEDOT Poly(3,4 - Ethylenedioxythiophene)

perfluoropolyether-silane Perfluoropolyether-silyltriethoxy-terminated

PMMA Poly(methyl methacrylate)

PVC Polyvinyl chloride

pyrrole-silane N-(3-Trimethoxysilylpropyl)pyrrole

RIE Reactive Ion Etching

SAED Selected Area Electron Diffraction

SAMs Self-Assembly Monolayers

SEM Scanning Electron Microscopy

STM Scanning Tunneling Microscopy

TBAPF$_6$ Tetrabutylammonium hexafluorophosphate

TBTA Tris [(1-benzyl-1H-1,2,3-triazol-4-yl)methyl)]amine

TEM Transmission Electron Microscopy

ToF-SIMS Time-of-Flight Secondary Ion Mass Spectrometry

WLI White Light Interferometry

XPS X-ray Photoelectron Spectroscopy

XRD X-ray Diffraction

1

GENERAL INTRODUCTION

1.1 INTRODUCTION TO CONDUCTING POLYMERS

Polymers are defined as compounds made of repeating units, called monomers. During synthesis, or polymerization, the electronic configuration of monomers is altered, inducing the formation of bonds and joining the monomers together in a chainlike or network configuration. The diversity in monomers and their derivatives gives rise to many types of polymeric materials, from natural to synthetic. Thus, polymers are widely spread in nature as in the case of proteins (polyamides), nucleic acids (polynucleotides), and polysaccharides, which are fundamental elements for biological structures and functions (Figure 1.1a), but also as part of other common materials such as amber, wool or silk, which have been used for centuries in ornaments and clothing. Regarding synthetic polymers, plastics are the most popular type, with examples as neoprene, nylon or polystyrene, frequently used in our everyday life for instance in CD's cases, bottles, trays, etc. (Figure 1.1b).

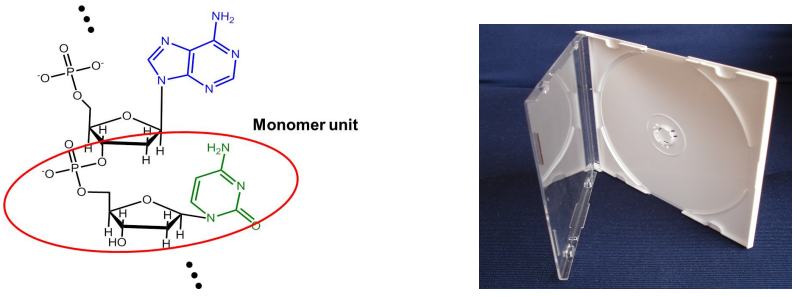

(a) (b)

Figure 1.1: Natural and synthetic polymers. a) Single stranded DNA, monomer unit highlighted in red. b) CD case made of polystyrene.

A special group of polymers, named conducting polymers (CPs), have attracted enormous interest over the last three decades due to their appealing electrical properties, which allowed their application in a wide range of fields, from electronics to biomedicine. First reports of conducting polymers are from 1862, when Henry Letheby prepared polyaniline by the anodic oxidation of aniline, showing conducting and electrochromic behaviors [1]. However, it was Heeger, MacDiarmid and Shirakawa in 1977, who put conducting polymers into focus due to their studies about oxidized iodine-doped polyacetylene [2]. They discovered the large increase in the conductivity of polyacetylene after a doping process, opening the door for their practical use in commercial applications and for which they were awarded the Nobel Prize of Chemistry in 2000.

1.1.1 *Origin of conducting polymers properties*

The origin of the properties of conducting polymers is their conjugated structure. This structure consists of a backbone formed of alternating single and double bounds, as depicted in Figure 1.2 [3].

Figure 1.2: Conjugated structure of polyacetylene, where it can be seen the alternation of double and single bonds.

As shown in Figure 1.3, while single bonds (sigma, σ) are strong and keep electrons localized between two atoms, double bonds (pi, π) are weaker and leave the electrons in lobes above and below the σ-bonds.

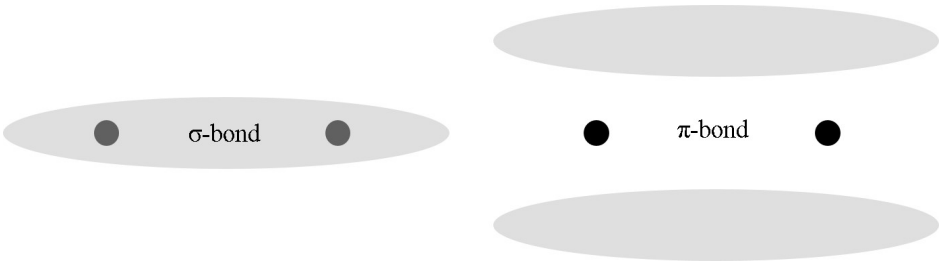

Figure 1.3: Schematics of the single and double bonds existing in conducting polymers.

Since the neighboring π-bonds overlap, one electron for each atom remains delocalized, giving these polymers an intrinsic metallic behaviour [4]. However,

these one-dimensional materials are unstable and undergo a spontaneous dimerization called Peierls distortion [5]. This distortion forces the bonds to alternate between long and short, making the unit cell twice as long, opening a gap and thus transforming conjugated polymers into intrinsic semiconductors. In consequence, as in conventional intrinsic semiconductors, conducting polymers need doping to reach high values of conductivity. In addition, conducting polymers are generally synthesized by oxidative polymerization, through which the fabricated polymer ends in the oxidized state. As a result, polymers require the incorporation of negative ions (dopants or counter anions) to balance their positively charged backbone and maintain charge neutrality, as seen in Figure 1.4 [6].

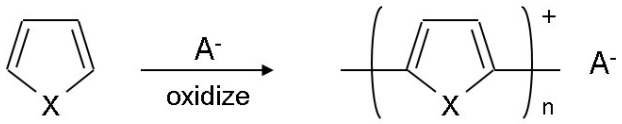

Figure 1.4: Charge balance of conducting polymers while synthesis.

Therefore, doping is not only a process required to obtain highly conducting polymers, but it is also necessary to maintain stability and charge neutrality of the polymer backbone.

Due to this charge balance requirement, conducting polymers are said to be permeable to ions. They can be reversibly doped and de-doped during redox processes, absorbing and desorbing ions coming from the electrolyte [7]. This process includes volume variations and a good reversibility between their conducting (oxidized form) and insulating states (reduced or neutral form).

1.2 APPLICATIONS FOR CONDUCTING POLYMERS

One of the most interesting properties of conducting polymers is the possibility of tuning the electrical conductivity of the material over several orders of magnitude by adjusting the synthetic parameters (dopant, solvent, synthetic method, oxidation state, etc.). In addition, the wide availability of monomers, their inexpensive cost, the ease of processing, the good mechanical performance of polymers, the wide range of functionalization possibilities, etc. [8], promote the use of conducting polymers in many divergent fields as alternatives to conventional inorganic materials.

The combination of all these properties has opened a wide range of applications in which conducting polymers are routinely implemented. For instance, the computer industry uses conducting polymers as coating for the insulators contained in microcircuits, thus preventing the buildup of static electricity and avoiding damage due to undesirable discharges. Other standard applications of conducting polymers include their use as conductive adhesive materials, electromagnetic shielding, electrochemical actuators, etc. [8].

Here, some cutting-edge areas for the use of conducting polymers are presented in detail. Such leading areas include electronics, optoelectronics and biomedical devices [9]. The use of conducting polymers for biomedical applications will be highlighted since is the main context for the development of this thesis.

1.2.1 *Conducting polymers for electronics and optoelectronics*

A Field Effect Transistor (FET) is an electronic component so named because a small electrical signal applied to one of its electrodes (gate) creates an electric field through the rest of the transistor. This field controls a current, traveling between two other electrodes (source and drain), allowing its modulation. Moreover, the high input impedance provided by FETs avoids the loading of signal sources, which makes them useful for almost any electronic application.

The ease of processing of conducting polymers make them ideal candidates for the fabrication of FETs, with the perspective to obtain low-cost, large-area, but most importantly, biocompatible (or in some applications biodegradable) and flexible electronic devices. Conducting polymer-based FETs can be deposited and patterned at room temperature by a combination of low-cost solution processing and direct-write printing. This substantially reduces the cost of manufacture. This kind of FETs have found applications in new technological areas[10], as for instance in flexible displays (Figure 1.5).

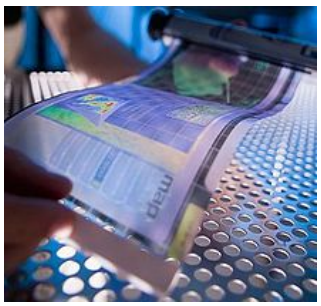

Figure 1.5: Flexible display using polymer-based FETs.

Other basic electronic component is the capacitor. In particular, supercapacitors are electrochemical capacitor devices with very high capacitance values, a virtually unlimited cycle life, fast and simple charging, low resistances and excellent low-temperature operation performance among others [11]. They have a potential use for instance in electric vehicles, where they are used for recovery energy from braking, but also in new portable and flexible electronic devices, where it is strongly required to develop a next-generation of inexpensive, flexible, light-weight, and sustainable energy storage systems, with large energy and power density [12].

Conducting polymers are used in a specific type of supercapacitors called pseudocapacitors, which obtain their capacitance from the storage of charge in the bulk of a redox material in response to a redox reaction [11]. Conducting polymers have been employed for supercapacitors because of their high redox-active capacitance, high conductivity and, most importantly, high intrinsic flexibility, which may bring new opportunities of energy-storage devices to the future portable electronic area [13].

A Light Emitting Diode (LED) is a device, where conducting polymers can also be incorporated. A LED is a p-n junction diode, which emits light when activated. When a suitable voltage is applied between the two electrodes of the diode, electrons are able to recombine with holes, releasing energy in the form of photons. The colour emitted by the diode, called electroluminescence, is characterized by the energy band gap of the semiconductor composing the diode [14]. Generally in a LED, the electroluminescent material is placed between two electrodes, one of which is transparent and normally made from Indium tin oxide (ITO). Conducting polymers have been used in LEDs either as electroluminescent materials or as transparent electrodes, thus replacing the ITO electrode [14, 15]. They are ideal alternatives for such purposes due to their fast response times, their easy processability, their possibility of uniformly covering large areas, their transparency, their low operating voltages and their ability for fine-tuning their optical and electrical properties by varying their structure.

Conducting polymer-based LEDs can be found in the fabrication of digital displays (Figure 1.6), such as television screens, computer monitors, mobile phones, PDAs, etc.

In the research of renewable energy resources, solar energy represents one of the most important energy sources, due to its nearly unlimited supply capability and wide distribution all over the earth. However the cost of photovoltaic modules, which can efficiently convert energy from sun light, is still too high to

Figure 1.6: LEDs based on electroluminescent conducting polymers.

be afforded by common energy consumption. The high cost of silicon solar cells and their complex production process launched the investigation of new materials such as conducting polymers. Polymer solar cells have been investigated (Figure 1.7) as an alternative due to their light weight, disposability, inexpensive fabrication, flexible nature, capability of being customized on the molecular level, smaller environmental impact, etc. However, these attractive polymer-based solar cells still lack of conversion efficiency (about 10%), which is a significant disadvantage when compared to their silicon counterparts (with best results of about 46% efficiency) [16].

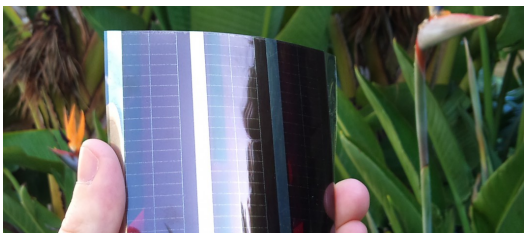

Figure 1.7: Flexible solar cell made of conducting polymer.

These examples reveal the capability of conducting polymers for substituting conventional inorganic materials in areas such as electronics and optoelectronics. However, although convenient in many aspects, conducting polymers still have to solve some limitations regarding performance when compared to conventional materials. Fortunately, the large spectrum of polymer chemistries available, not yet explored, opens a door for the development of new materials, which can meet the expectations for such applications.

1.2.2 *Conducting polymers for biomedical applications*

One of the biggest challenges in biomedicine is the design and development of biomedical devices, which provide not only therapies but also diagnoses of

multiple diseases [17]. Some of the most relevant biomedical devices such as implants, drug delivery systems and biological sensors require a good interface of the device with biology, in order to be effective and reliable. However, traditional materials such as metals and inorganic semiconductors, which proved to be very efficient in transmitting and processing electronic information, showed not to fit the chemical and mechanical requirements for such biological environments [18]. Alternatively, conducting polymers (CPs) are capable of providing mechanically compatible interfaces with biology. Moreover, conducting polymers possess a tunable electrical behaviour (with conductivities from 10^{-12} to 10^{5} S/cm) with an added conduction of ions, which is of great importance for the communication with biological systems [19, 20]. Besides, there is a wide range of functionalization strategies, which permit the incorporation of molecules to the polymers, enhancing bio-integration and facilitating the stability of the devices [21]. The electrical and mechanical performance of conducting polymers together with their permeability to ions, launched their use in many of the most important fields of biomedicine such as biosensors, cell/tissue stimulation, drug delivery and implantable devices.

Conducting polymers have been used in biosensors for being capable to behave both as immobilization and as transduction agents at the same time [22], which allow the conversion of a biological event into an electrical signal. In particular, conducting polymers exhibit variations in their electrochemical, optical and electronic properties due to environmental changes occurring at their surface, as the ones produced by a recognition process [23]. Moreover, the wide range of functionalization strategies available for conducting polymers allows an easy biological functionalization, which imparts the required selectivity for a sensor and provides an intimate contact between the bio-recognition element and the electronic transducer, thus enhancing the stability and the speed of the responses [24]. Conducting polymers have been used in biosensors to detect many types of biological analytes such as proteins, microorganisms, oligonucleotides, small biomolecules and even cells [3].

Furthermore, conducting polymers have been reported to trigger biological processes, such as cell migration, adhesion or even differentiation by means of electrical stimuli and also by delivering key drugs to cells or tissues [25]. For instance, cell adhesion and migration have been traditionally studied on passive surfaces, where topographical and chemical micropatterns were used to study their interaction with cells [26]. By contrast, the use of electroactive polymers, which can apply electrical stimuli on cell seeded polymers, avoid the use of

chemical treatments without compromising the cell integrity [17]. As an example, polypyrrole substrates have been widely used for the stimulation of neurons, demonstrating the enhancement of the in vitro neuritogenesis, the first step of neuronal differentiation [27].

Additionally, conducting polymers have been used for the development of bioactive implantable devices due to their biocompatibility. This becomes an imperative property, required to cause minimal and reversible disturbance to the working environment [23]. Conducting polymers became of great significance in fields such as the one of neuroprosthetic devices, used for neural recording and stimulation [17]. The most used neural interfaces are the cochlear implants, which traditionally are based on metallic electrodes. However, these implants are not mechanically compatible with the host tissue. This mechanical incompatibility produces inflammation and glial scarring, ending up in a loss of device efficiency after sometime of the implantation [28]. Alternatively, conducting polymers emerged as a unique class of materials which match the mechanical requirements of neural tissue interfaces, while exhibiting metallic behavior [29, 30]. Moreover, it is easy to functionalize them with biological species that allow control of the neural response after the implantation, avoiding the initial wound healing response and improving the life-time of the device [31, 32].

As seen here, conducting polymers have also shown to be excellent materials for their use in biomedicine. In particular, there is an increasing demand for new generation of biomedical devices (new cochlear implants, bionic eyes, brain-machine interfaces, multiplexed biosensors, etc.), requiring an enhanced performance of the device. For the application of conducting polymers to such devices is desirable the fabrication of high-density arrays of microelectrodes with a good spatial resolution of the polymeric electronic components [22, 33, 34]. However, the fabrication of high-performance devices based on conducting polymers still has to cross some barriers related to degradation, resolution and adhesion. First, the micro- and nanofabrication of conducting polymers by very well-known methods, such as photolithography or focused ion beam lithography, can induce thermal damage during the process. Besides, these standard fabrication methods are generally incompatible with the functional molecules incorporated into the polymer, which complicates the use of bio-functionalized conducting polymers in routine protocols [35]. Instead, ink-jet printing has appeared as the preferred alternative choice for the fabrication of polymer microelectrodes, allowing the direct deposition of polymer microstructures on a wide variety of surfaces. However, this technique offers a limited feature resolution in the range

of 20-50 µm, which sometimes is insufficient for achieving the required device performance [36]. These direct printing techniques (like ink-jet printing) suffer from the poor interaction polymer-surface, which results in bad adhesion properties. Furthermore, they usually require the use of chemical modifications to increase the polymer solubility in the carrier fluid, which in some cases affects the final properties of the polymer. Therefore, the development of simple and robust processes for the fabrication of stable conducting polymers structures with micrometer and even nanometer resolution, is one of the most important challenges in the polymer-device field.

In this thesis, those problems were investigated first at the microscale, by evaluating a new biocatalytical method for the fabrication of polypyrrole microelectrodes to subsequently test their functionality. At the nanoscale, different nanofabrication strategies were investigated for the achievement of polypyrrole nanowires, implemented into functional FET devices. These studies contribute to the field of micro- and nanofabrication of conducting polymers, with new fabrication strategies for the implementation of such materials into functional devices.

But besides these technical problems, there is also a rising interest in developing new environmentally respectful synthetic routes, novel biological functionalization strategies, biocompatible and biodegradable polymers, non-toxic systems, etc., which can replace conventional materials, while keeping the electroactive behavior of conducting polymers.

In the work presented here, some of these issues were studied based on two synthetic strategies: the electrochemical and the biocatalytical polymerization. On one side, the electrochemical strategy included the use of a home-made functionalized precursor monomer, which allowed the separation of the polymerization and the bio-functionalization processes, thus preserving functional biomolecules from degradation during synthesis. On the other side, the biocatalytical strategy provided sufficient soft environments, to incorporate biological entities during the polymer synthesis while avoiding their degradation due to harsh synthetic conditions. Moreover, the biocatalytical approach occurred in aqueous media, without toxic by-product formation, which is one of the requirements for the so called "green" chemistries. These polymeric designs provide the field of biomedicine with new approaches for the fabrication of bioactive devices.

At the end, the question of how to build these conducting polymer devices for biomedical applications will not be answered exclusively by an expert of a single field. Instead, multidisciplinary effort in polymer science, micro- and nan-

otechnology, biology, medicine, sensors, surface chemistry etc. will be necessary to obtain the appropriate properties for a biomedical device base on conducting polymers. The work presented here attempts to address some of these issues, by developing novel polymer fabrication (micro- and nano-) and functionalization strategies, as will be discussed in next section and will be detailed in the following chapters.

1.3 THESIS OBJECTIVES

This thesis, entitled "Conducting polymers for micro and nano electrodes. Application to biomolecule sensing and release", aims at providing a better understanding of the micro- and nanofabrication of conducting polymers for biomedical devices and present novel processes that widen the application range of conducting polymers in this field.

The main objectives of this work are:

the development of micro- and nanofabrication methodologies appropriate for conducting polymers,

the study of different polymerization methods and functionalization strategies compatible with the construction of bioactive devices based on conducting polymers

and the evaluation of the fabricated conducting polymers platforms in areas such as biological sensing and release.

1.4 THESIS STRUCTURE

The thesis is divided in four chapters, namely "Materials and Methods", "Biocatalytically-produced polypyrrole thin films and microelectrodes on insulating surfaces", "Azide-PEDOT electrodes. Application to DNA sensors" and "Fabrication of polypyrrole single nanowire devices". Every chapter, except chapter 1: "Materials and Methods", are preceded by an introduction section in which a summary of the state of the art, related to the specific topic of the chapter, is presented. These introductions put in context the results obtained in this work and compare them with the existing literature. The main conclusions of the developed work are summarized at the end of each chapter. The content of each chapter is detailed below.

Chapter 1, entitled "Materials and Methods", describes the materials used in this work and the fabrication and characterization methods required for the de-

velopment of the thesis. Here, theoretical and experimental details about the techniques employed, are provided.

Chapter 2, entitled "Biocatalytically-produced polypyrrole thin films and microelectrodes on insulating surfaces", presents a new on-surface biocatalytical procedure for the fabrication of polypyrrole microelectrodes on insulating surfaces, with resolutions comparable to the ones of conventional photolitography. This is an environmentally respectful microfabrication method that allows the entrapment of biomolecules during the polymer synthesis in a single step. As a proof of concept, biotin was trapped in the polypyrrole matrix and then released in a controlled way through electrical stimulation. It was proven that the polymer keeps its electroactivity after the fabrication and functionalization processes. This biocatalytical-based technique represents a straightforward method for the microfabrication of biological-active conducting polymers, which could be implemented in implantable devices for remotely controlled tissue interactions.

Chapter 3, entitled "Azide-PEDOT electrodes. Application to DNA sensors", describes the fabrication and testing of an electrochemical label-free DNA hybridization sensor, based on novel Azidomethyl-modified Poly(3,4 - Ethylenedioxythiophene) (Azide-PEDOT) electrodes. These Azide-PEDOT electrodes were used as platforms for the immobilization of acetylene-DNA probes, complementary to the "Hepatitis C" virus. The acetylene-DNA probes were covalently grafted to the polymer backbone via the robust "Click" reaction, which a part from being a very selective functionalization method, preserves DNA from denaturation during the synthesis of the polymer. DNA hybridization was detected by Differential Pulse Voltammetry (DPV), where the electrochemical change of the polymer behaviour, produced by the recognition event, was directly evaluated. This fabrication procedure is a powerful tool for the preparation of label-free DNA sensors able to selectively recognize a specific DNA sequence, down to the nanomolar range.

Finally, chapter 4, entitled "Fabrication of polypyrrole single nanowire devices", discusses the fabrication of polypyrrole at the nanoscale. Two fabrication techniques were investigated here, namely dip pen nanolithography and electrochemical polymerization on template-assisted surfaces. On one hand, the dip pen nanolithography proved to be a simple deposition technique with good control over size and location of the polypyrrole nanowires. On the other hand, the electrochemical polymerization on template-assisted surfaces provided as well nanoscaled polypyrrole, but added the possibility to chemically manipulate the polymer. This chemical manipulation was translated into polymer devices with

different electrical properties. By the use of these techniques, the capability of fabricating single nanowire devices (ready to use in different applications) and arrays of ordered nanowires based on conducting polymers is demonstrated.

Additionally, two appendixes can be found at the end of the thesis: Appendix A: "Fabrication of Azide-PEDOT microwire-based devices" and Appendix B: "Fabrication of nanopatterns by electron-sensitive silanes". They provide short experimental results obtained during the course of this work, which are first steps for future investigations.

A general conclusions section can be found at the end of the thesis, where a summary of the main achievements and contributions of this thesis are listed.

1.5 REFERENCES

[1] H Letheby. "On the Production of a Blue Substance by Electrolysis of Sulphate of Aniline". In: *Journal of Chemical Society* 161 (1862), pp. 161–163 (cit. on p. 2).

[2] Hideki Shirakawa et al. "Synthesis of Electrically Conducting Organic Polymers : Halogen Derivatives of Polyacetylene, (CH)x". In: *Journal of Chemical Society* 578 (1977), pp. 578–580 (cit. on p. 2).

[3] Khalil Arshak et al. "Conducting Polymers and Their Applications to Biosensors: Emphasizing on Foodborne Pathogen Detection". In: *IEEE Sensors Journal* 9.12 (2009), pp. 1942–1951 (cit. on pp. 2, 7).

[4] Karin Potje-Kamloth. "Semiconductor junction gas sensors". In: *Chemical reviews* 108.2 (2008), pp. 367–399 (cit. on p. 2).

[5] R E Peierls. *Quantum Theory of Solids*. Oxford University Press, 1955, p. 108 (cit. on p. 3).

[6] Tat'yana V Vernitskaya and Oleg N Efimov. "Polypyrrole: a conducting polymer; its synthesis, properties and applications". In: *Russian Chemical Reviews* 66.5 (May 1997), pp. 443–457 (cit. on p. 3).

[7] a. Mirmohseni et al. "Adaptive Membrane Systems Based on Conductive Electroactive Polymers". In: *Journal of Intelligent Material Systems and Structures* 4.1 (1993), pp. 43–49 (cit. on p. 3).

[8] Joel S Miller. "Conducting Polymers-Materials of Commerce". In: *Advanced Materials* 5.7/8 (1993), pp. 587–589 (cit. on pp. 3, 4).

[9] Murat Ates, Tolga Karazehir, and a. Sezai Sarac. "Conducting Polymers and their Applications". In: *Current Physical Chemistrye* 2.3 (May 2012), pp. 224–240 (cit. on p. 4).

[10] Hagen Klauk. "Organic thin-film transistors". In: *Chem. Soc. Rev.* 39.7 (2010), pp. 2643–2666 (cit. on p. 4).

[11] Marina Mastragostino, Catia Arbizzani, and Francesca Soavi. "Polymer-based supercapacitors". In: *Journal of Power Sources* 97-98 (July 2001), pp. 812–815 (cit. on p. 5).

[12] Indrajit Shown et al. "Conducting polymer-based flexible supercapacitor". In: *Energy Science and Engineering* 3.1 (Jan. 2015), pp. 2–26 (cit. on p. 5).

[13] Chuizhou Meng et al. “Highly Flexible and All-Solid-State Paperlike Polymer Supercapacitors”. In: *Nano Letters* 10.10 (2010), pp. 4025–4031 (cit. on p. 5).

[14] Tze-Bin Song and Ning Li. “Emerging Transparent Conducting Electrodes for Organic Light Emitting Diodes”. In: *Electronics* 3.1 (Mar. 2014), pp. 190–204 (cit. on p. 5).

[15] Deng Xian Yu. “Light-emitting devices with conjugated polymers”. In: *International journal of molecular sciences* 12.3 (Jan. 2011), pp. 1575–94 (cit. on p. 5).

[16] Gang Li, Rui Zhu, and Yang Yang. “Polymer solar cells”. In: *Nature Photonics* 6.3 (Feb. 2012), pp. 153–161 (cit. on p. 6).

[17] Meredith Muskovich and Christopher J Bettinger. “Biomaterials-Based Electronics: Polymers and Interfaces for Biology and Medicine”. In: *Advanced Healthcare Materials* 1.3 (2013), pp. 248–266 (cit. on pp. 7, 8).

[18] Laura Poole-Warren et al. “Development of bioactive conducting polymers for neural interfaces”. In: *Expert review of medical devices* 7.1 (Jan. 2010), pp. 35–49 (cit. on p. 7).

[19] Carlos M. Hangarter et al. “Conducting polymer nanowires for chemiresistive and FET-based bio/chemical sensors”. In: *Journal of Materials Chemistry* 20.16 (2010), p. 3131 (cit. on p. 7).

[20] Róisín M Owens and George G Malliaras. “Organic Electronics at the Interface with Biology”. In: *MRS Bulletin* 35.June (2010), pp. 449–456 (cit. on p. 7).

[21] Catalina Vallejo-Giraldo, Adriona Kelly, and Manus J P Biggs. “Biofunctionalisation pf electrically conducting polymers”. In: *Drug Discovery Today* 19.1 (2014), pp. 88–94 (cit. on p. 7).

[22] Hui Peng et al. “Conducting polymers for electrochemical DNA sensing”. In: *Biomaterials* 30.11 (Apr. 2009), pp. 2132–48 (cit. on pp. 7, 8).

[23] G.G. Adeloju, S.B., Wallace. “Conducting Polymers and the Bioanalytical Sciences : New Tools for Biomolecular Communications: A Review”. In: *The Analyst* I.June (1996) (cit. on pp. 7, 8).

[24] M I Pividori, A Merkoçi, and S Alegret. “Electrochemical genosensor design : immobilisation of oligonucleotides onto transducer surfaces and detection methods”. In: *Biosensors & bioelectronics* 15 (2000), pp. 291–303 (cit. on p. 7).

[25] Leandro Forciniti et al. “Schwann cell response on polypyrrole substrates upon electrical stimulation”. In: *Acta Biomaterialia* 10.6 (2014), pp. 2423–2433 (cit. on p. 7).

[26] Jordi Comelles et al. “Versatile Gradients of Covalently Bound Proteins on Microstructured Substrates”. In: *Langmuir* 28.38 (2012), pp. 13688–13697. DOI: 10.1021/la3025638 (cit. on p. 7).

[27] Robert L. Anger et al. “Stimulation of neurite outgrowth using an electrically conducting polymer”. In: *Proceedings of the National Academy of Sciences* 94.August (1997), pp. 8948–8953 (cit. on p. 8).

[28] Vadim S Polikov, Patrick a Tresco, and William M Reichert. “Response of brain tissue to chronically implanted neural electrodes”. In: *Journal of neuroscience methods* 148.1 (Oct. 2005), pp. 1–18 (cit. on p. 8).

[29] Manrico Fabretto et al. “High conductivity PEDOT resulting from glycol/oxidant complex and glycol/polymer intercalation during vacuum vapour phase polymerisation”. In: *Polymer* 52.8 (Apr. 2011), pp. 1725–1730 (cit. on p. 8).

[30] Kwanghee Lee et al. “Metallic transport in polyaniline”. In: *Nature* 441.7089 (May 2006), pp. 65–68 (cit. on p. 8).

[31] Brianna C Thompson et al. “Optimising the incorporation and release of a neurotrophic factor using conducting polypyrrole”. In: *Journal of controlled release : official journal of the Controlled Release Society* 116.3 (Dec. 2006), pp. 285–294 (cit. on p. 8).

[32] D H Szarowski et al. “Brain responses to micro-machined silicon devices”. In: *Brain Research* 983 (2003), pp. 23–35 (cit. on p. 8).

[33] Uta Reich et al. “Differential fine-tuning of cochlear implant material-cell interactions by femtosecond laser microstructuring”. In: *Journal of biomedical materials research. Part B, Applied biomaterials* 87.1 (2008), pp. 146–153 (cit. on p. 8).

[34] Mikhail a Lebedev and Miguel a L Nicolelis. “Brain-machine interfaces: past, present and future”. In: *Trends in neurosciences* 29.9 (2006), pp. 536–546 (cit. on p. 8).

[35] Hyeonseok Yoon et al. “A novel sensor platform based on aptamer-conjugated polypyrrole nanotubes for label-free electrochemical protein detection”. In: *Chembiochem : a European journal of chemical biology* 9.4 (Mar. 2008), pp. 634–41 (cit. on p. 8).

[36] Jun Xu, Chengmei Zhong, and Chun Fu. "Novel method for printing high-quality metal wires". In: *SPIE* (2007) (cit. on p. 9).

2

MATERIALS AND METHODS

This chapter describes the materials used in this work and the fabrication and characterization methods required for the development of the thesis.

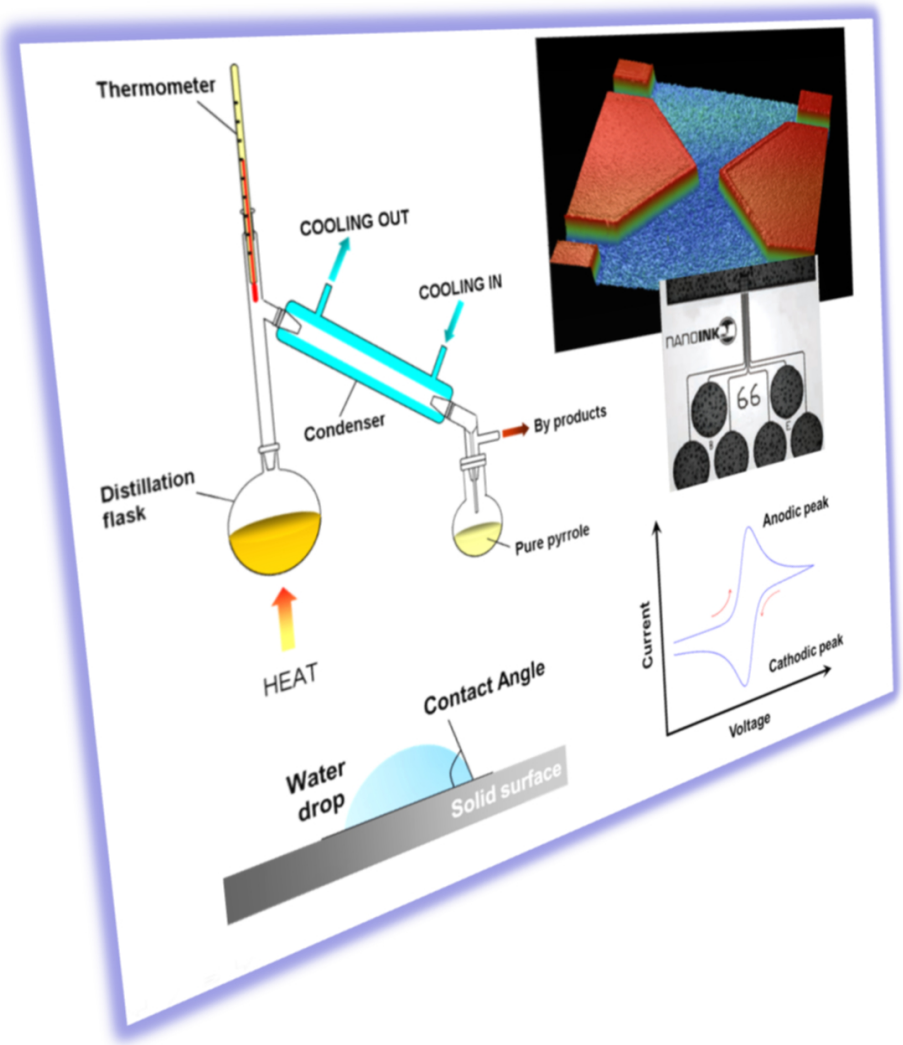

2.1 MATERIALS

The precursor monomers and reagents needed to perform the synthesis of conducting polymers are presented in this section, as well as the substrates used to deposit the polymers and the materials required for the generation of polymeric patterns.

2.1.1 *Conducting Polymers*

Conducting polymers are generally synthesized by oxidative polymerization, i.e. by the oxidation of a precursor monomer. The precursor monomer usually has an oxidation potential higher than that corresponding to the polymer, which results in polymers in the oxidized state. Therefore, polymers synthesized by this method require the incorporation of negative ions (doping or counter anions) to balance their positively charged backbone and maintain charge neutrality [1].

In this work, two conducting polymers were used namely Polypyrrole and Poly(3,4 - Ethylenedioxythiophene) (PEDOT). They are the most widely used conducting polymers in biomedical applications, due to their biocompatibility, stability and good electrical performance [2, 3]. In particular, these conducting polymers were synthesized from a pyrrole precursor monomer (from Sigma - Aldrich Co (USA)) and an Azidomethyl-modified 3,4 - Ethylenedioxythiophene (Azide-EDOT) monomer (obtained through collaboration with the "Institute of Organic Chemistry II and New Materials", at the University of Ulm, Germany) [4], shown in Figure 2.1

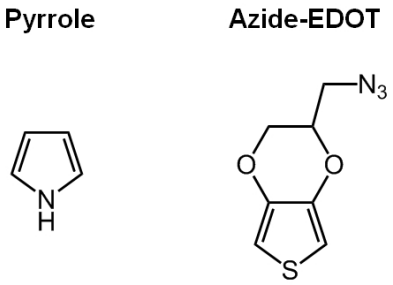

Figure 2.1: Precursor monomers. Pyrrole and Azide-EDOT.

The doping anions were chosen according to the polymerization mechanism applied and the final application. Thus, polypyrrole thin films and microelectrodes biocatalytically grown in aqueous medium, employed the redox mediator

2,2'-Azinobis(3-ethylbenzothiazoline-6-sulfonate) (ABTS) (from Sigma-Aldrich Co (USA)) to generate the counter anion $ABTS^-$. Azide-PEDOT thin films, electrochemically grown in 99.8% anhydrous Dichloromethane (DCM) (CH_2Cl_2, supplied by Sigma-Aldrich Co (USA)), used Tetrabutylammonium hexafluorophosphate ($TBAPF_6$) (from Sigma-Aldrich Co (USA)) as supporting electrolyte, which provided the negative hexafluorophosphate ion ($PF_6{}^-$). Polypyrrole nanowires grown by electrochemical method in water and Acetonitrile (ACN) (C_2H_3N, Sigma-Aldrich Co (USA)), were electrochemically balanced by Cl^- (Cl^- from sodium chloride, NaCl, Sigma-Aldrich Co (USA)) and PF_6-.

The biocatalytical synthesis of polypyrrole was performed using the enzyme Horseradish peroxidase (HRP) (brown powder, 50-150 units/mg, pyrogallol units, from Sigma-Aldrich Co (USA)), activated by hydrogen peroxide (H_2O_2). In this process, a potassium biphtalate buffer (Sigma-Aldrich Co (USA)) with pH 4.0 was used to maintain the activity of the enzyme during the polymerization reaction. Additionally, Ethylenediaminetetraacetic acid (EDTA) (Sigma-Aldrich Co (USA)) was employed to trap traces of metal ions that could eventually inactivate the enzyme.

Furthermore, Dip-Pen Nanolithography (DPN) was attempted for the direct deposition of polypyrrole nanowires. This direct polymer writing approach employs a doped polypyrrole suspension (Sigma-Aldrich Co (USA), Inc. 5 wt.% in H_2O), which has a solid bulk conductivity of 10-40 S/cm and a density of 1 g/cm^3.

All components and reagents were used without any prior treatment, except the precursor monomers, which were purified before use (see section 2.2.1.1).

2.1.2 *Substrates*

Polymerization was studied on-surface, for applications in biomedical devices. Therefore, several surfaces were used, including silicon/silicon oxide (Si/SiO_2) substrates, gold surfaces and Si/SiO_2 substrates with deposited metallic contacts.

P-type silicon wafers, (1 1 1) oriented with 1 µm thermally grown native oxide (Siltronix (Archamps, France)), were used for the fabrication of biocatalytic polypyrrole layers and microelectrodes. When an external electrical connection was required for further applications, metallic microelectrodes were deposited on the wafers by evaporation, consisting in 10 nm of a titanium adhesion layer and 70 nm of gold layer.

Azide-PEDOT films were electrochemically deposited on rod-like gold working electrodes with disk diameters of 1.6 mm (BASi, Indiana, USA). 1-0.25 µm diamond paste (Buehler, Dusseldorf, Germany) and alumina powder of 0.05 µm of grain's size (CH Instruments, Inc. Austin, USA) were used to polish the working electrodes after every use, to obtain clean and homogeneous working areas.

For the fabrication of polypyrrole nanowires by electrochemical polymerization, n-doped silicon wafers, (1 0 0) oriented, with 20 nm of thermally grown oxide (Siltronix (Archamps, France)) were used. Metallic contacts (10 nm of Ti adhesion layer and 50 nm of gold) were deposited on the silicon oxide wafers by evaporation.

2.1.3 *Patterning mediators*

The generation of micro- and nanopatterns made out of conducting polymers is of great importance in this work and the materials required for their development are described in this section.

On one side, the fabrication of micropatterns based on biocatalytically generated polypyrrole was achieved by tuning the adhesion properties of the surfaces, taking advantage of the selective deposition of silane compounds. Thus, a chemical confinement of the polymer was obtained. The silane compounds used for the investigation of biocatalytical polypyrrole micropatterns were N-(3-Trimethoxysilylpropyl)pyrrole (pyrrole-silane) and Perfluoropolyether-silyltriethoxy-terminated (perfluoropolyether-silane), both supplied by ABCR GmbH & CO. KG (Karlsruhe, Germany). Also, (3-Aminopropyl)triethoxysilane (APTES) and Trichloro (1H,1H,2H,2H-perfluorooctyl)silane (FDTES) were used from Sigma-Aldrich Co (USA).

Alternatively, the electrochemical synthesis of polypyrrole nanowires was accomplished by confining the polymer growth within nanochannels patterned on the surface. Si/SiO_2 surfaces, containing pre-fabricated metallic contacts, were coated with a passivation layer that was later opened bridging contacts by nanolitographic techniques (Figure 2.2). The materials used as passivation layers were silicon oxide (SiO_2) and Poly(methyl methacrylate) (PMMA) (Microchemicals GmbH, Germany).

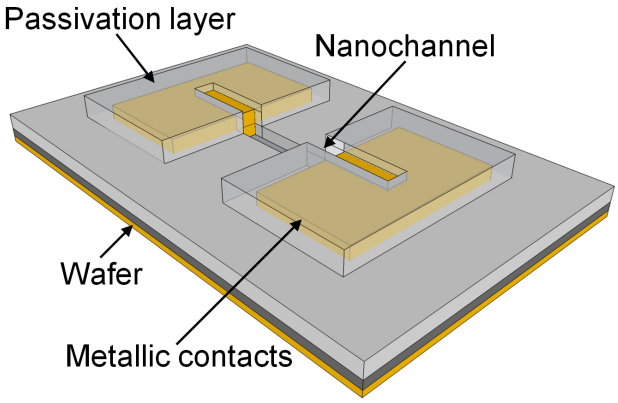

Figure 2.2: Schematics of surface patterning for the electropolymerization of polypyrrole nanowires. One can see the nanochannel opened on the passivation layer deposited on the wafer containing electrical contacts.

2.1.4 *Other supporting materials*

Sulphuric acid (H_2SO_4) 95-98%, hydrogen peroxide (H_2O_2), acetone and ethanol absolute were used in washing, surface activation and patterning processes (from Sima Aldrich Co (USA)).

A Sylgard® 184 Silicone Elastomer Kit was employed for Polydimethylsiloxane (PDMS) (Dow Corning (Seneffe, Belgium)) stamp fabrication, in microcontact printing experiments.

For biomolecule entrapment and drug-delivery experiments based on biocatalytically generated polypyrrole electrodes, streptavidin-modified gold colloids (~10 nm Au-nanoparticle diameter, 1.5x 10^{13} Au-nano particles/mL), simple streptavidin and D-biotin (Sigma-Aldrich Co (USA)) were used.

For DNA immobilization experiments, a 21-mer oligonucleotide extracted from the "Hepatitis C virus" was synthesized bearing an acetylene group (provided by Dr. Ramón Eritja, IQAC-CSIC Barcelona, Spain). It was used as immobilization probe to functionalize Azide-PEDOT electrodes by "Click" reaction. For hybridization experiments, the DNA probe was incubated with complementary, non-complementary and two-base mismatch targets (all provided by Sigma Aldrich Co (USA)). All DNA sequences were supplied as lyophilized powder. Oligonucleotide stock solutions (100 µM) were prepared in Milli-Q water and kept frozen. Next aliquots were prepared using Tris-HCl buffer (50 mM, pH 7.0). Milli-Q water was used in all DNA solution preparation.

Dimetyl sulfoxide (DMSO), Tris [(1-benzyl-1H-1,2,3-triazol-4-yl)methyl)]amine (TBTA), N,N-diisopropylethylamine (DIPEA) and Copper iodide (Cu(I)) (supplied

by Sigma-Aldrich Co (USA)) were mixed and used as catalyst solution for the immobilization reaction between the acetylene-modified DNA and the Azide-PEDOT ("Click" reaction).

2.2 FABRICATION METHODS

In this section, the oxidative polymerization mechanism and the specific polymerization techniques employed in the thesis are introduced. There is also a description of the methods used for the preparation of the surfaces, on which the polymers were grown, and the patterning techniques applied for the generation of micro- and nanopatterns of conducting polymers.

2.2.1 *Polymerization*

As briefly explained in subsection 2.1.1, the most common polymerization mechanism for conducting polymers occurs through a monomer oxidation. Although some controversy exists about the exact reaction route of oxidative polymerization, all theories agree that it starts with a cation radical formation [1, 5]. Two main polymerization mechanisms have been proposed [6]. The first is composed of the coupling of two cation radicals, subsequent generation of a dimer and the loss of two protons in the process (Figure 2.3).

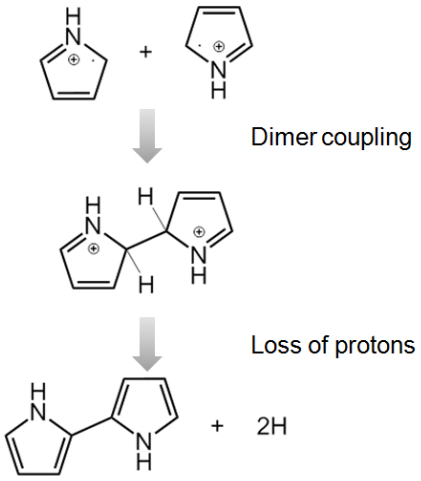

Figure 2.3: Polymerization mechanism based on cation radical coupling. From top to bottom: two cation radicals react and subsequently lose two protons. Afterwards, oxidation of the dimer occurs. (Pyrrole model is chosen for representation).

Dimers are more easily oxidized than monomers, which favors chain formation by the addition of other cation radicals (not shown in the schematics) [7].

The alternative mechanism is the free radical reaction with a neutral monomer, as shown in Figure 2.4. After the cation radical formation, a proton is lost and the radical attacks a neutral monomer. Then, after oxidation of the resulting dimeric radical and subsequent loss of a proton, the dimer can be oxidized again yielding to the chain growth (not shown in the schematics).

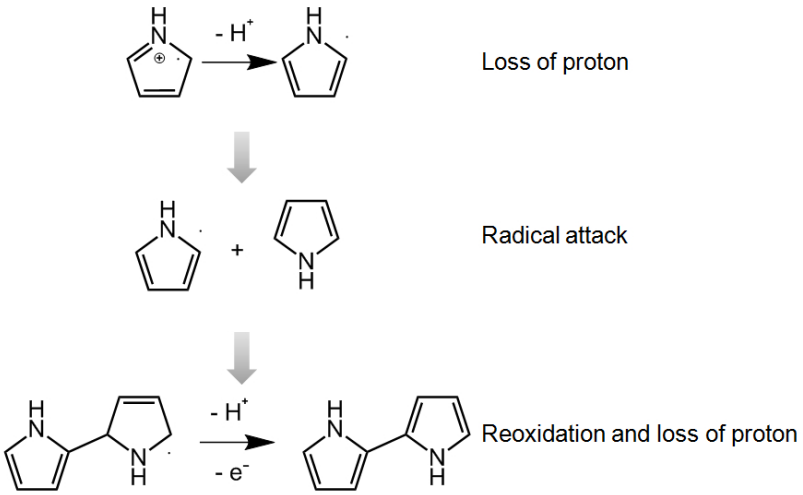

Figure 2.4: Polymerization mechanism based on cation radical coupling with neutral monomer. From top to bottom: a cation radical loses a proton and subsequently attacks a neutral monomer. Then, the dimer radical is reoxidized and loses another proton. (Pyrrole model is chosen for representation).

Monomer oxidation can be accomplished by electrochemical, chemical or biocatlytical methods. The electrochemical polymerization is initiated by applying high anodic potentials, while chemical and biocatalytical synthesis require chemical or biological oxidants to trigger the reaction. During the polymerization process, the electroneutrality of the polymer matrix is maintained by the incorporation of anions (doping anions), which balance the charge of the oxidized backbone, as seen in Figure 2.5. Therefore, the polymerization technique employed and the doping anion used will determine the final behaviour of the polymer [8].

In this work, electrochemical and biocatalytical methods were used for the fabrication of conducting polymer thin films, micro- and nanoelectrodes.

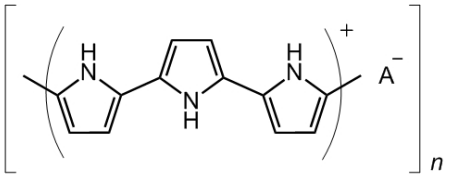

Figure 2.5: Structure of doped polypyrrole. A^- represents the doping anion.

2.2.1.1 *Monomer purification*

To assure good polymer properties, the reaction conditions must be carefully controlled. In particular, the purity of reagents, including the precursor monomer is essential. Therefore, while pure Azide-EDOT was obtained from collaboration and stored in the freezer protected from light, commercially provided pyrrole, required purification before use.

Pyrrole was purified by distillation under reduced pressure. Pyrrole has a boiling point of 129 ºC- 131 °C. By using low pressure conditions, distillation can be performed at lower temperatures, thus preserving the integrity of the components [9]. Here, impure pyrrole was kept under magnetic stirring and argon purge. Vacuum (200- 250 mbar approx.) was then applied to the distillation setup to decrease the pressure. At 50 °C (temperature measured inside the distillation balloon) distillation started, resulting in the collection of purified pyrrole after discarding the non-usable by-products (Figure 2.6). Pyrrole was stored under Argon, in the fridge and in the dark.

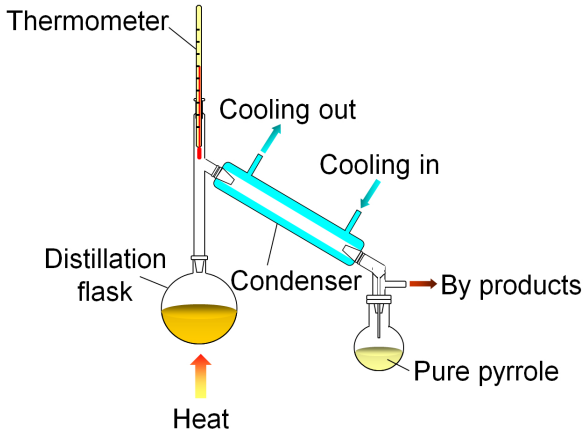

Figure 2.6: Distillation of pyrrole.

2.2.1.2 *Electrochemical polymerization*

The electrochemical synthesis of conducting polymers is accomplished by the application of high anodic potentials in electrolyte solutions containing the monomer. Since electropolymerization results in readily conductive and electroactive polymer films formed directly on the electrode surface, it is preferred when the polymer wants to be used as an electrode. Moreover, this technique provides an accurate control over the polymer thickness and the polymer properties during growth [8].

The polymer coating of an electrode starts by the generation of dimers and oligomers in solution, which only nucleate on the electrode surface when the chains are long enough to become insoluble [7]. After the nucleation step, the monomers and oligomers still present in solution are preferentially oxidized on the polymer surface rather than on the bare electrode, which results in a nuclei expansion and in the total coverage of the electrode [1].

Electrochemical polymerization can be performed by different electrical methods such as potentiostatic techniques, where a constant potential is applied between the electrodes, galvanostatic techniques, in which a constant current is injected between the electrodes and potentiodynamic techniques, which apply variable currents or potentials [8]. Here, we studied the electrochemical polymerization of Azide-PEDOT electrodes on gold surfaces by cyclic voltammetry (CV, potentiodynamic method), in DCM with $TBAPF_6$ as supporting electrolyte. A solution of 100 mM $TBAPF_6$ in DCM was prepared in a 3-electrode electrochemical cell and kept under Argon atmosphere. 1.5 mM Azide-EDOT was added to the electrochemical cell and cyclic voltammetry, between -1.5 V and +1.2 V (vs. Ferrocene-Ferrocenium (Fc/Fc^+)), was applied. All potentials were referred versus an Ag/AgCl pseudoreference electrode, consisting in an Ag/AgCl wire (only used for organic solvents), which was referenced after each use against Fc/Fc^+. A platinum wire was used as counter electrode. A BioLogic SP150 electrochemical analysis system (from Science Instruments) was employed to apply cyclic voltammetry.

Additionally, we investigated the electrochemical growth of polypyrrole nanowires between metallic contacts, by galvanostatic mode and by a system of alternating pulses of current (Figure 2.7).

The process was assisted by a second electrical filed, perpendicular to the electrode surface, used to favor the confinement of the oxidized monomers inside the nanochannel patterned on the surface, as envisioned in Figure 2.8. Drops of 2 µL of electrolyte solution and the monomer were placed on the nanochannel

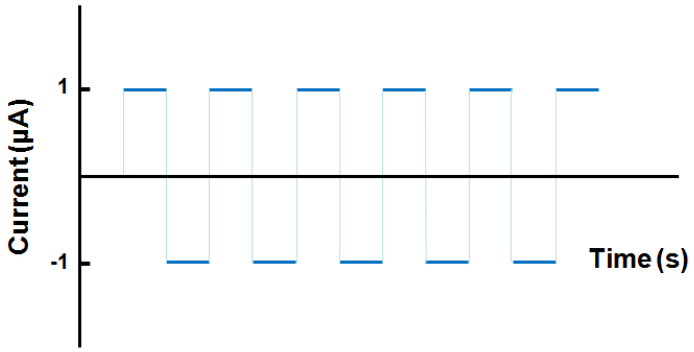

Figure 2.7: Alternating pulses of current applied between metallic contacts for polypyrrole nanowire fabrication.

and the process was started. The magnitude of the applied current was of 1 μA and the frequency of the alternating current was set at 0.5 kHz, with a duty of the 50%. The confinement field was generated by a voltage of -1 V and the reactions were conducted between 1 and 3 minutes. A S-1000 analytical probing station (Signatone Corporation), micropositioners and tungsten probes T20-50, with 5 μm tip radius (Everbeing INT'L corporation) were used to contact accurately the external electrical pads. A 6430 Sub-Femtoamp Remote SourceMeter (Keithley Instruments Inc.) together with a 50 MS/s single-channel arbitrary waveform generator, model WW5061 (Tabor Electronics Ltd.) were used to apply the two fields necessary for the electropolymerization and the confinement.

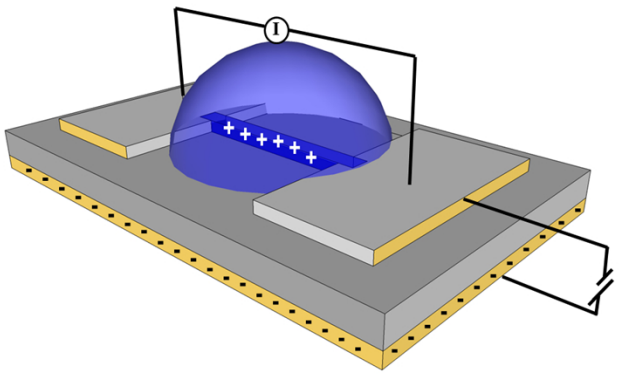

Figure 2.8: Electrolyte-monomer drop on top of nanochannel, ready to perform polymerization and confinement of polypyrrole nanowire.

Experiments in water solvent were conducted using 10 mM sodium chloride (NaCl) and 24 mM pyrrole monomer. For experiments in organic solvent, ACN was employed with 100 mM $TBAPF_6$ and 10 mM pyrrole.

2.2.1.3 *Biocatalytical polymerization*

Biocatalytical polymerization has emerged as a softer alternative to chemical polymerization methods, which require the use of extreme conditions such as strong oxidants and low pHs. By contrast, biocatalysis offers the possibility of working under mild reaction conditions, matching physiological requirements if needed, with low by-product formation and without compromising the electrical performance of the polymer [10].

This polymerization method was first attempted by using hydrogen peroxide, which is a natural and safe oxidant capable to perform the polymerization of several monomers. However, the polymerization in this way has low yields and causes structural defects in the final polymer [11], which brought enzymes into focus. Due to their high potential in catalyzing oxidation-reduction reactions, oxidoreductases have been used as natural catalysts to accelerate and improve polymerization reactions. In particular, two classes of oxidoreductases are the most relevant biocatalysts for the synthesis of conducting polymers: laccases and peroxidases [12].

Laccase is a copper-containing oxidase, which possesses four copper ions classified in one copper ion, Type1, and a cluster, Type2/Type3, as represented in Figure 2.9. The activation of the enzyme is produced by molecular oxygen (O_2), which oxidizes the enzyme and allows catalyzing four oxidation reactions. These four electron transfer steps return the enzyme back to its reduced (inactive) state, permitting its further "re-activation" through a new oxygen oxidation [10].

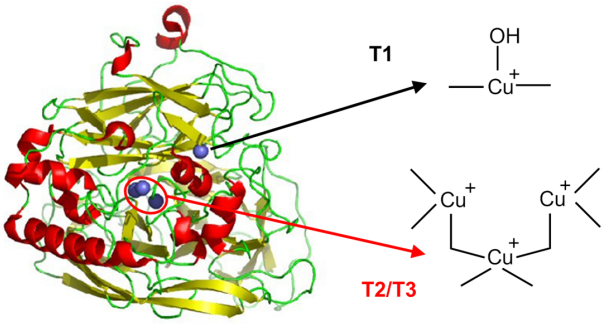

Figure 2.9: 3D structure of laccase, showing the copper centers T1 and T2/T3.

On the other hand, peroxidases such as horseradish peroxidase (HRP), soybean peroxidase (SBP) or palm tree peroxidase (PTP) are the most commonly used enzymes for conductive polymerization [13, 14, 15]. They belong to the heme-peroxidases group, whose active center is a heme (a ferrous ion (Fe^{2+}) containing cofactor needed to perform catalysis). These peroxidases can oxidize several monomers by using hydrogen peroxide in a very efficient process [12]. In the case of HRP, two calcium atoms and the iron heme group constitute its two metal centers (Figure 2.10). But it is the heme group which is open for hydrogen peroxide, oxidizing the enzyme. This process can catalyze two oxidation reactions, after which the enzyme is reduced back, like in the case of laccase [10].

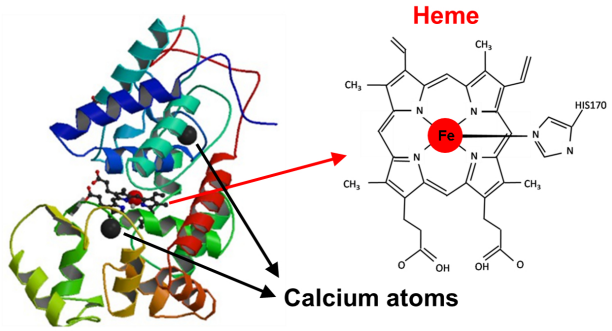

Figure 2.10: Structure of horseradish peroxidase, showing the active heme group.

These two enzymes are quite different regarding catalytic mechanism and active site structure, but both catalyze hydrogen abstraction reactions, which produce radical species and thus start the polymerization. However, sometimes the direct reaction of the monomer with the enzyme is not possible, as in the case of pyrrole. Since pyrrole is not a specific substrate for these enzymes, the oxidizing capability of Laccase and HRP towards pyrrole is considerably low, which has been solved by the incorporation of redox mediators [16, 17]. Redox mediators demonstrated to be useful in expanding the catalytic power of the enzymes and therefore facilitating the oxidation of compounds that could not be efficiently oxidized under the influence of the enzyme alone. Thus, as shown in Figure 2.11, the active form of the enzyme oxidizes the redox mediator, transferring its cation radical to the monomer and triggering the reaction [12].

Here, 3.35 mmol pyrrole, 0.123 mmol ABTS and 0.042 mmol EDTA, were mixed in 50 mM potassium biphtalate buffer (4.0 pH). The mixture was degassed through an argon flow to remove the oxygen present in the solution and was kept at room temperature (R.T.) under magnetic stirring and argon purge. Then, 7.32 mg HRP (from 50 to 150 pyrogallol units/mg approx.) were dissolved in 1.68 mL

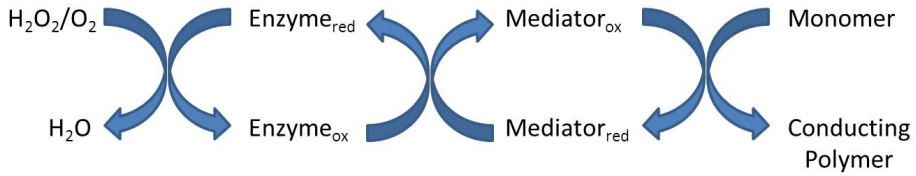

Figure 2.11: Enzymatic polymerization reaction assisted by redox mediators.

phosphate buffered saline (10x PBS, pH 7.0 buffer) and added to the reactor. Finally, the reaction was initiated by adding 3.35 mmol hydrogen peroxide (H_2O_2) to the mixture in a slow manner to avoid enzyme inactivation.

2.2.2 *Substrate Preparation*

In those cases where a good electrical connection between the conducting polymer and an external operator was required, metallic electrodes were deposited on the surface before polymer growth. Ti/Au microelectrodes were fabricated on bare Si/SiO_2 substrates and then polymers were grown between contacts, allowing its electrical manipulation. This section reviews the microfabrication procedures applied to obtain suitable surfaces on which conducting polymers were deposited afterwards.

2.2.2.1 *Microelectrode design*

The first step in every microfabrication process is the design of a hard mask to transfer a certain microelectrode layout to a substrate. The layout of the microelectrodes used in this work was generated by a layout editor (CleWin Ver. 4.0, MESA+ Institute for Nanotechnology, University of Twente, Netherlands). Figure 2.12a shows the layout of a mask that contained a general design in which two microelectrodes are separated by a distance of 5 µm (Figure 2.12c). The microelectrodes are connected by two large contact pads in order to apply bias, as shown in Figure 2.12b.

The designed microelectrode layouts were printed on acetate hard masks, which were used later in photolithography processes.

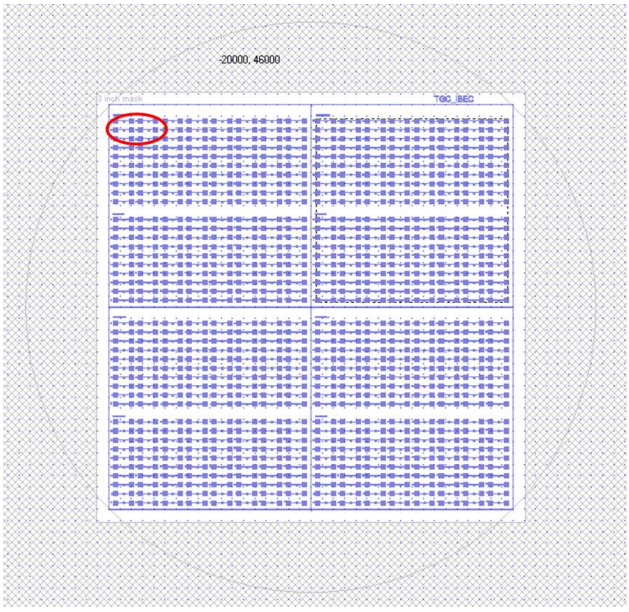

(a)

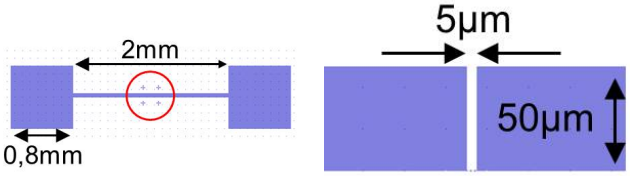

(b) (c)

Figure 2.12: Electrode design. Clewin layout. a) Layout of an acetate hard mask. b) Geometry of two microelectrodes with external large pads. c) Dimensions of microelectrode endings.

2.2.2.2 *UV- lithography*

Once a hard mask is obtained, with a desired microelectrode design on it, the microelectrodes were transferred to the substrate by UV-lithography.

UV-lithography, or photolithography, is a microfabrication process that uses light-sensitive materials, called photoresists, to selectively create micropatterns on surfaces. The surfaces to be treated are coated with photoresist and exposed to a pattern of intense light by means of the shadow hard mask (Figure 2.13). UV-light causes a chemical change on the photoresist, which allows some of the photoresist to be removed later by exposure to a solvent. Once a micropattern is formed on the photoresist, two different approaches can be applied in order to transfer the micropattern from the photoresist to the substrate underneath [18],

namely Top-Down (etching of the material exposed through the photoresist) and Bottom-Up (deposition of materials on the non-covered areas of the substrate underneath).

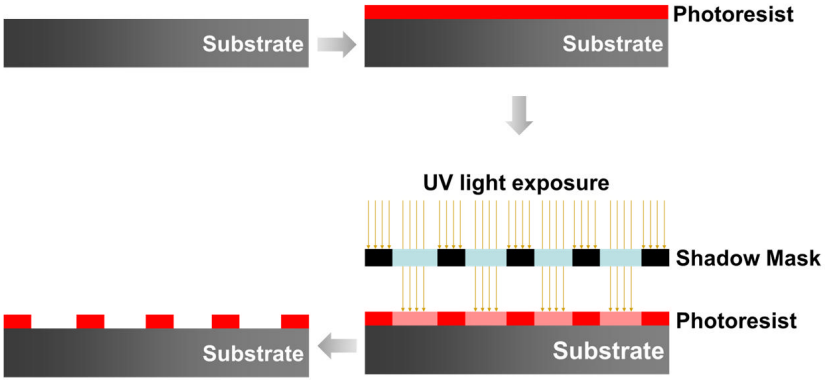

Figure 2.13: Photolithography. Steps of a photolithographic process consisting in spin coating, UV exposure and resist development.

Here, the substrates were spin coated with a photoresist AZ 5214-E (Microchemical GmbH, Germany) at 2000 rpm for 30 seconds (spin coater from Laurell Technologies Corporation, Figure 2.14a). The resulting film had a thickness of approximately 2 µm. This was followed by a soft-bake step, at 95 °C for 2 minutes on a hot-plate (Figure 2.14b), in order to evaporate the solvent remaining in the resist. The coated wafer and the hard mask were then brought into contact by a mask aligner MJB4 equipment (350 W Mercury light, SÜSS Microtec AG, Germany). The resist was UV-exposed at a constant intensity of 200 mJ/cm·s for 8 seconds (Figure 2.14c).

(a) (b) (c)

Figure 2.14: Photolithography equipment. a) Spin coater, b) hot plate for solvent evaporation and c) mask aligner..

The AZ 5214-E is a positive photoresist, which means that its exposure to UV-light breaks the polymeric links of the resist in the areas defined by the mask openings. The areas which are shadowed by the mask are not changed (the opposite occurs for negative resists). Thus, after immersion in an organic solvent, called developer (AZ developer 726MIF, Microchemical GmbH, Germany), for 25 seconds, the areas which have been exposed to UV-light (i.e. which have broken or weaker polymeric links) are dissolved, while the non-exposed areas (i.e. not altered) remain on the wafer. The reaction was stopped by rinsing the wafer in DI water, resulting in a photoresist pattern as seen in Figure 2.15. Up to 5 µm features can be obtained with this technique and a high-resolution hard mask.

Figure 2.15: Photoresist micropattern. Micropattern obtained after a photolithographic process.

2.2.2.3 *Direct Write Laser lithography (DWL)*

Additionally, for exceptional fabrication processes that require accurate control of electrode geometry, Direct Write Laser lithography (DWL) was used (DWL 66FS, Heidelberg Instruments, 50 mW diode laser with a wavelength of 405 nm). DWL is a high-precision, optical maskless lithography tool, for mask making and direct patterning of microstructures (Figure 2.16). As in conventional lithography, DWL is based on the exposure of a photo-sensitive resist that changes its solubility properties when a laser beam strikes the surface. This technique allows for a fabrication resolution down to 1 µm.

Figure 2.16: Mask plotter equipment (DWL).

In this case, the surfaces were coated with 1.4 µm of AZ1512 positive photoresist (Microchemical, GmbH, Germany). Then the micropattern was created by laser exposure of the microelectrode zones. After that, the wafers were developed in AZ726MIF developer for 6 seconds. The reaction was stopped with DI water, resulting in a photoresist micropattern.

2.2.2.4 *Etching: Top-Down fabrication*

Etching processes were used to transfer the patterns obtained on the photoresist, by UV-lithography, to the substrate underneath.

Top-Down fabrication approaches are based on removing material from a surface to generate features on it. In this work, after patterning the surface of metallized wafers (Si/SiO_2 wafers with 10 nm Ti and 70 nm Au) with photoresist microstructures, removal of the exposed metallic areas was achieved by wet and dry etching. Wet etching is an isotropic etching technique, which results in rounded profiles of the etched area as seen in Figure 2.17a. Here, wet etching was used to remove Au exposed areas from the substrates, by immersing the samples in a wet gold etching solution (Gold Etchant TFA, 14pH, Transene Company Inc., USA) with an etching rate of 28 Å/s. In the following step, the resist film was removed, whereby the remaining Au layer acted as a mask for the following Ti etching step.

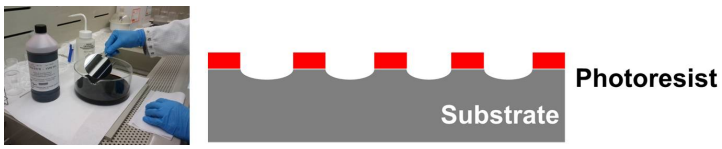

(a)

(b)

Figure 2.17: Etching. a) Wet etching of gold layer and b) dry etching of titanium layer by RIE.

The removal of the exposed titanium layer was performed by dry etching, which is an anisotropic process that results in sharp and well defined profiles

as sketched in Figure 2.17b. However, when titanium is exposed to air, a thin titanium oxide film (TiO_x) forms rapidly, which has to be removed prior etching the underneath Ti layer. By using dry etching in a series of gas processes, this problem was overcome without damaging the gold layer (the gases used have a negligible etching rate for gold). Substrates were subjected to a series of plasma processes in the same vacuum chamber by reactive ion etching (RIE, Plasmalab 80, Oxford Instruments pic, UK). First, 1 min of fluoroform plasma (CHF_3) was applied to remove the titanium oxide layer (50 sccm, 40 mTorr and 205 W), after it and without breaking the vacuum, a Cl_2 plasma was applied for 1 min more to remove the last Ti layer (50 sccm, 40 mTorr and 205 W). The etching rate of Cl_2 on SiO_2 is not significant and therefore SiO_2 acts as an etch-stop layer.

2.2.2.5 *Lift-off: Bottom-Up fabrication*

Alternatively, the fabrication of microstructures could also be achieved by Bottom-Up approaches, which are based on the deposition of materials on a bare substrate. In this case, titanium and gold metals were deposited on photoresist-microstructured flat SiO_2 surfaces, for the fabrication of electrical contacts (Figure 2.18b). 10 nm of titanium adhesive layer and 50 nm of gold were deposited by E-beam evaporation (Univex 450B, Oerlikon Leybold Vacuum, Figure 2.18a). After the metallic deposition was performed, a lift-off process was conducted (Figure 2.18b), which removed the photoresist coated areas after 1 hour of immersion in AZ100 remover (from Microchemicals GmbH).

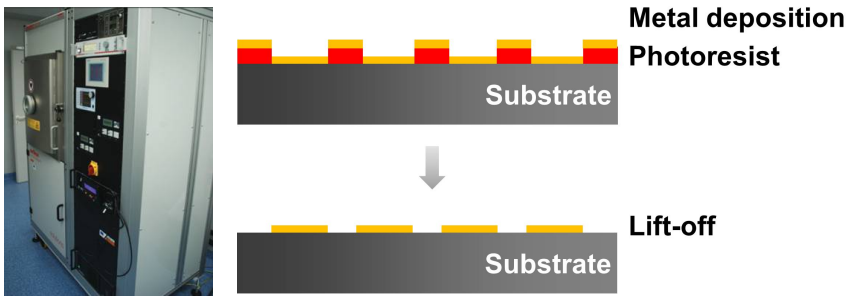

(a) (b)

Figure 2.18: Deposition of metallic micropatterns. a) Evaporator machine and b) lift-off process, consisting in deposition of metals on a micropatterned photoresist and removal of the resist.

The resulting patterned Ti/Au electrodes were characterized by several techniques such as Scanning Electron Microscopy (SEM), Atomic Force Microscopy (AFM) and optical microscopy .

2.2.3 *Patterning techniques*

This section describes the methods used to develop micro and nanopatterns made out of conducting polymers. Soft lithography techniques such as µCP and Dip-Pen Nanolithography (DPN) are introduced. Also, nanolithographic procedures such as Focused Ion Beam (FIB) and Electron Beam Lithography (EBL) are described.

2.2.3.1 *PDMS fabrication*

Generally, PDMS is used for the fabrication of replicating-microstructures (and also nanostructures) in the so called soft lithographic techniques [19]. In this thesis, soft lithography was used to transfer silane molecules from PDMS stamps to SiO_2 surfaces (see chapter 3). Therefore, PDMS replicas of hard microstructured silicon molds were fabricated (Figure 2.19a), by pouring a mixture of a PDMS precursor and a polymer cross linker (1:10 ratio, Sylgard® 184 Silicone Elastomer Kit) on top of the structures of the hard mold. Thus, a negative replica of the mold was obtained. Curing the mixture at 100 °C for one hour on a flat surface was required for obtaining a physically stable replica.

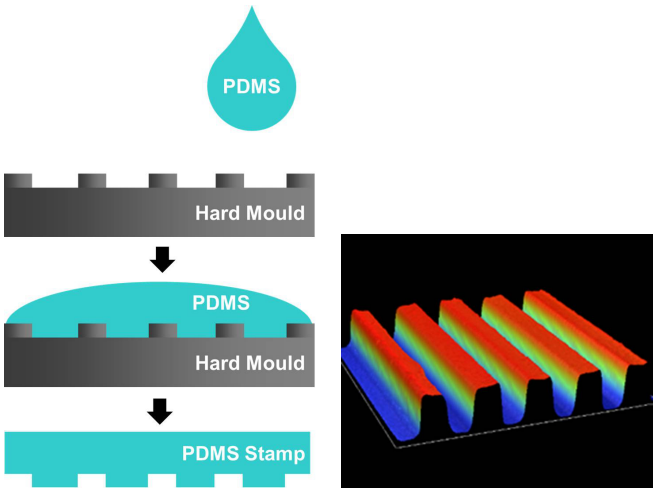

(a) (b)

Figure 2.19: PDMS stamp fabrication. a) Schematics of the PDMS fabrication process. b) Interferometric image of a PDMS stamp.

Figure 2.19b shows a white light interferometry (WLI) graph of a PDMS stamp, containing lines of 5 µm wide separated 5 µm.

2.2.3.2 *Microcontact printing (µCP)*

Microcontact printing (µCP) is one of the most popular forms of the so called soft-lithographic techniques to create micropatterns. µCP uses an elastomer stamp, generally made of PDMS, to transfer a desired molecule to a surface, via conformal contact. First, the PDMS stamp is inked with the molecule to be selectively deposited on the surface and then, the ink is transferred from the stamp to the substrate only in the area of contact. The µCP process is depicted in Figure 2.20. Since the development of µCP in the 90's by Kumma and Whitesides [20], where it was firstly used for the fabrication of thiol micropatterns on gold surfaces, µCP was adapted to different surfaces from metallic to insulating and was used with a large variety of inks. Particularly interesting inks include silanes, lipids, proteins, DNA, nanoparticles (NPs) and even metal nanofilms [21]. Resolutions down to 100 nm can be achieved by this method [22].

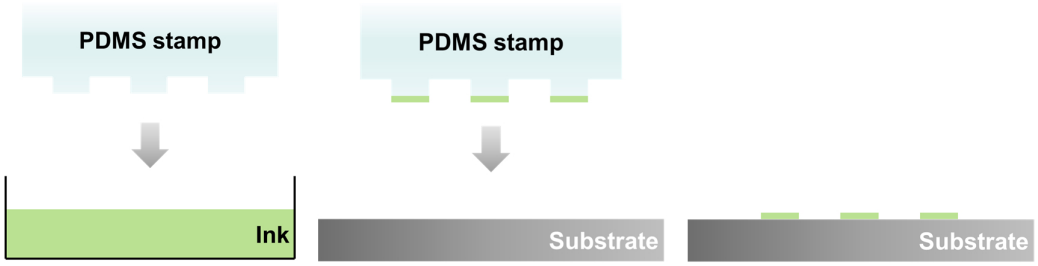

Figure 2.20: Microcontact printing (µCP) procedure. For µCP, PDMS stamp is inked with the molecule to stamp and the stamp is brought into contact with the surface, transferring the molecule to it.

2.2.3.3 *Dip Pen Nanolithography (DPN)*

Dip-pen nanolithography (DPN) is discussed for the fabrication of polypyrrole nanowires in chapter 5.

DPN is a direct-writing maskless fabrication technique that allows fine alignment and positioning of molecules over a surface in a convenient way. This nanolithographic technique, based on the atomic force microscope (AFM), uses AFM cantilevers coated with a desired molecule, to transport the molecule towards the surface via a water meniscus (unavoidably formed under ambient conditions), thus creating molecule-based nanofeatures (Figure 2.21a) [23].

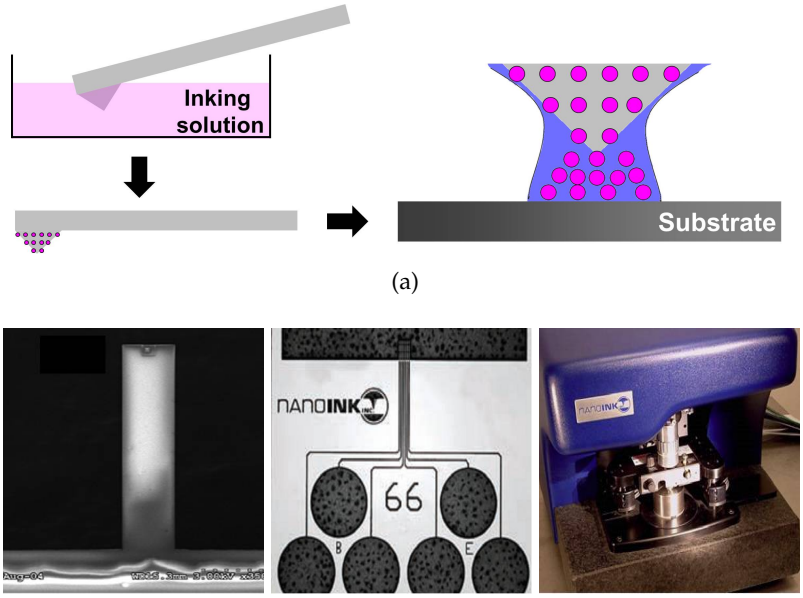

Figure 2.21: Dip-Pen Nanolithography a) Schematic of DPN process, b) DPN cantilever tip, c) DPN inkwells and d) Nscriptor equipment.

Contact mode AFM probes were obtained from NanoInk Inc. (type A, S-1, NanoInk, Inc. II., U.S.A. (Figure 2.21b)) with a spring constant of 0.041 N/m. Inking of the tips in the polypyrrole suspension was performed using the so called inkwells (special microfluidic channels, Figure 2.21c). The inkwells have a large reservoir of 2 mm of diameter, from where the ink flows to the microchannels with an approximate volume of 0.5 µL solution. DPN experiments have been performed with a NSCRIPTOR system from NanoInk (Skokie, USA Figure 2.21d) at room temperature (20 °C ± 1 °C) and humidity ranging from 30% to 40%, controlled with an environmental chamber and the EChamber software from NanoInk (ver. 1.01). InkCad Software (ver. 3.6.2, from NanoInk,) was used to design and program the nanolithography process. AFM images were taken with the same equipment, for characterization purposes. They were analyzed using nanoRule++ software (Ver. 2.5, Pacific Nanotechnology, II. U.S.A.)

2.2.3.4 *Focused Ion Beam (FIB)*

Focused ion beam (FIB) was employed in chapter 5 for the fabrication of SiO_2 nanochannels containing polymer nanowires.

FIB uses a focused beam of ions (generally gallium ions, Ga+) to image a sample, when operated at low beam currents, or for deposition and sputtering of

materials, when high beam currents are applied [24]. In a gallium liquid metal ion source, gallium metal is placed in contact with a tungsten needle and heated. The tip radius (~2 nm) of the needle is excited by an electric field, causing ionization and field emission of the gallium atoms, called source ions or primary ions. Then, the source ions are accelerated and focused onto the sample by electrostatic lenses. In a standard operation, the gallium primary ion beam hits the sample surface and sputters a small amount of material; this material leaves the surface as either secondary ions, neutral atoms or producing secondary electrons. As the primary beam rasters across the sample surface, the signal from the sputtered ions or secondary electrons is collected to form an image (Figure 2.22), with resolutions down to 5 nm. At higher primary currents, a great deal of material can be removed by sputtering, allowing precision milling of the specimen down to a sub micrometer or even a nanometer scale.

30 pA currents were used and 30 keV energies were applied. Channels with dimensions of 120 nm depth, 200 nm width and 15 µm length were fabricated.

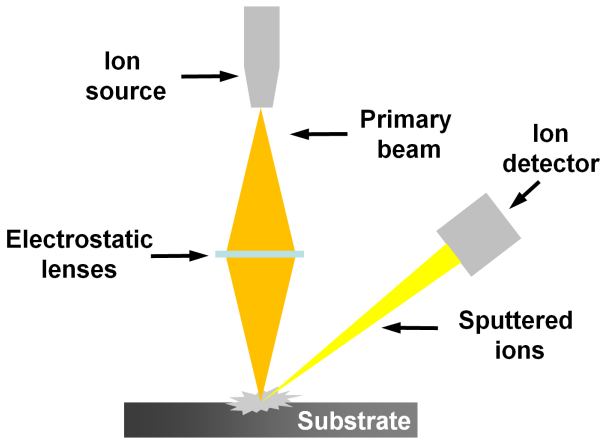

Figure 2.22: Focused Ion Beam schematics.

2.2.3.5 *Electron Beam Lithography (EBL)*

Electron beam lithography (EBL) is another maskless lithographic technique, which uses a focused beam of electrons to draw custom shapes on a surface, covered with an electron sensitive resist. As in photolitography, areas exposed to the electron beam change their solubility properties. This allows for the fabrication of patterns with sub-10 nm resolution [25]. First, a primary electron beam is emitted by thermal excitation of a tungsten filament cathode (other sources are also available). Then, the electron beam is focused by one or two condenser lenses and is deflected by pairs of scanning coils. They control the beam in the

x and y directions, scanning a certain area in a raster configuration (Figure 2.23). Typical EBL operation energies range from 10 keV and 50 keV.

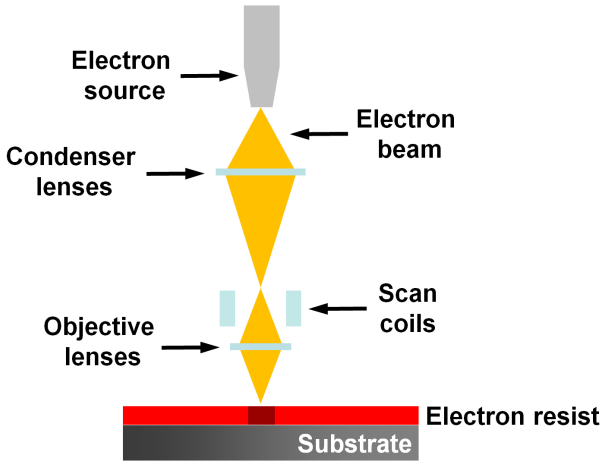

Figure 2.23: Electron Beam Lithography schematics.

An EBL equipment (Elphy Plus (SEM based system), Raith) was used to create nanopatterns on traditional electron-resists (PMMA) and on silanized SiO_2, for the fabrication of conducting polymer nanowires (see chapter 5) and nanostructures (see Appendix B).

In the case of PMMA, the resist was spin-coated on SiO_2 surfaces yielding a thickness of 300 nm. The exposure to electron beam was conducted using doses between 380 $\mu As/cm^2$ and 440 $\mu As/cm^2$. After exposure, development of PMMA was performed using a mixture of Methyl isobutyl ketone (MIBK) and Isopropanol (IPA) (MIBK:IPA 1:3) for 30 seconds, followed by an immersion of the substrates in IPA for 30 seconds. Surfaces with PMMA nanochannels could be used directly to grow electrochemically polypyrrole nanowires, when no SiO_2 layer was present under it. Therefore, PMMA acted as passivation layer. On the contrary, when a SiO_2 layer existed under the PMMA electron resist, an extra process of RIE was performed, to transfer the nanochannel to the oxide surface.

The use of silanes as electron resist is described in Appendix B.

2.3 CHARACTERIZATION METHODS

This section presents a summary of the techniques employed to characterize the fabricated polymers. The range of techniques applied includes structural, chemical, electrochemical and electrical characterizations. Some additional techniques are also introduced.

2.3.1 *Structural characterization*

2.3.1.1 *Atomic Force Microscopy (AFM)*

Atomic force microscopy (AFM) is a high-resolution type of scanning probe microscopy, able to resolve fractions of nanometers. Invented in 1986 by Binnig, Quate and Gerber, the AFM has become one of the most used tools for imaging, measuring, and manipulating matter at the nanoscale. An AFM is composed of a reflecting cantilever with a sharp and small tip (tip radius of few nanometers), used to scan the surface under study. When the tip is brought into proximity of a surface, forces between the tip and the sample cause a deflection of the cantilever according to Hooke's law. The deflection of the cantilever is measured using a laser, which reflects from the cantilever's backside to a photodiode (2.24) [26]. The photodiode signal corresponds to the change in deflection of the cantilever, providing a measurement of the surface topography. Scanning surfaces at a constant tip height is unfeasible due to an eventual damage of the tip, so to solve this problem, a feedback mechanism is employed to adjust the tip-to-sample distance and maintain a constant force between them. Piezoelectric elements facilitate accurate and precise movements in x, y and z directions, commanded by the feedback signals. AFM can be operated in contact and non-contact modes. In contact mode, the cantilever scans the sample and the contours of the surface are measured directly using the deflection of the cantilever. In the non-contact mode, the cantilever is externally oscillated at its fundamental resonance frequency. The oscillation amplitude, phase and resonance frequency are modified by tip-to-sample forces. These changes in oscillation with respect to the external reference oscillation provide information about the sample characteristics [26].

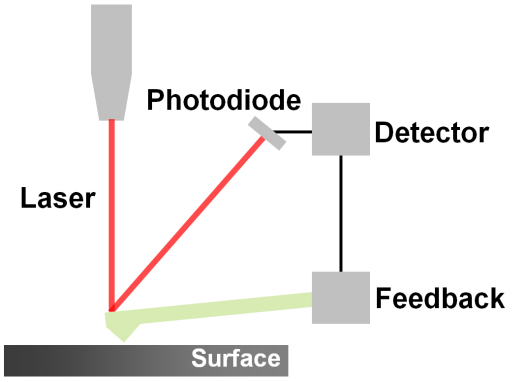

Figure 2.24: Atomic Force Microscope operation.

Chapters 3, 4 and 5 of the thesis discuss the use of AFM contact and non-contact modes, to investigate samples surface. Specifically, a Dimension 3100 AFM instrument (Veeco Instruments, USA) equipped with silicon AFM tips of spring constants of 40 N/m and 0.15 N/m, and radius of curvature smaller than 10 nm (Tap300Al-G and Contact300Al-G, 30 nm Al backside coating. BudgetSensors, Bulgaria) were used for the acquisition of topography images in tapping and contact modes, respectively. Images were obtained by area raster-scanning at several positions along the samples, for at least three samples per experiment. The acquired AFM measurements were processed with WSxM 5.0 software (Nanotec Electronica, Spain).

2.3.1.2 *Scanning Electron Microscopy (SEM)*

Scanning electron microscopy (SEM) is a high resolution imaging technique capable of resolving details in the nanometer range. SEM is based on the exchange of energy between a primary electron beam that scans the surface and the results of its interaction with the sample. These interactions include high energy electrons (reflected by elastic scattering), secondary electrons (emitted by inelastic scattering) and the emission of electromagnetic radiation [27]. Each of these signals can be collected by different detectors, giving different types of information like surface topography, composition or electrical conductivity. Commonly, the primary electron beam is emitted by thermal excitation of a tungsten filament cathode, but other sources are also available (Figure 2.25).

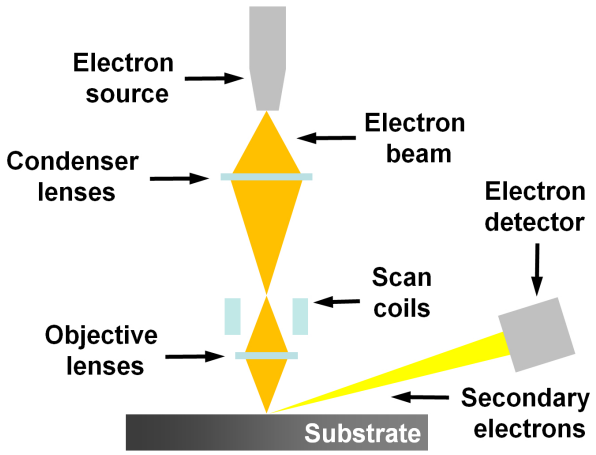

Figure 2.25: Scanning Electron Microscope.

The electron beam is then focused by one or two condenser lenses and it is deflected by pairs of scanning coils, controlling the beam in the x and y directions,

so it scans in a raster configuration over a rectangular area. Electronic amplifiers of various types are used to amplify the signals, which are displayed as variations in brightness on a screen .

SEM was used here, to analyze dimensions of micro- and nanofeatures and the morphology of different surfaces in chapters 3, 4 and 5. SEM micrographs were taken with a NOVA NANOSEM 230-FEI electron microscope, operating from 5 KV to 15 kV depending on the sample, with a spot size of 3 and at 5 mm distance from the electron gun.

2.3.1.3 *White Light Interferometry (WLI)*

White Light Interferometry (WLI) combines an interferometer and a microscope into one instrument. This technique provides a non-contact three dimensional measurement of surface roughness, with a resolution of tens of nanometers. Illumination from a white light beam passes through a filter and through a microscope objective lens to reach the sample surface. The objective lens is coupled with a beam splitter in such a way that some of the light is reflected from a reference mirror and recombined with the light reflected back from the surface (Figure 2.26).

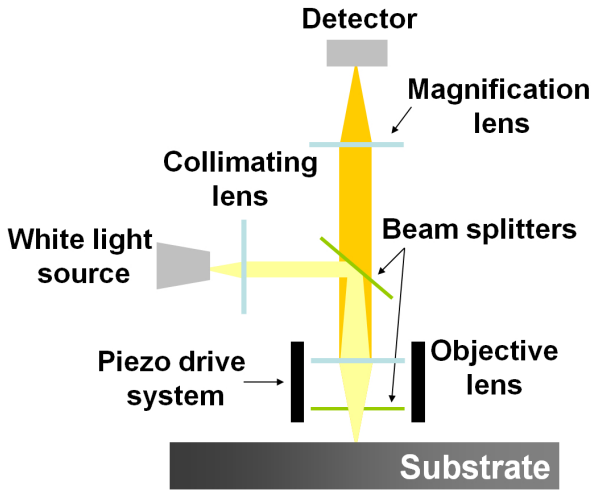

Figure 2.26: White Light Interferometry schematics.

Since the topography (height or roughness) of the sample will induce a change in the beam phase, the recombined beams create bright and dark bands called fringes, which represent the object topography and are captured by a CCD camera [28].

White light interferometry was used for PDMS stamps, and electrodes characterization in chapters 3 and 5.

2.3.1.4 *X-ray Diffraction (XRD)*

X-ray Diffraction (XRD) gives information about the crystal structure of materials. When X-rays hit an atom, the electronic cloud displaces, producing a charge movement that emits waves in the same frequency. These re-emitted wave fields interfere with each other either constructively or destructively, producing a diffraction pattern on a detector. This diffraction pattern is the basis of the diffraction analysis known as Bragg diffraction, which was first proposed by William Lawrence Bragg and William Henry Bragg in 1913, when they discovered that crystalline solids produced patterns of reflected X-rays. They found that at certain specific wavelengths and incident angles, crystals produced intense peaks of reflected radiation. They explained this result by modeling the crystal as a set of discrete parallel planes separated by a constant parameter d. It was proposed that the incident X-ray radiation would produce a Bragg peak if the reflections of various planes interfered constructively. The interference is constructive when the phase shift is a multiple of 2π. This condition can be expressed by Bragg's law (equation 2.1) (see also Figure 2.27):

$$n\lambda = 2d \sin\theta \tag{2.1}$$

Where n is an integer, λ is the wavelength of incident wave, d is the spacing between the planes in the atomic lattice, and θ is the angle between the incident ray and the scattering planes [29].

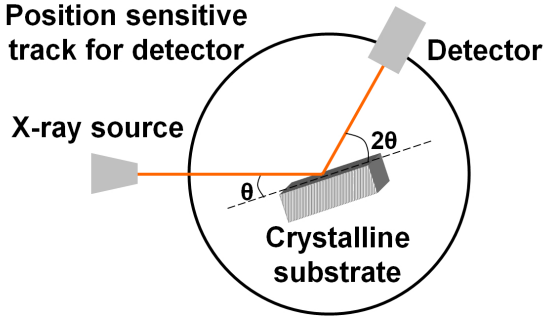

Figure 2.27: X-ray Diffraction operation.

XRD was applied in experiments of chapter 3, to obtain information about the crystalline structure of polypyrrole films and compare them to ones grown under

different conditions. The X-ray diffraction patterns of the polypyrrole samples were registered in a X'Pert PRO MRD system (PANalytical B.V, The Netherlands), using Cu K$\alpha(\lambda = 1.540598)$ Å. The diffractograms were registered in terms of 2θ in the range from 3° to 50° approximately with a scan step of 0.0196954°.

2.3.1.5 *Transmission Electron Microscopy (TEM)*

Transmission Electron Microscopy (TEM) is a microscopy technique in which an electron beam interacts with a very thin sample and passes through it. Then, an image produced from the interaction of the electrons transmitted through the sample can be obtained [30]. A TEM microscope is composed of several parts with different functions as the emission source, the vacuum system, the specimen stage, and the electromagnetic lenses (Figure 2.28). To avoid scattering of electrons with gases and allow efficient control of the electron beam, a vacuum system is required inside the TEM chamber. The emission source (or emission gun), which commonly consists of a tungsten filament connected to a high voltage source (typically ~100 kV – 300 kV), is responsible of the generation of the electrons. Once the electrons are extracted from the source, they are accelerated by an electric field and focused on a desired size and location by means of the electromagnetic lenses. The specimen stage, which allows the insertion, removal and motion of the sample in the beam path, is used to locate the area of interest in the sample through which electrons should pass.

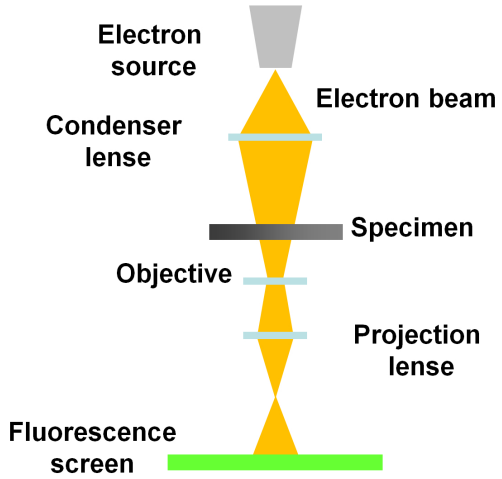

Figure 2.28: Transmission Electron Microscopy scheme.

TEM can operate in bright field imaging mode or in diffraction contrast mode. For bright field imaging mode, thicker regions of the sample (or regions with a higher atomic number) will appear dark, whilst regions transparent to electrons

(where electrons pass through) will appear bright, giving a final image of the studied sample. Simultaneously, if the wavelength of the electrons is comparable to the spacing between atoms of the sample, the scattering of a fraction of electrons that strike the sample occurs, to particular angles in the back focal plane. The main fraction of electrons will continue to pass through the sample without deflection. The diffracted electrons determine the crystal structure of the sample, and define the diffraction contrast image (selected area diffraction pattern, SAED), where each spot corresponds to a satisfied diffraction condition of the sample's crystal structure.

For thin crystalline samples, an image consisting of a pattern of dots is produced, while a series of rings are generated in the case of a polycrystalline and no pattern is obtained for amorphous solid materials.

TEM was used to investigate the crystallinity of biocatalytically produced polypyrrole samples, grown at room and low temperatures, in chapter 3. A TEM JEOL, JEM1210, with an accelerating voltage of 120 kV was used. Biocatalytic polypyrrole thin films were scratched from SiO_2 surfaces and prepared by dispersing the films in anhydrous hexane. A drop of suspended solution was placed onto a carbon-coated copper grid and dried naturally under ambient conditions. Finally, the samples were introduced in the TEM vacuum chamber to analyze their morphology and diffraction by electron beam.

2.3.2 *Chemical characterization*

2.3.2.1 *X-ray Photoelectron Spectroscopy (XPS)*

X-ray Photoelectron Spectroscopy (XPS) is a quantitative spectroscopic technique that measures the surface chemistry of any material in a non-destructive way. The first XPS spectrum was obtained in 1907, by P. D. Innes, who recorded broad bands of emitted electrons as a function of velocity when irradiating a material with X-rays. These investigations were interrupted by the first and second world wars, and it was not before 1954, after the second world war, Kai Siegbahn and his group developed several significant improvements to the equipment, recording the first high-energy-resolution XPS spectrum and revealing the potential of XPS [31].

XPS spectra are obtained by irradiating a material with a beam of X-rays which penetrates up to 5 µm in the sample volume. Simultaneously, the kinetic energy and number of electrons that escape from the first 10 nm of the material are analyzed (Figure 2.29). All of the deeper photo-emitted electrons, generated by

the X-rays penetration, are either recaptured or trapped in various excited states within the material. A typical XPS spectrum is a plot of the number of electrons detected versus their binding energy. Each element produces a characteristic set of XPS peaks at a certain binding energy, which directly identifies each element that exists in the material surface. These characteristic peaks correspond to the configuration of the electrons within the atoms. Such information allows the determination of elemental composition, empirical formula, chemical state and electronic state of the material being analyzed. The number of detected electrons in each of the characteristic peaks is directly related to the amount of element within the irradiated volume.

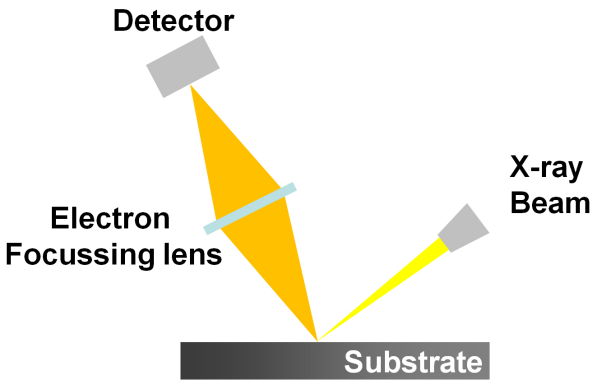

Figure 2.29: X-ray Photoelectron Spectroscopy cartoon.

XPS analysis was conducted in chapters 3 and 4 with a Perkin-Elmer PHI 5500 Multi-technique system (Physical Electronics, Inc., Minnesota, USA), operating in ultrahigh vacuum, (from $5{\cdot}10^{-9}$ torr to $2{\cdot}10^{-8}$ torr). Measurements were taken with a X-ray monochromatic source (Aluminium Kα 1486.6 eV and 350 W) placed perpendicularly to the analyzer axis and calibrated using the 3d5/2 line of Ag with a full width at half maximum (FWHM) of 0.8 eV. A circle of 0.8 mm of diameter was analyzed with a resolution for pass energy of 187.5 eV/step and 0.8 eV/step for full spectra and 11.75 eV/step of pass energy and 0.05 eV/step for the high resolution spectra of each element. Analysis of the full and high resolution spectra was done by MultiPak V6.0A software (Physical Electronics Inc., Minnesota, USA). Calibration of the spectra was done using de C1s line at 284.6 eV.

2.3.2.2 *Time-of-Flight Secondary Ion Spectroscopy (ToF-SIMS)*

Time-of-Flight Secondary Ion Mass Spectrometry (ToF-SIMS) provides qualitative surface elemental and chemical analysis of organic and inorganic materials, along

with elemental and chemical imaging. ToF-SIMS uses a pulsed ion beam, generally of cesium (Cs), gallium (Ga) or, as in this work, bismuth (Bi), to remove molecules from the surface of the sample in the form of secondary ions. These ions are then accelerated into a "flight tube" to determine their mass by measuring the exact time at which they reach the detector (Figure 2.30) [32]. ToF-SIMS can operate in several modes, namely mass spectrometry analysis, chemical imaging and depth profiling. In the mass spectrometry analysis and chemical imaging modes, only the outermost layers of the surface are analyzed (1 nm approx.) to determine the nature of the elemental and/or molecular species present on the surface. In the imaging mode, visualization of the distribution of individual species across the surface is accomplished by scanning the ion beam across the sample surface and acquiring an entire mass spectrum from every pixel in the image. In a different mode, depth profiles are used to determine the distribution of different chemical species as a function of depth from the surface. For this purpose, an ion gun is operated in DC mode during sputtering phases (O_2 and Cs), in order to remove material, and a second ion gun (Bi) is operated in the pulsed mode during data acquisition phases. Phases of sputtering and data acquisition are alternated until the complete depth profile is recorded (dual beam mode). With ToF-SIMS depth profiling, all species of interest are monitored simultaneously and with high mass resolution. Contrary to XPS, this technique is destructive, but allows chemical analysis in large depth profiles.

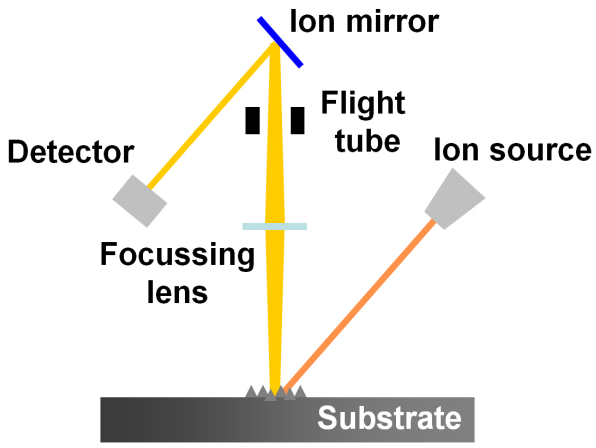

Figure 2.30: Time-of-Flight Secondary Ion Spectroscopy.

The study of biological samples by ToF-SIMS analysis is a challenging task, since such type of samples are enormously complex, contain hundreds of peaks which can be quite similar to each other. Thus, it is unfeasible to detect differences

between different surfaces by simple comparison of their individual mass spectra. Such a situation is traditionally handled by data processing approaches where only few peaks from the spectra are selected for the analysis, wasting most of the information present in the spectra [33]. Nevertheless, when MutiVariate Analysis (MVA) methods are applied to ToF-SIMS analysis, useful information from large data sets can be obtained, showing evident differences between samples that otherwise would need the use of labeled targets for distinction [34].

MVA requires multiple ToF-SIMS measurements on which statistical methods are applied. It summarizes the variance patterns within a dataset, describing the differences between samples. Principal Component Analysis (PCA) is the most commonly used MVA method for ToF-SIMS data analysis. It reduces a large set of correlated variables (peak intensities in a mass spectrum) to a smaller number of uncorrelated variables, called Principal Components (PCs) [33, 34, 35]. PCs represent linear combination of the original variables and capture the greatest variation within the dataset. This reduction in variables renders an easier interpretation of complex spectra while retaining all the information present in the entire set of mass spectra. The input of PCA is a correlation matrix where the rows are samples (spectra) and the columns are variables (peak intensities) and each cell in the matrix is the peak area for a given mass peak from a given spectrum [34, 36]. This matrix is decomposed into "scores" and "loadings" matrices, which describe the relationship between samples. Scores give the relationship between samples in the new axis system, while loadings show the relationship between the old variables (peak intensities) and new variables (PCs) [34]. However, before reducing the dataset by PCA, it is necessary to pre-treat the data to assure that the variance patterns are due to the chemical differences between samples and not to mathematical differences in peak intensities [37].

ToF-SIMS was used in chapters 3 and 4 with a ToF-SIMS4 from IonToF (Münster, Germany) operating at $5{\cdot}10^{-9}$ mbar of pressure. Bismuth liquid metal ions (Bi^{3+}) bombarded the samples at energy of 25 keV. The ion beam had a 20 ns pulse width and a 0.3 pA pulsed ion current for a dosage lower than $5{\cdot}10^{11}$ ions/cm^2, below the threshold level of $1{\cdot}10^{13}$ ions/cm^2 generally accepted for static SIMS conditions. Secondary ions were detected by a reflection time-of-flight analyser, a multichannel plate and a time-to-digital converter. Measurements were performed with a typical acquisition time of 20 s, at time resolution of 200 ps. Charge neutralization was achieved with a low energy (20 eV) electron flood gun, thus conductive coatings were not needed before measurements. Secondary ions were extracted with 2 kV voltage and were post-accelerated to 10 keV kinetic energy

just before hitting the detector. The maximum mass resolution, $R = m/\Delta m$, was around 8000, where m is the target ion mass and Δm is the resolved mass difference at the peak half-width. Secondary ion spectra in positive and negative mode were acquired from randomly rastered surface areas of 500 μm x 500 μm along the sample. Signal intensity of different ion fragments were extracted and compared for different samples.

Additionally, MVA was applied to ToF-SIMS to confirm the presence of biotin and streptavidin in polypyrrole thin films. PCA was then employed to reduce and analyze the ToF-SIMS dataset using XLSTAT software (Addinsoft SARL). PCA was used to describe the variance within the input matrix data, so identification of similarities and differences between spectra was possible.

2.3.2.3 *Infrared Spectroscopy (IR)*

Infrared Spectroscopy (IR spectroscopy) uses the infrared region of the electromagnetic spectrum to identify and study chemicals. IR spectroscopy exploits the fact that molecules absorb specific frequencies that are characteristic of their structure. Actually, the frequency of the absorbed radiation matches the frequency of the vibrating bond, thus associating vibration frequency with particular type of bond, represented by the strength and mass of the atoms that compose it [38]. The infrared spectrum of a sample is recorded by passing a beam of infrared light through the sample (Figure 2.31). When the frequency of the infrared is the same as the vibrational frequency of a bond, absorption occurs. Examination of the transmitted light reveals how much energy was absorbed at each frequency. Analysis of the position, shape and intensity of peaks in the obtained spectrum reveals details about the molecular structure of the sample.

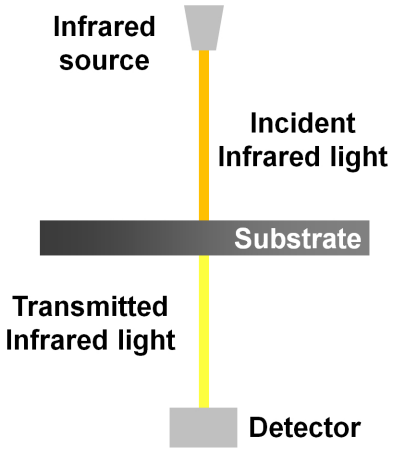

Figure 2.31: Infrared Spectroscopy.

IR spectroscopy was used in chapter 3, to identify chemical species based on their infrared absorbance. Polypyrrole powders were studied by this technique to evaluate and confirm polypyrrole formation under enzymatic method. An iZ10 infrared spectrophotometer with a fast recovery deuterated triglycine sulfate detector (DTGS) (Thermofisher Scientific, Inc.) was used to perform experiments accumulating 32 scans, with a spectral resolution of 4 cm^{-1} and operating in a spectral range from 650 cm^{-1} to 4000 cm^{-1}.

2.3.3 *Electrical characterization*

2.3.3.1 *Conductivity Measurements*

Ohm's law is used to determine unknown resistances. A known current (I) is applied through the resistance (R) to be measured and the voltage (V) developing across the resistance is recorded. Extraction of the resistance is achieved from the division of voltage and current values [39] as shown in equation 2.2.

$$R = \frac{V}{I} \tag{2.2}$$

In this work, 2-contacts conductivity measurements were performed for material characterization (see chapters 3 and 5). Therefore, direct current electrical measurements were performed on enzymatic polypyrrole layers with fabricated electrodes in 2-contcts geometry, for chapter 3. A sweep of potential from -1 V to +1 V was applied between two electrodes, using the recorded current to obtain the resistance of the enzymatic polypyrrole layers. In chapter 5, potentials from -0.1 V to +0.1 V were applied to fabricated polymeric nanowire-devices, recording the current and obtaining the resistance across the nanostructure.

A S-1000 analytical probing station (Signatone Corporation, California, USA), micropositioners and tungsten probes T20-50, with 5 µm radius tip (Everbeing INT'L corporation, Hsinchu, Taiwan), 6430 Sub-Femtoamp Remote SourceMeter with a 6430's Remote PreAmp, for a very sensitive bi-directional amplification (Keithley Instruments Inc., Ohio, USA) and LabTracer 2.0 (ver. 2.8) software (National Intruments Corporation) were employed for electrical characterization and electropolymerization experiments, together with a 50 MS/s single-channel arbitrary waveform generator, model WW5061 (Tabor Electronics Ltd., Israel).

2.3.4 *Electrochemical characterization*

Voltammetry comprises a group of electroanalytical methods, which study the current as a response to an applied potential. Voltammetry provides information about the thermodynamics and kinetics of chemical reactions and can be used to identify and quantify different species in solution. In this method, a certain potential (or current) is applied and varied between a couple of electrodes and the resulting current (or potential) is measured, giving information about the analyte under investigation [40]. Therefore, an electrode in contact with the analyte (working electrode), is subjected to a certain potential, thus facilitating the charge transfer with the analyte. Additionally, another electrode is needed to measure and control the potential of the working electrode and to balance the charge added or removed by the working electrode. However, it is difficult for a single electrode to assume these two functions, and generally two separated electrodes are used in a three-electrode-cell configuration. Thus, a reference electrode (with a known and stable potential) is responsible of gauging the working electrode potential and a counter electrode supplies all the current needed to balance the charge at the working electrode.

2.3.4.1 *Cyclic Voltammetry*

Cyclic Voltammetry (CV) is a useful technique to characterize a material and to acquire qualitative information about electrochemical reactions. It offers a rapid location of redox potentials of the electroactive species.

In this method, the electrode potential increases linearly versus time as shown in Figure 2.32a. The experiment is characterized by its ramping, known as the experiment's scan rate (V/s). The forward scan produces a current peak for any analyte that can be oxidized through the range of the potential scanned. On the waveform (Figure 2.32b), it can be observed how the current increases as the potential reaches the oxidation potential of the analyte. Then, it falls off as the concentration of the analyte is depleted close to the electrode surface. If the redox couple is reversible, the application of an opposite potential scan reduces back the product formed in the first oxidation reaction, and produces a current of reverse polarity from the forward scan. The reduction peak usually has a similar shape to the oxidation peak [41]. As a result, information about the redox potential and electrochemical reaction rates of the compounds are obtained [37].

In chapter 3, controlled drug release experiments were investigated by CV in a BioLogic SP150 electrochemical analysis system (Science Instruments, France).

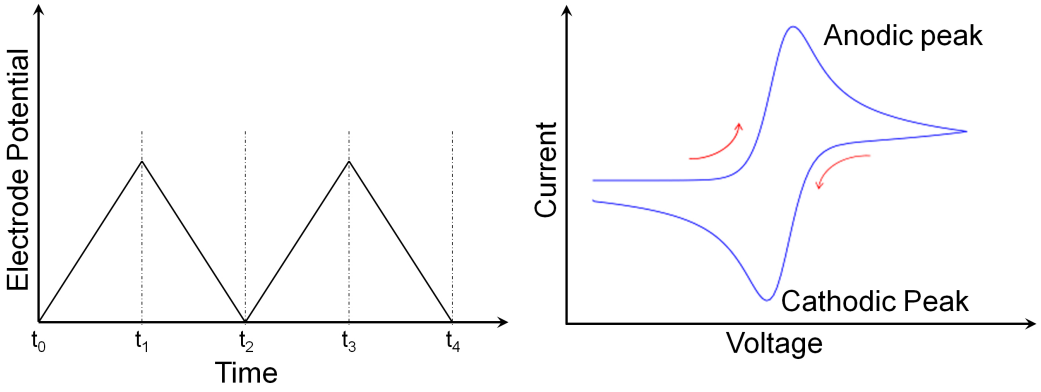

(a) (b)

Figure 2.32: Cyclic Voltammetry. a) Evolution of potential with time and b) cyclic voltammogram.

A three-electrode electrochemical cell was used with a platinum counter electrode and an Ag/AgCl reference electrode. The working electrode consisted on a Polypyrrole/ SiO_2/ Si surface that contained pre-fabricated gold electrodes, which were connected to external pads for electrical stimulation. Partial passivation of the working electrode was done with Teflon tape, to avoid electrochemical interferences with the external pads and to assure a constant liquid-exposed area (Figure 2.33). Measurements were done in Phosphate buffered saline (PBS) buffer (7.35 pH) and voltage sweeps from -0.9 V to +0.9 V and vice versa were applied to the polymeric working electrode at a scan speed of 100 mV/s. Then, changes in current intensity were registered against applied potential and analyzed.

In chapter 4, CV was used to polymerize Azide-EDOT on gold working electrodes, and to characterize the synthesized azide-modified PEDOT layers. PEDOT polymerization was conducted between -1.5 V and +1.2 V (vs Fc/Fc^+), in dichloromethane and characterization was done between -0.85 V and +0.6 V (vs. Ag/AgCl reference electrode) in Tris-HCl solution.

2.3.4.2 *Differential Pulse Voltammetry*

Differential Pulse Voltammetry (DPV) is another electrochemical measurement, where a series of regular voltage pulses (constant in amplitude) superimpose upon a staircase wave form (Figure 2.34a) [42, 43]. The current is sampled twice in each pulse period (once before the pulse and once at the end of the pulse) and the current difference is plotted as a function of potential (Figure 2.34b). By sampling the current just before the potential is changed, the effect of the charg-

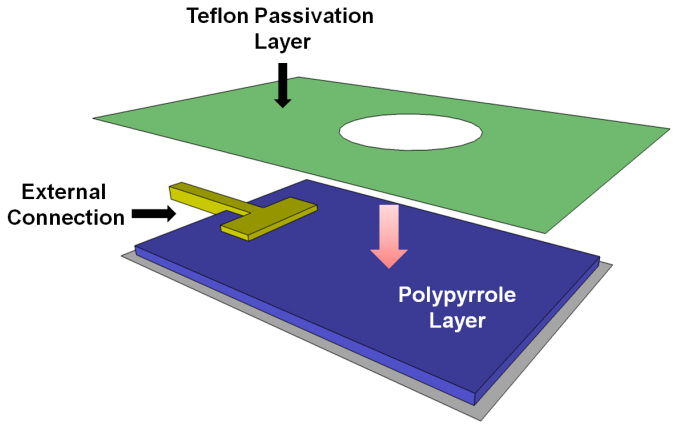

Figure 2.33: Diagram of polypyrrole electrodes. For redox experiments, polypyrrole was grown on SiO_2 surfaces containing prefabricated gold electrodes (which act as external connections). A Teflon passivation layer is added before electrical stimulation.

ing current can be decreased and high sensitivity is achieved [38]. Additionally, faradaic current is extracted, so electrode reactions can be analyzed more precisely, allowing the study of redox properties of extremely small amounts of chemicals.

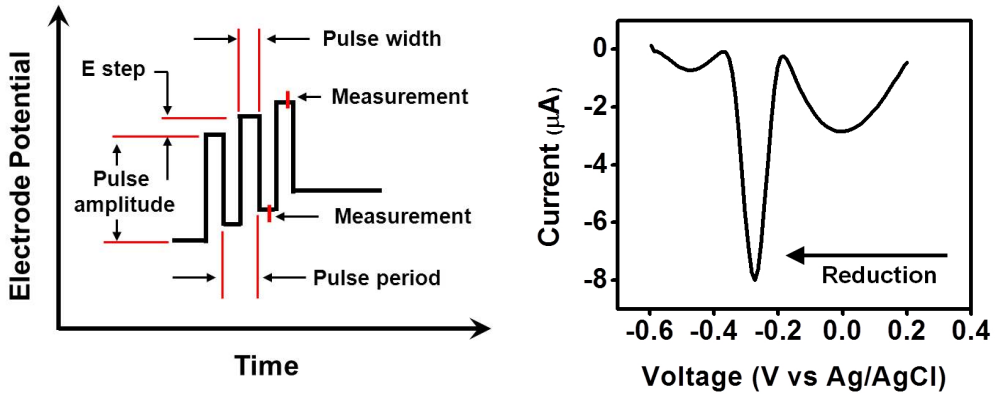

(a) (b)

Figure 2.34: Differential Pulse Voltammetry. a) Evolution of potential with time and b) differential pulse voltammogram.

This technique was used in chapter 4, to quantitatively detect DNA hybridization events, using an AUTOLAB PGSTAT 30 electrochemical analysis system (Eco Chemie, The Netherlands). DPV measurements were done in 20 mM Tris-HCl buffer (7.0 pH) using voltage sweeps applied to the working electrodes consist-

ing on PEDOT-modified gold electrodes. Then, changes in current intensity were registered against applied potential and analysed with GPES 4.7 software package (Eco Chemie, The Netherlands). Raw data were treated using the Savitzky and Golay filter, followed by the moving average baseline correction (peak width of 0.01) provided by the software.

2.3.5 *Other characterization techniques*

2.3.5.1 *Contact Angle*

The wettability of a solid surface by a certain liquid is quantified by the contact angle between the liquid and the solid surface. The contact angle measures the affinity between liquid and solid molecules compared to the interactions with their own kind. Experimentally, angles between surface and profiles of water droplets are compared (Figure 2.35). In this work we will study water contact angles, giving as a result a parameter called hydrophobicity, specific for the interaction of the solid surface with liquid water. If a drop of water spreads on the solid, the water contact angle of the surface will be small and we will consider it hydrophilic, but if the water contact angle is large (65°), the surface will be considered hydrophobic [44]. Different hydrophobicities are characteristic of different surfaces. Even for the same material, as in silicon, different surface treatments can yield different wettability and the surface can be made hydrophilic or hydrophobic. Thus this technique is an ideal method for the characterization of surface modifications, studied in chapters 3, 4 and 5.

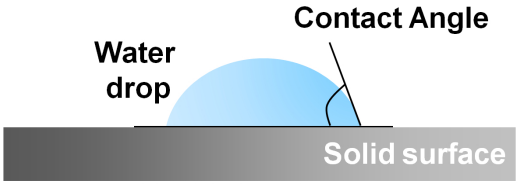

Figure 2.35: Contact Angle.

Contact angle measurements using Milli-Q ultrapure water drops (MilliPore Ibérica S.A.U, Spain) were performed in an OCA contact angle instrument (Dataphysics, Germany), where the droplets were placed at room temperature on the surfaces to be studied. Using the application drop analysis from ImageJ 1.460 software (National Institutes of Health, USA) droplet profiles were fitted to a sphere or an ellipse to extract the contact angle formed with the surfaces.

2.3.5.2 *High-Performance Liquid Chromatography Mass Spectrometry (HPLC-MS)*

High-Performance Liquid Chromatography Mass Spectrometry (HPLC-MS) is an extremely versatile instrumental technique capable of separating the components in a mixture, identifying them and quantifying them if necessary. As its name suggests, HPLC-MS (Figure 2.36) combines a high-performance liquid chromatograph (HPLC) attached, via a suitable interface, to a mass spectrometer (MS). Its primary advantage over other chromatographic techniques is that it is capable of analyzing a much wider range of components [45]. For instance, compounds that are thermally labile, with high polarity or with a high molecular mass such as proteins, can all be analyzed using HPLC-MS. Solutions derived from samples of interest are injected at high pressure into an HPLC column that comprises a narrow stainless steel tube (usually 150 mm in length and 2 mm or smaller in internal diameter) packed with fine, irregularly or spherically shaped particles, which are chemically modified to accomplish particular types of separations. Compounds are separated on the basis of their relative interaction with the chemical coating of these particles (stationary phase) and the solvent eluting through the column (mobile phase). Generally, in HPLC-MS instrumentation, octadecylsilyl (C18) and related organically-modified particles are used as stationary phase with pure or pH-adjusted mixtures of water and organic solvents such as water-acetonitrile and water-methanol. Components eluting from the chromatographic column are then ionized and introduced into the mass spectrometer via a specialized interface. The two most common interfaces used for HPLC-MS are the electrospray ionization and the atmospheric pressure chemical ionization interfaces, however the atmospheric pressure chemical ionization interface is not suitable for the analysis of thermally labile species and it is indicated for low mass compounds.

The electrospray ionization interface is composed of an electrospray needle and a source sampling cone, between which a high potential difference is applied. The analyte flows into the needle and leaves its tip towards the cone as a spray of charged droplets with a surface charge of the same polarity as the charge of the needle. Then, as the droplets travel through the space between needle tip and cone, solvent evaporation occurs and the droplets shrink until they reach a point where the surface tension can no longer sustain the charge. At that point, a "Coulombic explosion" occurs and the droplet is ripped apart, producing smaller droplets that can repeat the process until naked charged analyte molecules are obtained. The analyzer then subjects the charged molecules to electrical and magnetic fields, which accelerate and deflect the charged molecules, separating them

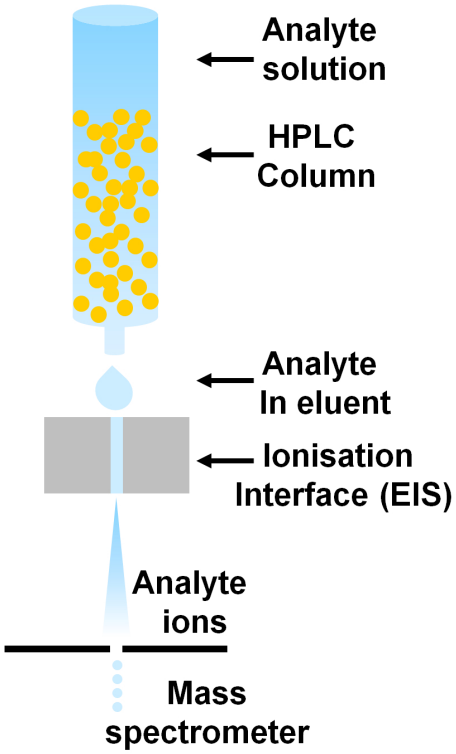

Figure 2.36: High-Performance Liquid Chromatography Mass Spectrometry.

according to their mass to charge ratio. This process is especially useful for studying high molecular mass such as proteins, since it avoids the fragmentation of large molecules when they are ionized. Moreover, it offers the possibility of creating singly or multiply charged analyte molecules, thus extending the mass range of the analyzer to higher orders of magnitude.

In the thesis, the presence of biotin into release buffers, after electrical stimulation of biotin-functionalized biocatalytic polypyrrole (see chapter 3), was confirmed by HPLC-MS. 200 µL liquid samples from the release measuring solution (PBS) were taken after certain electrochemical cycles and times. A mass spectrometer LTQ-Orbitrap from Thermo Scientific, equipped with a chromatographic module Accela was used. A Luna reversed phase column (C18) of 150 mm length and 2 mm internal diameter and particle size of 5 µm operated at 7000 psi with MeCN/H_2O eluent. Ionization was achieved with an electrospray source (ESI) and the acquisition data was done in positive polarity mode.

2.4 REFERENCES

[1] Tat'yana V Vernitskaya and Oleg N Efimov. "Polypyrrole: a conducting polymer; its synthesis, properties and applications". In: *Russian Chemical Reviews* 66.5 (May 1997), pp. 443–457. DOI: 10.1070/RC1997v066n05ABEH000261 (cit. on pp. 18, 22, 25).

[2] Sarah M Richardson-Burns et al. "Polymerization of the conducting polymer poly(3,4-ethylenedioxythiophene) (PEDOT) around living neural cells." In: *Biomaterials* 28.8 (Mar. 2007), pp. 1539–52. DOI: 10.1016/j.biomaterials.2006.11.026 (cit. on p. 18).

[3] Gordon Wallace and Geoffrey Spinks. "Conducting polymers - bridging the bionic interface". In: *Soft Matter* 3 (2007), pp. 665–671. DOI: 10.1039/b618204f (cit. on p. 18).

[4] Hang-Beom Bu et al. ""Click"-functionalization of conducting poly (3, 4-ethylenedioxythiophene) (PEDOT)". In: *Chem. Commun.* (11 2008), pp. 1320–1322. DOI: 10.1039/b718077b (cit. on p. 18).

[5] Dragos Brezoi. "Polypyrrole Films Prepared by Chemical Ooxidation of Pyrrole in Aqueous FeCl3 Solution". In: *Journal of Science and Arts* 1.1 (2010), pp. 53–58 (cit. on p. 22).

[6] HIDEYUKI Higashimura and SHIRO Kobayasi. "Oxidative polymerization". In: *Encyclopedia of Polymer Science and Technology*. Vol. 10. 4, pp. 740–764 (cit. on p. 22).

[7] B R Scharifker. "The growth of polypyrrole films on electrodes". In: *Journal of Electroanalytical Chemistry* 300 (1991), pp. 85–98 (cit. on pp. 23, 25).

[8] Darren Svirskis et al. "Electrochemically controlled drug delivery based on intrinsically conducting polymers." In: *Journal of controlled release : official journal of the Controlled Release Society* 146.1 (Aug. 2010), pp. 6–15. DOI: 10.1016/j.jconrel.2010.03.023 (cit. on pp. 23, 25).

[9] L.L. Armarego, Wilfred, L.F.; Chai, Christina. *Purification of Laboratory Chemicals*. Ed. by Elsevier. 2003, p. 346 (cit. on p. 24).

[10] Frank Hollmann and Isabel W. C. E. Arends. "Enzyme Initiated Radical Polymerizations". In: *Polymers* 4.4 (Mar. 2012), pp. 759–793. DOI: 10.3390/polym4010759 (cit. on pp. 27, 28).

[11] V Rocchi and G P Gardini. "ON PYRROLE OXIDATION WITH HYDROGEN PEROXIDE". In: *Tetrahedron* 26 (1970), p. 4073 (cit. on p. 27).

[12] G V Otrokhov et al. “Biocatalytic synthesis of conducting polymers and prospects for its application.” In: *Biochemistry. Biokhimiya* 78.13 (Dec. 2013), pp. 1539–53. DOI: 10.1134/S0006297913130117 (cit. on pp. 27, 28).

[13] Yong Hwan Kim et al. “Polymerization of cardanol using soybean peroxidase and its potential application as anti-biofilm coating material”. In: *Biotechnology letters* 25.18 (Sept. 2003), pp. 1521–4 (cit. on p. 28).

[14] H. B Dunford. *Peroxidases in Chemistry and Biology*. Ed. by J. Everse and M. B. Grisham. 1991, pp. 1–24 (cit. on p. 28).

[15] Ryan Bouldin et al. “Enzymatic Synthesis of Electrically Conducting Polymers”. In: *American Chemical Society* X.Symposium series (2010), pp. 315–341 (cit. on p. 28).

[16] R Cruz-Silva et al. “Biocatalytic synthesis of polypyrrole powder, colloids, and films using horseradish peroxidase”. In: *Journal of colloid and interface science* 328.2 (Dec. 2008), pp. 263–269. DOI: 10.1016/j.jcis.2008.09.021 (cit. on p. 28).

[17] Hyun-Kon Song and G Tayhas R Palmore. “Conductive polypyrrole via enzyme catalysis”. In: *The journal of physical chemistry. B* 109.41 (Oct. 2005), pp. 19278–19287. DOI: 10.1021/jp0514978 (cit. on p. 28).

[18] *Lithography. Theory and Application of Photoresists, Developers, Solvents and Etchants*. MicroChemicals (cit. on p. 30).

[19] John A Rogers and Ralph G Nuzzo. “Recent progress in soft lithography”. In: *Materials Today* February (2005), pp. 50–56 (cit. on p. 35).

[20] Amit Kumar and George M. Whitesides. “Features of gold having micrometer to centimeter dimensions can be formed through a combination of stamping with an elastomeric stamp and an alkanethiol "ink" followed by chemical etching”. In: *Applied Physics Letters* 4.14 (1993), pp. 2002–2004. DOI: 10.1063/1.110628 (cit. on p. 36).

[21] A. Perl, David N Reinhoudt, and Jurriaan Huskens. “Microcontact Printing: Limitations and Achievements”. In: *Advanced Materials* 21.22 (2009), pp. 2257–2268. DOI: 10.1002/adma.200801864 (cit. on p. 36).

[22] Tobias Kaufmann and Bart Jan Ravoo. “Stamps, inks and substrates: polymers in microcontact printing”. In: *Polymer Chemistry* 1.4 (2010), p. 371. ISSN: 1759-9954. DOI: 10.1039/b9py00281b (cit. on p. 36).

[23] “Applications of dip-pen nanolithography”. In: *Nature nanotechnology* 2.3 (Mar. 2007), pp. 145–55. DOI: 10.1038/nnano.2007.39 (cit. on p. 36).

[24] Jon Orloff. "Fundamental limits to imaging resolution for focused ion beams". In: *Journal of Vacuum Science and Technology B: Microelectronics and Nanometer Structures* 14.6 (1996) (cit. on p. 38).

[25] C Vieu et al. "Electron beam lithography : resolution limits and applications". In: (2000), pp. 111–117 (cit. on p. 38).

[26] Franz J Giessibl. "Advances in atomic force microscopy". In: *Reviews of Modern Physics* 75 (2003), p. 949 (cit. on p. 40).

[27] Pease RFW Oatley CW, Nixon WC. "Scanning electron microscopy". In: *Advanced Electronics and Electron Physics* 21 (1965), pp. 181–247 (cit. on p. 41).

[28] C. Schmit, J., Creath, K. and Wyant. "Surface Profilers, Multiple Wavelength, and White Light Intereferometry". In: *Optical Shop Testing*. Ed. by Daniel Malcara. John Wiley & Sons, Inc., 2007, pp. 667–755 (cit. on p. 42).

[29] C. Kittel. *Introduction to Solid State Physics*. Ed. by New York Wiley. 1976 (cit. on p. 43).

[30] Julius Ruska et al. "THE DEVELOPMENT OF THE ELECTRON MICROSCOPE AND OF ELECTRON MICROSCOPY". In: *Nobel Lecture* (1986) (cit. on p. 44).

[31] K. I. Al Siegbahn, K.; Edvarson. "beta-Ray spectroscopy in the precision range of 1 : 1e6". In: *Nuclear Physics* 1.8 (1956), pp. 137–159 (cit. on p. 45).

[32] a. Benninghoven. "Chemical Analysis of Inorganic and Organic Surfaces and Thin Films by Static Time-of-Flight Secondary Ion Mass Spectrometry (TOF-SIMS)". In: *Angewandte Chemie International Edition* 33 (Aug. 1994), pp. 1023–1043. DOI: 10.1002/chin.199437319 (cit. on p. 47).

[33] Daniel J. Graham, Matthew S. Wagner, and David G. Castner. "Information from complexity: Challenges of TOF-SIMS data interpretation". In: *Applied Surface Science* 252.19 (July 2006), pp. 6860–6868. DOI: 10.1016/j.apsusc.2006.02.149 (cit. on p. 48).

[34] M S Wagner and David G Castner. "Characterization of Adsorbed Protein Films by Time-of-Flight Secondary Ion Mass Spectrometry with Principal Component Analysis". In: *Langmuir* 17.30 (2001), pp. 4649–4660 (cit. on p. 48).

[35] Elena S F Berman et al. "Distinguishing monosaccharide stereo- and structural isomers with TOF-SIMS and multivariate statistical analysis". In: *Analytical chemistry* 78.18 (Sept. 2006), pp. 6497–6503. DOI: 10.1021/ac060865g (cit. on p. 48).

[36] J B Lhoest et al. "Characterization of adsorbed protein films by time of flight secondary ion mass spectrometry". In: *Journal of biomedical materials research* 57.3 (Dec. 2001), pp. 432–440. URL: http://www.ncbi.nlm.nih.gov/pubmed/11523038 (cit. on p. 48).

[37] Steven J. Pachuta. "Enhancing and automating TOF-SIMS data interpretation using principal component analysis". In: *Applied Surface Science* 231-232 (June 2004), pp. 217–223. DOI: 10.1016/j.apsusc.2004.03.204 (cit. on pp. 48, 51).

[38] C. P. Sherman Hsu. "Infrared Spectroscopy". In: *Handbook of Instrumental Techniques for Analytical Chemistry*. 1997, pp. 247–284 (cit. on pp. 49, 53).

[39] Tony R. Kuphaldt. *Lessons In Electric Circuits, Volume I- DC*. Fifth Edit. 2006, pp. 282–289 (cit. on p. 50).

[40] Cynthia G Zoski. *Handbook of Electrochemistry*. Ed. by Elsevier. Elsevier, 2007, pp. 1–935. ISBN: 9780444519580 (cit. on p. 51).

[41] Peter T Kissinger, West Lafayette, and William R Heineman. "Cyclic voltammetry". In: *Journal of Chemical Education* 60.9 (1983), pp. 702–706 (cit. on p. 51).

[42] Allen J Bard et al. *Electrochemical Methods: Fundamentals and Applications*. Ed. by Wiley. Wiley, 2001. ISBN: 0471043729 (cit. on p. 52).

[43] *INSTRUCTION MANUAL FOR BASi EPSILON FOR ELECTROCHEMISTRY* (cit. on p. 52).

[44] J. Comelles. "The role of surface energy of technical polymers in serum protein adsorption and MG-63 cells adhesion". In: *Nanomedicine: naotechnology, bioloy and medicine* 6 (2010), pp. 44–51 (cit. on p. 54).

[45] Arjen R. de Boer et al. "Mass spectrometry-based biochemical assays for enzyme-inhibitor screening". In: *TrAC Trends in Analytical Chemistry* 26.9 (Oct. 2007), pp. 867–883. ISSN: 01659936. DOI: 10.1016/j.trac.2007.08.004 (cit. on p. 55).

3

BIOCATALYTICALLY-PRODUCED POLYPYRROLE THIN FILMS AND MICROELECTRODES ON INSULATING SURFACES

This chapter presents a new on-surface biocatalytical procedure for the fabrication of polypyrrole microelectrodes on insulating surfaces. This is an environmentally respectful method that allows the entrapment of biomolecules during the polymer synthesis in a single step fabrication process. As a proof of concept, biotin has been trapped in the polymer matrix and then released in a controlled way through electrical stimulation. This result represents a straightforward method for the microfabrication of biological-active conducting polymers, which could be implemented in implantable devices for remotely controlled tissue interactions.

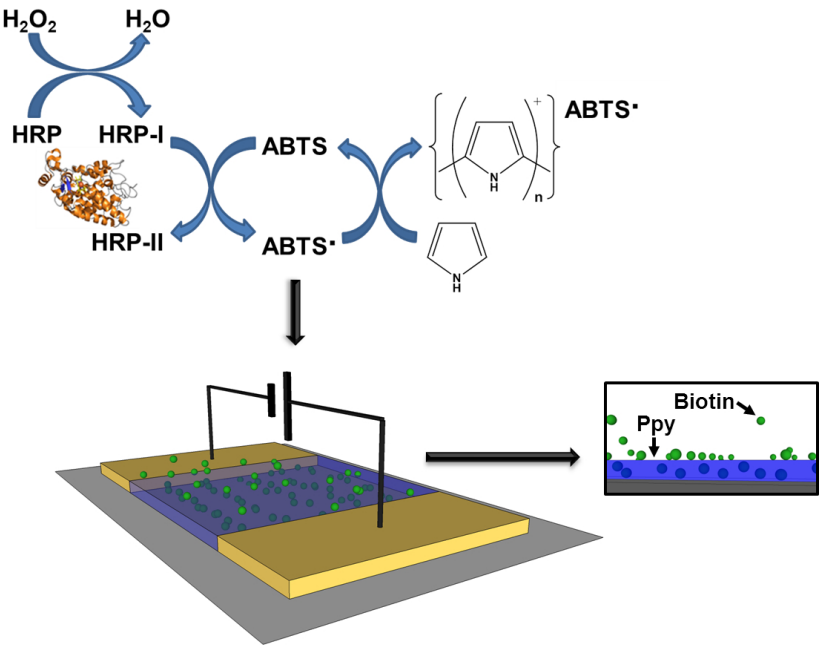

3.1 INTRODUCTION

Among all conducting polymers, polypyrrole (Figure 3.1) has become one of the most attractive alternatives to metals and inorganic semiconductors in the development of biomedical devices [1, 2]. Its good thermal and environmental stability, its high conductivity at room temperature (up to 100 S/cm) [3] and most importantly its biocompatibility [4], are key properties to put polypyrrole at the top of conducting polymers in this field. In particular, polypyrrole has been shown to behave as an excellent interface material to biology, providing good biomechanical interaction and efficient biomolecule loading properties, which enhance the life-time of the devices [5, 6].

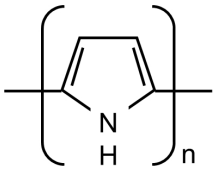

Figure 3.1: Polypyrrole chemical structure.

There are recent reports, in which polypyrrole has been tailored with biomolecules that influence a certain cell response, such as adhesion or differentiation [7, 8, 9]. Moreover, it has been used to deliver biological targets through the application of electrical stimulation [5, 10, 11], which reveals the potential of polypyrrole as a material for cell and tissue engineering. In this regard, polypyrrole has been used to coat implantable devices. It showed to match the biomechanical needs of the tissue interfaces, by being modified with drugs that improve integration and minimize the wound-healing response generated by conventional materials [12, 13]. It also provides a good electrical performance compatible with stimulation and recording, which allows an electrical interaction with the tissue [1]. In the new generation of neural implants, such as the bionic eye, the new cochlear implants, or the brain-machine interfaces, a demand for arrays of microelectrodes which allow the independent stimulation (or recording) of very close independent brain areas, is of great importance [14, 15]. However, the development of a simple and robust process for the fabrication of conducting polymer microelectrodes still remains a challenge. The conventional photolithographic methods used for microfabrication are not suitable for polymers, as they degrade the optical and conducting properties of the material upon exposure to radiation. Thus, direct-polymer-printing methods have been attempted as an alternative for the fabrication of conducting polymer microelectrodes, allowing

their direct deposition with micrometer resolution on a wide variety of surfaces. Different approaches have been reported, including screen-printing [16, 17, 18], Ink-Jet Printing (IJP) [19, 20, 21], thermal-laser-printing [22] and soft-lithography techniques [23, 24].

The screen-printing methods (Figure 3.2) use a polymer-inked mesh, attached to a blocking mask that forms open areas. By pressing through the mesh, the ink is transferred to the substrate, creating sharp-edged images with feature resolutions down to 100 µm.

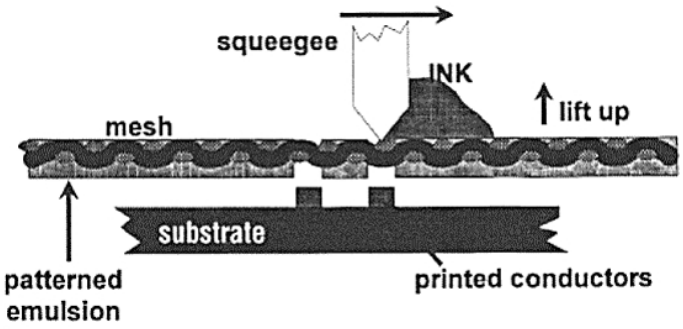

Figure 3.2: Screen printing technique. A polymer ink is transferred to a substrate pressing through a mesh on a blocking mask. (Image taken from reference [18])

IJP (Figure 3.3) is based on the common office printers, daily used for transferring electronic data to paper. This process has been translated to industrial manufacturing processes, becoming the most widely used fabrication technique applied to organic microelectronics.

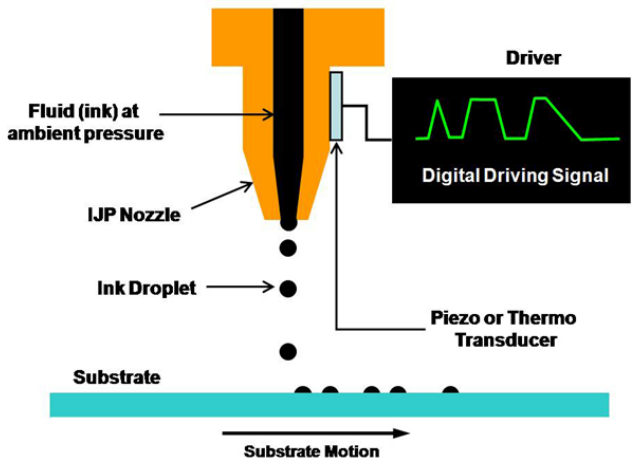

Figure 3.3: Ink-Jet printing technique. Polymer-ink droplets are deposited on a surface by computer control. (Image taken from reference [21]).

Digital images are created by computer aid, which control a piezoelectric inkjet printer that deposits polymer-ink droplets onto a substrate. This process can achieve polymer features in the range of 20 µm to 50 µm.

In a different way, thermal-laser-printing techniques (Figure 3.4) use a laser source to create a pattern on a thin solid polymer layer in contact with the substrate. The laser is focused onto a thin absorbing layer attached to the polymer, which converts light into heat. Then, heat decomposes the surrounding organic material of the interface into gaseous products, which expands and propels the polymer layer onto the substrate. This microfabrication technique reaches a resolution down to 10 µm.

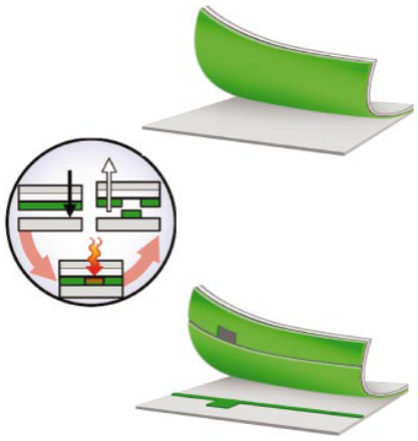

Figure 3.4: Thermal-laser printing technique. A polymer layer is patterned on a surface by laser stimulation. (Image taken from reference [22]).

The use of an elastomer stamp is the basis of the so called soft-lithographic techniques (Figure 3.5). Here, a microstructured stamp (generally fabricated in polymethylsiloxane, PDMS) is brought into conformal contact with a substrate, to create a micropattern. The stamps have been used in different manners as for instance in the microcontact printing technique (µCP). Here, the stamp is coated with a polymer ink, to transfer the polymer molecules to the surface after the contact. Alternatively, the substrates can be coated with the polymer, using later a clean stamp to partially remove the polymer. Also, fresh stamps can be used to create free microchannels at the interface with the surface, the polymer ink is sent into the channels left in the interface stamp-surface and later on, the polymer is cured obtaining the polymeric pattern after stamp removal. Resolutions down to 100 nm can be achieved by the use of these methods [24].

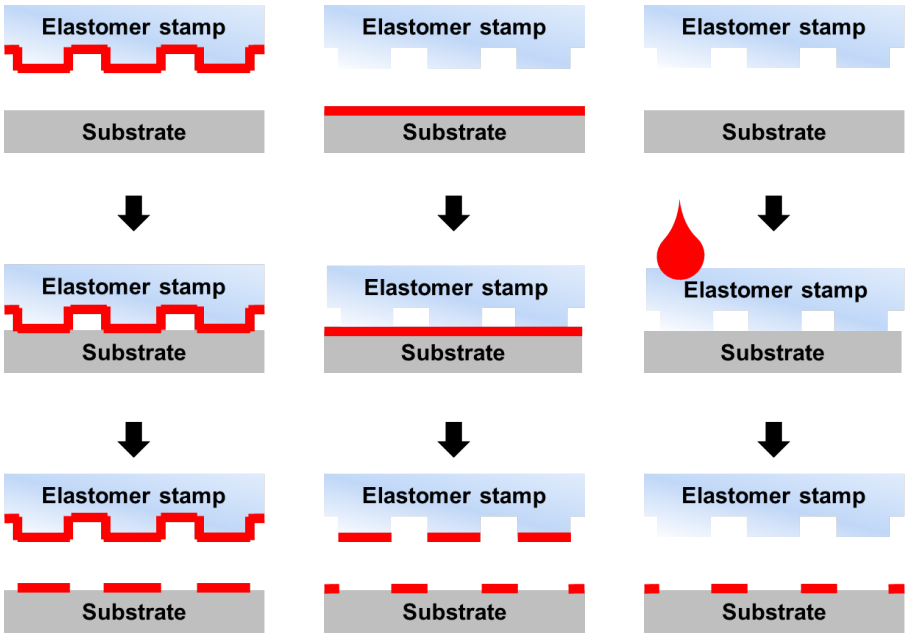

Figure 3.5: Soft lithography techniques. An elastomer stamp is brought into contact with a surface to create polymeric patterns in different manners. a) the stamp is wetted with a polymer ink and transferred by contact pressing to the surface, b) the stamp is brought into contact with a surface coated with polymer, then, contacting areas are removed together with the stamp and c) the stamp is brought into contact with the surface, the polymer ink is sent into the channels left in the interface stamp-surface and later on, the polymer is cured obtaining the polymeric pattern after stamp removal.

However, these microfabrication techniques, applied to conducting polymers, suffer from the poor interaction between polymer and surface, which results in bad adhesion properties. In addition, they usually require the use of chemical modifications to increase the polymer solubility in the carrier fluid, which in some cases affects the final properties of the polymer.

Alternatively, conducting polymers have been grown on-place by electrochemical oxidative polymerization [25, 26]. Here, the oxidation of a precursor monomer takes place under the application of a high positive potential on a working electrode. This technique provides highly conductive polymers and a good spatial resolution, but it is restricted to electrically conductive surfaces. For insulating surfaces, oxidative chemical polymerization has been used, assisted by the selective deposition of Self-Assembly Monolayers (SAMs) (Figure 3.6) [27]. The use of SAMs has been proven to increase adherence of polymers to substrates, but the

long times required for processing, the poor electrical performance of the polymers obtained and the harsh reaction conditions involved (low pHs), limit its application in biomedical devices [28, 29].

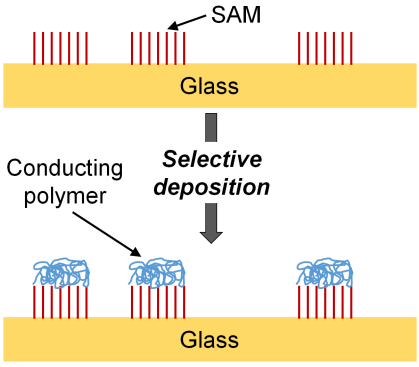

Figure 3.6: Chemical oxidative polymerization. Polymer patterns are obtained by chemical polymerization on SAMs-modified surfaces. (After [27])

To overcome this problem, the recently explored enzyme catalysis polymerization (or biocatalytical polymerization) has been presented as an environment friendly option for conducting polymer synthesis. Enzyme catalysis offers the advantage of working in aqueous media, under mild reaction conditions, with high selectivity, low by-product formation and without compromising the electric performance of the polymer. The first approaches to the environment friendly polymerization methods were done by the use of hydrogen peroxide. However, this polymerization route shows low yields and causes structural defects in the final polymer [30].

These problems have been solved by the use of enzymes, which act as natural catalysts to accelerate and improve the polymerization reaction. Due to their high performance for catalyzing oxidation-reduction reactions, oxidoreductases are the most relevant class of biocatalysts for the synthesis of conducting polymers. Laccase and peroxidases such as horseradish peroxidase (HRP), the soybean peroxidase (SBP) or the palm tree peroxidase (PTP) are the most commonly used enzymes for conductive polymerization [31, 32, 33]. They can efficiently oxidize several monomers by using either oxygen or hydrogen peroxide, but their activity towards pyrrole is insufficient. In some cases, an unfavorable steric interaction with the active site of the enzyme and/or an unfavorable redox potential of the monomer, make unfeasible the direct reaction with the enzyme [34]. It has been demonstrated that redox mediators are useful in expanding the catalytic power of oxidoreductases, making possible the oxidation of compounds that could not

be oxidized by the enzyme alone [35]. Figure 3.7 shows how the active form of the enzyme oxidizes the redox mediator, transferring its cation radical to the monomer and triggering the reaction.

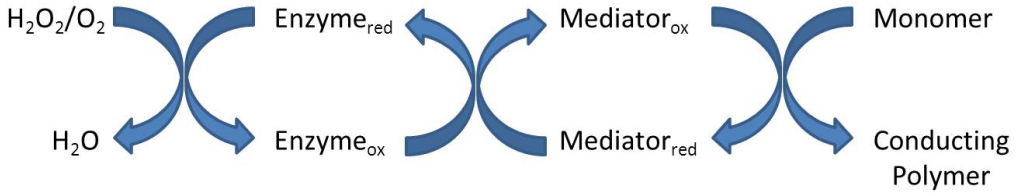

Figure 3.7: Enzymatic polymerization reaction assisted by redox mediators. The enzyme is activated by H_2O_2 or O_2, oxidizing the redox mediator, which catalyzes the monomer oxidation and initiates polymerization.

Moreover, it has been observed that redox mediators increase reaction rate, favoring film formation against oligomeric precipitates and render to polymers with a more linear and defect-free structure [36]. Also, they remain trapped in the final conducting polymer, acting as dopants and introducing some structural features that can favor charge transport between polymer chains. For instance, redox mediators such as ABTS, have shown to increase charge mobility of polypyrrole in two orders of magnitude when compared to polypyrrole obtained in the absence of it, with conductivity values up to 0.2 S/cm [36].

Specifically, horseradish peroxidase with hydrogen peroxide as a substrate, has been shown to catalyze the synthesis of a highly conductive form of polyaniline [37, 38]. However, the direct reaction with polypyrrole is hampered by its high oxidation potential (E_p(HRP) = 0.7 V and E_p(pyrrole) = 0.8 V to 1.0 V (vs. Ag/AgCl)) [33, 39]. Therefore, by using ABTS (E_p(ABTS) = 0.5 to 1.0 V (vs. Ag/AgCl)) [33], the biocatalytical synthesis of polypyrrole powders by HRP could be performed [40, 41]. In this process, the activated form of HRP can oxidize two ABTS molecules, going back to its reduced (or inactive) state after it. Then, the two ABTS radicals generated, are capable of oxidizing two pyrrole monomers, initiating the reaction. Although this process has been shown to deposit films of biocatalytical polypyrrole on the reaction container during synthesis [41], no selective surface deposition has been addressed to date.

Here, the biocatalytical (enzyme catalysis) polymerization technique was used for the production of polypyrrole thin films and arrays of polypyrrole microelectrodes on insulating surfaces. The enzyme HRP was used, with hydrogen peroxide as a substrate, in the presence of ABTS as redox mediator (Figure 3.8).

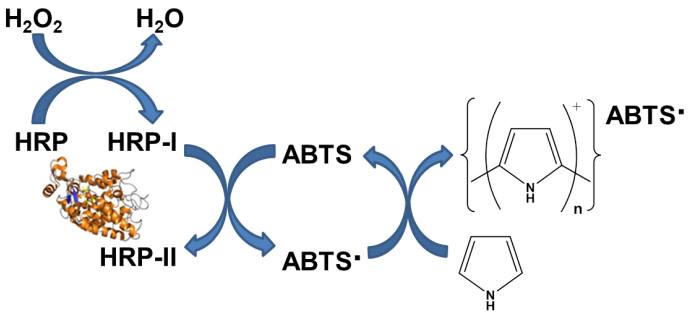

Figure 3.8: Half reaction of enzymatic polymerization of polypyrrole by means of HRP and the ABTS redox mediator. The activated HRP can oxidize the ABTS molecule, which can form a pyrrole cation radical, initiating polymerization of polypyrrole.

Biocatalytical polypyrrole thin films were strongly adhered onto SiO_2 surfaces by means of an adhesive pyrrole-terminated silane self-assembly monolayer. Then, the chemical composition of biocatalytical polypyrrole thin films was characterized by time-of-flight secondary ion mass spectroscopy (ToF-SIMS) and X-ray photoelectron spectroscopy (XPS). Electrical and microstructural properties of the biocatalytically fabricated polypyrrole layers were studied depending on the synthesis parameters: the use of silane and the growth temperature. For that, I-V characteristics, transmission electron microscopy (TEM) and X-ray diffraction (XRD) were used. Afterwards, the biocatalytical polypyrrole microelectrode fabrication was accomplished by tuning the surface adhesion of the substrates through a micropattern of a non-adhesive hydrophobic fluorosilane and an adhesive pyrrole-terminated silane (Figure 3.9).

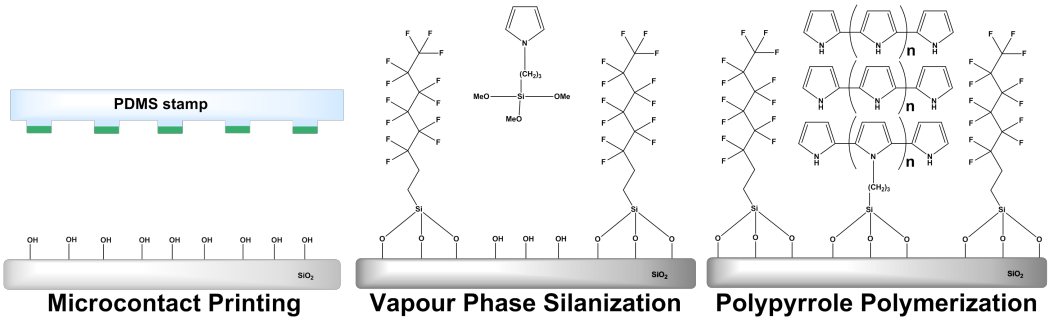

Figure 3.9: Polypyrrole microelectrode fabrication process. a) Microcontact printing of non-adhesive silane pattern, b) backfilling with an adhesive silane and c) biocatalytical polymerization .

Microelectrodes fabricated with an up to 5 µm resolution were characterized by atomic force microscopy (AFM), scanning electron microscopy (SEM) and ToF-SIMS.

Additionally, the benefits of the mild reaction conditions offered by the enzymatic polymerization method were demonstrated by the entrapment of biotin during the polymer synthesis in a single step functionalization process. Polypyrrole electrodes were then used for the controlled release of biotin through cyclic voltammetry. The electroactive character of the biocatalytical polypyrrole layers, after the functionalization process, was mantained. Moreover, it offered the possibility of controllable biomolecule delivery through electrical stimulation as envisioned in Figure 3.10.

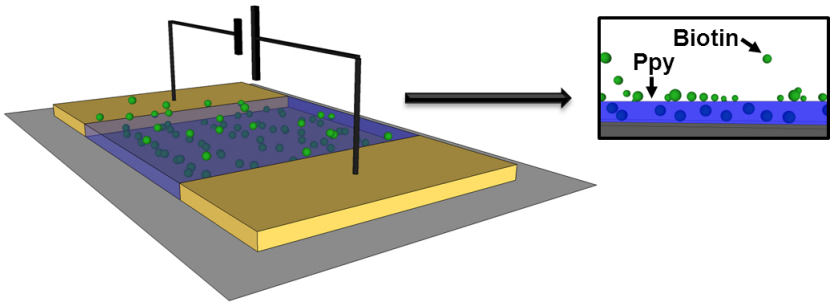

Figure 3.10: Biotin release. Representation of biotin release from biocatalytical polypyrrole electrodes, performed under electrical stimulation.

These results are very promiding and pave the way to the development of bioactive arrays of microelectrodes based on conducting polymers, which could be integrated in implantable devices for remotely controlled tissue interactions.

3.2 FABRICATION OF BIOCATALYTICALLY PRODUCED POLYPYRROLE THIN FILMS

A well-known problem regarding the fabrication of conducting polymer devices is the poor adhesion of polymers to substrates, which normally ends up in polymer film detachment, making their implementation unreliable and sometimes unfeasible [42]. This might be the reason why although polypyrrole has been successfully fabricated by biocatalytical methods in the past [41], there is no

study to date which reports the selective deposition of biocatalytically produced polypyrrole on surface.

To overcome this problem, SAMs have been proposed to be used at the interface between the substrate and chemically synthesized conducting polymers [28]. They have been shown to enhance the surface adhesion strength, by increasing the affinity between the surface and the polymer. However, the use of SAMs has been never applied to the fabrication of biocatalytical polymeric devices.

Here, the use of a pyrrole-terminated SAMs (pyrrole-silane) is presented for the production of stable biocatalytical polypyrrole layers on insulating silicon oxide surfaces. The process was accomplished by introducing a covalent bond between the surface and the biocatalytical polymer, via the pyrrole-silane adhesive layer.

3.2.1 *Silanization of SiO_2 surfaces with pyrrole-silane*

The first step in the fabrication of biocatalytically-produced polypyrrole layers consists in the formation of pyrrole-silane SAMs on SiO_2 surfaces, as depicted in Figure 3.11.

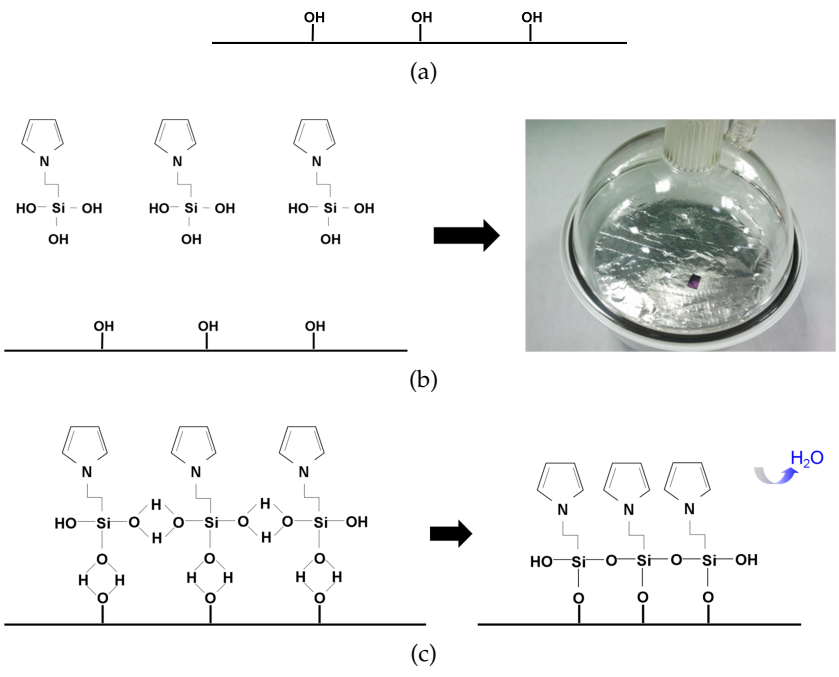

Figure 3.11: Vapour phase silanization of SiO_2 surfaces with pyrrole-silane. a) hydroxylation of SiO_2 surface, b) vapour phase silane deposition method and c) annealing.

Fresh SiO_2 surfaces were treated with "piranha" solution (7:3 (v/v) of concentrated H_2SO_4 and 30% H_2O_2) for 30 minutes. This treatment is crucial for obtaining high density of terminal hydroxyl groups on the surface, which is necessary to couple the silane compound. Then, the so called vapour phase method was used to deposit the silane on the surface [43]. This silanization technique is based on the formation of a silane atmosphere while applying low pressure conditions, and results in the uniform coating of silicon-based substrates. Thus, a drop of pyrrole-silane and the activated SiO_2 surfaces were placed inside a dissecator on which vacuum was applied. The process was conducted for 1h and it was followed by an annealing step of 1h at 80 °C. Annealing was required to promote covalent Si-O-Si bonds between the surface and the silane. Afterwards, characterization of the silanized surfaces was done by SEM, AFM and XPS.

Figure 3.12a shows two SEM images, comparing an untreated SiO_2 surface and a pyrrole-silanized surface. Both surfaces showed the same morphology, indicating that almost no polymerization of the silane occurred on the sample and that a homogeneous deposition of the pyrrole-silane was achieved.

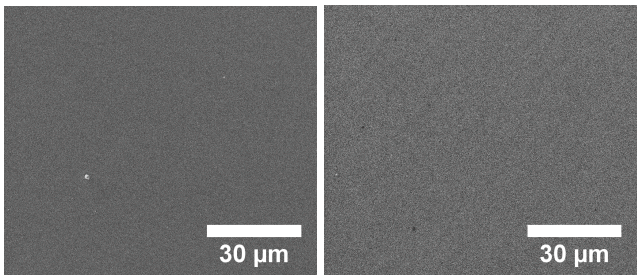

(a)

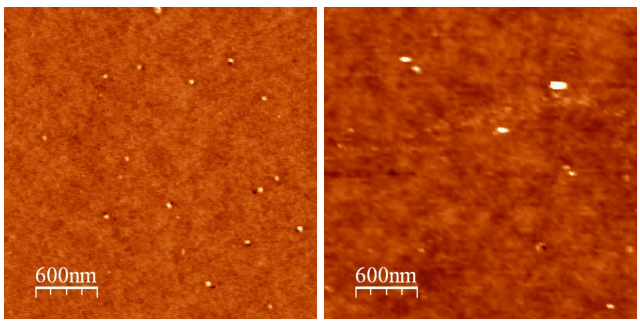

(b)

Figure 3.12: Morphology of SiO_2 and pyrrole-silanized SiO_2 surfaces. From left to right bare SiO_2 surface and pyrrole-silanized surface. a) SEM images and b) AFM graphs.

This was confirmed by topographic AFM (Figure 3.12b) measurements, which showed a minimum increase of the surface roughness values (arithmetic average of absolute values of roughness, Ra) from 0.17 nm for bare SiO_2, to 0.19 nm for silanized SiO_2. This is a key point when good polymer quality has to be achieved. It has been shown that formation of multilayers of SAMs, although leads to polymers with better adhesion, possesses worse and inhomogeneous physical properties [44].

To corroborate the successful deposition of the pyrrole-silane on the SiO_2 surface, XPS measurements were performed. The XPS wide range spectrum of the silanized sample (Figure 3.13) showed a nitrogen 1s peak at a binding energy of 400.1 eV. This peak was attributed to the presence of the pyrrole-silane, which is the only source of nitrogen, thus confirming the existence of the silane layer.

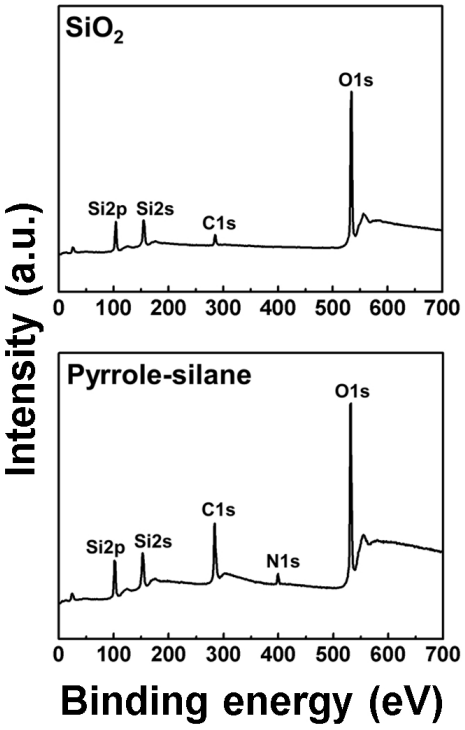

Element	At. %
O 1s	60,7
Si 2p	29,0
C 1s	10,3

Element	At. %
O 1s	41,3
Si 2p	21,4
C 1s	33,9
N 1s	3,4

Figure 3.13: XPS wide scan spectra of SiO_2 and pyrrole silanized surfaces. Upper image: SiO_2 spectrum accompanied by the atomic percentages present in the sample, and lower image: pyrrole-silanized XPS spectrum accompanied by the atomic percentages present in the sample.

Additional analysis of these XPS spectra provided extra information about the composition of the surfaces. Thus, for the bare SiO_2, the atomic percentages found for oxygen (60.7%) and silicon (29.0%) were consistent with the stoichiom-

etry of the bare substrate (SiO_2, 2O : 1Si). While a 10.3% of carbon was found, which was identified with contamination present on the substrate.

Regarding the silanized surface, the relations between nitrogen, carbon, oxygen and silicon mantained the following ratios according to the silane chemical structure: 1N:1Si, 1N:7C, 1N:3O (Figure 3.11). Therefore, since all the nitrogen found in the analysis (3.4%) is expected to come from the silane, the same percentage of the total silicon amount (3.4%) belonged to the monolayer, seven times more of the total carbon (23.8%) and three times more of total oxygen (10.2%) pertained to the monolayer composition. Moreover, the 23.8% of carbon corresponding to the silane added to the 10.3% of carbon previously identified with contamination, results in a 34.1% of theoretically calculated carbon, which is in good agreement with the experimental value obtained of 33.9% (see table of Figure 3.13). In relation to the silicon signal, two parts could be distinguished, namely the silane component and the silicon oxide component. As explained above, the silane compound is present in a 3.4%, which leads to a 18% of silicon corresponding to the oxide, after subtracting the silane part from the total silicon signal obtained (21.4%, see table of Figure 3.13). Finally, by using these results to calculate the distribution of oxygen present in the sample, one obtains: a 36% of oxygen coming from the SiO_2 (SiO_2 keeps a 2O : 1Si ratio. Si% = 18%, O% = 36%) and a 10.2% from the silane (silane keeps a 1N : 3O ratio. N% = 3.4%, O% = 10.2%), which finally gave a total theoretical value of 46.2%, which is close to the experimental result obtained for this sample of 41.3% (see table of Figure 3.13).

These analyses confirmed the appropriate deposition of the pyrrole-silane SAM on SiO_2 substrates, allowing for the next processing step: the biocatalytical polymerization of polypyrrole on silanized SiO_2 surfaces.

3.2.2 *Biocatalytical polymerization of polypyrrole on silanized SiO_2 surfaces*

Biocatalytical polymerization* was performed by immersing the substrates in a reactor with a mixture solution of pyrrole, ABTS and EDTA at pH 4.0. The mixture was degassed through an argon flow, to remove the oxygen present in the solution and was kept at room temperature (R.T.) under magnetic stirring and argon purge. Then, a previously prepared solution of

**Polymerization details:*
In 15 mL buffer 4.0 pH (50 mM potassium biphtalate): 3.35 mmol pyrrole, 0.123 mmol ABTS and 0.042 mmol EDTA.
Addition of 7.32 mg HRP in 1.68 mL pH 7.0 PBS buffer.
Slow addition of 3.35 mmol H_2O_2.

HRP, with a HRP amount large enough to oxidize all the ABTS present in the reaction, was added to the reactor. Finally, the reaction was initiated by adding hydrogen peroxide to the mixture and left to proceed for two hours. Immediately after incorporating the oxidizer (H_2O_2), a black precipitate appeared, indicating the presence of polypyrrole (Figure 3.14). After polymerization, all the surfaces were rinsed with ultrapure water and dried with nitrogen.

Figure 3.14: Polymerization reactor.

The presence of polypyrrole layers on SiO_2 surfaces was confirmed using AFM, SEM and ToF-SIMS analysis (Figure 3.15).

AFM studies of polymerized and non-polymerized surfaces (Figure 3.15a) revealed higher values of roughness (Ra) for polymerized surfaces (from 0.19 nm for silanized surfaces to 7.4 nm for polymerized surfaces), which indicated that the polymerization process produced a layer on silanized SiO_2 substrates, whose nature had to be determined.

Figure 3.15b shows the ToF-SIMS spectra obtained for three different samples, namely, a SiO_2 surface, a pyrrole-silanized substrate and a polymerized SiO_2. The arrows in the figure indicate the typical mass fragments of polypyrrole, corresponding to CN^- (26 mass/z), CNO^- (42 mass/z) and C_3N^- (50 mass/z) ions. While negligible amount of characteristic polypyrrole ions appears in the spectra of SiO_2 surfaces and pyrrole-silanized samples, the successful growth of polypyrrole layers on silanized SiO_2 surfaces was evident by the sharp increase in the polypyrrole characteristic signals corresponding to polymerized samples.

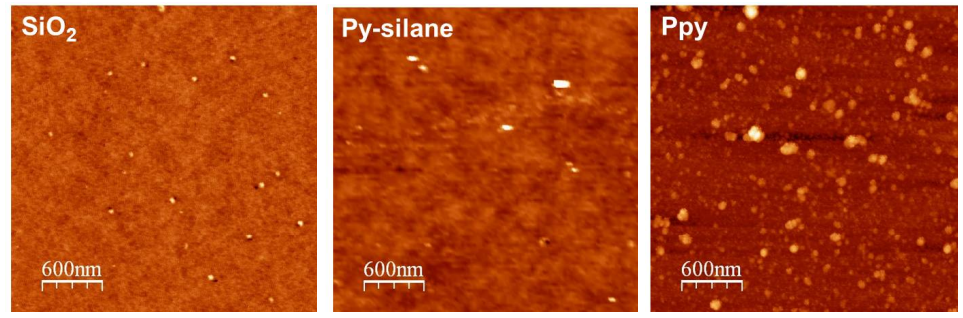

(a)

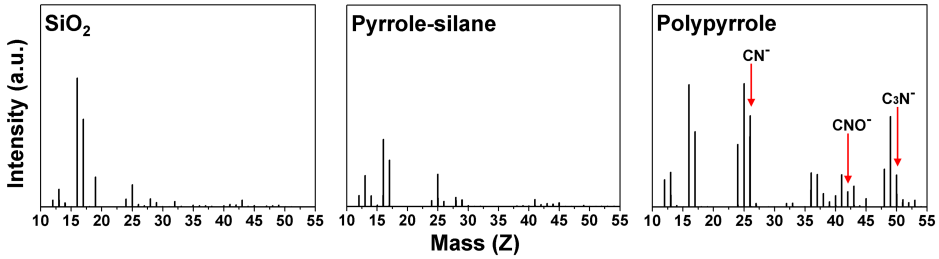

(b)

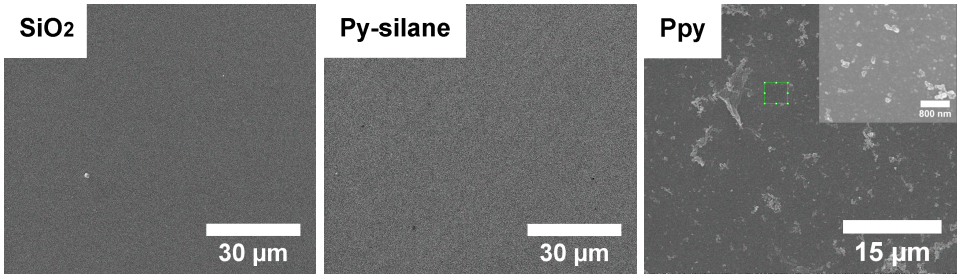

(c)

Figure 3.15: Characterization of biocatalytical polypyrrole layers. From left to right: bare SiO_2, pyrrole-silanized SiO_2 and polypyrrole surfaces. a) AFM graphs, b) ToF-SIMS spectra and c) SEM images of the different surfaces.

SEM images of polypyrrole films were obtained as well (Figure 3.15c), showing that full coverage of the surface was achieved and that small aggregates appeared on the surface. According to the mechanism proposed for conducting polymer deposition in precipitation polymerization [45, 46], these aggregates are most likely to be polypyrrole particles formed in solution that became trapped in the film during its growth.

After this, a detailed characterization of the polypyrrole layers was conducted.

3.3 CHARACTERIZATION OF BIOCATALYCALLY PRODUCED POLYPYRROLE THIN FILMS

In this section, the chemical, electrical, microstructural and electrochemical properties of the biocatalytically fabricated polypyrrole films were determined using spectroscopic methods (IR spectroscopy and XPS), electrical measurements (IV characteristics), diffraction techniques (XRD and TEM) and electrochemical methods (CV).

3.3.1 *Chemical characterization of biocatalytically produced polypyrrole thin films*

To exactly determine the nature of the fabricated biocatalytical polypyrrole compound, chemical characterization was conducted on powders grown from solution, by IR spectroscopy and on polymerized surfaces by XPS.

Infrared absorbance graph of Figure 3.16 shows that the prints of the examined powder fits the ones for polypyrrole [47, 48, 49].

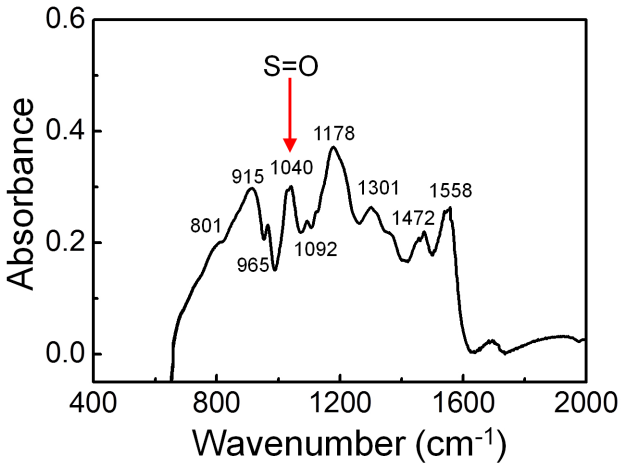

Figure 3.16: Absorbance infrared spectrum of polypyrrole. Sulphur from dopant appeared at 1040 cm^{-1}.

Thus, starting from high to low wavenumbers, the C-C and C-N stretching vibrations of the pyrrole rings were associated to bands appearing at 1558 cm^{-1} and at 1472 cm^{-1}. The C-N in plane deformation was identified with a band observed at 1301 cm^{-1} and the breathing vibration of the pyrrole ring was shown at 1178 cm^{-1}. At 1092 cm^{-1}, the band of C-H and N-H in plane deformation vibrations were found. And finally, the out of plane ring deformation vibrations were observed at peak 965 cm^{-1} for C-C and at 915 cm^{-1} and 801 cm^{-1} for C-H.

Additionally, the existence of another band at 1040 cm^{-1}, corresponding to the asymmetrical stretching of the group S=O, indicated the incorporation of ABTS as dopant into the structure, as previously reported [48].

On surface, XPS spectra of polypyrrole were taken to quantitatively analyze the surface chemistry. Figure 3.17 shows a XPS wide spectrum of polypyrrole, where seven main peaks were identified with carbon (C 1s), oxygen (O 1s), silicon (Si 2s and Si 2p), nitrogen (N 1s) and sulphur (S 2s and S 2p). The existence of sulphur in the analysis, indicated again the presence of the ABTS used for the polymerization reaction, which remained in the polymer matrix [36, 41].

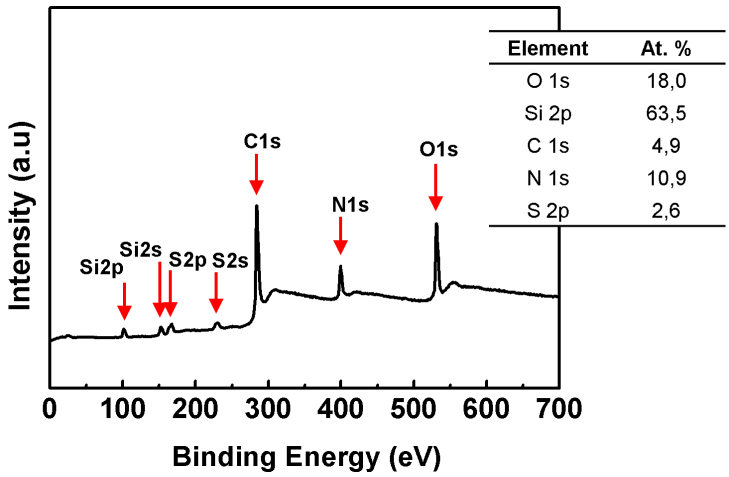

Figure 3.17: Wide scan XPS spectrum of polypyrrole. On it we can identify the peaks corresponding to C 1s, O 1s, Si 2s and Si 2p, N 1s and S 2s and S 2p.

Moreover, deconvolution of the high resolution spectra of the aforementioned collection of peaks (Figure 3.18) was performed. The position and the relative intensities of the deconvoluted signals provided specific information about the chemical structure and composition of the polymer. Deconvolution of the C 1s peak resulted in three components. The first at 284.70 eV corresponded to C-C, the second at 286.40 eV accounted for C-O and C-N and the third at 288.20 eV was due to C=O (Figure 3.18a) [50]. In a similar way, Figure 3.18b showed deconvolution of the N 1s signal, divided in nitrogen in imine state (-N= at 398.5 eV), due to oxidized polypyrrole, secondary amine nitrogen coming from the polypyrrole backbone (NH at 400.1 eV) and a 28% of positively charged atomic nitrogen (N+ at 401.6 eV and 403.1 eV). It was in well agreement with the theoretical percentage of positively charged nitrogen existing in fully doped polypyrrole, corresponding to a 25% of the total nitrogen signal (one in every four atoms) [42]. The same analyses were conducted on the Si 2p (Figure 3.18c) and O 1s (Figure 3.18d)

signals. For the silicon peak, energies of 100.78 eV and 103.26 eV were identified with signals coming from silanes and from silicon oxide respectively [51, 52]. The analysis of the oxygen peak showed a signal at 533.07 eV, which corresponded to oxides (SiO_2 in this case), and a signal at 530.90 eV, belonging to carbonates ($CO_3{}^{-2}$) [51, 52].

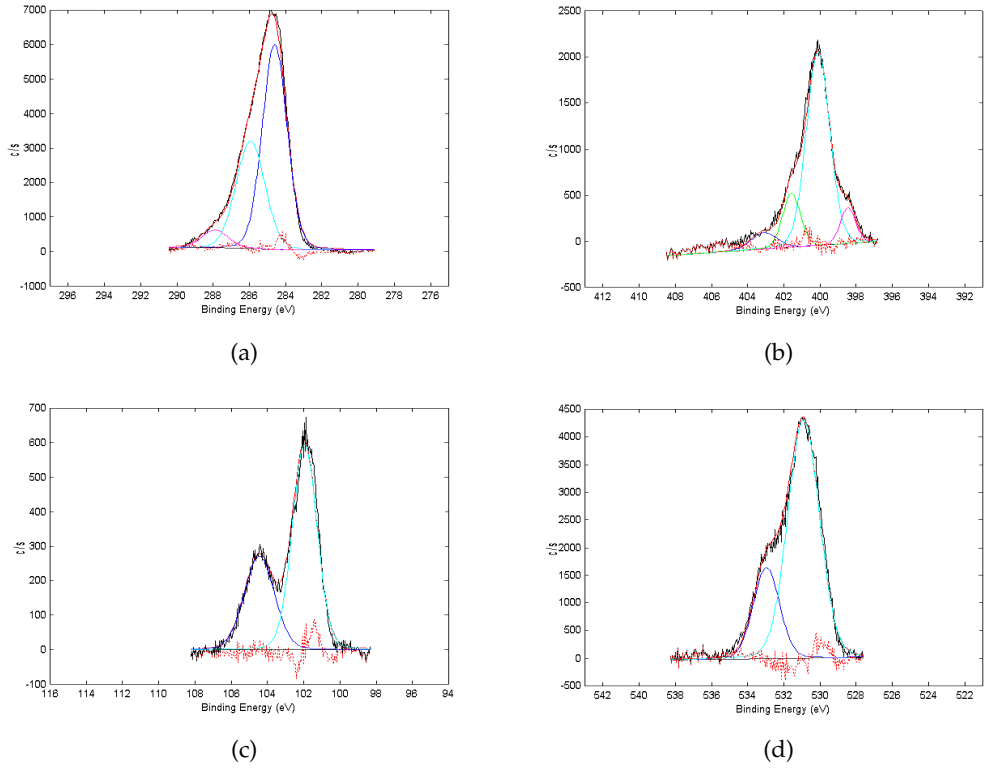

Figure 3.18: High resolution XPS spectra of polypyrrole. a) C 1s peak deconvoluted in three components, b) N 1s peak deconvoluted in four components, Si 2p peak deconvoluted in two components and d) O 1s peak deconvoluted in two components.

These results show that the polypyrrole thin films fabricated by biocatalytical method in this work were fully doped by the ABTS redox mediator as could be seen using IR spectroscopy and XPS analyses.

3.3.2 *Kinetics of growth of biocatalytically produced polypyrrole thin films*

To understand the mechanism of growth of biocatalytical polypyrrole films, experiments at different growth times, between 5 minutes and 2 hours, were conducted. Three series of experiments were done at 5, 10, 15, 20, 25, 30, 60, 90 and

120 minutes and characterized by AFM measurements. Thickness and roughness of the resulting films were determined.

AFM profiles taken from scan areas of 3 µm x 3 µm, at different times during the film growth revealed an increase of the thickness within the first hour as shown in Figure 3.19 (red triangles). Polymer thickness reached a maximum value of 80 nm (in average) at 60 minutes, decreasing later to an approximated value of 30 nm. The dispersion in the thickness values obtained, suggested that small aggregates got trapped in the film during growth, affecting the thickness of the film in height and distribution along the sample, which is consistent with the mechanism of deposition in precipitation polymerization [46].

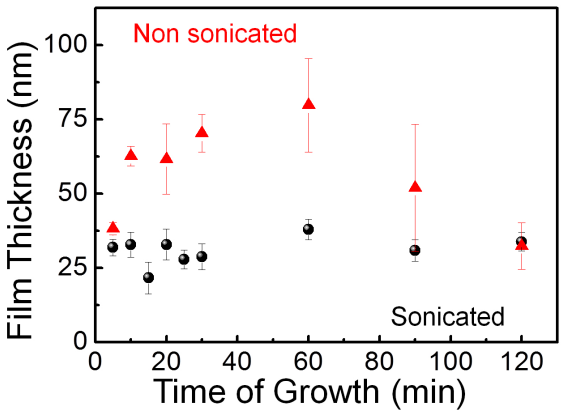

Figure 3.19: Polypyrrole thickness versus time of growth. Red triangles correspond to not sonicated samples and black dots belong to sonicated experiments.

These results suggested that from a certain thickness, the non-well attached polypyrrole material peels off, probably due to the competition between surface stress tensions and the $\pi - \pi$ bond mediated by the adhesive silane layer. To support this hypothesis, the same experiments were repeated with the addition of a sonication step of 15 minutes, before the AFM characterization. In this way, any deposited but not well attached polypyrrole product was removed from the surface, as revealed by the smoother thickness evolution observed on this set of experiments (black dots in Figure 3.19). After the sonication step, the thickness remained almost constant during all the time, ranging from 25 nm to 40 nm, with an averaged thickness of 31 nm $\pm$ 5 nm. The roughness (Ra) of these films (at 120 nm of growth) showed an averaged value of 4.7 nm $\pm$ 0.7 nm

Additionally, to confirm the need of the silane adhesive layer, polypyrrole layers were grown on bare SiO_2 surfaces (without the use of the py-silane). The morphology of the polypyrrole films obtained in this way was studied after two

hours of growth and 15 minutes of sonication using AFM. Thus, approximated values of thickness and roughness were determined, being 27 nm and 6 nm respectively. These values are quite similar to the results obtained for layers grown on the pyrrole-silane. However, the surfaces appeared with many open areas, on which the polymer seemed to detach after the sonication step (Figure 3.20). These observations suggested that the pyrrole-silane is necessary for obtaining more homogeneous polypyrrole layers.

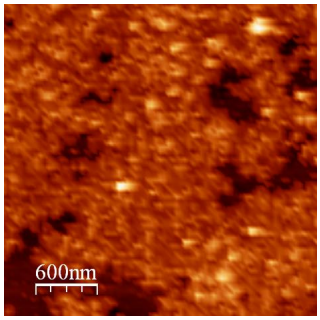

Figure 3.20: AFM graph of a polypyrrole layer grown on bare SiO_2 surface (without a pyrrole-silane adhesion layer). After 15 min of sonication, polymer detaches from certain areas..

Therefore, from the kinetics studies performed in this work it can be said that stable and homogeneous polypyrrole layers could be obtained after the first minutes of biocatalytical growth. The stability of the polymer layer was provided by the existence of the pyrrole-silane adhesion layer, as expected. The polymer cohesion was maintained up to 30 nm thickness, for polypyrrole layers grown on pyrrole-silanized surfaces, after an ultrasonic cleaning step, required to remove any loosely attached polypyrrole on the surface. Probably above this thickness, the surface tension is superior to the inter-chain forces, causing the detachment of the polymer beyond this limit.

3.3.3 *Effect of the py-silane and the temperature of growth on the polypyrrole thin films*

The electrical and microstructural properties of the biocatalytically produced polypyrrole layers were tested under two fabrication parameters, namely the use of the pyrrole-silane and the variation of the growth temperature. Electrical and diffraction experiments (XRD and TEM) were performed on samples grown with and without the use of the pyrrole-silane adhesion layer, at both room and low temperatures (0 °C).

I-V characteristics from biocatalytical polypyrrole layers were obtained by two-contact measurements.* Conductivity was estimated by applying equation 3.1, where σ is the conductivity, R the measured resistance, A the area of the film section between electrodes multiplied by the layer thickness, and l the separation between contacts. Results were obtained from at least three independent samples, with at least three measurements taken from each sample.

Two-contact measurements:
Biocatalytic polypyrrole was grown on SiO_2 surfaces containing squared metallic electrodes. Afterwards, the polymer between electrodes was isolated, by scratching the polymer around the electrodes, as sketched below. I-V characteristics were recorded.

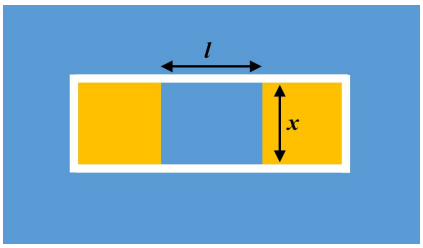

$$\sigma = \frac{l}{A \times R} \tag{3.1}$$

In addition, XRD measurements and TEM experiments were conducted.

Apart from the described lack of homogeneity of samples grown without the silane adhesion layer, polypyrrole grown on bare SiO_2 showed a slightly poorer electrical performance (Figure 3.21a). While polypyrrole layers grown on silanized SiO_2 surfaces showed conductivities of 2.9 S/cm $\pm$ 0.3 S/cm, the SiO_2 surfaces that were not silanized before the polymerization, produced a conductivity value of 1.7 S/cm $\pm$ 0.3 S/cm. It has been shown that the presence of silane self-assembled monolayers, such as the ones employed here, can induce the ordered deposition of the conducting polymers grown above them, enhancing charge mobility and leading to higher conductivity values [53]. Therefore, the increase of conductivity observed for polypyrrole layers grown on silanized surfaces, was attributed to the presence of the pyrrole-silane monolayer. The silane layer is more likely to induce a better organization of the polymer, as it was confirmed by XRD measurements (Figure 3.21b). The XRD spectrum belonging to polypyrrole layers grown on silanized surfaces, showed a broad peak at 20.32°, near the reported values for polypyrrole [49, 54, 55]. On the contrary, no peak was observed for samples without the use of the silane compound, indicating the existence of an amorphous layer.

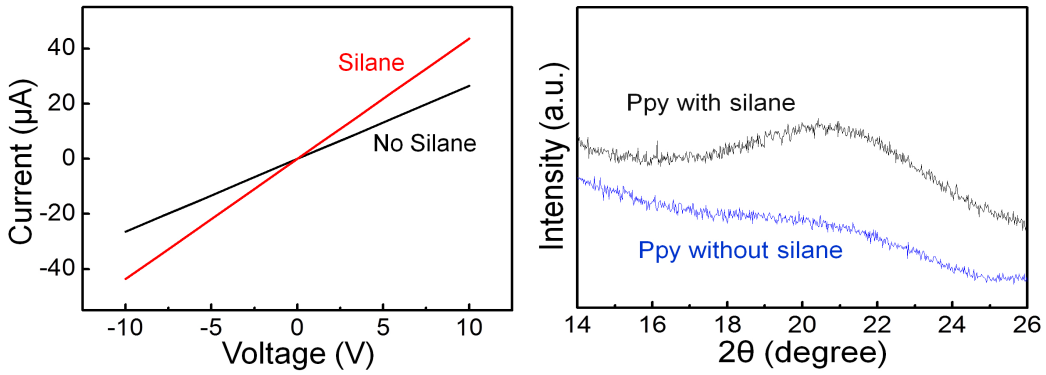

(a) (b)

Figure 3.21: Comparison between polypyrrole layers on bare SiO_2 and on pyrrole-silane surface. a) I-V characteristics of both polypyrrole layers, showing an increased conductivity for layers grown on pyrrole-silane (red line). b) XRD spectra of polypyrrole. Black line corresponds to a polypyrrole layer grown on a silanized silicon oxide surface and blue line corresponds to a polypyrrole layer grown on a bare SiO_2 substrate.

Theoretically, the pyrrole-silane forces the growth to occur in the same direction for most of the chains, introducing a certain degree of order in the polymer. It does not depend on the SiO_2 surface, but on the silane organization [56], as depicted in Figure 3.22.

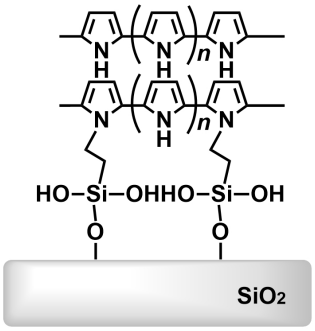

Figure 3.22: Schematics of polypyrrole. Arrangement of the polymer chains depending on silane orientation.

However, defects in the silane deposition can lead to the formation of heterogeneous silane multilayers, which prevent the generation of ordered polymeric structures and affects dramatically the conductivity values [44]. This suggests that achieving ordered silane monolayers is a key factor in developing highly ordered and conducting polymer films.

In this work, silane deposition was performed by vapor phase method, an easy and cheap technique that limits the concentration of alkoxysilanes on the surface, favoring homogeneous silane formation [43]. However, although this method is easy and does not require clean room environment, it is hardly controllable in comparison with more sophisticated deposition techniques, such as Chemical Vapour Deposition (CVD). CVD is one of the most efficient technique in producing silane monolayers [57], and leads to a higher degree of order and even lower resistances. However, it requires expensive CVD growth chambers in a clean room environment, not available in this case.

Right after, the effect of the temperature of growth on the formation and arrangement of the polymer layers was investigated by conducting experiments at low temperature. For that, the polymerization reactor was immersed in a cooling bath with crushed ice and water, leading to an approximated reaction temperature of 0°C. Temperature was monitored during the process to keep it stable, adding ice if necessary.

Electrical measurements performed on biocatalytical polypyrrole layers grown at low temperature, resulted in conductivity values of 8.6 S/cm $\pm$ 1.8 S/cm, which is almost three times higher than the value obtained for samples grown at room temperature (Figure 3.23).

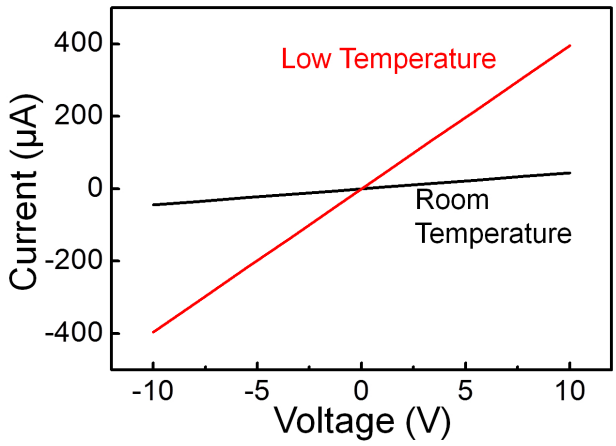

Figure 3.23: I-V characteristics of polypyrrole. Black line corresponds to a polypyrrole layer grown at room temperature (lower conductivity) and red line corresponds to a polypyrrole layer grown at low temperature (higher conductivity).

This increase in conductivity was attributed to a more organized polymer [54], as was evident by electron diffraction experiments. Figure 3.24 shows a TEM

micrograph of a biocatalytical polypyrrole layer and two Selected Area Electron Diffraction (SAED) patterns of polypyrrole at room temperature and 0°C, respectively. Clear diffraction patterns, similar to patterns previously observed for crystalline polypyrrole [58, 59, 60, 61] were obtained for samples grown at low temperature (Figure 3.24b), which therefore suggested the presence of a crystalline structure. On the other hand, samples grown at room temperatures did not produce any diffraction pattern (Figure 3.24c), indicating the existence of an amorphous material.

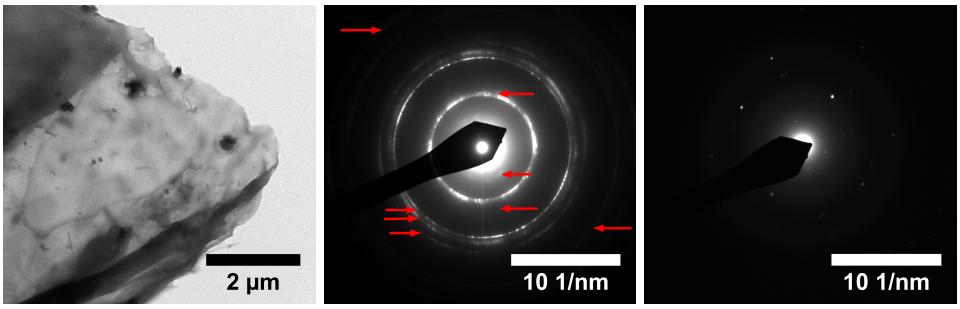

(a) (b) (c)

Figure 3.24: a) Transmission electron micrograph of biocatalytically grown polypyrrole thin layer. b) SAED pattern of biocatalytically grown polypyrrole thin layer at low temperature. c) SAED pattern of biocatalytically grown polypyrrole thin layer at room temperature.

These results demonstrate that the relatively cheap and straightforward fabrication method applied, yielded biocatalytical polypyrrole thin films with conductivities one order of magnitude higher than those values reported for biocatalytical polypyrrole films (below 0.6 S/cm) [36], and three orders of magnitude higher than HRP-mediated polypyrrole powders (1.6×10^{-3} S/cm) [41]. These values could be slightly varied by manipulating fabrication parameters, such as the presence/absence of a SAMs at the interface substrate-polymer and the temperature of growth, which influenced the organization of the polymer film.

3.3.4 *Redox performance of biocatalytically produced polypyrrole thin films*

The electroactivity of biocatalytically produced polypyrrole layers was under study in this section.

Generally, the synthesis of a conducting polymer involves the oxidative polymerization of its monomer unit by an oxidant. In this process the oxidation poten-

tial of pyrrole is higher than that corresponding to polypyrrole, which generates a polymer in the oxidized state. Therefore, to maintain charge neutrality, negative ions are incorporated to the structure of the polymer, balancing its positively charged backbone [62]. Thus, when polypyrrole is subjected to reduction, the charge balance is broken and the anions can leave the polymer matrix, a process in which the polymer reaches its neutral state. This capture and release of ions, maintains polymer neutrality and conforms the redox behaviour of a polymer. Here, the electroactivity of the biocatalytically produced polypyrrole layers was investigated using cyclic voltammetry studies, in which the polymer film was used as working electrode (see chapter 2 for more details). Cyclic voltammetry is a useful technique to characterize a material and to acquire qualitative information about electrochemical reactions. It offers a rapid location of redox potentials of the electroactive species. Figure 3.25 shows a cyclic voltammogram run on a biocatalytical polypyrrole electrode between -0.9 V and +0.9 V, at 100 mV/s scan speed. A certain tilt was observed in the voltammogram, which could be explained by the existence of a parasitic resistance due to the film thickness and the electrical connections with the external electrodes.

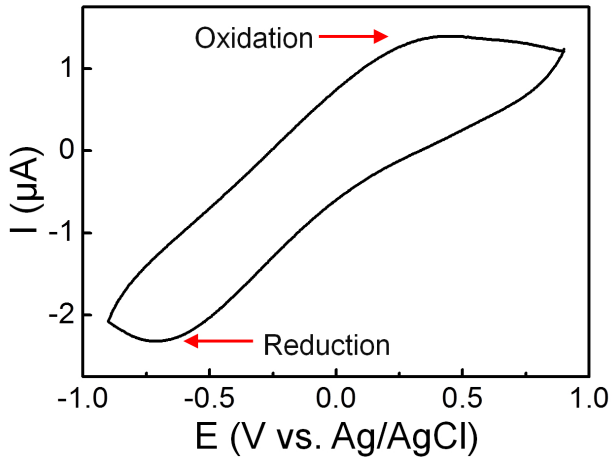

Figure 3.25: Cyclic Voltammogram of biocatalytically fabricated polypyrrole working electrode.

However, despite the resistive effect, wide anodic and cathodic peaks (typical of conducting polymers) [63] could be identified at potentials 0.45 V and -0.75 V respectively, demonstrating the existence of a redox wave, compatible with an electroactive behaviour of the polymeric films.

3.4 FABRICATION OF BIOCATALYTICALLY PRODUCED POLYPYRROLE MICROELECTRODES

In this section, the fabrication process of biocatalytically produced polypyrrole microelectrodes is presented. This fabrication process does not require clean room environment and can be readily accomplished by tuning the surface adhesion properties of silicon oxide substrates by the use of silane compounds. Polypyrrole microelectrode fabrication was firstly attempted by the deposition of pyrrole-silane micropatterns, applying the microcontact printing technique (µCP, for more details about the technique see section 2.2.3.2). PDMS stamps with lines in the micrometer range were fabricated as described in section 2.2.3.1. Figure 3.26a shows a white light interferometer graph of a PDMS stamp, after fabrication (5 µm wide lines with 5 µm pitch). The fabricated PDMS stamps were then inked with the pyrrole-silane by contact inking*, and the pattern was transferred to activated SiO_2 surfaces by contacting for 5 minutes. This was followed by an annealing step at 80 °C for one hour.

Contact Inking:
As opposed to wet inking this technique does not permeate the PDMS bulk. The ink molecules only contact the protruding areas of the stamp that are going to be used for the patterning. This is done by the direct contact of a feature stamp and a flat PDMS substrate that has ink on it [64]. Here, a flat PDMS stamp was wet inked in a 5 mM solution of pyrrole-silane in ethanol, and used to contact the micropatterned stamp.

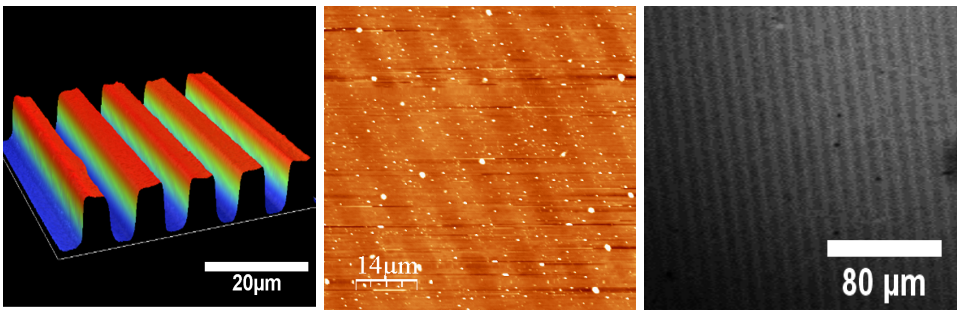

(a) (b) (c)

Figure 3.26: Polypyrrole microelectrodes by µCP deposition of pyrrole-silane. a) WLI image of PDMS stamp (lines 5 µm width with 5 µm pitch) used for µCP, b) AFM friction image of pyrrole-silane micropattern and c) optical microscope image of polymerized micropattern.

Figure 3.26b shows a contact-mode AFM image of a selectively pyrrole-silanized SiO_2 surface. The geometry of the stamp was reasonably conserved through the µCP process, and thus the polymerization process could follow. After biocatalytical polymerization (described in section 3.2.2 of this chapter) was applied on selectively silanized surfaces, polypyrrole patterns were obtained, as shown in the optical microscope image of Figure 3.26c.

However, closer inspection of the samples by AFM, revealed that the polymer growth also extended laterally to the not silanized areas (Figure 3.27a). This weakly bonded lateral growth on not silanized areas could be removed by sonication cycles. Figures 3.27b, 3.27c and 3.27d , show AFM images of a sample after different sonication times, in which weakly attached polymer progressively peeled off, revealing the SiO_2 surface underneath. Unfortunately, after 30 minutes of sonication (Figure 3.27d), the patterns were not completely clean and homogeneous, thus requiring the use of a complementary technique to optimize the microfabrication process.

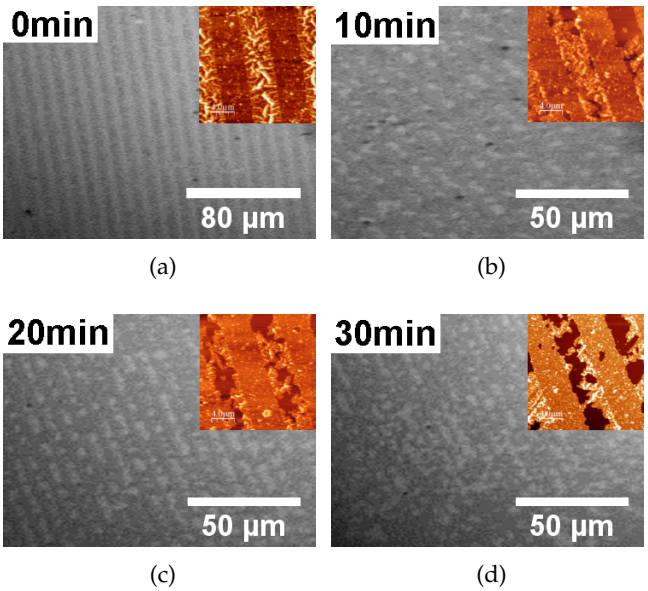

(a) (b) (c) (d)

Figure 3.27: AFM images of polypyrrole microelectrodes. a) After polymerization, surface is completely covered by the polymer. b) After ultrasonic cleaning for 10 minutes, the pattern started to appear. c) After ultrasonic cleaning for 20 minutes. d) After ultrasonic cleaning for 30 minutes.

It was reported that differences in hydrophobicity leads to selectivity in polypyrrole growth [65, 66]. Therefore, to improve the easy removal of undesired polypyrrole products and to increase homogeneity in the polymeric patterns, sev-

eral surface modifications that affected the hydrophobicity of the not silanized regions, were studied.

Hydrophobicity properties of different non-adhesive silane compounds namely, APTES, perfluoropolyether-silane and FDTES, were investigated by water contact angle measurements (for more details about contact angle measurements, see section 2.3.5.1). To do so, silicon oxide surfaces, from dices of the same wafer, were coated by vapour phase method with the different silanes. Table 3.1 shows water contact angle of surfaces coated with pyrrole-silane (53.96°), APTES (55.97°), perfluoropolyether-silane (88.06°) and FDTES (109°). Additionally a piranha pre-treated SiO_2 surface was tested, as comparison with silanized surfaces.

SILANE COMPOUND	CONTACT ANGLE [°]
Pyrrole-silane	53.96
APTES	55.97
Perfluoropoly- ether silane	88.06
FDTES	109.00
Piranha treated SiO_2	< 10

Table 3.1: Water contact angle measurements of the silanes used for the selectively growth of polypyrrole.

Then, to investigate the effect of the different surface treatments on the overall fabrication process, microlelectrode fabrication using the non-adhesive silanes, was conducted as follows: microelectrode dimensions were defined by the patterning of the non-adhesive silane onto the insulating SiO_2 surfaces by microcontact printing (μCP). On the remaining hydrophilic regions, polymer adhesion was promoted by a back-filling with the pyrrole-silane, performed by vapour phase method. Then, substrates were immersed in a polymerization reactor for 60 minutes, followed by an ultrasonic cleaning step in order to remove the excess of polymer which was poorly attached to the surface.

Microfabrication results for the different combinations of silanes are presented in Figure 3.28. The most uniform patterns were obtained when FDTES was employed as non-adhesive layer, for which differences in contact angle with the pyrrole-silane were higher. On the contrary, when the differences in contact an-

gle were almost negligible, as in the case of APTES, a total absence of pattern was observed.

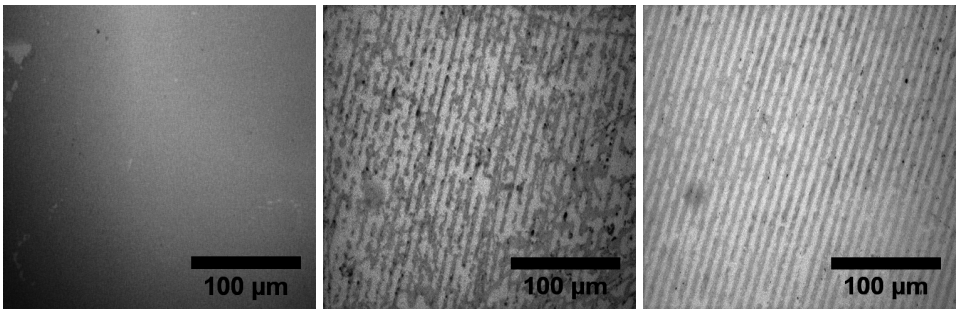

(a) (b) (c)

Figure 3.28: Optical images of polypyrrole patterns generated by different silanes. a) Combination APTES and pyrrole-silane, b) combination perfluoropolyether-silane and pyrrole-silane and c) combination FDTES and pyrrole-silane.

Thus, the fabrication process using FDTES as non-adhesive silane, was characterized at each step by SEM and ToF-SIMS (Figure 3.29), demonstrating the successful site-selective growth of polypyrrole onto the pyrrole-silane regions. Figure 3.29a shows the schematics of the microelectrode fabrication. As previously explained, the first step consisted in the microcontact printing of the FDTES silane on the activated SiO_2 surfaces. It was followed by back-filling the free areas with the pyrrole-silane (by vapour phase method). And the process finished with the biocatalytical polymerization of the selectively silanized surfaces. SEM graphs (Figure 3.29b) showed that the pattern geometry was conserved through the process at each step of it, while ToF-SIMS (Figure 3.29c) confirmed the appropriate chemistry distribution along the sequence. In particular, ToF-SIMS images of the FDTES pattern on bare SiO_2, revealed the presence of oxygen ions (O^-), belonging to the substrate (SiO_2), well distinguished from the Fluor ions (F^-), coming from the hydrophobic silane (FDTES). When the surface was backfilled with the adhesive pyrrole-silane, ToF-SIMS images showed a signal associated to pyrrole (CN^-) on the backfilled areas, which was still resolved from the FDTES signal (F^-). And finally, when the biocatalytical polymerization was applied, ToF-SIMS exhibited alternation of FDTES ions (F^-) and polypyrrole ions (CN^-), which confirmed the correct distribution of the polymer on the pyrrole-silane areas.

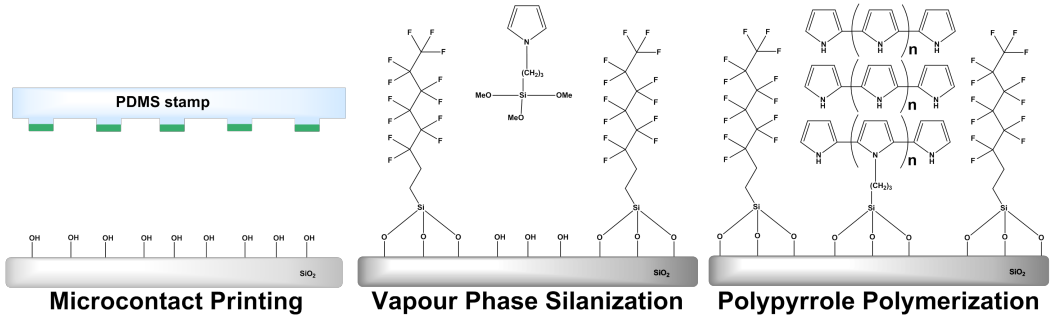

(a)

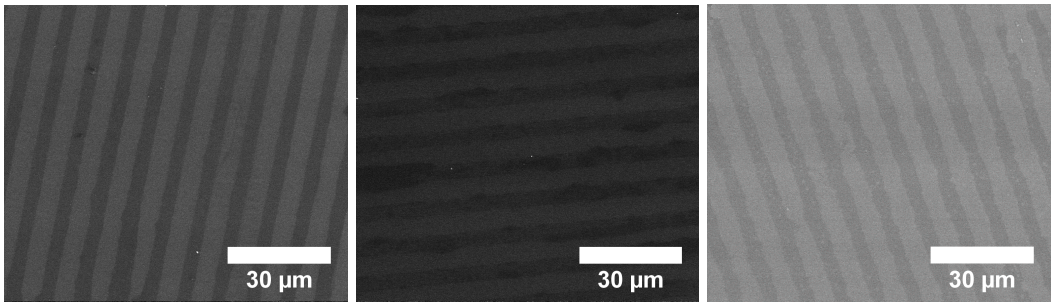

(b)

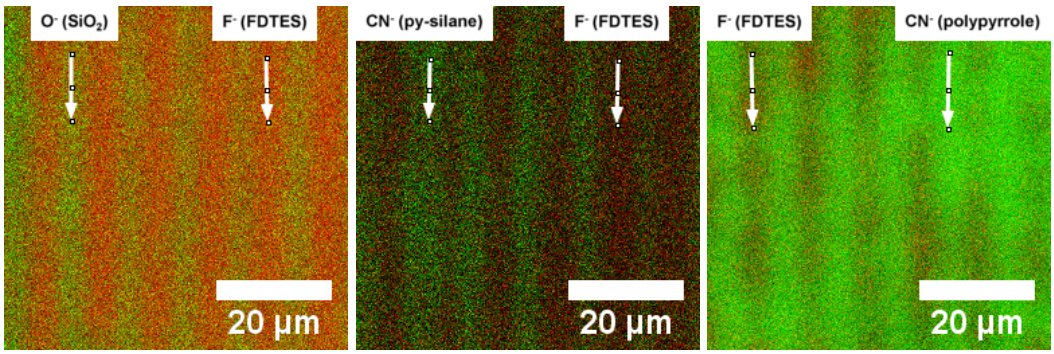

(c)

Figure 3.29: Site-selective deposition of biocatalytically produced polypyrrole on insulating SiO_2 surfaces. a) Schematics of the procedure steps that from left to right are: µCP of FDTES, backfilling of the hydrophilic regions with pyrrole-silane, and biocatalytical polymerization. b) SEM images obtained after each corresponding step given in (a). c) ToF-SIMS images of the indicated ions, obtained after each step given in (a).

Moreover, the versatility of the site-selective biocatalytical polypyrrole growth was validated on different pattern dimensions (Figure 3.30). Lines of 20 µm width with 20 µm pitch, lines of 5 µm width with 5 µm pitch and lines of 5 µm width with 1 µm pitch were grown, surpassing the resolution limits of inkjet printing

(20-50 μm), which is the most widely used method for the construction of organic microelectrodes.

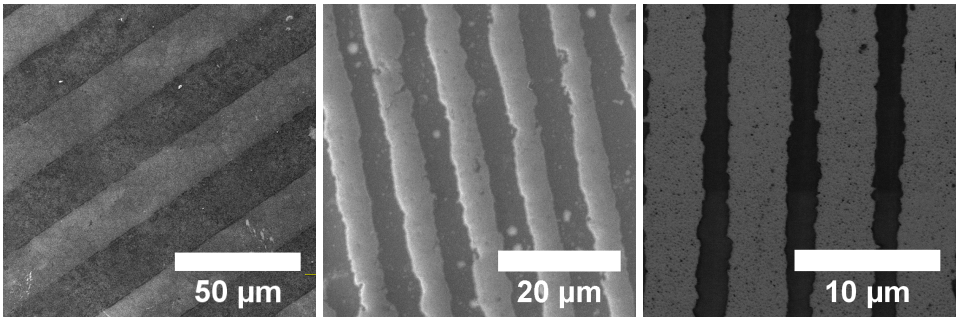

(a) (b) (c)

Figure 3.30: SEM images of a) 20 μm width lines with 20 μm pitch, b) 5 μm width lines with 5 μm pitch and c) 5 μm width lines with 1 μm pitch.

3.5 BIO-FUNCTIONALIZATION OF BIOCATALYTICALLY PRODUCED POLYPYRROLE

Since biocatalytical polymerization offered the possibility of working under mild reaction conditions, such as aqueous media and pH values within the physiological range, the entrapment of biomolecules during the polymer growth in a single step fabrication process was attempted.

The couple streptavidin-biotin was taken here, as biomolecule model. Streptavidin is a protein with high affinity for biotin, which is a small vitamin that couples into streptavidin structure (Figure 3.31).

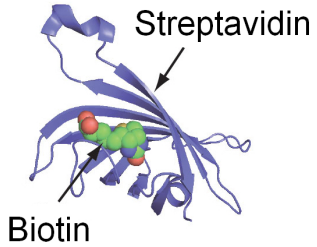

Figure 3.31: Biotin-Streptavidin representation.

Biotin binds to streptavidin in one of the strongest non-covalent interactions existing in nature, with an extremely high affinity, fast on-rate, and high specificity [67]. Moreover, many molecules can be covalently attached to biotin (biotinylation) without altering their natural functions, which allows a wide variety

of functionalizations compatible with streptavidin conjugation, and thus being extremely useful for biotechnology applications.

3.5.1 *Bio-functionalization of biocatalytically produced polypyrrole thin films*

Functionalization of biocatalytically fabricated polypyrrole samples was studied through the fabrication of streptavidin-functionalized and biotin-functionalized polypyrrole layers.

Biotin and streptavidin were physically trapped into the polymer matrix by adding them to the reaction during the polymerization process, thus obtaining biologically functionalized polypyrrole surfaces in a single step*. The presence of biotin and streptavidin in the final polymer surface was investigated by ToF-SIMS and XPS analyses. Statistics were applied to complex biological data recorded from ToF-SIMS (for more details see section 2.3.2.2). Multivariate analysis method (MVA) was selected to conduct this study. For MVA analysis, certain ToF-SIMS peaks from the samples were chosen and normalized to the maximum ion intensity of the spectra. This process allowed accounting for variations in the data acquisition that may not relate to actual surface chemical differences such as variations in primary ion current or detector efficiency. Principal component analysis (PCA) was then employed to reduce and analyse the ToF-SIMS dataset.

**Single step biologically functionalized polypyrrole fabrication:*
For biological functionalization experiments, biotin and streptavidin concentrations 2 µg/mL and 100 µg/mL were used.
For streptavidin-modified gold nanoparticles a concentration of 2 µg/mL of streptavidin was used which corresponded to $1.5x10^{13}$ Au-nano particles/mL (~10 nm Au-nanoparticle diameter, ~6 streptavidin molecules per Au-nanoparticle).

Four samples were studied by PCA, namely a bare polypyrrole layer, a streptavidin-functionalized polypyrrole layer, a biotin-functionalized polypyrrole layer and a streptavidin-functionalized polypyrrole layer incubated with biotin. Eight mass spectra from each of the four samples were evaluated, and eighteen representative peaks from the dataset were selected and normalized to the maximum intensity of the positive spectra. These peaks accounted for biotin fragments [68, 69] and amino acid fragments corresponding to streptavidin [70, 71, 72]. PCA analysis resulted in differentiation of the samples in clusters based on their spectra, as seen in the score plot represented in Figure 3.32a.

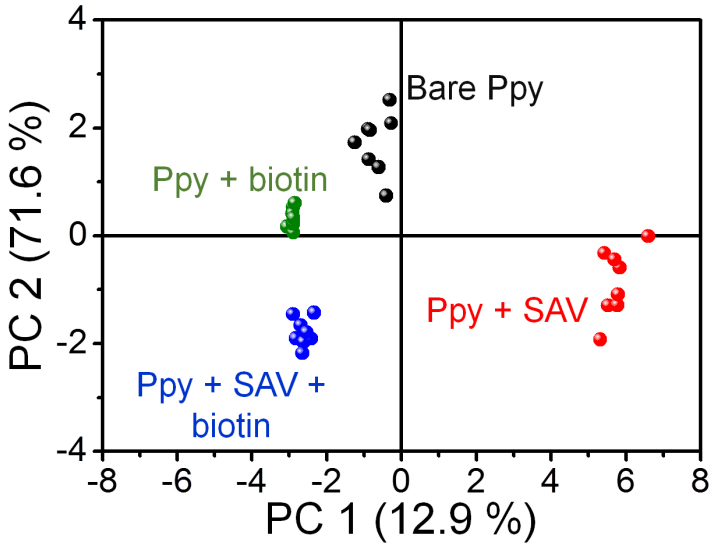

(a)

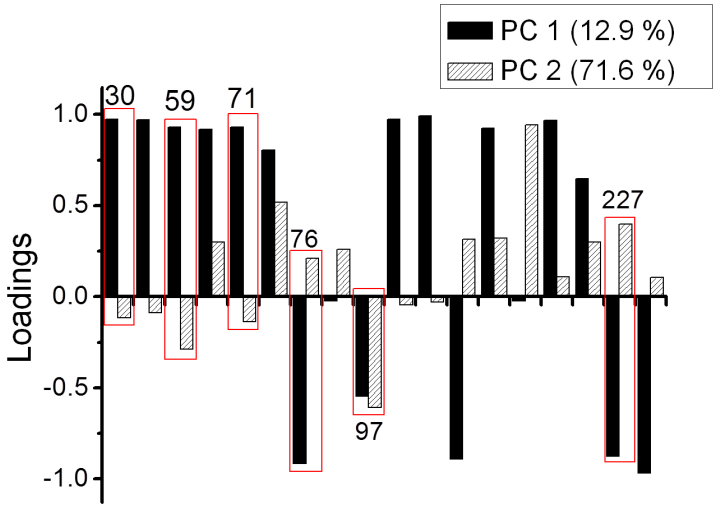

(b)

Figure 3.32: MVA of ToF-SIMS. Results corresponding to four samples namely bare polypyrrole layer, streptavidin-functionalized polypyrrole layer, biotin-functionalized polypyrrole layer and streptavidin-functionalized polypyrrole layer incubated with biotin. a) In scores plot four clusters can be distinguished (black: bare polypyrrole, green: biotin-functionalized polypyrrole, red: streptavidin-functionalized polypyrrole and blue: streptavidin-functionalized polypyrrole incubated with biotin). b) In loadings plot the most representative ions of each sample are shown.

The score plot indicates how different are spectra from each other, i.e. spectra clusters in the plot are from the same kind and distributed spectra correspond to different surface chemistries. The total variance represented in this plot was 84.5%, meaning that over 80% of the variance among the four samples was described just by the first two principal components (new variables PC1 and PC2). Therefore, the first principal component (PC1) clearly separated the samples containing biotin at the negative part of the axis from the ones free of it at the positive and neutral part. Similarly, the second principal component (PC2) differentiated the samples which contain streptavidin in their structure at the negative side of the axis, from the ones free of it at the positive side.

The correlation existing between scores and loadings of the same sign (negative loadings correspond to negative scores, analogous for the positive case) provides information as to which mass peaks are important in driving the achieved classification of clusters [73]. Thus, Figure 3.32b identified the mass fragments 30 mass/z, 59 mass/z and 71 mass/z (positive PC1 and negative PC2 in scores and loadings plots) as highly contributing to the separation of the streptavidin-functionalized polypyrrole cluster. These mass fragments correspond to streptavidin fragments and turned out to be present in significant amounts in the streptavidin-functionalized polypyrrole sample, but not in the other ones. In a similar way, the separation of the biotin-functionalized polypyrrole cluster (negative PC1 and positive PC2 in scores and loadings plots) was due to mass fragments reported to be from biotin (76 mass/z and 227 mass/z). And, the streptavidin-functionalized polypyrrole sample that was incubated with biotin showed to be resolved from the other samples in the third quarter of the scores plot (negatives PC1 and PC2). This cluster isolation could be attributed to the presence of the biotin-streptavidin union, since a new ion (97 mass/z) appeared to be predominantly present in this sample, but not in the samples that contained only biotin or only streptavidin. These results suggested that the streptavidin-biotin union was formed and therefore that the entrapment of biomolecules (such as streptavidin) into the polypyrrole electrodes occurs without loss of biomolecule functionality. Correlation between ion masses and molecule fragments are shown in Table 3.2.

Additionally, ToF-SIMS experiments in depth profile mode were conducted on biologically functionalized samples to verify the homogeneous distribution of the biomolecule across the polymer thickness.

In ToF-SIMS depth profiles, the intensity of certain ions is plotted against time of bombarding, which afterwards can be translated to sample thickness. However,

MASS (Z)	CORRESPONDING ION	IDENTIFIABLE FRAGMENT
30	CH_4N^+	streptavidin
59	CNH_5^+	streptavidin
71	$C_3H_{33}O_2^+$	streptavidin
76	$C_{22}H_6NS^+$	biotin
97	$C_4H_7N_{33}^+$	streptavidin + biotin
227	$C_4H_{77}N_{22}O_7S^+$	biotin

Table 3.2: ToF-SIMS data of biotin and streptavidin functionalized polypyrrole.

the etching nature of the experiment, destroys molecular fragments giving only elemental information, which makes impossible to distinguish between similar mass fragments.

Thus, to eliminate the uncertainty in ion identification, labelled targets were trapped into the polypyrrole layers. Here, streptavidin-modified gold nanoparticles were added during polymerization synthesis. ToF-SIMS depth profiles were taken across the thickness of functionalized samples, collecting the signals of the ions composing the sample. Figure 3.33 shows ion signals of gold, polypyrrole (CN^-, CNO^-) and ABTS (HS^-), which suddenly decrease at the time that silicon and silicon dioxide signals increase.

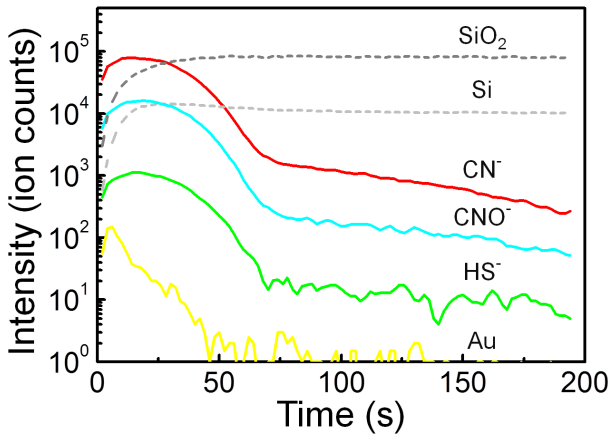

Figure 3.33: ToF-SIMS depth profile. Streptavidin-modified gold nanoparticles included in the polypyrrole film.

This crossing point of signals determines the thickness of the polymer (~60 nm measured by AFM) and indicates the presence of gold in the sample and consequently streptavidin across all the polypyrrole layer thickness.

Finally, XPS analysis was also conducted to confirm the chemical composition of polypyrrole thin layers grown in the presence of biotin. Figure 3.34 shows high-resolution spectra recorded for the core-level peaks of S 2p of polypyrrole with biotin (black solid line) and without biotin (red dashed line). In both cases, S 2p signal showed two strong components centered at 165.1 eV and 162.0 eV, respectively. The oxidized sulfur species (-SO_3H) at 165 eV was most likely to correlate with the use of ABTS as dopant, and the peak centered at 162 eV could be attributed to C-S-C and C-SH species [74]. In the absence of biotin, the peak at 162 eV could be due to the contribution of the enzyme HRP that is also entrapped in the polymer structure during the polymerization process [75, 76]. The peak area ratio between the two sulfur components at 162 eV and 165 eV is 0.90. Due to the presence of biotin, the contribution of the 162 eV peak increased, reaching a peak area ratio of 1.14.

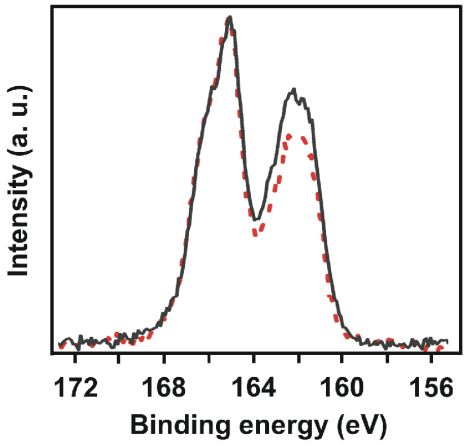

Figure 3.34: S 2p core-level XPS analysis of biocatalytically synthesized polypyrrole with (solid black line) and without biotin (dashed red line), showing the increase in the 162.0 eV peak due to the contribution of sulfur from biotin.

These results indicate that polypyrrole layers grown by biocatalytical method can physically trap biological species in a single step process, maintaining the biomolecule functional and consequently reducing the number of functionalization steps.

3.5.2 *Bio-functionalization of biocatalytically produced polypyrrole microelectrodes*

Here, biological functionalization was applied to biocatalytically produced microelectrodes. The previously developed site-selective fabrication process of polypyrrole microelectrodes (section 3.4) was used in the presence of biotin and streptavidin respectively.

It was possible to fabricate lines of biocatalytically produced polypyrrole functionalized with biotin down to 20 µm width (Figure 3.35a). However, the stability of the assembled polymer layers was compromised by the presence of the entrapped biotin, which affected polymer cohesion and required accurate control of the ultrasonic cleaning time for an appropriate lift off (times between 2 and 5 minutes). Some troubles have been reported previously when biological species were incorporated into polymeric structures during synthesis, including interference with the polymer growth and a decreased adherence of the polymer to the surface [62]. In particular, effects of molecule entrapment on the mechanical and adhesion properties have been previously described for electrochemically grown polypyrrole, requiring as well fine tuning of the experimental conditions [5]. In contrast, when streptavidin was included in the synthesis reaction, features of the same size were obtained without apparent loss of cohesion properties (Figure 3.35b).

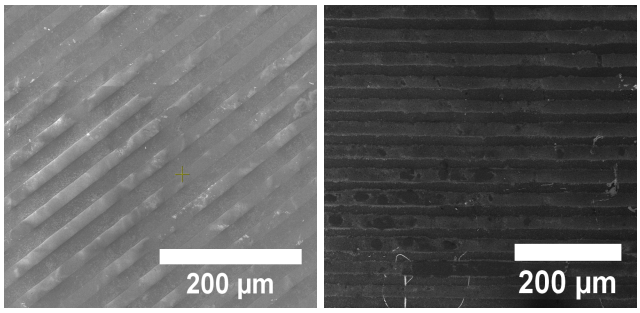

(a) (b)

Figure 3.35: SEM images of biologically functionalized polypyrrole. a) Biotin functionalized polypyrrole and b) streptavidin modified polypyrrole.

This phenomenon could be explained by the charge carried by the biomolecule during the polymerization process. On one hand, the biocatalytical polymerization reaction developed in this work occurs at pH 4.0 and the isoelectric points of streptavidin and biotin at this pH are 5 and 3.5 respectively. It becomes clear that streptavidin is positively charged during the polymerization reaction, whereas

biotin is negatively charged. Biotin's negative charge could lead to its participation as doping ion in the polymerization reaction. This could be the reason why biotin functionalized polypyrrole lacks internal cohesion when compared with streptavidin functionalized samples. However, by applying suitable conditions at the ultrasonic cleaning step, both functionalized micropatterns were successfully obtained.

3.6 APPLICATION OF BIOCATALYTICALLY PRODUCED POLYPYRROLE THIN FILMS IN THE CONTROLLED DELIVERY OF BIOMOLECULES

In this section, controlled biomolecule delivery experiments are discussed as an example of application for biologically-functionalized biocatalytical polypyrrole electrodes.

As explained in section 3.4 of this chapter, negatively charged species are known to behave as polymer dopants, which can be released under controlled electrical stimulation. In the case of small molecules such as biotin, the electrochemical switching between the oxidized and reduced states of polypyrrole allows the release of biotin from the polymer structure [56].

Here, the fabrication of biotin-functionalized polypyrrole electrodes was conducted to perform biotin-release experiments under cyclic voltammetry (CV) stimulation. Biotin release into the electrolyte solution was monitored by means of high-performance liquid chromatography mass spectrometry (HPLC-MS) analysis, which is a chromatographic technique used to identify and quantify the components present in a mixture (for more details about HPLC-MS see section 2.3.5.2).

Biotin-functionalized polypyrrole layers were grown on SiO_2 surfaces that contained pre-fabricated gold electrodes. In this manner, good electrical contact with the polymer film was achieved, allowing for a stable external connection. Additionally, the use of biotin-saturated solutions to perform the polymer growth (8.2 mM), assured a dense functionalization of the polymer layers, which is convenient for release experiments [56]. The samples were rinsed with Milli-Q water to remove any loosely attached biotin onto the surface. Then, samples were connected to the external pads for electrical stimulation and passivated with Teflon tape, as shown in Figure 3.36, to avoid interferences with connections and assure a fixed liquid-exposed area for all samples.

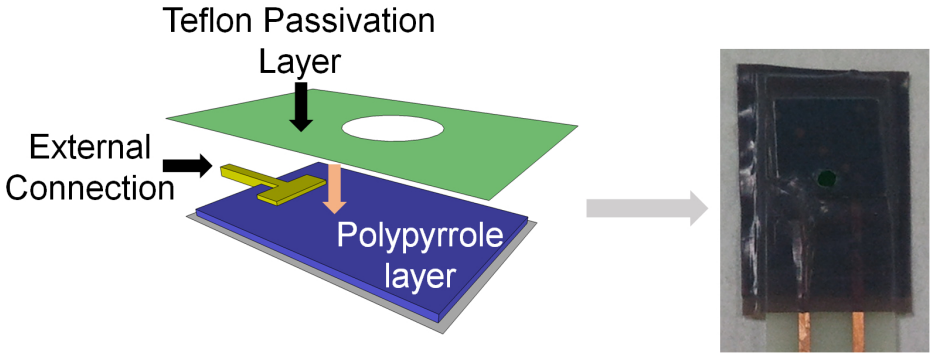

Figure 3.36: Passivation step of polypyrrole working electrodes. Teflon covers external electrical pads and defines the electrochemical working area.

Cyclic voltammetry was used to apply electrical stimulation to biocatalytical polypyrrole layers. This technique is reported to be the most efficient method for drug release experiments based on conducting polymers [5].

Controlled drug release experiments are based on the redox behaviour of the biocatalytical polypyrrole layers, shown in section 3.3.4 of this chapter. The mechanism of drug release is explained by the switching behaviour of the polymer between its oxidized and reduced states. During reduction, the applied negative potential, neutralizes the positive charge of the polymeric backbone and thus eliminates the electrostatic interaction between polypyrrole and the anion of interest (biotin) [11]. On the other hand, when positive potentials are used on polypyrrole layers, the positive charge of the backbone is increased further by the oxidation, avoiding the diffusion of the anions present in the matrix (Figure 3.37).

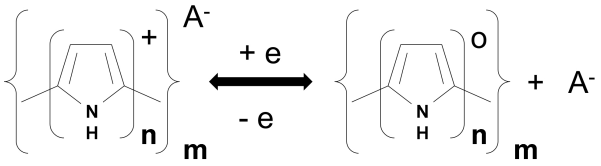

Figure 3.37: Redox mechanism of polypyrrole. The redox process allows biomolecule release.

Controlled release experiments were performed at different conditions namely constant oxidation experiment, non-electrical-connection experiment and CV experiment. In the constant oxidation experiments, a fixed positive potential of +0.9 V was applied to functionalized polypyrrole working electrodes. For the non-electrical-connection experiments, biotin-modified polypyrrole working elec-

trodes were simply soaked in measuring solution (PBS). And for the CV experiments, electrical stimulation by means of cyclic voltammetry (scans between -0.9 V and +0.9 V, at 100 mV/s) was applied on the polymer electrodes.

Biotin release into the electrolyte solution was monitored at different times (1, 5, 10, 15, 20, 25 minutes) by means of HPLC-MS analysis. 200 µL liquid samples from the release measuring solution (PBS) were taken after reduction of polypyrrole at the indicated times. Then, the area corresponding to the characteristic biotin fragment (m/z = 245.09) obtained after polypyrrole reduction, was compared with the same fragment area obtained during the oxidation experiment and the non-electrical-connection experiment.

Figure 3.38 shows the HPLC-MS data where the red line corresponds to the CV experiment, the blue line corresponds to the non-electrical-connection experiment and the green line belongs to the oxidation experiment. For CV experiments, the biotin release decreased abruptly during the first five minutes of the cathodic stimulation, as expected for thin polymer layers where diffusion of dopants through the polymer matrix is not a limiting step [11, 5].

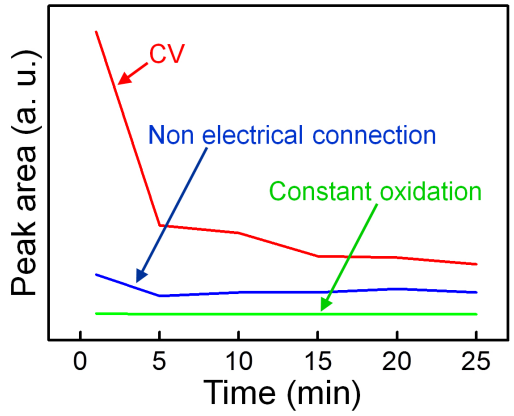

Figure 3.38: HPLC-MS for biotin release experiments. Plot of the evolution of the characteristic peak area fragment at m/z = 245.09 of biotin obtained from HPLC-MS analysis of the electrolyte solution at different time-points during the reduction step (red line), oxidation step (green line) and without electrical stimulation (blue line).

On the other hand, a minimal release was produced during the non-electrical-connection experiments, attributed to a phenomenon of ionic exchange with the electrolyte of the medium [77]. The driving force of the ionic exchange is the concentration gradients between doping ions in the polymer and ions present in the solution. This does not require stimulation to occur and the polymer backbone

remains with the same charge during the process. Finally, negligible release was registered for constant oxidation experiments, avoiding biotin diffusion from the polypyrrole matrix and demonstrating the voltage-dependent release behaviour of the biocatalytically grown polypyrrole.

These results indicate that the biocatalytically produced polypyrrole electrodes fabricated in this work, retain their electroactivity after a biological functionalization process. Therefore, they could be used for the release of small biomolecules, such as biotin, in a controlled manner under electrical stimulation

3.7 CONCLUSIONS

Organic electronic devices based on conducting polymers have emerged as a versatile alternative to silicon-based technologies in the biomedical field. Patterning of conducting polymers with good spatial resolution is a key step in the microfabrication of devices, with applications in new generation of implants and biosensors. Here, we presented the fabrication of conducting polymer microelectrodes through an environmentally friendly method that puts forward the state-of-the-art in the surface patterning of conducting polymers on insulating substrates. We fabricated bioactive polypyrrole microelectrodes on insulating substrates by a surface-guided biocatalytical polymerization method that does not require cleanroom environment and that can be straightforwardly scaled up to device fabrication. Polypyrrole microelectrode fabrication was controlled by tuning the surface adhesion through a non-adhesive/adhesive micropattern of silanes, generated by microcontact printing technique. Polymer cohesion was maintained up to 30 nm thickness after an ultrasonic cleaning step. X-ray photoelectron spectroscopy (XPS) studies revealed that fully doped polypyrrole was obtained, with conductivity values (3 S/cm approx.) one order of magnitude higher than other reported biocatalytic polypyrroles.

Polypyrrole microelectrodes were fabricated with an up to 5 μm resolution, what surpassed the resolution of the most used technique for organic electrodes printing. Moreover, the mild reaction conditions of the biocatalytical approach were compatible with the entrapment of biomolecules during the polymer synthesis in a single step process. Thus, as an example for the application of biologically-functionalized biocatalytical polypyrrole electrodes, biotin-functionalized electrodes were used for the controlled release of biotin through the application of an external electric field, thus demonstrating the potential of these systems for drug delivery devices. These are very promising results that pave

the way for the development of arrays of bioactive microelectrodes based on conducting polymers, which could be integrated in implantable devices for remotely controlled tissue interactions.

3.8 REFERENCES

[1] Laura Poole-Warren et al. "Development of bioactive conducting polymers for neural interfaces". In: *Expert review of medical devices* 7.1 (Jan. 2010), pp. 35–49. DOI: 10.1586/erd.09.58 (cit. on p. 62).

[2] Meredith Muskovich and Christopher J. Bettinger. "Biomaterials-Based Electronics: Polymers and Interfaces for Biology and Medicine". In: *Advanced Healthcare Materials* 1.3 (2013), pp. 248–266. DOI: 10.1002/adhm.201200071.Biomaterials-Based (cit. on p. 62).

[3] Md. Aminur Rahman et al. "Electrochemical Sensors Based on Organic Conjugated Polymers". In: *Sensors* 8.1 (Jan. 2008), pp. 118–141. DOI: 10.3390/s8010118 (cit. on p. 62).

[4] Harold Castano et al. "Polypyrrole thin films formed by admicellar polymerization support the osteogenic differentiation of mesenchymal stem cells". In: *Macromolecular bioscience* 4.8 (Aug. 2004), pp. 785–94. DOI: 10.1002/mabi.200300123 (cit. on p. 62).

[5] Brianna C Thompson et al. "Optimising the incorporation and release of a neurotrophic factor using conducting polypyrrole." In: *Journal of controlled release : official journal of the Controlled Release Society* 116.3 (Dec. 2006), pp. 285–94. DOI: 10.1016/j.jconrel.2006.09.004 (cit. on pp. 62, 97, 99, 100).

[6] D H Szarowski et al. "Brain responses to micro-machined silicon devices". In: *Brain Research* 983 (2003), pp. 23–35 (cit. on p. 62).

[7] S. et al. Aznar.Cervantes. "Fabrication of conductive electrospun silk fibroin scaffolds by coating with polypyrrole for biomedical applications". In: *Bioelectrochemistry* 85 (2012), pp. 36–43 (cit. on p. 62).

[8] Manisha Sarma et al. "High surface area polypyrrole scaffolds for tunable drug delivery". In: *International Journal of Pharmaceutics* 443.1-2 (2013), pp. 163–168 (cit. on p. 62).

[9] Daniel V. Bax et al. "Cell patterning via linker-free protein functionalization of an organic conducting polymer (polypyrrole) electrode". In: *Acta Biomaterialia* 8.7 (2012), pp. 2538–2548 (cit. on p. 62).

[10] Sirinrath Sirivisoot, Rajesh Pareta, and Thomas J. Webster. "Electrically controlled durg release from nanostructures polypyrrole coated on titanium". In: *Nanotechnology* 22 (2011), p. 085101 (cit. on p. 62).

[11] Reecha Wadhwa, Carl F Lagenaur, and Xinyan Tracy Cui. "Electrochemically controlled release of dexamethasone from conducting polymer polypyrrole coated electrode". In: *Journal of controlled release : official journal of the Controlled Release Society* 110.3 (Feb. 2006), pp. 531–41. DOI: 10.1016/j.jconrel.2005.10.027 (cit. on pp. 62, 99, 100).

[12] Vadim S Polikov, Patrick a Tresco, and William M Reichert. "Response of brain tissue to chronically implanted neural electrodes". In: *Journal of neuroscience methods* 148.1 (Oct. 2005), pp. 1–18. DOI: 10.1016/j.jneumeth.2005.08.015 (cit. on p. 62).

[13] Xinyan Cui et al. "In vivo studies of polypyrrole/peptide coated neural probes". In: *Biomaterials* 24.5 (Feb. 2003), pp. 777–87 (cit. on p. 62).

[14] Uta Reich et al. "Differential fine-tuning of cochlear implant material-cell interactions by femtosecond laser microstructuring." In: *Journal of biomedical materials research. Part B, Applied biomaterials* 87.1 (Oct. 2008), pp. 146–53. DOI: 10.1002/jbm.b.31084 (cit. on p. 62).

[15] Mikhail a Lebedev and Miguel a L Nicolelis. "Brain-machine interfaces: past, present and future". In: *Trends in neurosciences* 29.9 (Sept. 2006), pp. 536–46. DOI: 10.1016/j.tins.2006.07.004 (cit. on p. 62).

[16] Francis Garnier et al. "All-Polymer Field-Effect Transistor Realized by Printing Techniques". In: *Science* 265 (1994), p. 1684 (cit. on p. 63).

[17] Sunappan Vasudivan. "Fine line screen printed electrodes for polymer microfluidics". In: *2010 12th Electronics Packaging Technology Conference* (Dec. 2010), pp. 89–93. DOI: 10.1109/EPTC.2010.5702612 (cit. on p. 63).

[18] Ken Gilleo. "POLYMER THICK FILM TECHNOLOGY". In: *Pollution Prevention Review* (1996), pp. 65–74 (cit. on p. 63).

[19] T. R. Hebner et al. "Ink-jet printing of doped polymers for organic light emitting devices". In: *Applied Physics Letters* 72.5 (1998), p. 519. DOI: 10.1063/1.120807 (cit. on p. 63).

[20] Yang Yang et al. "Organic / polymeric electroluminescent devices processed by hybrid ink-jet printing". In: *Journal of Materials Science: Materials in Electronics* 1 (2000), pp. 89–96 (cit. on p. 63).

[21] Jun Xu, Chengmei Zhong, and Chun Fu. "Novel method for printing high-quality metal wires". In: *SPIE* (2007). DOI: 10.1117/2.1200712.0969 (cit. on p. 63).

[22] Graciela B. Blanchet et al. "Large area, high resolution, dry printing of conducting polymers for organic electronics". In: *Applied Physics Letters* 82.3 (2003), p. 463. DOI: 10.1063/1.1533110 (cit. on pp. 63, 64).

[23] J R Sheats et al. "Patterning of Polymer Light-Emitting Diodes with Soft Lithography". In: *Advanced Materials* 12 (2000), pp. 269–273 (cit. on p. 63).

[24] Tobias Kaufmann and Bart Jan Ravoo. "Stamps, inks and substrates: polymers in microcontact printing". In: *Polymer Chemistry* 1.4 (2010), p. 371. DOI: 10.1039/b9py00281b (cit. on pp. 63, 64).

[25] Sarah M Richardson-Burns et al. "Polymerization of the conducting polymer poly(3,4-ethylenedioxythiophene) (PEDOT) around living neural cells". In: *Biomaterials* 28.8 (Mar. 2007), pp. 1539–52. DOI: 10.1016/j.biomaterials.2006.11.026 (cit. on p. 65).

[26] Luigi Sasso et al. "Doped overoxidized polypyrrole microelectrodes as sensors for the detection of dopamine released from cell populations." In: *The Analyst* 138.13 (July 2013), pp. 3651–9. DOI: 10.1039/c3an00085k (cit. on p. 65).

[27] Zheyuan Huang et al. "Selective Deposition of Conducting Polymers on Hydroxyl-Terminated Surfaces with Printed Monolayers of Alkylsiloxanes as Templates". In: *Langmuir* 7463.12 (1997), pp. 6480–6484 (cit. on pp. 65, 66).

[28] Gyoujin Cho and Daniel T Glatzhoferc. "Enhanced adhesion of polypyrrole film through a novel grafting method". In: *Journal of Materials Chemistry* (1999), pp. 345–347 (cit. on pp. 66, 70).

[29] Rajeswari Ravichandran et al. "Applications of conducting polymers and their issues in biomedical engineering". In: *Journal of the Royal Society, Interface / the Royal Society* 7 Suppl 5 (Oct. 2010), S559–79. DOI: 10.1098/rsif.2010.0120.focus (cit. on p. 66).

[30] V Rocchi and G P Gardini. "On Pyrrole Ooxidation with Hydrogen Peroxide". In: *Tetrahedron* 26 (1970), p. 4073 (cit. on p. 66).

[31] Yong Hwan Kim et al. "Polymerization of cardanol using soybean peroxidase and its potential application as anti-biofilm coating material." In: *Biotechnology letters* 25.18 (Sept. 2003), pp. 1521–4 (cit. on p. 66).

[32] H. B Dunford. *Peroxidases in Chemistry and Biology*. Ed. by J. Everse and M. B. Grisham. 1991, pp. 1–24 (cit. on p. 66).

[33] Ryan Bouldin et al. "Enzymatic Synthesis of Electrically Conducting Polymers". In: *American Chemical Society* X.Symposium series (2010), pp. 315–341 (cit. on pp. 66, 67).

[34] Frank Hollmann and Isabel W C E Arends. "Enzyme Initiated Radical Polymerizations". In: *Polymers* 4 (2012), pp. 759–793. DOI: 10.3390/polym4010759 (cit. on p. 66).

[35] G V Otrokhov et al. "Biocatalytic synthesis of conducting polymers and prospects for its application". In: *Biochemistry. Biokhimiya* 78.13 (Dec. 2013), pp. 1539–53. DOI: 10.1134/S0006297913130117 (cit. on p. 67).

[36] Hyun-Kon Song and G Tayhas R Palmore. "Conductive polypyrrole via enzyme catalysis". In: *The journal of physical chemistry. B* 109.41 (Oct. 2005), pp. 19278–87. DOI: 10.1021/jp0514978 (cit. on pp. 67, 77, 84).

[37] Seong-Cheol Kim et al. "Self-Doped Polyaniline/Poly(diallyldimethyl ammonium chloride) Complex: N-Type Doping with High Stability". In: *Chemistry of Materials* 18.9 (May 2006), pp. 2201–2204. DOI: 10.1021/cm052206a (cit. on p. 67).

[38] Rodolfo Cruz-Silva et al. "pH- and thermosensitive polyaniline colloidal particles prepared by enzymatic polymerization". In: *Langmuir : the ACS journal of surfaces and colloids* 23.1 (Jan. 2007), pp. 8–12. DOI: 10.1021/la0618418 (cit. on p. 67).

[39] Jalal Arjomandi and Rudolf Holze. "Spectroelectrochemistry of conducting polypyrrole and poly (pyrrole-cyclodextrin) prepared in aqueous and nonaqueous solvents". In: *Journal of Solid State Electrochemistry* 11.8 (Jan. 2007), pp. 1093–1100. DOI: 10.1007/s10008-006-0243-7 (cit. on p. 67).

[40] Yulia N. Kupriyanovich et al. "Peroxidase-catalysed synthesis of electroconductive polypyrrole". In: *Mendeleev Communications* 18.1 (Jan. 2008), pp. 56–58. DOI: 10.1016/j.mencom.2008.01.021 (cit. on p. 67).

[41] R Cruz-Silva et al. "Biocatalytic synthesis of polypyrrole powder, colloids, and films using horseradish peroxidase." In: *Journal of colloid and interface science* 328.2 (Dec. 2008), pp. 263–9. DOI: 10.1016/j.jcis.2008.09.021 (cit. on pp. 67, 69, 77, 84).

[42] Eeva-liisa Kupila and Jouko Kankare. "Influence of electrode pretreatment , counter anions and additives on the electropolymerization of pyrrole in aqueous solutions". In: *Synthetic Metals* 74 (1995), pp. 241–249 (cit. on pp. 69, 77).

[43] C M Halliwell and a E Cass. "A factorial analysis of silanization conditions for the immobilization of oligonucleotides on glass surfaces". In: *Analytical chemistry* 73.11 (June 2001), pp. 2476–83 (cit. on pp. 71, 83).

[44] Chun-Guey Wu and Ching-Yuh Chen. "Chemical deposition of ordered conducting polypyrrole films on modified inorganic substrates". In: *Journal of Materials Chemistry* 7.8 (1997), pp. 1409–1413. DOI: 10.1039/a608365j (cit. on pp. 72, 82).

[45] Jaroslav Stejskal and Irina Sapurina. "In-situ polymerized polyaniline films". In: *Synthetic metals* 105 (1999), pp. 195–202 (cit. on p. 75).

[46] A Riede, M Helmstedt, and V Riede. "In Situ Polymerized Polyaniline Films . 2 . Dispersion Polymerization of Aniline in the Presence of Colloidal Silica". In: *Langmuir* 19 (2000), pp. 6240–6244 (cit. on pp. 75, 79).

[47] Walaiporn Prissanaroon et al. "Electrical conductivity response of dodecylbenzene sulfonic acid-doped polypyrrole films to SO2-N2 mixtures". In: *Synthetic Metals* 114.1 (July 2000), pp. 65–72. DOI: 10.1016/S0379-6779(00)00230-7 (cit. on p. 76).

[48] Miroslava Trchova and Jana Kova. "Synthesis and structural study of polypyrroles prepared in the presence of surfactants". In: *Synthetic metals* 138 (2003), pp. 447–455 (cit. on pp. 76, 77).

[49] T. K. Vishnuvardhan et al. "Synthesis, characterization and a.c. conductivity of polypyrrole/Y2O3 composites". In: *Bulletin of Materials Science* 29.1 (Feb. 2006), pp. 77–83. DOI: 10.1007/BF02709360 (cit. on pp. 76, 81).

[50] Wenbin Liang, Junting Lei, and Charles R. Martin. "Effect of synthesis temperature on the structure, doping level and charge-transport properties of polypyrrole". In: *Synthetic Metals* 52.2 (1992), pp. 227–239 (cit. on p. 77).

[51] J. F. Moulder C. D. Wanger, W. M. Riggs, L. E. Davis and G. E.Muilenberg. *Handbook of XPS*. Ed. by USA Physical Electronics Division, Eden Prairie, Minnesota. Perkin-Elmer Corp., 1979 (cit. on p. 78).

[52] A. Naumkin et al. "NIST Standard Reference Database 20, Version 4.1". In: Measurement Services Division of the National Institute of Standards and Technology (NIST), 2012. Chap. NIST X-ray Photoelectron Spectroscopy Database (cit. on p. 78).

[53] R. Joseph Kline, Michael D. McGehee, and Michael F. Toney. "Highly oriented crystals at the buried interface in polythiophene thin-film transistors". In: *Nature Materials* 5.3 (Feb. 2006), pp. 222–228. DOI: 10.1038/nmat1590 (cit. on p. 81).

[54] Anuar Kassim, Zarina Bte Basar, and H. N. M. Ekramul Mahmud. "Effects of preparation temperature on the conductivity of polypyrrole conducting polymer". In: *Journal of Chemical Sciences* 114.2 (Apr. 2002), pp. 155–162. DOI: 10.1007/BF02704308 (cit. on pp. 81, 83).

[55] S. Partch, R., Gangolli, G.S., Matijevic, E., Cai, W., Arajs. "Conducting Polymer Composites". In: *Journal of colloid and interface science* 111 (1991), pp. 27–35 (cit. on p. 81).

[56] P.M. George et al. "Electrically Controlled Drug Delivery from Biotin-Doped Conductive Polypyrrole". In: *Advanced Materials* 18.5 (Mar. 2006), pp. 577–581. DOI: 10.1002/adma.200501242 (cit. on pp. 82, 98).

[57] Gaurav Saini et al. "Two-silane chemical vapor deposition treatment of polymer (nylon) and oxide surfaces that yields hydrophobic (and superhydrophobic), abrasion - resistant thin films". In: *Journal of Vacuum Science & Technology A: Vacuum, Surfaces, and Films* 26.5 (2008), p. 1224. DOI: 10.1116/1.2953699 (cit. on p. 83).

[58] R. H. Geiss et al. "Polymer Structure Determination Using Electron Diffraction Techniques". In: *IBM Journal of Research and Development* 27 (1983), p. 321 (cit. on p. 84).

[59] X. Chu et al. "Crystalline fibers in chemically polymerized ultrathin polypyrrole films". In: *Journal of Applied Physics* 77.12 (1995), p. 6658. DOI: 10.1063/1.359078 (cit. on p. 84).

[60] Zhanhu Guo et al. "Fabrication and characterization of iron oxide nanoparticles filled polypyrrole nanocomposites". In: *Journal of Nanoparticle Research* 11.6 (Oct. 2008), pp. 1441–1452. DOI: 10.1007/s11051-008-9531-8 (cit. on p. 84).

[61] Yanju Wang et al. "Individually addressable crystalline conducting polymer nanowires in a microelectrode sensor array." In: *Nanotechnology* 18.42 (Oct. 2007), p. 424021. DOI: 10.1088/0957-4484/18/42/424021 (cit. on p. 84).

[62] Darren Svirskis et al. "Electrochemically controlled drug delivery based on intrinsically conducting polymers". In: *Journal of controlled release : official journal of the Controlled Release Society* 146.1 (Aug. 2010), pp. 6–15. DOI: 10.1016/j.jconrel.2010.03.023 (cit. on pp. 85, 97).

[63] G Garcia-Belmonte et al. "Doping-induced broadening of the hole density-of-states in conducting polymers". In: *Electrochimica Acta* 55.21 (2010), pp. 6123–6127. DOI: http://dx.doi.org/10.1016/j.electacta.2009.08.019 (cit. on p. 85).

[64] Laurent Libioulle et al. "Contact-Inking Stamps for Microcontact Printing of Alkanethiols on Gold". In: *Langmuir* 23 (1999), pp. 300–304 (cit. on p. 86).

[65] Sunil Kwon et al. "Patterning of polypyrrole using a fluoropolymer as an adsorption-protecting molecule". In: *Applied Surface Science* 257.1 (Oct. 2010), pp. 165–171. DOI: 10.1016/j.apsusc.2010.06.057 (cit. on p. 87).

[66] Feng Zhou et al. "Manipulation of the ultimate pattern of polypyrrole film on self-assembled monolayer patterned substrate by negative or positive electrodeposition". In: *Surface Science* 561.1 (July 2004), pp. 1–10. DOI: 10.1016/j.susc.2004.05.077 (cit. on p. 87).

[67] Michel N. Green. "Avidin and Streptavidin". In: *Methods in Enzymology* 184.1978 (1990) (cit. on p. 91).

[68] Young-Pil Kim et al. "Quantitative ToF-SIMS study of surface-immobilized streptavidin". In: *Applied Surface Science* 252.19 (2006), pp. 6801 –6804. DOI: http://dx.doi.org/10.1016/j.apsusc.2006.02.203 (cit. on p. 92).

[69] Young-Pil Kim et al. "Quantitative analysis of surface-immobilized protein by TOF-SIMS: effects of protein orientation and trehalose additive." In: *Analytical chemistry* 79.4 (Feb. 2007), pp. 1377–85. DOI: 10.1021/ac0616005 (cit. on p. 92).

[70] Bryan N Brown et al. "Surface characterization of extracellular matrix scaffolds". In: *Biomaterials* 31.3 (Jan. 2010), pp. 428–37. DOI: 10.1016/j.biomaterials.2009.09.061 (cit. on p. 92).

[71] M S Wagner and David G Castner. "Characterization of Adsorbed Protein Films by Time-of-Flight Secondary Ion Mass Spectrometry with Principal Component Analysis". In: *Langmuir* 17.30 (2001), pp. 4649–4660 (cit. on p. 92).

[72] J B Lhoest et al. "Characterization of adsorbed protein films by time of flight secondary ion mass spectrometry". In: *Journal of biomedical materials research* 57.3 (Dec. 2001), pp. 432–40 (cit. on p. 92).

[73] Elena S F Berman et al. "Distinguishing monosaccharide stereo- and structural isomers with TOF-SIMS and multivariate statistical analysis". In: *Analytical chemistry* 78.18 (Sept. 2006), pp. 6497–503. DOI: 10.1021/ac060865g (cit. on p. 94).

[74] Youngnam Cho and Richard Ben Borgens. "Biotin-doped porous polypyrrole films for electrically controlled nanoparticle release". In: *Langmuir : the ACS journal of surfaces and colloids* 27.10 (May 2011), pp. 6316–22. DOI: 10.1021/la200160q (cit. on p. 96).

[75] A. Ramanavicius et al. "Redox enzyme-glucose oxidase-initiated synthesis of polypyrrole". In: *Synthetic Metals* 156.5-6 (Mar. 2006), pp. 409–413. DOI: 10.1016/j.synthmet.2005.12.018 (cit. on p. 96).

[76] X. Cui et al. "Biocatalytic Generation of Ppy-Enzyme-CNT Nanocomposite: From Network Assembly to Film Growth". In: *Journal of Physical Chemistry C* 111.5 (Feb. 2007), pp. 2025–2031. DOI: 10.1021/jp0671594 (cit. on p. 96).

[77] Ryeo Yun Hwang et al. "Suppression of the loss of an electroactive dopant from polypyrrole by using a non-aqueous electrolyte of dopant-phobicity". In: *Journal of Electroanalytical Chemistry* 657.1-2 (July 2011), pp. 181–186. DOI: 10.1016/j.jelechem.2011.03.028 (cit. on p. 100).

4

AZIDE-PEDOT ELECTRODES. APPLICATION TO DNA SENSORS

This chapter describes the fabrication and testing of an electrochemical label-free DNA hybridization sensor, based on azidomethyl-modified poly(3,4-ethylenedioxythiophene) electrodes (azide-PEDOT electrodes). These azide-PEDOT electrodes are used as platforms for the immobilization of acetylene-DNA probes, complementary to the "Hepatitis C" virus, which are covalently grafted to the polymer backbone via "Click" reaction. DNA hybridization is detected by Differential Pulse Voltammetry (DPV), by evaluating the direct electrochemical change of the polymer behavior produced by the recognition event. This fabrication procedure is a powerful tool for the preparation of label-free DNA sensors able to selectively recognize a specific DNA sequence, down to the nanomolar range.

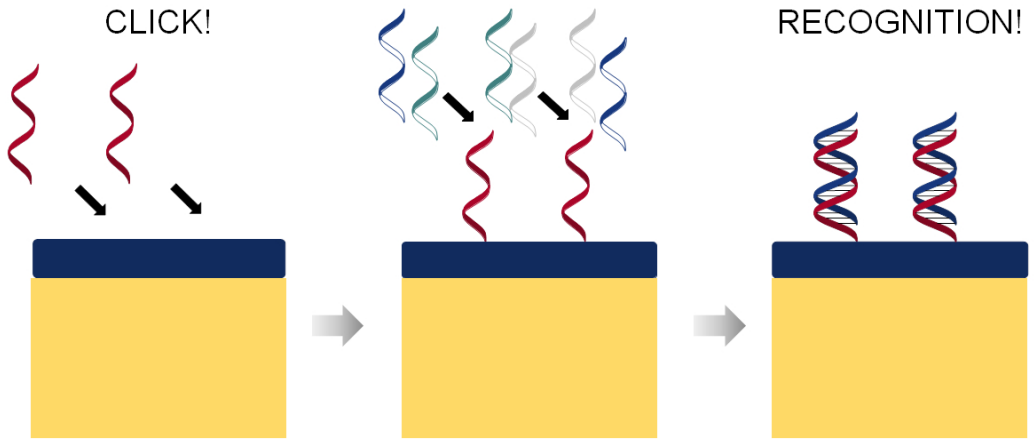

4.1 INTRODUCTION

Specific and quantitative DNA sequence detection is of great significance in the healthcare sector, not only for identification of pathogenic and genetic diseases but also to assess suitable therapies [1, 2]. In particular, since the completion of the "Human Genome Project" in 2003 [3], many DNA hybridization sensors have been developed for the investigation of different genetic mutations and human diseases, such as different types of cancer, human brain bacterial meningitis or HIV-1 infection [4, 5, 6]. DNA detection has also been applied to the environmental evaluation of water and food quality [7, 8], and to the screening of drugs that may bind to DNA or regulate gene expression [9]. Therefore, the interest in obtaining rapid and reliable methods for DNA detection has increased in the last years. This is reflected in the increasing number of publications related to this topic, as shown in Figure 4.1.

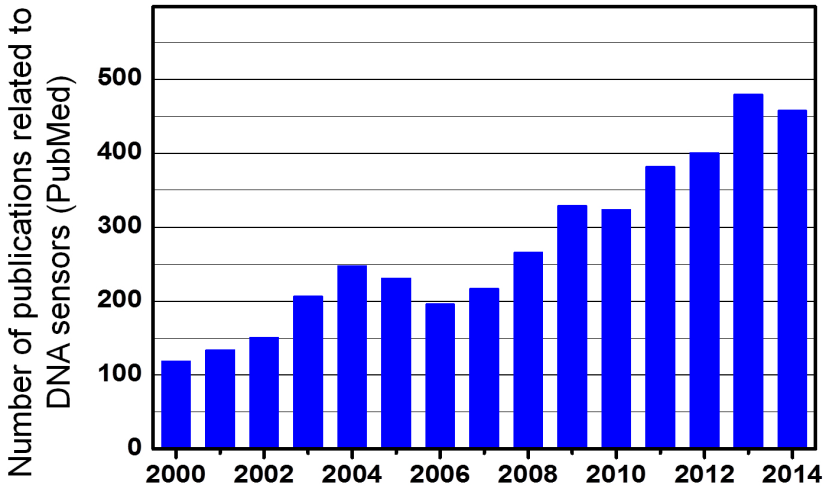

Figure 4.1: Number of publications related to DNA sensors from 2000 to date. Data obtained from PubMed source.

The identification of specific DNA sequences was accomplished for the first time in the 70's by direct sequencing [10, 11, 12]. Although this was a revolutionary invention, sequencing techniques are still limited in the number of DNA samples that can be analyzed at the same time, a part from being slow and poorly selective. Alternatively, DNA hybridization sensors soon appeared as an attractive substitute to direct sequencing, due to their simplicity and versatility [13]. They allow working on solid supports and also permit the construction of DNA array technologies [14].

Generally, a DNA hybridization sensor is composed of a transducing element on which a single-stranded probe (DNA probe) is immobilized. The system is then exposed to a specific target sequence (complementary DNA target), which is captured onto the surface during the recognition event, known as hybridization. Finally, the recognition event generates a response, which is transformed into a readable signal (Figure 4.2).

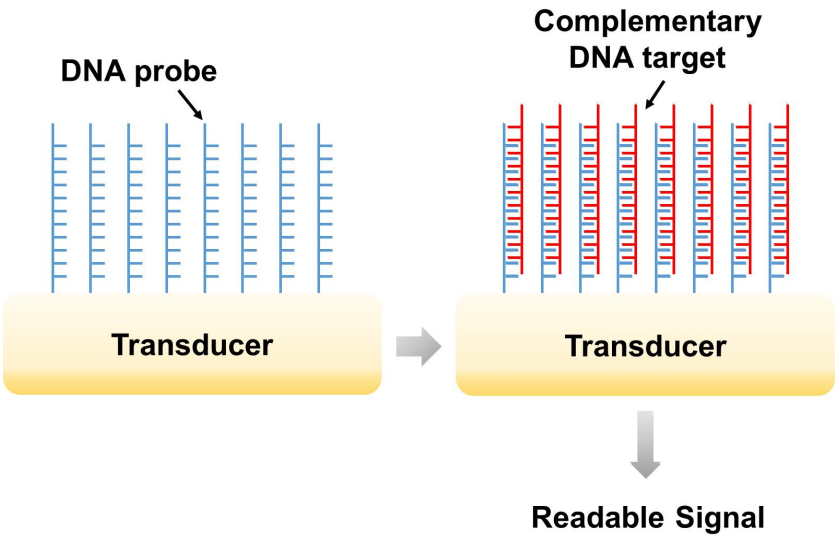

Figure 4.2: Schematics of a DNA hybridization sensor. It is composed of a transducing element, the recognition layer (DNA probe) and the analyte to detect (Complementary DNA target). After hybridization a readable signal is obtained through the transducer.

The performance of a DNA sensor relies on its selectivity and its sensitivity, which depend on the appropriate design of the sensing device. Firstly, the selectivity of a DNA sensor arises from the highly specific recognition process between two complementary DNA sequences. This specificity of DNA interactions is produced by steric and hydrogen bonding constrains between a purine base (adenine or guanine) and a pyrimidine base (thymine or cytosine) [15]. The space within the double helix is a perfect fit of a purine-pyrimidine pair, where adenine and thymine form two hydrogen bonds, while guanine and cytosine form three hydrogen bonds (Figure 4.3). These conditions unequivocally determine the specificity of the bases interaction.

Secondly, the sensitivity of a DNA sensor typically depends on technical parameters such as the immobilization matrix, the immobilization strategy or the transduction mechanism. One can find a wide variety of DNA immobilization

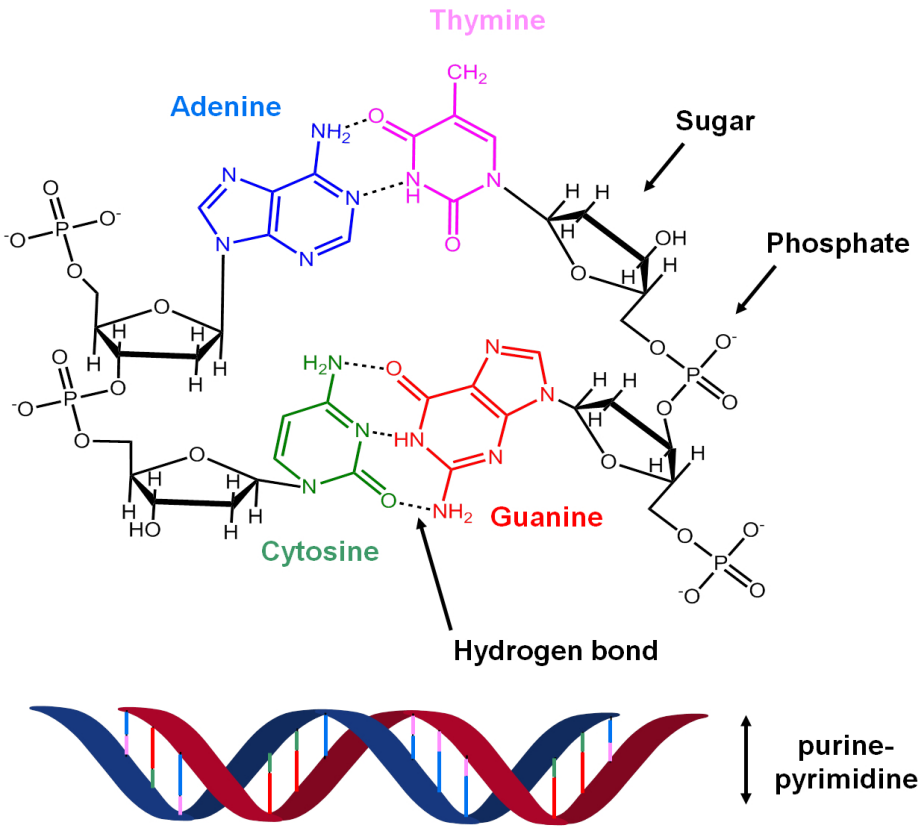

Figure 4.3: Watson-Crick's model for DNA double helix. Adenine and thymine share two hydrogen bonds, while cytosine and guanine share three hydrogen bonds. The space between the two phosphate backbones exactly fits a purine-pyrimidine pair.

techniques, ranging from simple adsorption, to covalent bonding and avidin-biotin complexation [16]. Different sensors have been developed based on various transduction mechanisms such as optical [17, 18], mass-sensitive [19, 20], or electrochemical methods [16].

Currently, fluorescence-based assays are one of the most widely used techniques for DNA detection and quantification. Their high sensitivity (sub-femtomolar concentrations) [21] paired with the possibility to fabricate microarrays by using multiple fluorescent species, allows simultaneous detection of different sequences in parallel [22, 23]. However, these techniques apart from being time consuming, often require expensive equipment, sophisticated mathematical algorithms to interpret the data and skilled personnel.

A powerful alternative are DNA sensors based on electrochemical detection, because of their reliable, simple and cost-effective detection procedures [16].

Therein, the electrode surface not only works as a substrate for DNA immobilization, but also as an active element. This is particularly suitable for fast sensing, since the hybridization event can be converted directly into an electrical signal. Moreover, electrochemical DNA sensing devices are compatible with microfabrication technology, which allows miniaturization and multiplexed detection, thus facilitating portable point-of-care-test applications [24].

The electrochemistry of such DNA sensors has so far been monitored by using amperometric and potentiometric techniques, such as cyclic voltammetry, pulse voltammetry, chronopotentiometry, etc. [25]. Electrochemical impedance spectroscopy (EIS) has been used as well, giving the possibility to directly detect DNA hybridization by using impedance measurements on functionalized surfaces [26]. Even though, this technique is highly sensitive, the drawback is that it requires complex interpretation. Nevertheless it can be replaced successfully by other less sophisticated electrochemical techniques, while still achieving quantitative results [27].

The electrochemical detection methods of DNA hybridization are classified as either direct or indirect. DNA sensors based on indirect detection methods demand the use of other electroactive species (labels) to detect the DNA hybridization, which have to be different from the electrode surface and the oligonucleotides. For example, the use of redox active indicators (ferrocenyl derivatives, quantum dots, enzyme reporters, etc.) has been reported, which are linked to the target sequence. Then, the electrochemical response of the indicator gives evidence of the DNA hybridization event [28, 29, 30]. Also, redox intercalators have been used, for example metal complex ions such as cobalt (III) ($Co(phen)_3^{3+}$) and hexaammineruthenium(III) ($Ru(NH3)_6^{3+}$) cations or organic dyes such as methylene blue (MB) [31, 32, 33]. They are intrinsically related with the double helix by electrostatic interactions, showing hybridization when the double helix is formed. These labeling techniques are the most extensively used DNA detection methods due to their low limits of detection, in the nano- and femtomolar range, and their capability to distinguish single-base mutations [34, 35]. However, most of these electrochemical methods used for DNA detection can affect the binding properties of the biological probe, thus interfering in the recognition process. Moreover, labelling requires extra time, expense and sample handling, and does not allow the detection of target-probe coupling in real time.

In contrast, direct detection methods are based on the electroactivity of the nucleic acids or on changes in the electronic properties of the substrate, which are induced by the hybridization event. Such direct detection methods are preferred

over indirect detection methods since they allow faster and a more versatile detection. They don't require extra time for labelling and are independent of the probe and/or target sequences used [36].

The electroactivity of nucleic acids was discovered in 1960 by the Palecek's group [37]. Guanine (G) is reported to be the most redox active nitrogenous base in DNA [38], and has been used, together with adenine (A), to detect the hybridization of DNA in label-free biosensors [39, 40]. However, this detection method still faces some problems, such as the variability on the oxidation potentials of Adenine (A) and Guanine (G) bases, depending on the nature of the electrode on which they are immobilized, and the controversy existing about the interpretation of the results. On one side, it is accepted that there is a decrease in the oxidation peak of guanine after hybridization due to the partial unavailability of the free G bases after recognition. But on the other side, an increase in the electrochemical signal of guanine after hybridization has been reported when the target sequence augments the total number of G bases [16]. This controversy has eventually been solved by using inosine-substituted probes (G-free probes) [40]. However, this approach means increased time and complexity, doesn't allow direct evaluation of the immobilization step due to the lack of G bases in the probe, and is limited to detection in the micromolar range [41].

Concerning the electroactivity of the substrate, conducting polymers (CP) have been used to directly detect DNA hybridization events because they serve as immobilization and transduction agents at the same time. Their electrochemical, optical and electronic properties are sensitive to environmental changes occurring at their surface, like the ones produced by a hybridization event [25, 42, 43]. Conducting polymers provide an intimate contact between the DNA probe and the electronic transducer, enhancing the stability and the speed of the response. Therefore, conducting polymers have been used in label-free DNA sensors, by monitoring changes in the electronic properties of their backbone caused by DNA hybridization events, where limits of detection lower than the micromole could be achieved [41].

The most popular conducting polymers used in biomedical applications are polypyrrole (Ppy), polyaniline (PANI) and polythiophene, due to their biocompatibility, good electrical performance, their stability under ambient conditions and the wide availability of the precursor monomers and their derivatives [25].

In DNA sensors, conducting polymers have typically been synthesized by electrochemical oxidation. This technique has been shown to be particularly advantageous over standard chemical methods, because it provides an efficient coverage

of the electronic component and a good adhesion to it [44]. Conducting polymers can be functionalized using many different strategies, including: adsorption, electrochemical entrapment, covalent attachment and affinity interactions (avidin-biotin) [25, 45, 46, 47]. Choosing the functionalization strategy greatly influences the performance of the sensor. The affinity between probe and target should be maintained, as well as the accessibility of the target to the probe. Simple adsorption has shown to be a tremendously simple approach. However, it is very unstable and can suffer from effects arising from constraints on the orientation of the DNA probe, resulting in high steric and kinetic barriers to hybridization. In a different manner, electrochemical entrapment occurs at the same time as the polymerization step and is a very simple technique, providing better anchoring of the DNA probe on the surface. However, the drawbacks here as compared to the previous method are less accessibility to the DNA probe and occasionally occurring damage to the oligonucleotides due to high oxidation potentials employed during the process. The avidin-biotin interaction offers the possibility of functionalizing a polymer (using a biotinylated target) without the use of chemical reactants which could damage DNA, and the distribution of biomolecules is concentrated at the surface of the polymer film, thus providing better accessibility and sensitivity. Nevertheless, the presence of the avidin layer with several available binding sites, can increase the non-specific interactions, compromising selectivity and sensitivity of the sensor [16].

Covalent bonding overcomes all these problems by providing better control over the concentration, stability and orientation of the DNA probe. Herein, precursor monomers modified with oligonucleotides or with reactive groups, such as carboxylic acids, amines, phosphates, etc., are used, which in turn will react with modified oligonucleotides [48]. Recently, the so called "Click" reactions have been investigated as appealing alternatives for polymer functionalization, due to their robustness and simplicity [49]. In particular, the copper-catalyzed Huisgen 1,3-dipolar cycloaddition has shown to be the most efficient reaction within the "Click" reactions. This reaction occurs between azide and alkyne groups and is not affected by other functional groups. The catalyst of choice is copper, which can be obtained from a wide variety of copper sources, while many different solvents (including water) can be used. The reaction takes place without the generation of by-products, thus making it suitable for biocompatible environments [50]. However, to the best of our knowledge, there is no report to date which applies "Click" reaction for the construction of label-free DNA hybridization sensors based on conducting polymers.

Here, a highly selective and sensitive electrochemical label-free DNA hybridization sensor is presented using a new approach, for the detection of "Hepatitis C" virus sequences (part of this work was done in collaboration with the Institute of Organic Chemistry II and Advanced Materials at the University of Ulm, Germany). The construction of the polymeric sensors includes the covalent grafting of a DNA probe to the polymer backbone, by "Click" reaction. The present work proposes the use of azidomethyl-poly(3,4-ethylenedioxythiophene electrodes (Azide-PEDOT) as platforms for the immobilization of an acetylene-DNA probe, which is complementary to a specific sequence of the "Hepatitis C" virus. For this purpose, an Azide-EDOT precursor monomer was electropolymerized on top of gold electrodes, thus including both the fabrication and functionalization of the polymer in a single step (Figure 4.4, Polymerization). Subsequently, an acetylene-modified DNA probe was covalently linked to the PEDOT films via "Click" reaction (Figure 4.4, "Click"), preserving the DNA probe from eventual damages during synthesis. The hybridization events were then detected by differential pulse voltammetry (DPV), by evaluating the electroactivity of the polymer after the DNA recognition process.

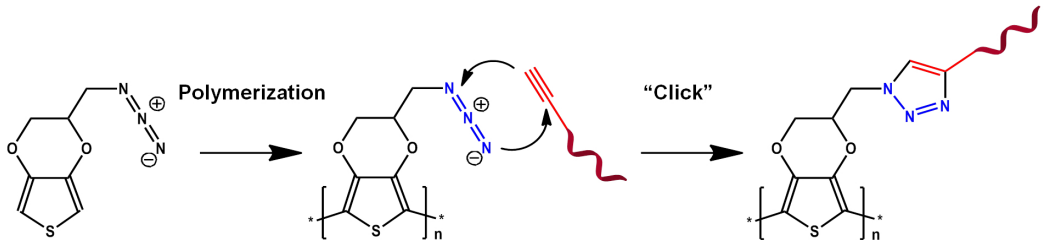

Figure 4.4: Construction of PEDOT DNA sensor. From left to right: polymerization of Azide-PEDOT electrode from monomer precursor and DNA immobilization process, by "Click" reaction.

To confirm the successful functionalization of the polymer, X-ray photoelectron spectroscopy (XPS), time-of-flight secondary ion spectroscopy (ToF-SIMS) and contact angle measurements were conducted. Full electrochemical characterization of the system was performed by cyclic voltammetry and differential pulse voltammetry.

Different parameters have been optimized, such as polymer layer thickness, oxidation state of the polymer, "Click" reaction time and temperature, in order to obtain a highly selective and sensitive DNA sensor.

The PEDOT sensor was tested under exposure to different concentrations of complementary target, resulting in calibration curves useful to find the detec-

tion limit of the system. DNA concentrations down to the nanomolar range were successfully detected, showing that the newly developed device is more sensitive than the so far reported electrochemical DNA sensors of the same type, thus avoiding the use of target amplification methods.

Moreover, the selectivity of the Azide-PEDOT electrochemical sensor was evaluated at a specific concentration for different target sequences. The test of complementary and non-complementary sequences resulted in a clear distinction of the hybridization event from the controls. A two-base mismatched sequence was tested being distinguished from the control experiment in a 60% approximately. Also, to demonstrate the clinical feasibility of the biosensor, mixed complementary/non complementary samples were measured simultaneously, showing good selectivity.

This system resulted in a new powerful tool for the preparation of label-free DNA sensors, revealing its potential for applications in the field of screening for genetic mutations and diseases, with special relevance in the detection of the "Hepatitis C" virus.

4.2 FABRICATION OF AZIDE-PEDOT ELECTRODES

In this section, the fabrication and characterization of Azide-PEDOT electrodes on gold surfaces is described. The fabricated Azide-PEDOT electrodes are then used for the detection of DNA sequences in a DNA sensor.

4.2.1 *Electrochemical synthesis of azide-PEDOT electrodes*

Rod-like gold electrodes, surrounded by an inert polymeric cover, were used to grow Azide-PEDOT films. Since these electrodes were used several times, a polishing pre-treatment was required before each use. To obtain a clean and smooth working area, diamond paste of different grain sizes was used to carefully polish the gold electrodes until specular surfaces were obtained (see details in section 2.2). Then, the electrodes were washed in ultrasonic baths of acetone and ethanol and finally used in electrochemical experiments.

Polymerization of Azide-EDOT was performed in organic solvent to avoid the overoxidation of the polymer. Polymer overoxidation is produced by the nucleophilic attack of water molecules on the monomer cation radicals, being responsible for a large amount of defects in the polymer and resulting in poor polymer conductivity [51, 52, 53]. In this work, Azide-PEDOT was polymerized in anhy-

drous dichloromethane (DCM) with tetrabutylammonium hexafluorophosphate ($TBAPF_6$) as supporting electrolyte.*

Before performing the polymerization, infrared spectroscopy characterization of the Azide-EDOT (in DCM) was conducted, to assure the integrity of the modified monomer. Figure 4.5 shows the infrared spectra of the solvent in comparison with the monomer in solution. Absorbance peaks corresponding to azide group [54] and 3,4 - Ethylenedioxythiophene (EDOT) prints [55] could be identified at wavenumbers of 2103 cm^{-1}, and from 1488 to 705 cm^{-1}, respectively.

** Polymerization details:*
100 mM $TBAPF_6$ in DCM was prepared in a 3-electrode electrochemical cell and kept under argon atmosphere. 1.5 mM Azide-EDOT was added to the electrochemical cell and cyclic voltammetry was applied. All potentials were referred versus an Ag/AgCl pseudoreference electrode, only used for organic solvents, consisting in an Ag/AgCl wire, which was referenced after each use against Fc/Fc^+.

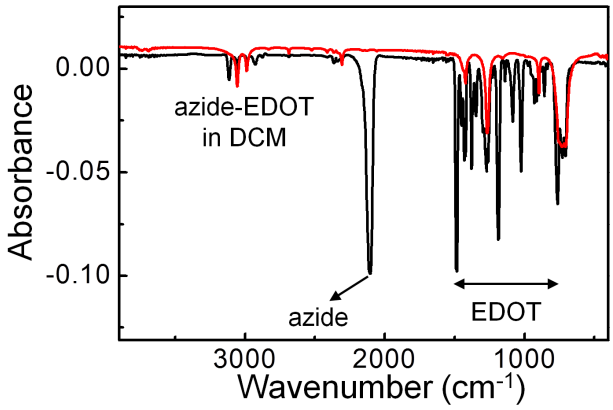

Figure 4.5: Infrared absorbance graph of Azide-EDOT monomer in dichloromethane (DCM). The red line represents the spectrum of DCM solvent and the black line is the spectrum of the Azide-EDOT monomer in DCM. The absorption peaks for the azidomethyl group and the EDOT monomer were identified.

Then, the electrochemical behavior of the Azide-EDOT system was investigated in DCM, using cyclic voltammetry between -1 V and +1.7 V at 100 mV/s, versus an Ag/AgCl pseudoreference electrode (-1.5 V and +1.2 V vs Fc/Fc^+), as depicted in Figure 4.6. A flat voltammogram (black cycle) was observed for a gold electrode, scanned in the absence of the modified monomer. On the other hand, when the Azide-EDOT monomer was added to the electrochemical cell (red voltammo-

grams), a large oxidation current was observed, corresponding to the polymerization of the monomer.

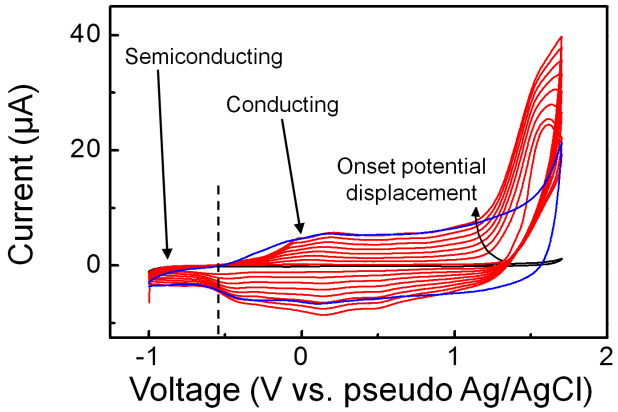

Figure 4.6: Electrochemical behavior of the Azide-EDOT monomer in DCM and $TBAPF_6$. Black line: cyclic voltammogram of a bare gold electrode in the absence of monomer in the electrolyte solution. Red lines: Electropolymerization cycles of Azide-EDOT in electrolyte solution. Blue line: characterization of Azide-PEDOT in an electrolyte solution free of monomer.

The oxidation process started at 1.28 V (polymerization onset potential, +0.78 V vs. Fc/Fc^+) with a maximum at +1.61 V (+1.11 V vs. Fc/Fc^+). The first scan presented a crossover between the cathodic and anodic branches, corresponding to the nucleation process typically occurring in the electrochemical synthesis of conducting polymers [56]. After that, the polymer deposition is much easier and the onset potential of the polymerization process shifted to lower potentials [57]. Moreover, after the first polymerization scan, a new irreversible redox wave appeared in the low-potential region, proving the deposition of polymer on the gold electrode. This redox wave gradually increased with the number of scans, indicating the rising amount of Azide-PEDOT deposited during every anodic sweep.

Azide-PEDOT voltammograms conducted in an electrolyte free of modified monomer (blue voltammogram), presented two well separated polymer behaviors. At -0.53 V (-1.03 V vs Fc/Fc^+) the fabricated polymer leaves the semiconducting regime to behave as a conductor.

The transition window was also characterized in Tris-HCl buffer (pH 7.0 , from -0.85 V to +0.6 V vs. Ag/AgCl reference electrode), since it was the medium employed for hybridization detection experiments. Up to 100 continuous cycles were conducted in Tris-HCl buffer to test the polymer stability under electrochemical stimulation in this medium. Figure 4.7 shows that 95.5% of electroactiv-

ity was retained after the series of cycles, providing an excellent basis for sensing applications.

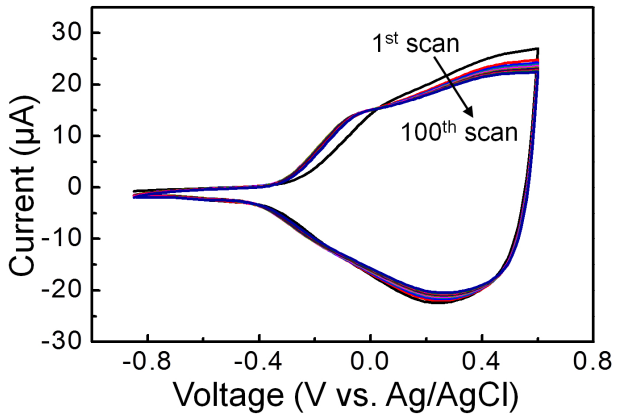

Figure 4.7: Stability test of Azide-PEDOT electrodes in Tris-HCl 20 mM. Cyclic voltammograms of an Azide-PEDOT electrode in Tris-HCl buffer where only a 4.5% of the electroactivity is lost after 100 cycles.

4.2.2 *Characterization of azide-PEDOT electrodes*

In this section, the characterization of Azide-PEDOT surfaces by scanning electron microscopy (SEM), atomic force microscopy (AFM), water contact angle, X-ray photoelectron spectroscopy (XPS) and differential pulse voltammetry (DPV) is discussed. For surface characterization experiments, gold-coated silicon wafers were used as working electrodes to grow Azide-PEDOT layers instead of rod-like electrodes, which showed to be not suitable for such purposes.

Figure 4.8 shows SEM and AFM graphs of Azide-PEDOT layers grown under the electrochemical conditions described in the previous section (section 4.2 of this chapter), but on gold-coated silicon wafers. The polymer surfaces presented a rough morphology covered by nano-fiber shaped features. This was accompanied by an increase of the hydrophobicity, as revealed by the water contact angle measurements, rising from $40.5^{o} \pm 2.6^{o}$ for bare gold surfaces to $67.4^{o} \pm 0.5^{o}$ for Azide-PEDOT surfaces. This increase in the active surface area of the gold electrodes is a convenient feature for sensing purposes, where a large sensing surface provides higher sensitivity [41].

The surface chemistry of the Azide-PEDOT electrodes was investigated using XPS. Figure 4.9a shows a wide scan spectrum of an Azide-PEDOT layer where the presence of the doping ion (PF_6^-) was confirmed by the existence of the F 1s and

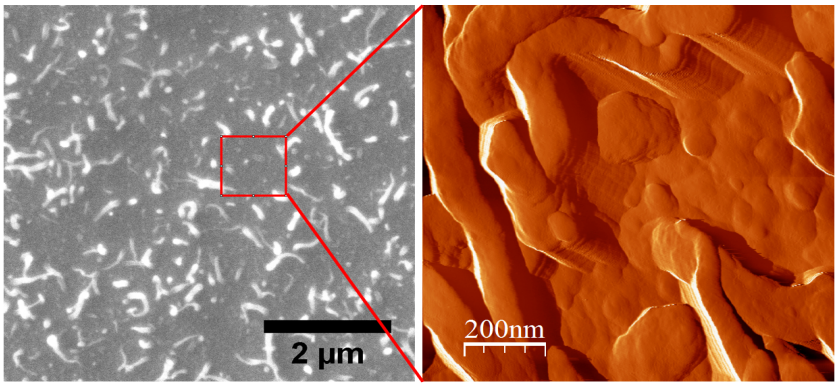

Figure 4.8: Morphological characterization of Azide-PEDOT electrodes. Left: SEM graph of an Azide-PEDOT electrode. Right: zoom of a smaller area of an Azide-PEDOT electrode by AFM.

P 2p peaks at 686.8 eV and 132.5 eV, respectively. Moreover, a 10.8% of atomic nitrogen and a 3.9% of atomic sulphur were found, being this ratio in good agreement with the proportion of sulphur and nitrogen contained in the Azide-PEDOT (1:3). Specifically, the high-resolution spectrum recorded for the core-level peak of N 1s of the Azide-PEDOT surface (Figure 4.9b) showed two deconvoluted peaks at 400.6 eV and 404.3 eV. They correspond to the two states of nitrogen in the azidomethyl group, with a peak area ratio of 2.1, as expected for the azide groups present on the surface [58, 59, 60].

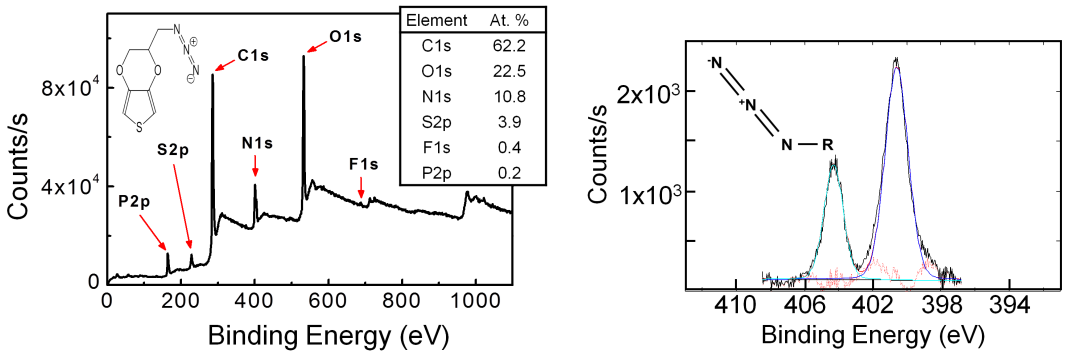

Figure 4.9: XPS analysis of Azide-PEDOT surfaces. a) wide-scan spectrum of an Azide-PEDOT surface where the presence of the doping ion was confirmed by the existence of the F 1s and P 2p peaks. b) high-resolution spectrum of the N 1s peak corresponding to the azide structure present on the surface.

Finally, the electrochemical characterization of the Azide-PEDOT electrodes was conducted again using rod-like electrodes, in Tris-HCl (20 mM, 7,0 pH) by DPV,

which is the electrochemical technique chosen for DNA detection. In Figure 4.10, a differential pulse voltammogram of an Azide-PEDOT electrode is shown, performed from +0.3 V to +1.5 V at 100 mV/s (vs. Ag/AgCl). DPV measurements were standardized, to allow comparison between results from different electrodes.*

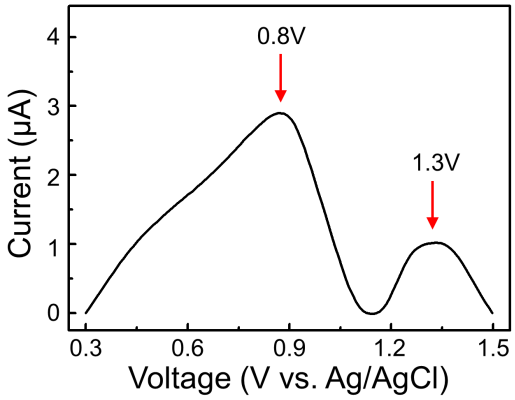

Figure 4.10: Differential pulse voltammetry of an Azide-PEDOT electrode in Tris-HCl buffer. The two oxidation peaks of the Azide-PEDOT marked with red arrows coincide with the oxidation peaks for guanine and adenine.

The oxidation of the polymer in this range showed several peaks, as described by Bäuerle's group [61]. In particular, there are two broad peaks at 0.8 V and 1.3 V approximately. These values are quite close to the reported values for the oxidation peaks of guanine (0.8 V-1.1 V) and adenine (1.1 V-1.4 V) [40, 62], thus rendering direct observation of the oxidation of G and A bases as an unfeasible method to determine the existence of DNA on the surface. Moreover, the peak close to 1.3 V could be related to the gold oxidation in aqueous solvents with halides or other complex ions, which suggested the use of moderate potentials to perform the electrochemical measurements. Therefore, DNA detection (immobilized and/or hybridized) was performed by monitoring the changes in the electrochemical behavior of the polymer during immobilization and hybridization processes, in a reduced potential window between 0.5 V and 1.0 V.

* *Mathematical treatment of raw DPV measurements:*
Raw data were analyzed with GPES 4.7 software package, using the Savitzky and Golay filter, followed by the moving average baseline correction (peak width of 0.01) provided by the software. Same corrections will be applied to all DPV measurements recorded in the following.

Summarizing, the fabrication of Azide-PEDOT electrodes from the electropolymerization of Azide-EDOT monomers was presented here. Morphological, chemical and electrochemical characterization of Azide-PEDOT surfaces was conducted, revealing the good performance of the modified polymer for sensing applications. Moreover, this fabrication strategy resulted in a ready to use azide-modified polymer, which will allow the direct functionalization with acetylene-terminated DNA sequences, by the fast and robust process of "Click" reaction.

4.3 IMMOBILIZATION OF "HEPATITIS C" VIRUS SEQUENCE ON AZIDE-PEDOT ELECTRODES

The immobilization of Acetylene-terminated "Hepatitis C" virus probe (HCV-probe) on the Azide-PEDOT electrodes was accomplished by applying the so called "Click" chemistry, between acetylene and azidomethyl groups. The DNA probe employed in this work was a complementary probe to a specific sequence of the "Hepatitis C" virus. Successful DNA immobilization was confirmed by X-ray photoelectron spectroscopy (XPS), time-of-flight secondary ion mass spectrometry (ToF-SIMS), water contact angle measurements and differential pulse voltammetry (DPV). Additionally, several "Click" reaction parameters like time and temperature of the reaction and some polymer parameters such as its thickness and oxidation state were adjusted in order to obtain the maximum immobilization efficiency possible.

Immobilization of HCV-probe on Azide-PEDOT electrodes was performed by means of the copper(I)-catalyzed Huisgen 1,3-dipolar cycloaddition between azidomethyl and acetylene groups, as depicted in Figure 4.11.

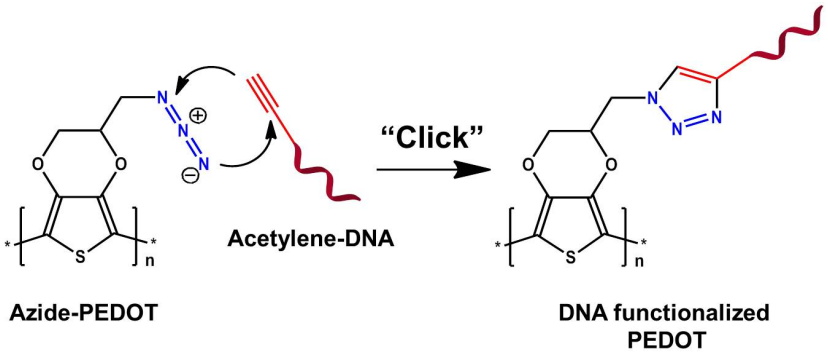

Figure 4.11: Schematics of the "Click" reaction between an Azide-PEDOT surface and an acetylene-terminated DNA probe.

The "click" reaction took place in a mixture of water and DMSO in a ratio 1:1. At least 50% of the solvent had to be water, in order to keep DNA soluble and functional. Thus, aqueous solutions (50 mM Tris-HCl buffer, pH 7.0) of HCV-probe were prepared at a concentration of 50 nM. Since the coupling reaction required a large excess of copper(I) source to proceed [63], a 100-fold excess of Cu(I) and TBTA and a 120-fold excess of DIPEA were dissolved in DMSO and added to the aqueous DNA solution.*

Then, Azide-PEDOT electrodes were incubated in the "Click" mixture and left to react for 20 to 24 hours (overnight) at room temperature. After the incubation period, electrodes were washed with a mixture of 0.05% Tween 20 in phosphate buffer saline (washing solution), to remove any HCV-probe not specifically adhered to the surface. Finally, the electrodes were rinsed with Milli-Q water to remove any remaining residue. Immediately afterwards, DNA-functionalized PEDOT surfaces were subjected to several studies to determine the success of the functionalization process.

* *Immobilization details:*
50 mM Tris-HCl and DMSO in a 1:1 ratio.
50 nM HCV-probe in 50 mM Tris-HCl.
5 μM Cu(I), 5 μM TBTA and 6 μM DIPEA in DMSO.

Fig.4.12 shows the XPS high-resolution spectra of the core-level peak of N 1s for an Azide-PEDOT surface (Fig.4.12a), and a DNA-functionalized PEDOT surface (Fig.4.12b).

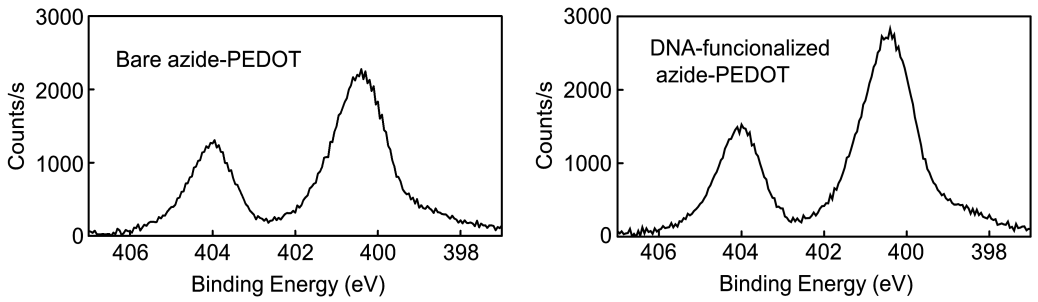

Figure 4.12: XPS high-resolution spectra of the core-level peak of N 1s for a bare Azide-PEDOT electrode and a DNA-functionalized PEDOT electrode. The area ratio between the two peaks at 400.6 eV and at 404.3 eV increased for DNA-functionalized PEDOT surface, indicating the successful DNA attachment to the polymer surface.

The polymer surfaces were prepared on gold-coated silicon wafers. As previously determined (section 4.2.2 of this chapter), an Azide-PEDOT surface presents two well resolved N 1s peaks at 400.6 eV and 404.3 eV, whose ratio is close to 2 (exactly 2.1 in this work). However, after the "Click" reaction took place, the peak at 404.3 eV decreased in favor of the lower energy peak (400.6 eV). This is likely due to the formation of triazoles and the incorporation of nitrogen contained in the HCV-probe [60, 64]. For Azide-PEDOT surfaces coupled with HCV-probe, the ratio between the two nitrogen peaks rose to 2.6 (an increase of approx. 19%), suggesting the partial functionalization of the polymer.

Additionally, ToF-SIMS analyses were performed on different polymer surfaces, namely "No DNA" (neither DNA nor acetylene were added to the reaction), "DNA without acetylene" (DNA without acetylene were added to the reaction) and "Acetylene-DNA" (HCV-probe probe was added to the reaction). Figure 4.13 shows the superposition of the three ToF-SIMS mass spectra (normalized to the total intensity of the spectra), in which only the Azide-PEDOT surface reacted with HCV-probe exhibited significant contributions of ion fragments representative of DNA (PO_2^-, PO_3^- and $PH_2O_4^-$) [64, 65]. On the other hand, samples on which the "Click" reaction did not occur (because of the absence of acetylene in the DNA probe or because no DNA at all was in the reaction mixture) showed negligible amounts of such ions. This suggested the successful immobilization of DNA probes carrying acetylene groups, with negligible presence of non-specifically adsorbed DNA.

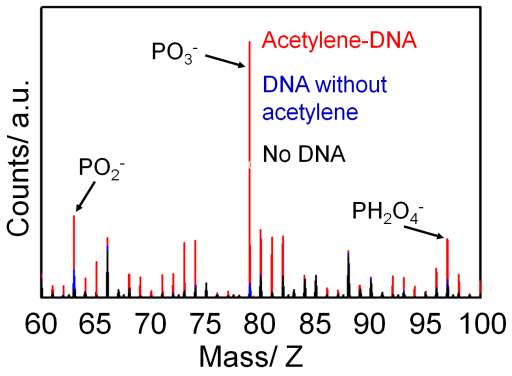

Figure 4.13: ToF-SIMS spectra of Azide-PEDOT surfaces incubated with different immobilization solutions. Black spectrum represents an Azide-PEDOT electrode incubated in a solution free of DNA, blue spectrum represents an Azide-PEDOT electrode incubated in a solution with a DNA without acetylene and red spectrum represents an Azide-PEDOT electrode incubated in a solution with the acetylene-terminated DNA (HCV-probe).

This result is in good agreement with the alternative study performed on the same surfaces by water contact angle measurements, which provided qualitative information about the differences between the mentioned surfaces. The value of the water contact angle decreased from 67.4° ± 0.5° for "No DNA" samples (neither DNA nor acetylene were added to the reaction), to 58.3° ± 0.5° for "HCV-probe" samples (HCV-probe were added to the reaction), on which the "Click" reaction took place. This change was attributed to the hydrophilic nature of DNA attached to the surface [64]. Moreover, water contact angle measurements of "acetylene-free DNA" samples (DNA probes without acetylene were added to the reaction) showed constant values (67.2° ± 1.2°), comparable to "No DNA" samples, indicating again negligible adsorption of the non-specific DNA on Azide-PEDOT surfaces.

Furthermore, in order to corroborate the previous results by electrochemical techniques, DPV measurements were conducted on Azide-PEDOT rod-like electrodes, which were incubated under the previous conditions ("No DNA", "acetylene-free DNA" and "HCV-probe"). DPV measurements were performed between +0.5 V and +1.0 V at 100 mV/s (vs. Ag/AgCl reference electrode) in 20 mM Tris-HCl buffer at room temperature. Figure 4.14 shows the standarized DPV measurements of the three types of samples.

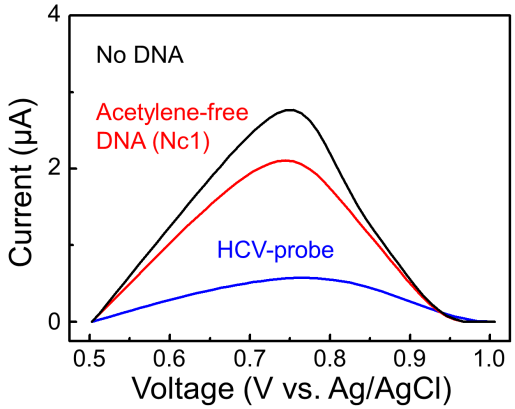

Figure 4.14: Differential pulse voltammetry of "Click" reaction. The "HCV-probe" sample (blue line) showed a decreased electroactivity as compared with non-functionalized samples, "acetylene-free DNA" (red line) and "No DNA" (black line).

The electroactivity of the "HCV-probe" samples (where the "click" reaction was accomplished) showed a big decrease compared to the "No DNA" samples (control samples, where there is no DNA at all). This is likely due to the bonding formation of HCV-probe, which acts as insulating layer on the polymeric film,

impeding ion exchange and hence reducing the electrochemical activity of the polymer [45, 66]. On the other hand, "acetylene-free DNA" samples, i.e. where the DNA probes were not anchored to the surface, did not show such large electrochemical change. This indicates that proper immobilization ("Click" reaction) was only accomplished when HCV-probe was used.

Finally, once the immobilization process was demonstrated by different techniques, key conditions such as the reaction time, reaction temperature, polymer thickness and oxidation state of the polymer were investigated, seeking for an improved immobilization efficiency.

It has been shown that when "Click" reactions are performed without the use of any catalyst, the reactions proceed in a slow manner, requiring the use of high temperatures and long reaction times to increase the yields [67]. This suggested that these two parameters (reaction time and temperature) play an important role in the efficiency of the immobilization process [68, 69, 70]. Electrochemical results, as the ones presented here in Figure 4.14, suggested that larger electrochemical changes of the polymer behaviour after the immobilization process were related to higher surface blockage and thus higher immobilization proportions. Therefore, the electrochemical change of the polymer after a certain "Click" reaction was evaluated against its control experiment ("Click" reaction using a DNA without acetylene) by DPV measurements. By alternatively varying the reaction parameters (time, temperature, oxidation state and polymer thickness), it was possible to select the optimal conditions that resulted in larger electrochemical changes of the polymer.

The electrochemical change of the polymer was evaluated after 2 h and 20 - 24 h of "Click" reaction, then at room temperature and 45°C, later by using reduced (-0.85 V) and oxidized (+0.6 V) polymers and finally with thin (grown by 2 polymerization cycles as described in section 4.2 of this chapter) and thick (grown by 8 polymerization cycles as described in section 4.2 of this chapter) polymer electrodes.*

* *Optimizing immobilization conditions:*
Reaction Time: experiments were conducted at R.T., polymer thickness corresponding to 2 polymerization scans and reduced state of the polymer (-0.6 V).
Reaction Temperature: experiments were conducted for 20 - 24 h, polymer thickness corresponding to 2 polymerization scans and reduced state of the polymer (-0.6 V).
Oxidation state: experiments were conducted at R.T., for 20 - 24 h and polymer thickness corresponding to 2 polymerization scans.
Polymer Thickness: experiments were conducted at R.T., for 20 - 24 h and reduced state of the polymer (-0.6 V).

Figure 4.15 shows the relative current changes of Azide-PEDOT electrodes where "Click" reaction took place, against their control experiments under the same conditions. The largest current change was taken as reference (100%).

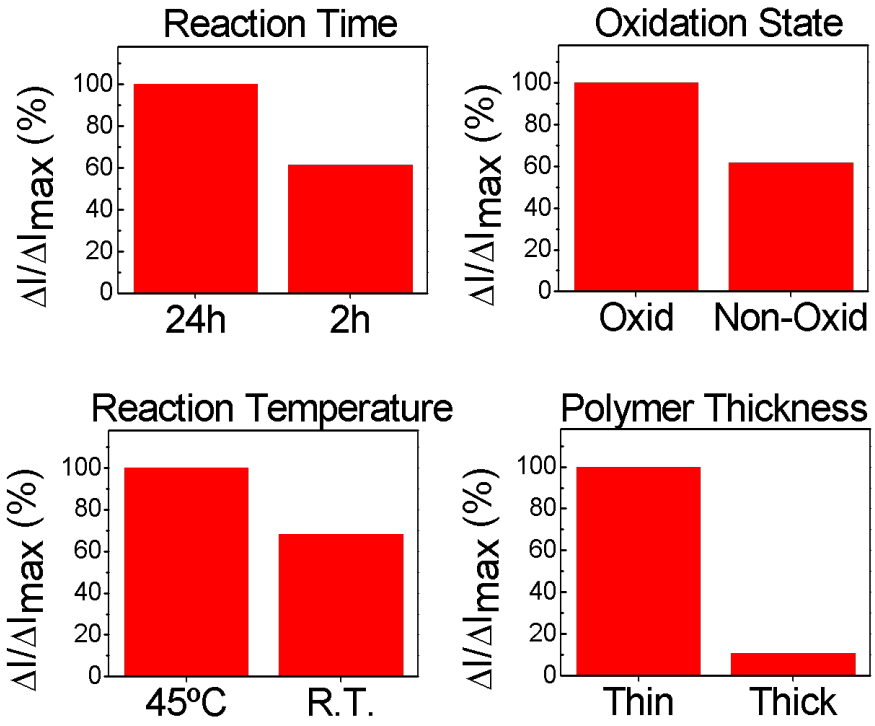

Figure 4.15: Optimization experiments of the immobilization reaction. When changing a reaction parameter, the rest of parameters were kept constant. The best results for the immobilization reaction were achieved after 24h of reaction at 45ºC, using thin polymers in their oxidized state.

One can observe how indeed, as reported by literature, the use of longer reaction times and higher temperatures results in larger electrochemical changes in the polymer behaviour. The use of shorter times and room temperatures does not improve the response of the polymer to the HCV-probe, which in those cases remains about the 60 - 70% of the maximum response. Moreover, electrodes that were oxidized before the "Click" reaction showed higher responses to the HCV-probe than the non-oxidized electrodes (whose response remained above the 60% of the maximum response). It was attributed to the increased electrostatic affinity between the oxidized polymer (positively charged) and the negatively charged DNA backbone, which eventually would lead to a higher DNA immobilization proportion. Finally, larger changes in the electrochemical response were

recorded by using thin polymers, which is in good agreement with other works that suggest that thicker polymers may hide the changes in the electrochemical behaviour [71]. In this work, this was supported by the electrochemical response of thick polymers, which was about the 10% of the one obtained for thin polymer electrodes.

This section described, by different techniques, the successful functionalization of Azide-PEDOT surfaces with HCV-probe by "Click" chemistry. The studies conducted on Azide-PEDOT electrodes showed that non-specific adsorption of DNA was negligible and did not interfere with the electrochemical measurements, proving the robustness of the "Click" process. The optimization of the immobilization parameters was achieved after 20 - 24 h of reaction, at 45°C, using thin polymer electrodes in their oxidized state. Additionally, it was confirmed the suitability of differential pulse voltammetry (DPV) as a fast electrochemical technique to assess the DNA functionalization of Azide-PEDOT surfaces.

4.4 HYBRIDIZATION OF "HEPATITIS C" VIRUS SEQUENCES ON AZIDE-PEDOT ELECTRODES

In this section, the use of the DNA-functionalized PEDOT electrodes is presented for the development of DNA hybridization sensors. A specific sequence of the "Hepatitis C" virus was investigated. The selectivity of the sensor, at a specific concentration, was studied under exposure to several targets, including complementary, non-complementary and two base mismatch sequences. Moreover, complex mixtures of complementary and non-complementary targets were tested. The sensor was also challenged with low concentrations of the complementary target, to obtain its limit of detection. Additionally, the reusability of the sensor was investigated by applying several de-hybridization protocols.

4.4.1 *Selectivity of the DNA sensor*

When a sensor responds only to a certain target analyte, it is called highly selective. In order to investigate the selectivity of the DNA sensor developed here, the PEDOT electrodes were tested against several DNA sequences (Table 4.1), at a specific concentration.

Hybridization reactions* were conducted for 30 minutes at room temperature, using the different DNA sequences. Then, PEDOT electrodes were washed with the washing solution described in section 4.3 of this chapter, to remove any not

DNA NAME	DNA SEQUENCE
Probe (HCV-probe)	5′-*6TT TTT* TGG GGA TCC CGT ATG ATA CCC-3′
Complementary target (HCV-target)	5′-GGG TAT CAT ACG GGA TCC CCA-3′
Non-complementary target 1 (Nc1-target))	5′-CTC GAT GAC TCA ATG ACT CG-3′
Non-complementary target 2 (Nc2-target)	5′-CCC GCA CTT CAC CAC TCC TCA CCA CTT CAC GCC C-3′
Two base mismatch target (2BM-target)	5′-GGG TAT CTT ACG GCA TCC CCA-3′

Table 4.1: List of oligonucleotides. In HCV-probe, *6* represents the acetylene group and the five next *T* bases were introduced as spacers. In red mismatched bases with respect HCV-target.

hybridized DNA target. After that, the electrodes were subjected to DPV measurements. Three series of experiments were performed, where DPV measurements were recorded from 3 independent electrodes per experiment. Raw data were standardized to perform comparisons between electrodes of different batches.

Since the oxidation peaks for A and G bases were definitely not evaluated in this work, DPV measurements were performed in the previously reduced potential range (between 0.5 V and 1.0 V vs Ag/AgCl reference electrode), thus avoiding unnecessary overoxidation of the polymer. The reference for the electrochemical behaviour of the polymer was taken as the current intensity corresponding to the oxidation peak appearing at 0.8 V approximately.

* *Hybridization details:* Azide-PEDOT *electrodes previously immobilized with 50 nM* HCV-probe *were incubated with Tris-HCl 20 mM, containing 20 mM NaCl and 50 nM* DNA *hybridization sequences.*

Figure 4.16 shows corrected DPV measurements of DNA-functionalized electrodes incubated with different hybridization solutions, namely a hybridization

solution free of DNA target (single stranded, black line), a solution containing a non-complementary target (Nc1-target in Table 4.1, blue line) and a solution containing the HCV-target (red line). The highest peak intensity was observed for target-free samples, which remained almost unvarying upon exposure to non-complementary DNA. In contrast, when the electrodes were incubated with the HCV-target, the current intensity abruptly decreased, revealing a change in the electrochemical behaviour of the system. These results suggested that the hybridization did not occur when the electrodes were exposed to non-complementary target sequences since the electroactivity of the polymer did not change in comparison with the non-hybridized control. By contrast, hybridization did occur when the electrodes were exposed to HCV-target. This decrease in the current intensity for electrodes incubated with HCV-target was attributed to changes in the polymer backbone. It was reported that the formation of hydrogen bonds after completed hybridization, creates potential barriers that slow down the diffusion of ions into the polymer [28, 56, 71, 72]. This reduces the electroactivity and conductivity of the polymer backbone, which is in good agreement with the observed electrochemical behaviour.

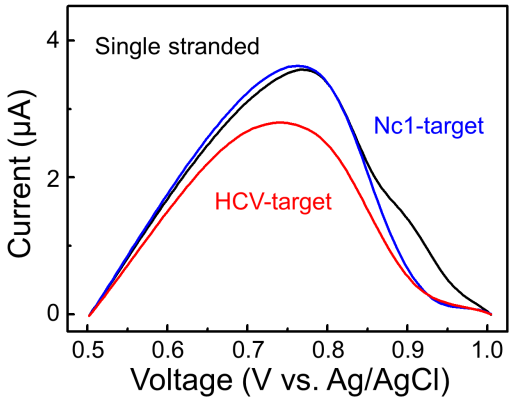

Figure 4.16: Corrected DPV measurements for DNA-functionalized PEDOT electrodes hybridized with a complementary target (HCV-target, red line), a non-complementary target (Nc1-target, blue line) and without any DNA target (Single stranded, black line).

Next step was to evaluate whether the sensor developed here was still able to detect the complementary target within a complex mixture. Therefore, a solution containing two non-complementary DNA sequences called Nc1-target and Nc2-target (see Table 4.1) and HCV-target was tested. The three target sequences were mixed at the same concentration of 50 nM, resulting in a total DNA concentration of 150 nM. Figure 4.17 shows the corrected DPV measurements of DNA-

functionalized electrodes which were incubated with a hybridization solution free of DNA (Single stranded, black line), with a solution containing the complementary sequence (HCV-target, red line), and with a solution that contained the mixture of the complementary sequence and the non-complementary sequences (Mixture, blue line). Exposing the polymer to the mixture of non-complementary and complementary sequences resulted in a similar change in electrochemical behaviour as observed before, when only HCV-target alone was used. This result proved that the DNA sensor developed here is capable of detecting the complementary target within a more complex mixture. Moreover, the sensor did not show remarkable interferences due to the presence of other non-complementary sequences, which is an important feature required for the analysis of real samples.

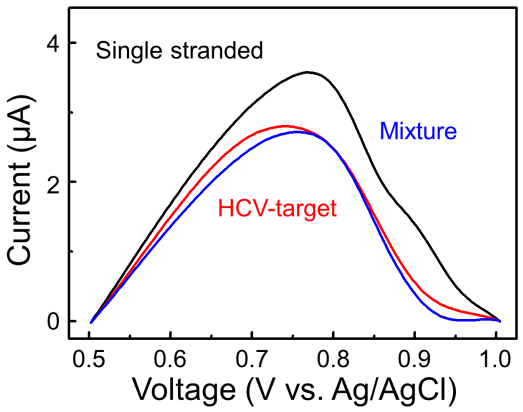

Figure 4.17: Corrected DPV measurements for DNA-functionalized PEDOT electrodes hybridized with a complementary target (HCV-target, red line), a mixture of non-complementary and complementary targets (Mixture, blue line) and without any DNA target (Single stranded, black line).

Finally, the discrimination against two-base mismatch was also studied. Figure 4.18 presents the DPV responses of the sensor to a two-base mismatch sequence (2BM-target), the one of a DNA-functionalized PEDOT electrode incubated without any target and another incubated with a fully complementary target (HCV-target). A decrease of almost half of the electrochemical signal was observed when the two-base mismatch sequence was used. Pairing between mismatched bases can occur when all the adjacent bases are perfectly matched. Although this situation is less stable, it can take place and in certain cases can be distinguished from totally matching sequences [25, 73, 74]. In this case, a strong attenuation of the electrochemical response of the polymer was observed without reaching

the value of the complementary target. The capability of distinguishing between both DNA sequences without the use of any redox label, commonly used for efficient detection of base mutations, improves the performance of the sensor in terms of costs and detection time. This is a convenient advantage for developing point-of-care-test sensors.

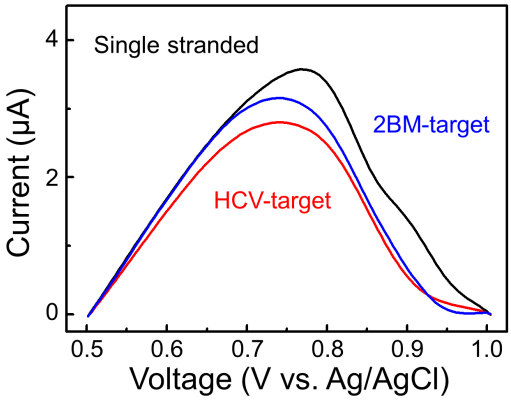

Figure 4.18: Corrected DPV measurements for DNA-functionalized PEDOT electrodes hybridized with a complementary target (HCV-target, red line), a two-base mismatch target (2BM-target, blue line) and without any DNA target (Single stranded, black line).

The selectivity of the sensor at a specific DNA concentration (50 nM) is summarized in Figure 4.19, showing the relative current changes against the not hybridized experiments. Thus, taking as reference the response of the sensor to a complementary target (100 ± 9.7%, "HCV" in Figure 4.19), the response to the non-complementary target ("NC" in Figure 4.19) did not exceed 20% (19.9 ± 3.3%), which separates the hybridization event from the non-specific DNA bonding to the surface. On the other hand, the response of the sensor to the cocktail of non-complementary and complementary targets ("Mix" in Figure 4.19) remained above 90% (90.33 ± 3.5%), which suggests that the sensor can still detect the complementary target over several non-complementary targets with good resolution. The two-base mismatch target ("2BM" in Figure 4.19) showed about 60% (58.1 ± 12.8%) of response of the total signal, permitting the distinction from the complementary and the non-complementary targets.

Thus, the DNA sensor developed in this work allows the effective discrimination between all the target sequences tested here, at a fixed concentration of 50 nM. This reveals the potential of the sensor for applications in the screening of genetic mutations and diseases, such as "Hepatitis C".

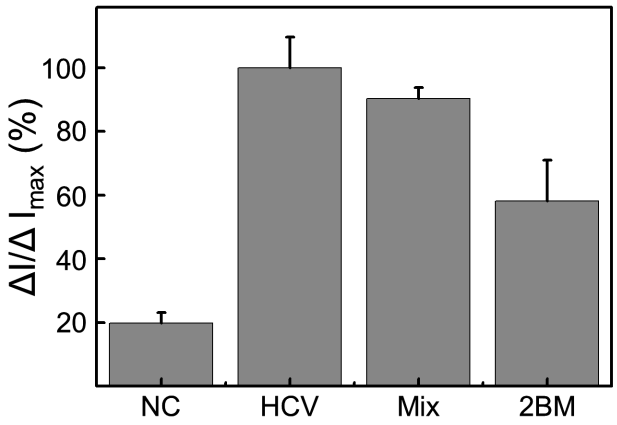

Figure 4.19: Selectivity of the DNA sensor. "NC" shows the response of the sensor to the non-complementary target. "C" shows the response to the complementary sequence (taken as reference, 100%). "Mix" shows the response of the sensor to a mixture of non-complementary (Nc1, Nc2) and complementary sequences. "Mis" is the response of the sensor to a two-base mismatch target sequence.

4.4.2 *Sensitivity of the DNA sensor*

As much as the selectivity, the sensitivity of a sensor to a concrete target sequence is important in the development of clinical devices.

The sensitivity of a sensor can be described as the smallest change of target concentration that can be detected reliably. Alternatively, the limit of detection (LOD) is used to measure the smallest concentration that can be detected with a certain precision and reproducibility. Generally, the precision is defined as the concentration producing a signal 3 times the standard deviation of a series of blank readings. This definition is equivalent to a 99% confidence level. Therefore, the Limit Of Detection (LOD) is a function of sensitivity and signal stability. Here, LOD is were calculated to perform comparisons with other reported works.

Hybridization experiments were performed for 30 minutes at room temperature, using different concentrations of HCV-target, from 20 nM to 1 nM.* Afterwards, PEDOT electrodes were washed with the washing solution and the electrodes were subjected to DPV measurements, using 3 independent electrodes per experiment. At

** Hybridization solution:*
Azide-PEDOT *electrodes previously immobilized with 20 nM* HCV-probe *were incubated with 20 mM Tris-HCl, containing 20 mM NaCl and* HCV-target *at several concentrations namely 20 nM, 10 nM, 5 nM, 2.5 nM and 1 nM.*

least three series of experiments were conducted. Raw data were standardized to perform comparisons between electrodes of different batches.

Figure 4.20 shows a gradual decrease in the oxidation current of the polymer when increasing the concentration of HCV-target. This suggested a change in the polymer backbone produced by hybridization, which is increasing with higher target concentrations. Moreover, the oxidation peaks of the polymer were shifted towards more positive potentials for increasing concentrations, which is in agreement with the formation of hydrogen bonds (potential barriers) that slow down the diffusion of ions through the polymer. These results evidenced the dependence of the electrochemical behaviour of the polymer on changes in the target concentration, showing its suitability to perform quantification experiments necessary for clinical analyses.

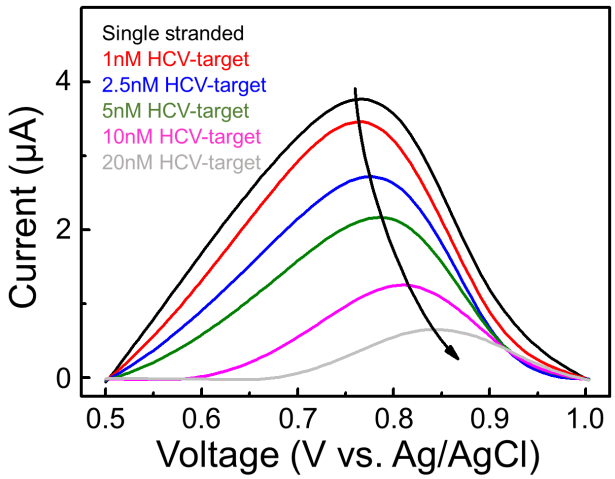

Figure 4.20: Corrected DPV measurements for DNA-functionalized PEDOT electrodes hybridized with different concentrations of complementary target, from 0 nM to 20 nM.

Figure 4.21 shows the calibration curve obtained from the quantitative electrochemical measurements, taken from at least three independent electrodes per concentration. When the current intensity is plotted against the logarithm of the target concentration, the graph is linear with a correlation coefficient of 0.990. The limit of detection (LOD) was obtained by application of the equation $Y_{LOD} = Y_B + 3\sigma_B$ and the regression equation Y(X) = 3.878 - 1.563X of the plot. Where Y_B represents the main current for the blank experiment (hybridization experiment without DNA target) and σ_B is the standard deviation of the blank experiment. In this way, a limit of detection of about 0.13 nM was estimated. This result is com-

parable to values achieved by other electrochemical DNA sensors with enhanced sensitivity, provided by the use of redox indicators or miniaturized systems [41].

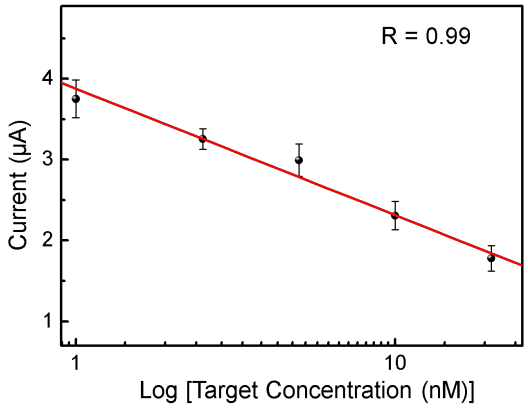

Figure 4.21: Calibration curve for the oxidation signal of DNA-functionalized PEDOT electrodes, hybridized at different concentrations of complementary target. Current intensity (Y = I) is plotted against the logarithm of the target concentration (X = log [Target Concentration]).

The PEDOT sensor presented here is therefore showing low limits of detection for the recognition of specific DNA sequences (down to the nanomolar range), without the need of labelling or complicated microfabrication methodologies. In addition, this work represents an important contribution to the label free detection of the "Hepatitis C" virus, since there are very few reports in this field. The existing reports related to label free electrochemical sensors for the "Hepatitis C" virus are based on either the oxidation signal of guanine or on the electrochemical behavior of conducting polymers [75]. On one side, Pournaghi-Azar et al. developed a label free sensor for the "Hepatitis C" virus, based on the detection of guanine oxidation, with a limit of detection of 6.5 nM. This sensor showed to be as sensitive as other DNA sensors of the same kind (sensors based on the guanine oxidation signal), but 50 times less sensitive than the PEDOT sensor presented here [62]. On the other hand, to the best of our knowledge, there is only a single report concerning the electrochemical label free detection of the "Hepatitis C" virus, using conducting polymers. This sensor, although shows very low limits of detection (10^{-21} M), includes the use microelectrode fabrication technology and is based on the electropolymerization of a probe-modified pyrrole monomer [76]. Instead, the system developed here uses a straightforward fabrication strategy that avoids the use of complex equipment and processes. Moreover, the

fabrication ends in a readily azide-functionalized platform for the further probe immobilization, which preserves the HCV-probe integrity from eventual damages during the electrochemical synthesis. Additionally, the PEDOT sensor offers excellent limits of detection, taking into account that the concentration analyzed in clinical tests for the "Hepatitis C" virus in serum or plasma is usually around 1.5 - 2.0 µM [77].

However, new trends in DNA sensors seek even lower limits of detection, for which nanomaterials, such as nanoparticles, carbon nanotubes, nanowires, etc., showed to be useful [78, 79, 80]. The combination of conducting polymers with those nanomaterials have shown to provide maximum benefit of the surface and electrical properties of the device, which could be applied on the presented sensor. Nevertheless, this would mean an increase in processing steps, time and cost and is therefore out of the scope of this chapter, although it was envisaged as future work.

4.4.3 *Reutilization of the DNA sensor*

Device reutilization is a crucial issue in biosensors. The importance of reutilizing a sensor after a first detection process is enormous, regarding the cost of the device and its application to real point-of-care-tests [44].

Since the DNA probe is covalently grafted to the polymer surface, the method of choice for reutilization is the de-hybridization of the complementary target sequence. However, both the complete de-hybridization of the system and also the re-hybridization are very important. It is desirable to achieve the same yields of hybridization after a recycling step, for many times, which depends on the resistance of the sensing device (transducer or DNA probe) upon degradation [27].

Techniques typically used for de-hybridization, i.e. breaking the hydrogen bonds of the DNA double strand, are based on either the use of very basic pHs (alkaline denaturation with pH values from 8 to 12.5) [81] or on the increment of the temperature to the melting point of the sequence (thermal denaturation) [82]. The use of solutions with very low pHs has also been reported [83]. However, this method ends in the depurination of DNA (release of purines) and the loss of up to 50% of the information of the strands.

In this thesis, the de-hybridization of the PEDOT sensors was attempted by two different protocols based on alkaline and thermal denaturation.

First, hybridized electrodes were de-hybridized by using a 10 mM solution of sodium hydroxide (NaOH, 12 pH) during 10 minutes. Then, the electrodes were washed for 5 minutes in Milli-Q water and for another 5 minutes in the washing solution described in 4.3, to remove any DNA target not specifically adsorbed on the surface. Then, the electrodes were subjected to DPV measurements. Results of de-hybridization (De-Hyb) experiments were compared with the ones obtained after the first hybridization of the system (1st-Hyb) and with the ones obtained after the second hybridization of the system, following de-hybridization (2nd-Hyb). Figure 4.22 shows the relative current intensity of the electrodes with respect to the blank experiment (no DNA was used for first hybridization, second hybridization and de-hybridization experiments).

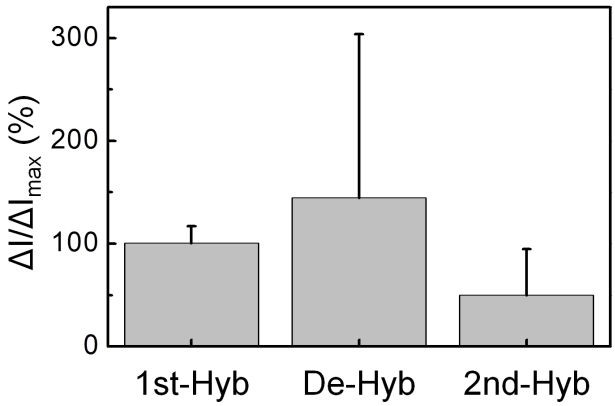

Figure 4.22: Reutilization of DNA sensor by alkaline protocol. The graph shows the relative response of the sensor with respect the blank experiment (without using DNA). 1st-Hyb: first hybridization of the system, whose response is taken as reference value (100%). De-Hyb: de-hybridization experiment and 2nd-Hyb: second hybridization experiment after de-hybridization.

A successful de-hybridization assay would result in a decrease of the relative current intensity, meaning the resemblance between the de-hybridized experiment and the blank. However, the experiments performed at this point using basic solutions, showed an increase of the relative current intensity. This means that the differences between the de-hybridization experiment and the blank were even higher than before the process. Moreover, the results of the second hybridization, after de-hybridization, showed a hybridization yield of only 50% as compared to the first hybridization process, being an insufficient response which cannot be considered a successful regeneration of the sensor. It is proposed that the process of alkaline denaturation used here affects the polymer backbone either by degrading it or because Na^+ residues remain in the porous

structure of the polymer. The increased ion contents of the system would affect the electrochemical response in a non-homogeneous way, as evidenced by the large standard deviation values of the de-hybridization experiment. Thus, it was concluded that the alkaline protocol was not suitable for the reutilization of the polymeric device developed here and the use of thermal denaturation, as an alternative method to reuse the DNA sensors, was investigated.

Here, hybridized sensors were incubated with Milli-Q water at 80°C for 5 minutes.* Then, the electrodes were washed as described before, with the washing solution. Afterwards, DPV measurements were conducted and compared with the hybridization experiment, before and after denaturation.

Figure 4.23 shows the relative current intensity of the electrodes with respect to the blank experiment, as in the previous case. Here, a smaller difference between the de-hybridized electrodes and the blank was observed, which at first indicates the successful de-hybridization of the system. However, the second hybridization process after the de-hybridization step, showed a response of the sensor of about 67% of the initial hybridization, which is still far from being considered an effective regeneration of the system.

** De-hybridization temperature:*
The melting temperature of the "Hepatitis C" virus sequence is 56.3°C [84]. An exceeding temperature of 80°C was used in order to completely ensure the denaturation of the double strand.

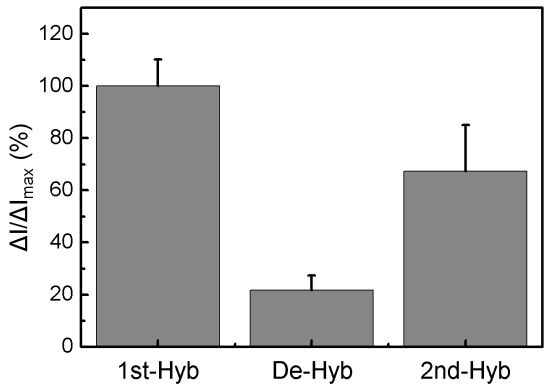

Figure 4.23: Reutilization of DNA sensor by thermal protocol. The graph shows the relative response of the sensor with respect the blank experiment (without using DNA). 1st-Hyb: first hybridization of the system, whose response is taken as reference value (100%). De-Hyb: de-hybridization experiment and 2nd-Hyb: second hybridization experiment after de-hybridization.

These are preliminary results, which need optimization. However, to the best of our knowledge, there are very few studies of DNA sensor based on conducting polymers which report successful regeneration and none of them correspond to label free sensors. Arora *et al*. [27] used thermal denaturation to regenerate polyaniline based DNA hybridization sensors (using methylene blue as redox intercalator) up to 7 times. However, they report a response to complementary targets of only 17% after the 7th regeneration process and first signs of polymer detachment after the 5th regeneration process.

Therefore, although the results obtained here are not ideal, they provide a better understanding of the regeneration process in polymer-based DNA sensors, indicating a promising future by performing more tests in this direction.

4.5 CONCLUSIONS

In this chapter, a highly selective and sensitive electrochemical label-free DNA hybridization sensor is presented in a new approach. This work proposes the use of Azide-PEDOT electrodes as platforms, using "Click" reaction for the immobilization of an acetylene-DNA probe, which is complementary to a specific sequence of the "Hepatitis C" virus. An Azide-EDOT precursor monomer was electropolymerized on top of gold electrodes, thus performing both the fabrication and functionalization of the polymer in a single step. Morphological, chemical and electrochemical characterization of Azide-PEDOT surfaces was conducted, revealing the good performance of the modified polymer for sensing applications. Moreover, this fabrication strategy resulted in a ready to use azide-modified polymer, which allowed the direct functionalization with acetylene-terminated DNA sequences by the fast and robust covalent coupling reaction known as "Click" reaction. This fabrication method preserved the integrity of the DNA probe from the synthetic process.

The hybridization events were then detected by differential pulse voltammetry (DPV), by evaluating the electroactivity of the polymer after the DNA recognition process. The selectivity of the Azide-PEDOT electrochemical sensor was evaluated at a specific concentration of 50 nM. Using complementary and non-complementary sequences, a clear distinction of both events in about 80% was possible. The response of the sensor to a mixture of non-complementary and complementary targets remained above 90% as compared to the complementary response, which suggests that the sensor can still detect the complementary target within a complex mixture with good resolution. A two-base mismatch target

showed a response of about 60% of the total signal, permitting the distinction from the complementary and the non-complementary targets. Therefore, the DNA sensor developed in this work allows the effective discrimination between all the target sequences tested at a fixed concentration, revealing its potential for applications in the screening of genetic mutations and diseases, such as "Hepatitis C" virus. The limit of detection (LOD) for complementary targets resulted in about 0.13 nM, which is one order of magnitude smaller than other reported label free sensors of the same kind. Additionally, the reusability of the sensor was studied with positive preliminary results, for protocols using thermal denaturation of DNA. The electrode reusability needs further improvement but contributes with new results to the regeneration of label free DNA sensors based on conducting polymers.

These results are very promising for the development of polymeric label free DNA hybridization sensors, which can be applied to point-of-care-tests due to their high selectivity and sensitivity. Moreover, the combination of conducting polymers with nanomaterials represents the next step for the further improvements of this sensor, which can be feasibly implemented in the system developed here.

4.6 REFERENCES

[1] Susan R Mikkelsen. "Electrochemical Biosensors for DNA Sequence Detection." In: *Electroanalysis* 8 (1996), pp. 15–19 (cit. on p. 112).

[2] Minhaz Uddin Ahmed and Mosharraf Hossain. "Electrochemical Biosensors for Medical and Food Applications." In: *Electroanalysis* (2008), pp. 616–626. DOI: 10.1002/elan.200704121 (cit. on p. 112).

[3] *National Human Genome Research Institute*. URL: www.genome.gov/10001772 (cit. on p. 112).

[4] Xin-hua Lin et al. "Electrochemical DNA biosensor for the detection of short DNA species of Chronic Myelogenous Leukemia by using methylene blue." In: *Talanta* 72 (2007), pp. 468–471. DOI: 10.1016/j.talanta.2006.11.015 (cit. on p. 112).

[5] Sandip Kumar Dash and Minakshi Sharma. "rmpM Genosensor for Detection of Human Brain Bacterial Meningitis in Cerebrospinal Fluid." In: *Applied Biochemistry and Biotechnology* (2013). DOI: 10.1007/s12010-013-0339-3 (cit. on p. 112).

[6] Gopala Krishna Darbha et al. "Gold-Nanorod-Based Sensing of Sequence Sepecific HIV-1 Virus DNA by Using Hyper-Rayleigh Scattering Spectroscopy." In: *Chemistry A European Journal* 14 (2008), p. 3896 (cit. on p. 112).

[7] F Lucarelli et al. "Electrochemical DNA biosensor as a screening tool for the detection of toxicants in water and wastewater samples." In: *Talanta* 56 (2002), pp. 949–957 (cit. on p. 112).

[8] Masaaki Kobayashi et al. "Electrochemical DNA quantification based on aggregation induced by Hoechst 33258." In: *Electrochemistry Communications* 6 (2004), pp. 337–343. DOI: 10.1016/j.elecom.2004.01.012 (cit. on p. 112).

[9] S Rauf et al. "Electrochemical approach of anticancer drugs–DNA interaction." In: *Journal of Pharmaceutical and Biomedical Analysis* 37 (2005), pp. 205–217. DOI: 10.1016/j.jpba.2004.10.037 (cit. on p. 112).

[10] Ray Wu. "Nucleotide Sequence Alanlysis of DNA." In: *Nature* 236 (1972), pp. 198–200 (cit. on p. 112).

[11] Allan M Maxam and Walter Gilbert. "A new method for sequencing DNA." In: *Proceedings of the National Academy of Sciences* 74.2 (1977), pp. 560–564 (cit. on p. 112).

[12] F. Sanger and S. Nicklen. "DNA sequencing with chain-terminating." In: *Proceedings of the National Academy of Sciences* 74.12 (1977), pp. 5463–5467 (cit. on p. 112).

[13] R.B. Wallace et al. "The use of synthetic oligodeoxyribonucleotides to phi chi 174 DNA: the effect of single base pair mismatch." In: *Nucleic acids research* 9.4 (1981), p. 879 (cit. on p. 112).

[14] A N N Caviani Pease et al. "Light-generated oligonucleotide arrays for rapid DNA sequence analysis." In: *Proceedings of the National Academy of Sciences* 91.May (1994), pp. 5022–5026 (cit. on p. 112).

[15] James D. Watson and Francis H. Crick. "Molecular Structure of Nucleic Acids." In: *Nature* (1953), p. 4356 (cit. on p. 113).

[16] M. I. Pividori, A. Merkoçi, and S. Alegret. "Electrochemical genosensor design : immobilisation of oligonucleotides onto transducer surfaces and detection methods." In: *Biosensors & bioelectronics* 15 (2000), pp. 291–303 (cit. on pp. 114, 116, 117).

[17] Hui Peng et al. "DNA Hybridization Detection with Blue Luminescent Quantum Dots and." In: *Journal of the American Chemical Society* c (2007), pp. 3048–3049 (cit. on p. 114).

[18] T Livache et al. "Polypyrrole electrospotting for the construction of oligonucleotide arrays compatible with surface plasmon resonance hybridization detection." In: *Synthetic metals* 121 (2001), pp. 1443–1444 (cit. on p. 114).

[19] Naomi Flowers Campbell, Jeffrey A. Evans, and Newton C. Fawcett. "Detection of Poly (U) hybridization using Azido modified Poly (A) coated piezoelectric crystals." In: *Biochemical and Biophysical Research Communications* 196 (1993), pp. 858–563 (cit. on p. 114).

[20] Jungyul Sakong, Heesu Roh, and Yongrae Roh. "Surface Acoustic Wave DNA Sensor with Micro-Fluidic Channels." In: *Jpn J Appl Phys* 46.7 (2007), pp. 4729–4733. ISSN: 0021-4922. DOI: 10.1143/JJAP.46.4729 (cit. on p. 114).

[21] Xiaojun Zhao, Rovelyn Tapec-dytioco, and Weihong Tan. "Ultrasensitive DNA Detection Using Highly Fluorescent Bioconjugated Nanoparticles." In: *Journal of the American Chemical Society* Figure 2 (2003), pp. 11474–11475 (cit. on p. 114).

[22] Rong Hu et al. "Multicolor Fluorescent Biosensor for Multiplexed Detection of DNA." In: *Analytical chemistry* 86 (2014), pp. 5009–5016 (cit. on p. 114).

[23] Jason R Epstein, Israel Biran, and David R Walt. "Fluorescence-based nucleic acid detection and microarrays." In: *Analytica Chimica Acta* 469 (2002), pp. 3–36 (cit. on p. 114).

[24] M Mir, Antoni Homs, and Josep Samitier. "Integrated electrochemical DNA biosensors for lab-on-a-chip devices." In: *Electrophoresis* 30 (2009), pp. 3386–3397. DOI: 10.1002/elps.200900319 (cit. on p. 115).

[25] Hui Peng et al. "Conducting polymers for electrochemical DNA sensing." In: *Biomaterials* 30.11 (Apr. 2009), pp. 2132–48. DOI: 10.1016/j.biomaterials.2008.12.065 (cit. on pp. 115–117, 134).

[26] Tae-young Lee and Yoon-bo Shim. "Direct DNA Hybridization Detection Based on the Oligonucleotide-Functionalized Conductive." In: *Analytical chemistry* 73.22 (2001), pp. 5629–5632 (cit. on p. 115).

[27] Kavita Arora et al. "Ultrasensitive DNA hybridization biosensor based on polyaniline." In: *Biosensors and bioelectronics* 23 (2007), pp. 613–620. DOI: 10.1016/j.bios.2007.07.010 (cit. on pp. 115, 139, 142).

[28] Aude-Emmanuelle Navarro et al. "Characterization of PEDOT film functionalized with a series of automated synthesis ferrocenyl-containing oligonucleotides." In: *Tetrahedron* 61.16 (Apr. 2005), pp. 3947–3952. DOI: 10.1016/j.tet.2005.02.058 (cit. on pp. 115, 133).

[29] Joseph Wang, Guodong Liu, and Arben Merkoc. "Electrochemical Coding Technology for Simultaneous Detection of Multiple DNA Targets." In: *Journal of the American Chemical Society* 125 (2003), pp. 3214–3215 (cit. on p. 115).

[30] Yongchao Zhang, Hyug-han Kim, and Adam Heller. "Enzyme-Amplified Amperometric Detection of 3000 Copies of DNA in a 10-microL Droplet at 0.5 fM Concentration." In: *Analytical chemistry* 75.13 (2003), pp. 3267–3269 (cit. on p. 115).

[31] Ningning Zhu et al. "Electrochemically fabricated polyaniline nanowire-modified electrode for voltammetric detection of DNA hybridization." In: *Electrochimica Acta* 51.18 (May 2006), pp. 3758–3762. ISSN: 00134686. DOI: 10.1016/j.electacta.2005.10.038 (cit. on p. 115).

[32] Kelly M Millan and Susan R Mikkelsen. "Sequence-Selective Biosensor for DNA Based on Electroactive Hybridization Indicators." In: *Analytical chemistry* (1993), pp. 2317–2323 (cit. on p. 115).

[33] Adam B Steel, Tonya M Herne, and Michael J Tarlov. "Electrochemical Quantitation of DNA Immobilized on Gold." In: *Analytical chemistry* 70.22 (1998), pp. 4670–4677 (cit. on p. 115).

[34] Yanli Zhang et al. "Electrochemical DNA Biosensor Based on the Proximity-Dependent Surface Hybridization Assay." In: *Analytical chemistry* 81.5 (2009), pp. 1982–1987 (cit. on p. 115).

[35] Boon Ping Ting et al. "Biosensors and Bioelectronics A DNA biosensor based on the detection of doxorubicin-conjugated Ag nanoparticle labels using solid-state voltammetry." In: *Biosensors & bioelectronics* 25 (2009), pp. 282–287. DOI: 10.1016/j.bios.2009.07.005 (cit. on p. 115).

[36] Nai-ying Wu et al. "Direct electrochemical sensor for label-free DNA detection based on zero current potentiometry." In: *Biosensors and Bioelectronic* 39.1 (2013), pp. 210–214. ISSN: 0956-5663. DOI: 10.1016/j.bios.2012.07.038 (cit. on p. 116).

[37] Emil Palecek. "Oscillographic Polarography of Highly Polymerized Deoxyribonucleic Acid." In: *Nature* 188.19 (1960), p. 656 (cit. on p. 116).

[38] Steen Steenken et al. "How Easily Oxidizable Is DNA? One-Electron Reduction Potentials of Adenosine and Guanosine Radicals in Aqueous Solution." In: *Journal of the American Chemical Society* 7863.20 (1997), pp. 617–618 (cit. on p. 116).

[39] Burcu Meric et al. "Indicator-Free Electrochemical DNA Biosensor Based on Adenine and Guanine Signals." In: *Electroanalysis* 14.18 (2002), pp. 1245–1250 (cit. on p. 116).

[40] Arzum Erdem et al. "Rigid carbon composites: a new transducing material for label-free electrochemical genosensing." In: *Journal of Electroanalytical Chemistry* 567.1 (June 2004), pp. 29–37. DOI: 10.1016/j.jelechem.2003.10.049 (cit. on pp. 116, 124).

[41] Bhuvaneswari Kannan et al. "High-sensitivity, label-free DNA sensors using electrochemically active conducting polymers." In: *Analytical chemistry* 83.9 (May 2011), pp. 3415–21. ISSN: 1520-6882. DOI: 10.1021/ac1033243 (cit. on pp. 116, 122, 138).

[42] Nirmal Prabhakar, Harpal Singh, and Bansi D. Malhotra. "Nucleic acid immobilized polypyrrole-polyvinylsulphonate film for Mycobacterium tuberculosis detection." In: *Electrochemistry Communications* 10.6 (June 2008), pp. 821–826. DOI: 10.1016/j.elecom.2008.03.006 (cit. on p. 116).

[43] By Francis Garnier. "Functionalized Conducting Intelligent Materials." In: *Advanced Materials* 4 (1989), pp. 117–121 (cit. on p. 116).

[44] A. Ramanavicius, A. Ramanaviciene, and A. Malinauskas. "Electrochemical sensors based on conducting polymer-polypyrrole (Review)." In: *Electrochimica Acta* (2006), pp. 6025–6037 (cit. on pp. 117, 139).

[45] Liz a Thompson et al. "Label-free DNA hybridization probe based on a conducting polymer." In: *Journal of the American Chemical Society* 125.2 (Jan. 2003), pp. 324–5. DOI: 10.1021/ja027929z (cit. on pp. 117, 129).

[46] Laura Poole-Warren et al. "Development of bioactive conducting polymers for neural interfaces." In: *Expert review of medical devices* 7.1 (Jan. 2010), pp. 35–49. DOI: 10.1586/erd.09.58 (cit. on p. 117).

[47] A Dupont-Filliard et al. "Biotin/avidin system for the generation of fully renewable DNA sensor based on biotinylated polypyrrole film." In: *Analytica Chimica Acta* 515 (2004), p. 271 (cit. on p. 117).

[48] Thierry Livache et al. "Preparation of a DNA matrix via an electrqchemically directed copolymerization of pyrrole and oligonucleotides bearing a pyrrole group." In: *Nucleic acids research* 22.15 (1994), pp. 2915–2921 (cit. on p. 117).

[49] Hang-Beom Bu et al. "Efficient post-polymerization functionalization of conducting poly(3,4-ethylenedioxythiophene)(PEDOT) via "click"-reaction." In: *Tetrahedron* 67 (2011), pp. 1114–1125. DOI: 10.1016/j.tet.2010.12.022 (cit. on p. 117).

[50] Liyuan Liang and Didier Astruc. "The copper (I) -catalyzed alkyne-azide cycloaddition (CuAAC) "click" reaction and its applications . An overview." In: *Coordination Chemistry Reviews* 255.23-24 (2011), pp. 2933–2945. DOI: 10.1016/j.ccr.2011.06.028 (cit. on p. 117).

[51] Ryeo Yun Hwang et al. "Suppression of the loss of an electroactive dopant from polypyrrole by using a non-aqueous electrolyte of dopant-phobicity." In: *Journal of Electroanalytical Chemistry* 657.1-2 (July 2011), pp. 181–186. DOI: 10.1016/j.jelechem.2011.03.028 (cit. on p. 119).

[52] Petr Novák. "Limitations of polypyrrole synthesis in water and their causes." In: *Electrochimica Acta* 37.7 (June 1992), pp. 1227–1230. DOI: 10.1016/0013-4686(92)85060-X (cit. on p. 119).

[53] Chun-Guey Wu and Ching-Yuh Chen. "Chemical deposition of ordered conducting polypyrrole films on modified inorganic substrates." In: *Journal of Materials Chemistry* 7.8 (1997), pp. 1409–1413. DOI: 10.1039/a608365j (cit. on p. 119).

[54] Nicola Vinson et al. "Optimised "click" synthesis of glycopolymers with mono/di- and trisaccharides." In: *Polymer Chemistry* 2.1 (2011), p. 107. DOI: 10.1039/c0py00260g (cit. on p. 120).

[55] S. Vinod Selvaganesh et al. "Chemical Synthesis of PEDOT-Au Nanocomposite." In: *Nanoscale Research Letters* 2.11 (Oct. 2007), pp. 546–549. DOI: 10.1007/s11671-007-9100-6 (cit. on p. 120).

[56] Junhoe Cha et al. "DNA hybridization electrochemical sensor using conducting polymer." In: *Biosensors and Bioelectronics* 18.10 (Sept. 2003), pp. 1241–1247. DOI: 10.1016/S0956-5663(03)00088-5 (cit. on pp. 121, 133).

[57] J. Arias-Pardilla et al. "Synthesis, electropolymerization and oxidation kinetics of an anthraquinone-functionalized poly (3,4-ethylenedioxythiophene)." In: *Electrochimica Acta* 55.5 (Feb. 2010), pp. 1535–1542. DOI: 10.1016/j.electacta.2009.10.011 (cit. on p. 121).

[58] Tim Nunney. *XPS Characterization of "Click" Surface Chemistry*. Tech. rep. East Grinstead, 2011, p. 52130 (cit. on p. 123).

[59] Simone Ciampi et al. "Functionalization of acetylene-terminated monolayers on Si(100) surfaces: a click chemistry approach." In: *Langmuir : the ACS journal of surfaces and colloids* 23.18 (Aug. 2007), pp. 9320–9. DOI: 10.1021/la701035g (cit. on p. 123).

[60] Anando Devadoss and Christopher E D Chidsey. "Azide-modified graphitic surfaces for covalent attachment of alkyne-terminated molecules by "click" chemistry." In: *Journal of the American Chemical Society* 129.17 (May 2007), pp. 5370–1. ISSN: 0002-7863. DOI: 10.1021/ja071291f (cit. on pp. 123, 127).

[61] Hang-Beom Bu et al. ""Click"-functionalization of conducting poly (3, 4-ethylenedioxythiophene) (PEDOT)." In: *Chem. Commun.* (11 2008), pp. 1320–1322. DOI: 10.1039/b718077b (cit. on p. 124).

[62] M.H. Pournaghi-Azar, F. Ahour, and M.S. Hejazi. "Differential Pulse Voltammetric Detection of Hepatitis C Virus- Oligonucleotide Chain by a Label-Free Electrochemical DNA Hybridization Biosensor Using Consensus Sequence of Hepatitis C Virus-Probe on the Pencil Graphite Electrode." In: *Electroanalysis* 21.16 (Aug. 2009), pp. 1822–1828. ISSN: 10400397. DOI: 10.1002/elan.200804570 (cit. on pp. 124, 138).

[63] Margarita Alvira and Ramón Eritja. "Synthesis of Oligonucleotides Carrying 5'-5' Linkages Using Copper-Catalyzed Cycloaddition Reactions." In: *Biochemistry and Biodiversity* 4.12 (2007), pp. 2798–2809 (cit. on p. 126).

[64] Xiaochun Zhang et al. "Covalent attachment of shape-restricted DNA molecules on amine-functionalized Si(111) surface." In: *Surface Science* 603.16 (Aug. 2009), pp. 2445–2457. DOI: 10.1016/j.susc.2009.05.023 (cit. on pp. 127, 128).

[65] H. F. Arlinghaus et al. "DNA sequencing with ToF-SIMS." In: *Surface and Interface Analysis* 34.1 (Aug. 2002), pp. 35–39. DOI: 10.1002/sia.1247 (cit. on p. 127).

[66] M C Pham et al. "Direct electrochemical detection of oligonucleotide hybridization on poly(5-hydroxy-1,4-naphthoquinone- co-5-hydroxy-3-thioacetic acid-1,4-naphthoquinone) film." In: *Analytical chemistry* 75.23 (Dec. 2003), pp. 6748–52. ISSN: 0003-2700. DOI: 10.1021/ac034770f (cit. on p. 129).

[67] Rolf Huisgen. "1.3-Dipolar Cycloadditions: Past and Future." In: *Angewandte Chemie International Edition* 2.10 (1963), pp. 565–632 (cit. on p. 129).

[68] Jena Bioscience. *Copper (I) Catalyzed Click Reactions Background Information and Protocols*. 2011 (cit. on p. 129).

[69] Vsevolod V Rostovtsev et al. "A stepwise huisgen cycloaddition process: copper(I)-catalyzed regioselective "ligation" of azides and terminal alkynes." In: *Angewandte Chemie (International ed. in English)* 41.14 (July 2002), pp. 2596–9. DOI: 10.1002/1521-3773(20020715)41:14<2596::AID-ANIE2596>3.0.CO;2-4 (cit. on p. 129).

[70] Christian W Tornø e, Caspar Christensen, and Morten Meldal. "Peptidotriazoles on solid phase: [1,2,3]-triazoles by regiospecific copper(i)-catalyzed 1,3-dipolar cycloadditions of terminal alkynes to azides." In: *The Journal of organic chemistry* 67.9 (May 2002), pp. 3057–64 (cit. on p. 129).

[71] Hafsa Korri-Youssoufi and Bouchra Makrouf. "Electrochemical biosensing of DNA hybridization by ferrocenyl groups functionalized polypyrrole." In: *Analytica Chimica Acta* 469.1 (Sept. 2002), pp. 85–92. DOI: 10.1016/S0003-2670(02)00539-1 (cit. on pp. 131, 133).

[72] Peter Bäuerle and Andreas Emge. "Specific Recognition of Nucleobase-Functionalized Polythiophenes." In: *Advanced Materials* 10.4 (Mar. 1998), pp. 324–330. DOI: 10.1002/(SICI)1521-4095(199803)10:4<324::AID-ADMA324>3.0.CO;2-E (cit. on p. 133).

[73] R Issa, N.A. Hamdan, and M.F.M Noh. "Differential Pulse Voltammetric Determination of DNA Hybridization using Methylene Blue on screen Orinted Carbon Electrode for the Detection of Mycrobacterium tuberculosis." In: *Biotechnology* 9 (2010), pp. 304–311 (cit. on p. 134).

[74] S O Kelley et al. "Single-base mismatch detection based on charge transduction through DNA." In: *Nucleic acids research* 27.24 (Dec. 1999), pp. 4830–7 (cit. on p. 134).

[75] Carolina V Uliana, Carla S Riccardi, and Hideko Yamanaka. "Diagnostic tests for hepatitis C: Recent trends in electrochemical immunosensor and genosensor analysis." In: *World journal of gastroenterology : WJG* 20.42 (Nov. 2014), pp. 15476–15491. DOI: 10.3748/wjg.v20.i42.15476 (cit. on p. 138).

[76] Carla dos Santos Riccardi et al. "Label-free DNA detection of hepatitis C virus based on modified conducting polypyrrole films at microelectrodes and atomic force microscopy tip-integrated electrodes." In: *Analytical chemistry* 80.1 (Jan. 2008), pp. 237–45. DOI: 10.1021/ac701613t (cit. on p. 138).

[77] Shuna Liu et al. "Electrochemical detection of hepatitis C virus based on site-specific DNA cleavage of BamHI endonuclease." In: *Chem. Commun.* 13 (2009), pp. 1635–1637. DOI: 10.1039/B900690G (cit. on p. 139).

[78] H V Tran et al. "Label-free and reagentless electrochemical detection of microRNAs using a conducting polymer nanostructured by carbon nanotubes : Application to prostate cancer biomarker miR-141." In: *Biosensors and Bioelectronic* 49 (2013), pp. 164–169. DOI: 10.1016/j.bios.2013.05.007 (cit. on p. 139).

[79] Elena Komarova, Matt Aldissi, and Anastasia Bogomolova. "Direct electrochemical sensor for fast reagent-free DNA detection." In: *Biosensors and bioelectronics* 21.July 2004 (2005), pp. 182–189. DOI: 10.1016/j.bios.2004.07.025 (cit. on p. 139).

[80] Wei Zhang, Tao Yang, and Kui Jiao. "Ultrasensitive indicator-free and enhanced self-signal nanohybrid DNA sensing platform based on electrochemically grown poly-xanthurenic acid / Fe 2 O 3 membranes." In: *Biosensors and Bioelectronics* 31.1 (2012), pp. 182–189. DOI: 10.1016/j.bios.2011.10.015 (cit. on p. 139).

[81] M Ageno, E Dore, and C Frontali. "The alkaline denaturation of dna." In: *Biophysical Journal* 9.11 (1969), pp. 1281–1311 (cit. on p. 139).

[82] Roger M. Wartell and Albert S. Benight. "Thermal denatiration of DNA molecules: A comparison of theory with experiments." In: *Physics Reports* 126.2 (1985), pp. 67–107 (cit. on p. 139).

[83] R. N. Maslova, V. V. Grechko, and Ja. M. Varshvsky. "Acid-base denaturation of DNA in heavy water." In: *Biochimica et Biophysica Acta (BBA)-Specialized Section on Nucleic Acids and Related Subjects* 87.2 (1967), pp. 314–325 (cit. on p. 139).

[84] *OligoCalc: Oligonucleotide Properties Calculator website*. URL: http://www.basic.northwestern.edu/biotools/oligocalc.html (cit. on p. 141).

5

FABRICATION OF POLYPYRROLE SINGLE NANOWIRE DEVICES

This chapter discusses the fabrication of polypyrrole single nanowire devices. Two fabrication techniques are investigated, namely dip-pen nanolithography and electrochemical polymerization on template-assisted surfaces. On one hand, dip-pen nanolithography proved to be a simple deposition technique with good control over size and location of the polypyrrole nanostructures. On the other hand, the electrochemical polymerization on template-assisted surfaces allows the chemical manipulation of the polymer, which permits tailoring the device properties. Applying these techniques, the capability of fabricating ready-to-use single nanowire devices, based on conducting polymers, is demonstrated.

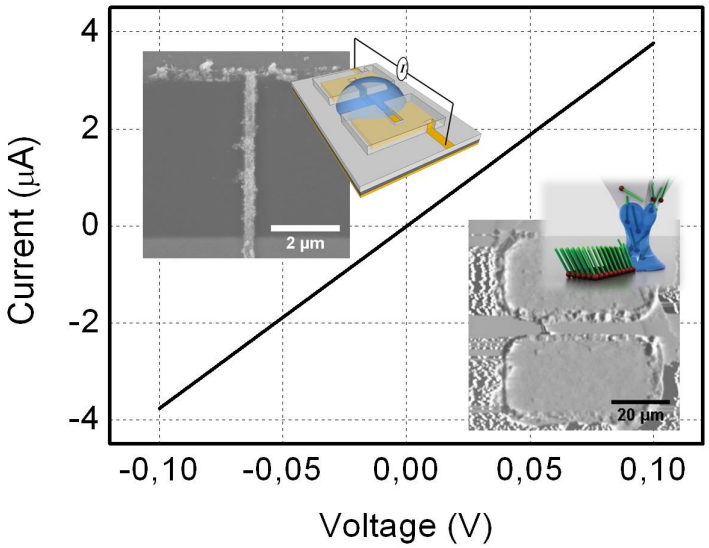

5.1 INTRODUCTION

Since Sakaki predicted in 1980 the enhanced electrical properties of nanowires due to the scattering suppression in one-dimensional structures [1], nanowires started to be used in electronic applications, with field effect transistors (FETs) as basic components to fabricate highly efficient devices [2, 3]. In these nanowire-based FETs, the nanowire connects two electrodes, called source and drain, on a highly doped silicon substrate (gate), which is coated with a thermally grown oxide layer (gate dielectric) (Figure 5.1) [2]. The FET operation consists in switching the conductance of the nanowire between full conduction (on-mode) and no conduction (off-mode) by the application of an electric field, through the gate electrode. These nanowire-based systems experience a greater influence on the channel conductivity, in comparison with conventional planar structures [2]. This is due to the similarity existing between the nanowire diameter's size and the Debye's length (a measure for the penetration of the electric field into the bulk), which confines the effects of the gate voltage to the nanowire's body.

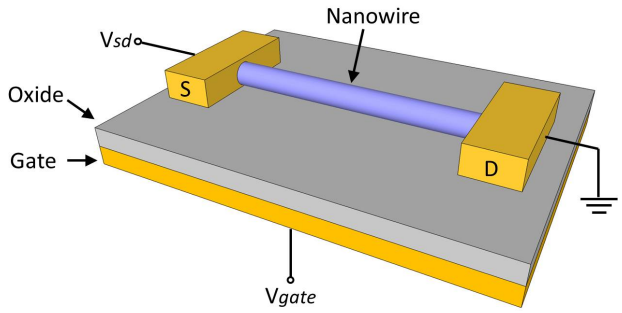

Figure 5.1: Field effect transistor configuration based on a single nanowire. A nanowire connects two metallic electrodes (source and drain) and lies on an insulating oxide layer, on top of the gate electrode.

Other nanowire's properties such as their high surface-to-volume ratio, their sub-wavelength optical properties, their high sensitivity to environmental changes occurring at their surface, their superior mechanical performance, etc., make them useful in many other applications such as optoelectronics, environmental care, as biomedical coatings, in chemical and biological sensors, etc. [4, 5, 6, 7, 8]. In biotechnological applications, the area that has shown to profit most from the nanowires' properties is the biosensors field, with detections in real-time and highly sensitive responses [9, 10]. Many works can be found reporting the use

of nanowires to detect important biological molecules, involved in common diseases such as glucose, or to detect specific DNA sequences, viruses and proteins [11, 12, 13, 14].

Of special interest is the case of nanowires based on conducting polymers (CP) such as polypyrrole (Ppy), polyaniline (PANI) or polythiophene [7]. As mentioned in previous chapters, conducting polymers have been used as alternatives to conventional materials (metals and inorganic semiconductors) in different fields, due to their extraordinary properties. They include the possibility of tuning the material's conductivity over several orders of magnitude by adjusting the synthetic parameters (dopant, solvent, synthetic method, oxidation state, etc.), the wide availability of monomers, their inexpensive cost, their capability to behave both as immobilization and as transduction agents at the same time and the multiple functionalization possibilities, which are so demanded in biotechnology [15].

Generally, electronic nanowire devices, based on conducting polymers, can be found either as arrays of nanowires (nanowire-networks) or as single-nanowire devices. On one side, nanowire-networks represent the easiest route to implement conducting polymer nanowires into electrical devices [16]. Nevertheless, these systems suffer from poor control over the number and position of nanowires bridging the electrodes, resulting in large variations of the contact resistance between different systems, which is translated into low reproducible devices [7]. Alternatively, single-nanowire devices offer a constant performance and their use provides an excellent control and understanding of the device properties and the operation mechanism [16]. Moreover, the capability of fabricating single-nanowire structures improve the spatial resolution of the device, allowing the construction of high density electronic devices. Used for instance, in recognition systems, where control assays can be included in a single experiment, thus reducing the false positive/negative responses [11].

However, single conducting polymer nanowires still suffer from serious fabrication limitations. Conventional micro- and nanofabrication techniques, such as photolithography and focus ion beam (FIB) showed to be incompatible with the fabrication of polymer nanostructures (they induce thermal damage during the process on the polymer and are incompatible with the incorporated functional groups) [16]. Instead, the most widely employed techniques to deposit conducting polymer nanowires over electrical contacts includes the synthesis of the nanowires in solution (by template methods) [17]. These nanowires are placed, after fabrication, between metallic electrodes by drop-casting. Then they are aligned

with the help of a complementary method, to obtain single-nanowire devices [18]. The nanowire's alignment has been typically performed by the use of electric and magnetic fields, which requires tedious steps of alignment and deposition, increasing the complexity of the fabrication process. Alternatively, other fabrication approaches have been investigated based on scanning probe microscopies. For instance, scanning tunneling microscopy (STM) has been used to locally electropolymerize a thin film of a precursor monomer on a surface, thus creating polymer nanostructures [19]. Also, polymer-based suspensions have been deposited in nanowire shape by dip-pen nanolithography (DPN), representing an attractive alternative to direct printing techniques, as ink-jet printing, with nanometer resolutions [20]. Recently, the in-situ electropolymerization of nanowires between electrical contacts has also been studied. Although, it seems a very convenient fabrication method that could overcome problems related to reproducibility, it is still an immature technique, where the experimental conditions showed to affect dramatically the course of the process and where the fabrication parameters should be optimized.

This chapter discusses the fabrication of polypyrrole nanowires between electrical contacts. Two different methods were attempted, namely dip-pen nanolithography and electrochemical polymerization on template-assisted surfaces. DPN operation conditions were investigated for a polypyrrole-based ink, obtaining the calibration of the nanowire's diameter against the writing speed and the relative humidity. DPN showed to be a suitable technique for the deposition of polypyrrole nanowires between metallic electrodes with resolutions down to 100 nm. Alternatively, the growth of polypyrrole nanowires by electrochemical synthesis offered higher control over the chemical and physical properties of the polymer. The absence of standard protocols to fabricate these types of nanowires motivated this study, which seeks an optimization of the fabrication parameters. The optimization process resulted in an increased reproducibility of fabricated devices in comparison with former studies, where reported protocols were applied. Two final devices, using different solvents and electrolytes were characterized electrically, demonstrating the capability of fabricating ready-to-work systems with potential applications in different fields.

5.2 POLYPYRROLE NANOWIRES BY DIP-PEN NANOLITHOGRAPHY (DPN)

In this section, dip-pen nanolithography (DPN) is introduced as a suitable technique for the deposition of polypyrrole nanowires. The principles of this tech-

nique are presented here, along with a description of the fabrication process and the characterization of the polymer nanowires.

5.2.1 *Principles of Dip-Pen Nanolithography*

In 1986, Binning and Rohrer were awarded with the Nobel Prize in Physics for the invention of the Scanning Tunneling Microscopy (STM) [21]. It was based on the tunneling currents generated between a conductive tip and a surface close to it, achieving lateral resolutions as low as 0.1 nm. STM was the first invention of the scanning probe microscopes, which are based on the intimate interaction between a probe and a surface. Shortly after, the Atomic Force Microscope (AFM) was developed with sub-nanometer resolution, exploiting the forces existing between a surface and a tip brought to its proximity (described by the Lennard-Jones potential) [22]. These techniques represented a tremendous advance for the study of biological samples, since they provided researchers with measurements of atomic resolution in air and liquid, overcoming the vacuum restrictions existing to that date [23].

However, scientists soon encountered a major problem when the measurements were done in air. It was related to the formation of a water meniscus between the tip and the surface (Figure 5.2), which altered the measurements. This phenomenon was extensively studied, obtaining a correlation between the meniscus's size and the relative humidity existing in the environment [24]. Based on this idea, Piner *et al.* took advantage of the water meniscus, using it as a vehicle for the deposition of molecules from a functionalized tip to the surface and calling it dip-pen nanolithography (DPN) technique [25].

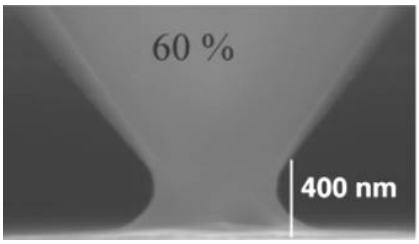

Figure 5.2: SEM image of a water meniscus between an AFM tip and a surface, at 60% relative humidity. (Picture taken from [24]).

DPN is a direct-writing fabrication method based on the AFM operation principle, which allows fine alignment and positioning of nanometer structures over a surface. In a standard DPN process (molecular inks DPN), an AFM probe is coated

with the desired molecule to be deposited (ink) and subsequently the molecule is transported via the water meniscus towards the surface. This process can occur if the surface tension is favorable and the molecule attaches preferably to the surface, for which a driving force is required. DPN permits the control of the nanopattern dimensions by changing operation parameters such as the contact time (time that the tip is in contact with the surface, dwell), the temperature and the relative humidity, achieving feature resolutions' down to 10 nm [26]. DPN has been shown to be compatible with many different inks such as small organic molecules, polymers, biomolecules, colloid particles, metal ions, etc. [27]. Also, a large variety of surfaces have been patterned using this method, from conventional substrates such as gold, silicon or silicon oxide to more biocompatible and flexible substrates like polyethylene terephthalate (PET) or polydimethylsiloxane (PDMS) [28].

Recent advances in DPN include not only the possibility of depositing the molecules via the water meniscus (molecular inks, Figure 5.3a), but also of dispensing nanodrops of a molecule in a certain solution (liquid inks, Figure 5.3b). This operation mode is suitable for biomolecules which are in need of a buffered solution to prevent their denaturing, like proteins, peptides, viruses or DNA [29, 30, 31]. When using molecular inks, is not only important the specific interaction between ink, tip and surface but also the viscosity of the solution, which typically limits the resolution of the features about 500 nm approximately [28].

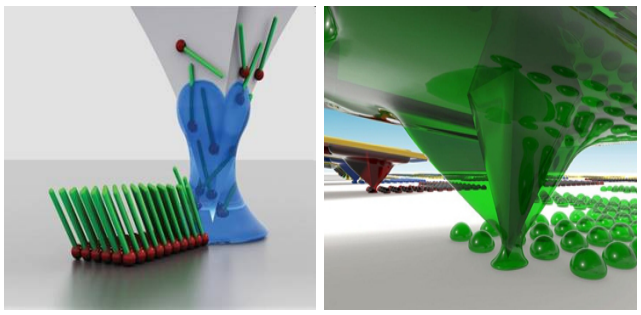

(a) (b)

Figure 5.3: Dip-Pen Nanolithography modes. a) Molecular inks, the water meniscus is used to transfer the molecule from tip to surface. b) Liquid inks, nanometre drops containing the molecule are dispensed on the surface. (Images taken from NanoInk Inc. and Scitech Pty Ltd.)

Moreover, DPN has been coupled with other techniques, resulting in new approaches as the thermal DPN or the electrochemical DPN [32, 33]. These techniques

use customized tips either to heat a solid tip coating, thus allowing deposition, or to generate electrochemical reactions on a meniscus-sized electrochemical cell, performing the deposition or even the synthesis of materials. In this section, the specific case of using conducting polymers as molecular inks is discussed. The deposition of these materials at the nanometer scale turned out to be very limited, when solution processable techniques such as ink jet printing or microcontact printing (useful in the micrometer range) are used [34]. Instead, DPN showed to be especially useful for fast patterning of conducting polymer nanofeatures [20].

5.2.2 *Fabrication of polypyrrole nanowires by Dip-Pen Nanolithography*

Dip-pen nanolithography (DPN) was conducted using polypyrrole as a molecular ink, along with soft DPN probes for contact operation (see section 2.2.3.3). The tips were dip coated with a commercial polypyrrole suspension, which was used without any prior treatment (described in section 2.1.1). Special microfluidic channels, called inkwells (presented in section 2.2.3.3), were used to coat the tips in such a way that no spreading of the polymer ocurred at the backside of the cantilever (Figure 5.4).

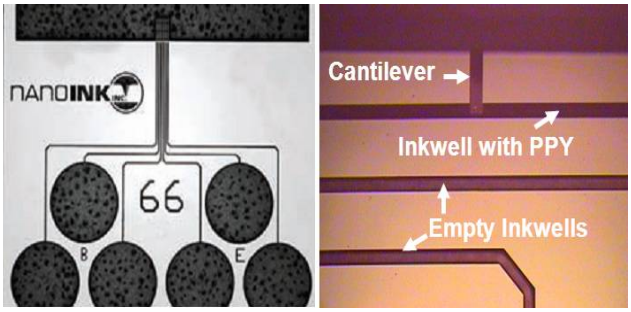

(a) (b)

Figure 5.4: Polymer inking process. a) optical image of an 6-inkwell microfluidic chip. b) Inking procedure, consisting in dipping the tip into the polymer contained in one microfluidic channel.

This is a crucial issue since a constant force mode was used to perform the lithography. In this operation mode, the tip is constantly controlled by a laser feedback, which requires a clean and reflective cantilever's backside, keeping a constant force with the surface. Therefore, after the tips were dip coated in the polymer suspension for 1 minute, they were retracted from the inkwells and

left to dry for 3 minutes under ambient conditions. Finally, the cantilevers were brought into contact with the surface and the writing process was initiated.

The doped polypyrrole used here has a positively charged backbone [35], which suggested the use of negatively charged surfaces to create an electrostatic driving force between the polymer and the surface. This driving force facilitates the polymer deposition and was generated by creating negative charges (OH^-) on the silicon oxide surfaces (Figure 5.5), by dipping the substrate for 15 minutes in "piranha" solution (7:3 (v/v) of concentrated H_2SO_4 and 30% H_2O_2). Then, sets of multiple polypyrrole nanowires were written on the activated SiO_2 substrates, to calibrate the writing process parameters such as humidity and writing speed, versus nanowire's diameter.

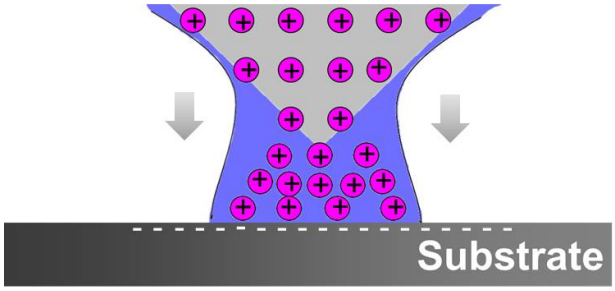

Figure 5.5: Driving force for polypyrrole deposition by dip-pen nanolithography. Electrostatic interaction between the polymer ink (positively charged) and the activated SiO_2 substrate (negatively charged).

DPN experiments were performed at room temperature (20°C ± 1°C) and relative humidity values of 30%, 35% and 40% (controlled by means of an environmental chamber). All experiments were conducted within the two hours after the piranha treatment, to keep the surface activation. Seven different writing speeds were studied from 0.1 µm/s to 2.0 µm/s (the nanowire's length was set to 5 µm, which results in writing frequencies from 0.02 Hz to 0.4 Hz). Additionally, single polypyrrole nanowires were deposited on gaps between metallic electrode pairs, to demonstrate the capability of patterning nanostructures on a specific location. A rigorous protocol, respecting activation and inking times was followed to obtain good reproducibility.

5.2.3 *Characterization of polypyrrole nanowires deposited by Dip-Pen Nanolithography*

The in-situ characterization of the polypyrrole nanowires was conducted by AFM analysis using the same instrumentation as the one used for the polymer de-

position DPN equipment and tip). Working in feedback operation mode allows performing both processes in a consecutive way without losing the relative position between surface and tip. By increasing the tip speed to a certain threshold, the ink deposition is avoided, permitting the direct verification of the patterns immediately after the writing process. In the case of the polypyrrole suspension used here, the writing frequencies (i.e. writing speeds) were varied from 0.02 Hz to 0.4 Hz, while the characterization frequencies (i.e. scan speeds) were fixed at values above 1.5 Hz.

Figure 5.6 shows a lateral force mode AFM image (LFM) of a set of nanowires, written at room temperature (21°C), 31% of relative humidity and 0.1 µm/s (0.02 Hz) writing speed. The characterization of the nanowires was conducted right after the deposition process, using the same tip. The scan area was enlarged to the whole set of wires and the scanning speed was increased to a frequency value of 2.5 Hz. The results revealed that under the mentioned conditions, nanowires with diameters between 150 nm and 180 nm could be obtained and that negligible ink deposition occurred during the characterization step.

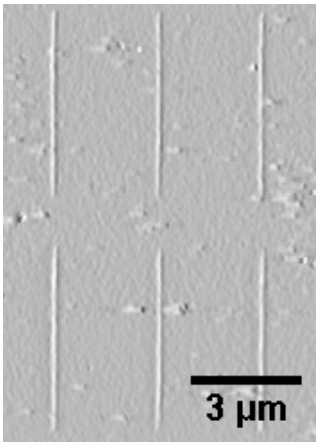

Figure 5.6: Lateral force microscopy image of a set of nanowires deposited at 0.02 Hz writing frequency and characterized at 2.5 Hz scan frequency.

Afterwards, calibration experiments were performed to establish the relation existing between the dimensions of the nanowire and the different operation parameters such as the relative humidity and the writing speed. Sets of 5 µm long nanowires were written using speeds ranging from 0.1 to 2.0 µm/s (0.1, 0.3, 0.5, 0.7, 1, 1.5 and 2 µm/s). A temperature of 20 ± 1°C was maintained and three different humidity conditions were used: 30%, 35% and 40%. Then, Lateral Force Microscopy (LFM) images were taken in order to characterize the size of the nanowires.

Figure 5.7 shows the dependence of the nanowire's diameter with the writing speed and the relative humidity at room temperature. Two conclusions could be extracted from these results. First, there is a decay tendency in the nanowire's diameter when the writing speed is increased and secondly, the size of the nanowires increases when the humidity values rise up.

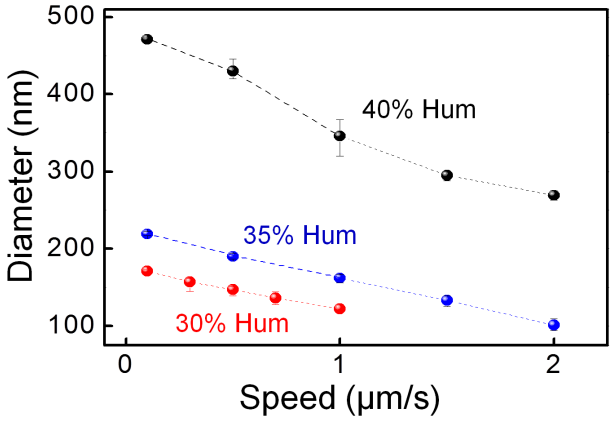

Figure 5.7: Dependence of the nanowire's diameter with writing speed and relative humidity. The black dots represent the nanowire's diameter obtained at 40% relative humidity, the blue dots show the results at 35% relative humidity and the red dots represent the results at 30% relative humidity. At least 3 measurements were done from 3 independent nanowires for the same conditions.

These results are consistent with the DPN diffusion models previously reported [36, 37, 38], which predict the reduction of the feature's dimensions when the writing speed is increased and the environmental humidity is decreased. In particular, the effect of the humidity on the nanowire's diameter can be explained by the existence of the water meniscus between tip and surface. The meniscus becomes larger at higher humidity values and thus allows a higher deposition rate, being in direct relation with the feature's size. Besides, the decrease of the nanowire's size when the writing speed increases, is related with the transport mechanisms participating in the deposition process. The molecules travel from the tip to the surface at a certain speed, which depends on the environmental conditions and the affinity of the molecules for the surface. Thus, if the writing speed is much higher than the velocity at which the molecules travel from the tip to the surface, no continuous deposition is achieved and the process becomes unfeasible. An example for this phenomenon could be found here, when the deposition was attempted at 30% relative humidity and the writing speeds were

over 1 μm/s. In this case, continuous deposition of polypyrrole was not obtained due to the low deposition rate exhibited under the mentioned conditions.

The smallest continuous diameter achieved in this work was 101 ± 8 nm, for 35% relative humidity and 2.0 μm/s writing speed. This is the smallest nanowire's diameter obtained for polypyrrole nanowires deposited as molecular ink [20]. Only other DPN-based techniques as the thermal and the electrochemical DPN showed to be successful in fabricating conducting polymer nanowires under 100 nm of resolution [32, 33].

Additionally, to prove the capability of positioning nanostructures in a precise area, polypyrrole nanowires were written between metallic contacts (Ti/Au), previously deposited on a Si/SiO_2 wafer. Figure 5.8 shows a topographical AFM image of a 339 nm thick polypyrrole nanowire, deposited at 21°C, 40% relative humidity and 1.0 μm/s writing speed. It was written on the SiO_2 gap (smaller than 2 μm) existing between two rectangular contacts of micrometer size (6 μm x 12 μm). These results prove the capability of selectively deposit polypyrrole nanowires in a very accurate manner in a simple fabrication process.

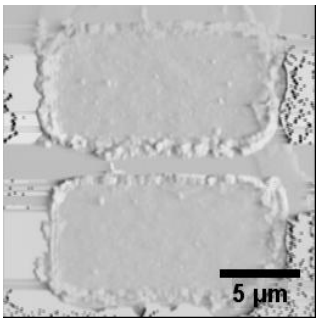

Figure 5.8: Topographical AFM image of a polypyrrole nanowire deposited between metallic contacts. The nanowire was deposited at 40% relative humidity and 1 μm/s speed. The diameter of the nanowire was 339 nm.

Typically, the techniques that have been mostly employed to deposit conducting polymer nanowires over electrical contacts are based on the synthesis of nanowires in solution (by template methods). In those methods, the nanowires are placed between metallic electrodes with the help of another complementary method [18]. This integration of nanowires in real devices has been attempted by simple drop casting or by using electric and magnetic fields, which increase the complexity of the fabrication process, requiring tedious steps of alignment and deposition. On the contrary, DPN has been shown to be a simple and efficient technique to fabricate conducting polymer nanowire devices due to its easy concept; however, it is not free of drawbacks. In this study, polypyrrole nanowire

based devices were subjected to vacuum and cleaning processes (as sonication baths), which resulted in polymer detachment, indicating the poor adhesion of the nanowires to the surface. This was previously reported for other DPN-based methods used to fabricate polymer nanowires, representing an important problem for real applications [33]. Additionally, since the ink used in this work is an already polymerized suspension, there is no possibility for structural modification. It has been shown that by, for instance, changing the doping anion used during the polymerization process, the physical and chemical properties of the material can be strongly influenced [39], which in this case is impossible. Moreover, DPN is a complex research tool, which is still under evolution and needs the permanent control of a trained operator to ensure reliable and reproducible results. For these reasons, although DPN has demonstrated to be a suitable technique for the fabrication of polypyrrole nanowires, with 100 nm of resolution and good control on the polymer location, some of the drawbacks found at this point suggested the study of alternative fabrication methods for the development of functional devices.

5.3 POLYPYRROLE NANOWIRES BY ELECTROCHEMICAL POLYMERIZATION ON TEMPLATE-ASSISTED SURFACES

Motivated by the need of finding improved methods for the fabrication of polypyrrole nanowires, whose structure could be easily tuned and with higher stability after integration in a device, the electrochemical polymerization of polypyrrole nanowires between metallic contacts was studied.

In this section, the fabrication of polypyrrole nanowires, which can function directly in an electronic device without any further processing steps, is presented.

Template-assisted surfaces are used to control dimensions, position and alignment of the nanowires. The electrochemical polymerization of pyrrole on these template-assisted surfaces is attempted using different electrolytes, which produce polypyrrole nanowires with different chemical composition and different electrical properties.

5.3.1 *Principles of electrochemical synthesis of conducting polymer nanowires*

The electrochemical synthesis of conducting polymer nanowires is based on the conventional process of electrochemical oxidative polymerization (discussed in section 2.2.1.2), which oxidizes a precursor monomer to its cation radical to ini-

tiate polymerization [35]. In the particular case of nanowires, two opposite electrodes are typically used and biased, inducing the monomer's oxidation at the anode surface [40, 41]. If the electric field is strong enough, the nanowire grows along the electric field direction until it reaches the opposite electrode (cathode) [40].

However, controlling the nanowire shape is not straightforward and requires modifications of the process, as will be presented here. Template-free approaches have been reported, resulting in random nets of conducting polymer nanowires bridging the electrodes [42, 43]. In these template-free approaches, bare gold electrodes are used without any further processing step different from their deposition. After fabrication of the gold electrodes, a bias is applied and polymerization occurs. Although these template-free approaches are appealing for avoiding extra lithographic steps, few works have shown the fabrication of single or ordered nanowire devices. Moreover, most of these reports state the great difficulty in reproducing and controlling the results, which are quite unstable and dependent on the experimental conditions [40, 44, 45]. Alternatively, template-assisted methods have been investigated, which include a lithographic step before the electrochemical polymerization, normally performed by, but not limited to, nanolithography techniques such as e-beam lithography or focused ion beam. This procedure results in an electrolytic channel which connects the metallic electrodes and thus defines the exact shape and location of the nanowire [41, 46, 47, 48]. Although the use of these methods increases the complexity of the substrate fabrication process, they allow an accurate control over the diameter of the nanowire and also over the number of nanowires bridging the electrode's gap. This becomes essential when a deep understanding of the device function is needed, avoiding the uncertainty of multiple random wires, where only averages can be obtained.

In next sections, the in-situ synthesis of conducting polymer nanowires by template-assisted method is presented. As explained above, this method allows not only the control of the physical and chemical properties of the device, but also the precise alignment of the nanowires. Thus, it results in ready connected nanowires, which allows their direct utilization in an electronic device without any post-processing step [49, 50]. By this procedure, the limitations existing regarding the integration of conducting polymer nanowires into devices shown by other methods, such as the direct writing methods or the synthesis of nanowires in solution, can be overcome.

5.3.2 *Fabrication of template-assisted surfaces for the electrochemical polymerization of polypyrrole nanowires*

The fabrication of an appropriate surface, in which a template for the nanowires is included, is crucial at this point since it will determine both diameter and location of the nanowires. In this work, parallel electrodes were fabricated as described in section 2.2.2. Briefly, microelectrodes consisting of a 10 nm titanium adhesion layer and a 70 nm gold layer were deposited by evaporation on Si/SiO_2 wafers with the help of direct write laser lithography (DWL). The two microelectrodes were separated by a distances of 5 µm and 15 µm. The electrodes were then coated by a passivation layer on which a nanochannel bridging the electrodes was patterned by electron-beam lithography (EBL), as envisioned in Figure 5.9. Nanochannels with widths between 200 nm and 450 nm were investigated.

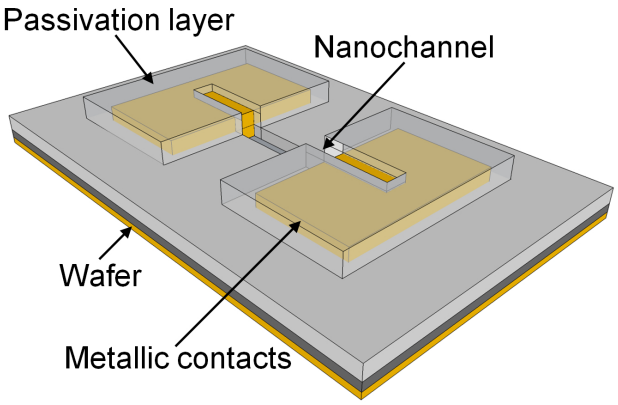

Figure 5.9: Schematics of surface patterning for the electropolymerization of polypyrrole nanowires. One can see the nanochannel opened on the passivation layer deposited on the wafer containing electrical contacts.

Figure 5.10 shows dark field optical microscope images of 200 nm wide nanochannels, patterned between electrodes. In the images, the exposed SiO_2 and gold surfaces under the passivation layer can be seen, confirming the success of the e-beam nanolithography process. High care should be taken during this fabrication process, since dirty channels with passivation residues may produce overgrowth of the polymer, ending in non-uniform nanostructures. Two passivation materials were studied here, namely Poly(methyl methacrylate) (PMMA) and silicon oxide (SiO_2).

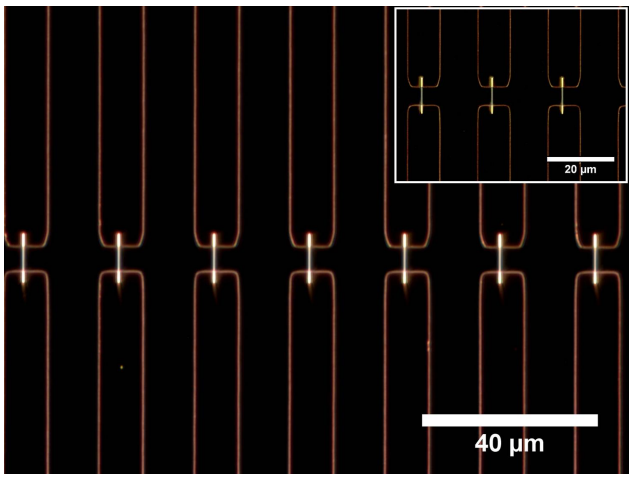

Figure 5.10: Optical microscope image of electrolyte nanochannels bridging metallic electrodes. PMMA is the passivation layer used in these electrodes.

PMMA is one of the most commonly used electron sensitive resists to perform EBL. The use of PMMA directly as passivation layer in this work, is an attractive option since it reduces the number of lithographic steps needed to achieve the surface nanopattern. However, PMMA is not a completely inert material and can be affected by the nature of the solvent used to perform the polymerization [51]. Therefore, the use of PMMA as passivation layer was restricted here to reactions in aqueous media. After coating the electrode-containing substrate with PMMA, e-beam lithography was used to fabricate the openings between the contacts (for more details about the e-beam process see section 2.2.3.5), as shown in Figure 5.9.

On the contrary, the use of SiO_2 as passivation layer increases the clean room processes, but it results in a very inert passivation layer compatible with most of the organic solvents used for polymerization. Here, SiO_2 was deposited by evaporation on surfaces containing electrodes. Then, they were coated by PMMA in order to perform the EBL step required to achieve a nanochannel between electrodes. After the nanochannels were patterned on the PMMA, an extra etching process was required to transfer the PMMA nanochannel to the SiO_2 passivation layer (reactive ion etching, more details about the technique see section 2.2.2.4). Finally, the PMMA was removed from the surface by ultrasonic bath in acetone, resulting in the configuration shown in Figure 5.9. Once the nanochannels were patterned on the passivation surface, the electrochemical polymerization was conducted by depositing a drop of electrolyte, containing the monomer, on the nanochannel and applying a current between the electrodes (Figure 5.11).

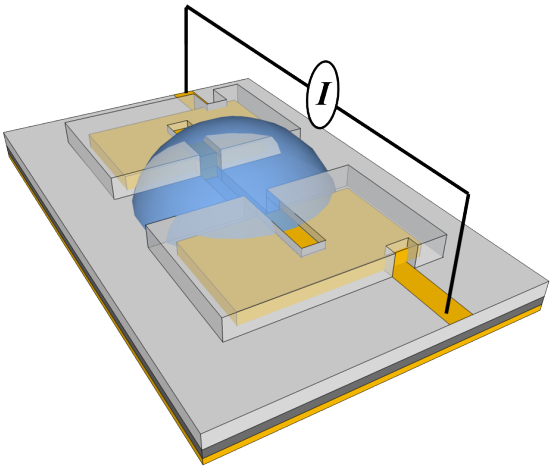

Figure 5.11: Polymerization scheme. Drop of electrolyte and monomer on the nanochannel. Electric field applied between parallel electrodes.

5.3.3 *Electrochemical polymerization of polypyrrole nanowires*

The electrochemical polymerization of polypyrrole nanowires is described in this section. As mentioned before, the existing works related to the electrochemical synthesis of conducting polymer nanowires still report poor success in the incorporation of these materials into routine functional integrated devices. The great difficulty in reproducing the simplest reports published in this area suggested that a more complex and uncontrollable process is occurring, which needed further optimization. During the course of our research, the simplest polymerization protocols were investigated, increasing their complexity in a gradual manner and seeking an increased reproducibility in the results. The experimental parameters were progressively limited at each step, achieving the optimization of the growing conditions and obtaining suitable polymeric devices.

5.3.3.1 *Polypyrrole nanowires grown in aqueous solvent*

First works reporting the fabrication of polymer nanowires by template assisted methods, use inorganic passivation layers (highly inert to side reactions), accompanied by widely available reagents as water solvent and sodium chloride electrolyte. Taking these reports as start point, the fabrication of SiO_2-based template assisted surfaces was conducted (see section 5.3.2).

Drops of electrolyte containing the monomer (2 µL of 10 mM NaCl and 25 mM pyrrole in Milli-Q water) were placed on the nanochannels between electrodes

and a constant current was applied, as shown in Figure 5.11. The current values investigated here ranged from 10 nA to 100 µA. It was observed that currents bellow 100 nA did not induce nanowire formation and currents above 1 µA produced degradation of the electrode surface. The obtained wires were stable and were not washed away by water rinsing or sonication, which indicated their good adhesion to the surface. Figure 5.12 shows a polypyrrole nanowire grown inside a 200 nm wide SiO_2 channel with a length of 15 µm. It was synthesized in an aqueous solution of NaCl electrolyte, under a current of 1 µA.

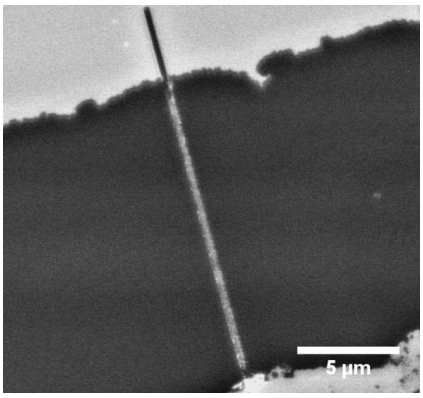

Figure 5.12: Polypyrrole nanowire (200 nm diameter) inside a SiO_2 nanochannel, highlighted by the arrows.

In the image one can see how the width of the electrolytic nanochannel defines the diameter of the nanowire, confining the polymer into it and thus obtaining a polypyrrole nanowire of 200 nm, comparable to the ones reported in literature [46]. However, very low success rates were obtained, being about 10% of the total number of polymerization trials. In most of the cases, where the polymerization between electrodes was achieved, overgrowth of the polymer was observed, as shown in Figure 5.13.

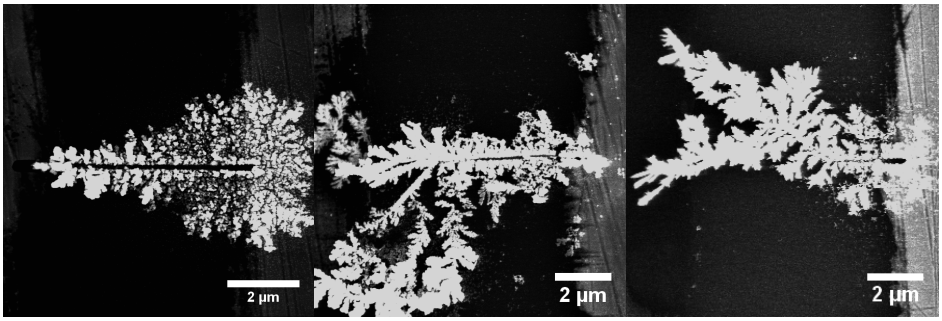

Figure 5.13: Overgrowth of polypyrrole nanowires.

This indicated that still a lot of optimization was required to obtain reliable fabrication protocols. To reduce time and costs of the process, PMMA was employed as passivation layer instead of SiO_2. This allowed to produce more samples and to increase the number of experiments. Currents were limited to values between 100 nA and 1 µA, showing similar results as before, but still with low rates of successful experiments. Figure 5.14 shows a polypyrrole nanowire of 200 nm in diameter, grown in a NaCl aqueous solution, under the application of a constant current of 1 µA, using PMMA-based templates.

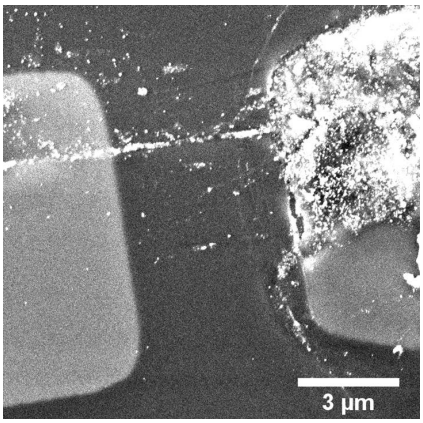

Figure 5.14: Polypyrrole nanowire (200 nm diameter) inside a PMMA nanochannel.

Although not fully optimized, these experiments were useful to confirm that the monomer oxidation was produced at the anode surface. This was supported by the observation of partially formed wires at the anode, oriented in the electric field direction (Figure 5.15).

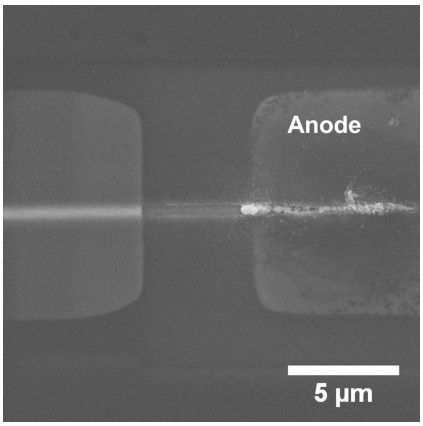

Figure 5.15: Polypyrrole growth starts at the anode.

In order to achieve higher efficiency and yields in the fabrication process, a different electrical configuration was investigated. It has been suggested by Hu *et al*. that a second electric field acting perpendicularly to the electrode surface, may increase the confinement of the positively charged monomers (oxidized monomers) inside the nanochannel. Consequently, polymerization time might be reduced and reproducibility increased [52]. Therefore, a second electric field was generated here by applying a negative potential under the 20 nm thick SiO_2 layer, by means of a back electrode. This back electrode consisted on a gold layer deposited by evaporation at the silicon doped side of the wafer. When the negative potential was applied to the back electrode, a negative charge was generated at the SiO_2 insulating bottom surface, inducing the accumulation of positively charged species inside the electrolytic channel, as depicted in Figure 5.16.

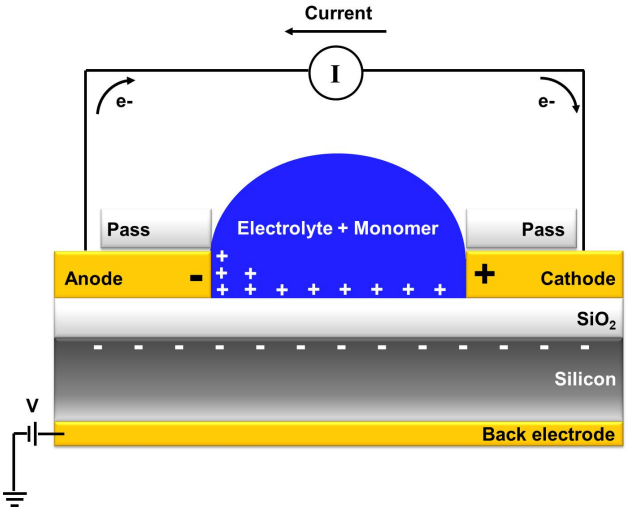

Figure 5.16: Schematics of the set-up used for polymerization. A current is applied to the anode, initiating polymerization. A perpendicular electric field is created to confine the positive monomers inside the nanochannel.

Voltages between 0 V and -10 V were tested, observing that no significant improvement of the polymerization process was obtained when the applied potential was smaller than -1 V. For voltages above -2 to -3 V the breakdown voltage of the thin SiO_2 layer is reached and a rupture of the layer occurred, generating a leakage current which produced undesired polymerization when no other currents were applied. The best results were achieved when voltages of -1 V were applied. These results demonstrated that the use of thin oxide insulating layers, as the ones employed here, reduce the power consumption of the device in comparison to previous works, as the one of Hu *et al*., where thicker dielectric layers

(10 times thicker) needed higher back voltages (-10 V) in order to obtain similar results. Moreover, the introduction of this second electric field increased the efficiency of the process to an approximated value of 60%, confirming the utility of this new electrical configuration in achieving higher success rates.

Figure 5.17 shows a polypyrrole nanowire, grown inside a 450 nm PMMA channel, using 10 mM NaCl and 25 mM pyrrole in water. It was grown by using a constant polymerization current of 1 µA and a back voltage of -1 V.

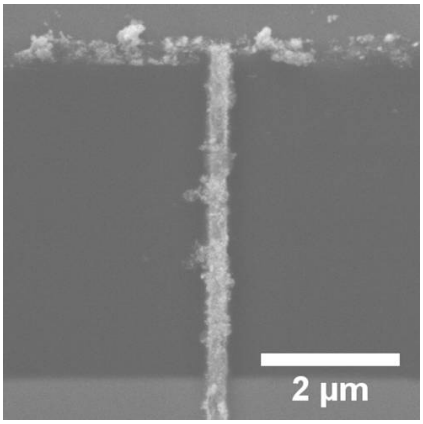

Figure 5.17: Polypyrrole nanowire (450 nm diameter) grown inside a PMMA channel, this time applying a second perpendicular electric field.

Figure 5.18 shows three nanowires grown in parallel, where the same optimized conditions were applied (10 mM NaCl and 25 mM pyrrole in water, polymerization current 1 µA and back voltage of -1 V). This result enables the fabrication of ordered arrays of polypyrrole nanowires, which could be applied to multiplexed devices.

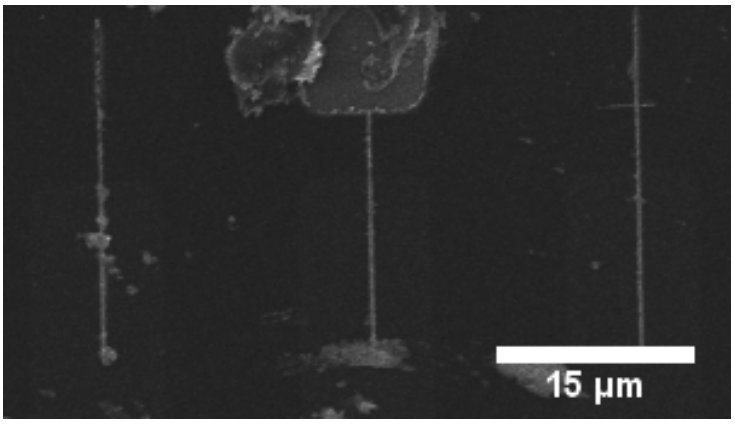

Figure 5.18: Set of three polypyrrole nanowires grown in parallel, using the field assisted method.

However, a degradation of the passivation layer was observed, suggesting that the electrical conditions applied here were still too aggressive for the preservation of the PMMA coating. In this regard, it has been shown that the use of AC voltages, for inducing polymerization, is useful in the electrode preservation [45]. In particular, square waves with 50% duty demonstrated to be the most conservative alternating stimulation applied in these cases [44]. Here, since the growing parameters were optimized to specific current values, the alternating stimulation was applied in terms of current instead of potential. Thus, current pulses of 1 µA were applied by means of square waves of 50% duty and 0.5 kHz frequency (Figure 5.19).

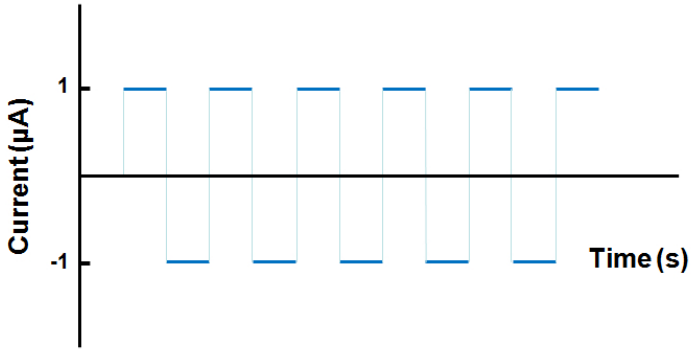

Figure 5.19: Alternating pulses of current applied between metallic contacts.

In this way, nanowires as the one shown in Figure 5.20 could be fabricated, resulting in the preservation of not only the electrodes but also their PMMA passivation coating.

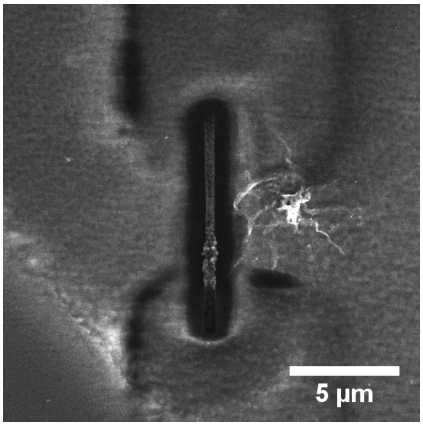

Figure 5.20: Polypyrrole nanowire (450 nm diameter) grown in a PMMA nanochannel, using a second perpendicular electric field and a squared alternating current.

These nanowires showed to be conducting as indicated by the I-V characteristics obtained (Figure 5.21), showing that they obey the ohm's law with negligible contact resistance with the electrode.

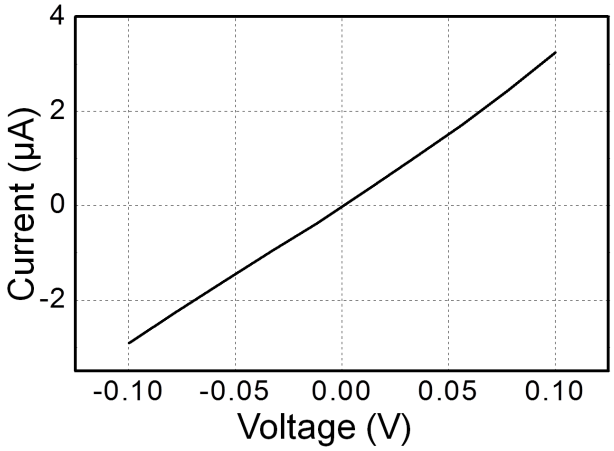

Figure 5.21: I-V characteristics of polypyrrole nanowires.

The conductivity of the polypyrrole nanowires was calculated by applying Equation 5.1, where σ is the conductivity, R the measured resistance, A the area of the nanowire's cross section and l de separation between contacts.

$$\sigma = \frac{l}{AxR} \tag{5.1}$$

Polypyrrole nanowires grown under the mentioned conditions and a final diameter of 450 nm, showed an approximated conductivity of 7 S/cm. The conductivity exhibited by these polypyrrole nanowires is approximately one order of magnitude higher as compared to other reported polypyrrole nanowires grown as well by electrochemical polymerization in aqueous solution (between 0.3 and 0.9 S/cm) [53].

5.3.3.2 *Polypyrrole nanowires grown in organic solvent*

The use of organic solvents for the fabrication of polypyrrole nanowires is discussed here. Using the previously optimized parameters with other chemical conditions increases the versatility of the fabrication method presented in this work, thus enabling the use of the fabricated nanowires for a wider range of applications.

The use of organic solvents in the electrochemical synthesis of conducting polymers is widely extended, since it avoids the overoxidation of the polymer occurring in aqueous media. It is reported that the nucleophilic attack of water

molecules on the monomer cation radicals, induce polymer degradation resulting in conducting polymer with poor physical properties [54, 55, 56]. Therefore, the polymerization under organic solvent conditions was attempted here, employing a model based on acetonitrile (ACN) and tetrabutylamonuim hexafluorophosphate ($TBAPF_6$) as compatible electrolyte.

The fabrication of polypyrrole nanowires was conducted on SiO_2-based template-assisted surfaces, avoiding the use of PMMA as passivation layer. The previously optimized conditions were used, consisting in alternating polymerization currents of 1 µA amplitude, 50% duty, 0.5 kHz frequency and a back voltage of -1 V. The polymerization solution included 10 mM pyrrole and 100 mM $TBAPF_6$ dissolved in acetonitrile.

Polypyrrole nanowires as the one shown in Figure 5.22a were obtained under the mentioned organic solvent conditions. These nanowires, showed good adhesion to the surface under washing processes with acetonitrile. The good ohmic contact of the polymer with the electrodes was evidenced by the I-V characteristics shown in Figure 5.22b, which resulted in calculated conductivity values of approximately 45 S/cm, obtained from Equation 5.1.

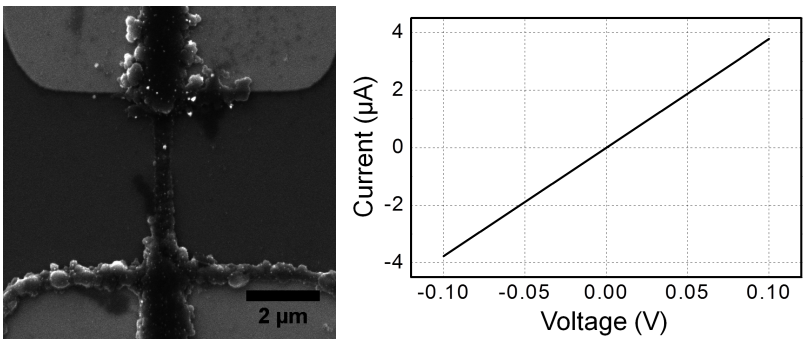

(a) (b)

Figure 5.22: Polypyrrole nanowire grown in SiO_2 nanochannel, applying an alternating polymerization current and a second perpendicular electric field, with tetrabutylammonium hexafluorophosphate in acetonitrile electrolyte. a) SEM image of a polypyrrole nanowire (450 nm in diameter). b) I-V characteristics of the polypyrrole nanowire.

This increase in conductivity with respect to nanowires grown in aqueous medium could be attributed to the use of the organic solvent itself, which avoids the large amount of defects produced by water-based solvents [54, 55, 56]. It is also known that the selection of the doping ion has a certain impact in the electrical performance of the final polymer [39, 57], which might be as well the reason

for the increase in the conductivity value. These electrical results are in good agreement with the only reported work of polypyrrole wires grown in organic solvent (propylene carbonate) using the PF_6^- doping ion, which exhibit values of 63 S/cm [58]. This proves that the fabrication method developed here is suitable under different chemical conditions, thus allowing tailoring of the polypyrrole nanowire devices properties.

5.4 CONCLUSIONS

Two polypyrrole nanowire fabrication techniques were presented in this chapter, namely dip-pen nanolithography (DPN) and electrochemical polymerization on template-assisted surfaces. Although completely different in working principle and resulting properties, both techniques resulted in polypyrrole nanowire devices with possible applications in different fields.

On one side, DPN showed to be a suitable technique for the fabrication of polypyrrole nanowires with a resolution of 100 nm and a good control on the polymer location. However, poor adhesion of the nanowires to the substrate indicated the limitation of this technique for fabricating functional devices. Moreover, as a strict deposition technique, it does not permit the chemical and physical modification of the polymer properties.

Alternatively, the growth of polypyrrole nanowires by electrochemical synthesis between electrical contacts, offers control over the chemical and physical properties of the polymer, by adjusting reaction parameters such as solvent and electrolyte. Polypyrrole nanowires in aqueous solvent were fabricated, with conductivity values (7 S/cm) one order of magnitude higher than other reported wires, grown under similar conditions. Additionally, higher conductivities were achieved for nanowires grown under organic solvent conditions (45 S/cm), similar to other analogous works. This confirms that variations on the synthesis parameters influence the final device performance.

At the end, the processes developed here resulted in ready-to-work systems based on single conducting polymer nanowires, contributing with new results to the reproducible fabrication of these nanomaterials, which might be useful for their integration into routine devices.

5.5 REFERENCES

[1] Hiroyuki Sakaki. "Scattering Suppression and High-Mobility Effect of Size-Quantized Electrons in Ultrafine Semiconductor Wire Structures." In: *Japanese Journal of Applied Physics* 19.12 (1980), pp. L735–L738 (cit. on p. 154).

[2] Neil P Dasgupta et al. "25Th Anniversary Article: Semiconductor Nanowires–Synthesis, Characterization, and Applications." In: *Advanced materials (Deerfield Beach, Fla.)* 26.14 (Apr. 2014), pp. 2137–84. DOI: 10.1002/adma.201305929 (cit. on p. 154).

[3] Yi Cui et al. "High Performance Silicon Nanowire Field Effect Transistors." In: *Nano Letters* 3.2 (Feb. 2003), pp. 149–152. DOI: 10.1021/nl025875l (cit. on p. 154).

[4] Hyesung Park et al. "Graphene Cathode-Based ZnO Nanowire Hybrid Solar Cells." In: *Nano Letters* 13.1 (2013), pp. 233–239. DOI: 10.1021/nl303920b (cit. on p. 154).

[5] David T Schoen et al. "High Speed Water Sterilization Using One-Dimensional Nanostructures." In: *Nano Letters* 10.9 (2010), pp. 3628–3632. DOI: 10.1021/nl101944e (cit. on p. 154).

[6] Wenjun Dong et al. "Multifunctional Nanowire Bioscaffolds on Titanium." In: *Chemistry of Materials* 19.18 (2007), pp. 4454–4459. DOI: 10.1021/cm070845a (cit. on p. 154).

[7] Carlos M. Hangarter et al. "Conducting polymer nanowires for chemiresistive and FET-based bio/chemical sensors." In: *Journal of Materials Chemistry* 20.16 (2010), p. 3131. DOI: 10.1039/b915717d (cit. on pp. 154, 155).

[8] Matt Law et al. "Nanoribbon Waveguides for Subwavelength Photonics Integration." In: *Science* 305.5688 (Aug. 2004), pp. 1269–1273. DOI: 10.1126/science.1100999 (cit. on p. 154).

[9] P. R. Nair and M. a. Alam. "Performance limits of nanobiosensors." In: *Applied Physics Letters* 88.23 (2006), p. 233120. ISSN: 00036951. DOI: 10.1063/1.2211310 (cit. on p. 154).

[10] Fernando Patolsky et al. "Electrical detection of single viruses." In: *Proceedings of the National Academy of Sciences of the United States of America* 101.39 (Sept. 2004), pp. 14017–14022. DOI: 10.1073/pnas.0406159101 (cit. on p. 154).

[11] Gengfeng Zheng et al. "Multiplexed electrical detection of cancer markers with nanowire sensor arrays." In: *Nat Biotech* 23.10 (Oct. 2005), pp. 1294–1301 (cit. on p. 155).

[12] Guo-Jun Zhang et al. "Highly sensitive measurements of PNA-DNA hybridization using oxide-etched silicon nanowire biosensors." In: *Biosensors and Bioelectronics* 23.11 (2008), pp. 1701–1707. DOI: 10.1016/j.bios.2008.02.006 (cit. on p. 155).

[13] Guo-Jun Zhang et al. "Silicon nanowire biosensor for highly sensitive and rapid detection of Dengue virus." In: *Sensors and Actuators B-chemical* 146.1 (2010), pp. 138–144. DOI: 10.1016/j.snb.2010.02.021 (cit. on p. 155).

[14] Ruomeng Yu et al. "Enhanced Performance of a ZnO Nanowire-Based Self-Powered Glucose Sensor by Piezotronic Effect." In: *Advanced functional materials* (2013), pp. 1–7. DOI: 10.1002/adfm.201300593 (cit. on p. 155).

[15] "Applications of conducting polymers and their issues in biomedical engineering." In: *Journal of the Royal Society, Interface / the Royal Society* 7 Suppl 5 (Oct. 2010), S559–79. DOI: 10.1098/rsif.2010.0120.focus (cit. on p. 155).

[16] Hyeonseok Yoon et al. "A novel sensor platform based on aptamer-conjugated polypyrrole nanotubes for label-free electrochemical protein detection." In: *Chembiochem : a European journal of chemical biology* 9.4 (Mar. 2008), pp. 634–41. DOI: 10.1002/cbic.200700660 (cit. on p. 155).

[17] Jeong In Lee et al. "Highly Aligned Ultrahigh Density Arrays of Conducting Polymer Nanorods using Block Copolymer Templates 2008." In: *Nano letters* 8 (2008), pp. 23–25 (cit. on p. 155).

[18] Yaping Dan et al. "Gas Sensing Properties of Single Conducting Polymer Nanowires and the Effect of Temperature." In: *Nanotechnology* 20 (2009), p. 434014 (cit. on pp. 156, 163).

[19] Sung-Yeon Jang, Manuel Marquez, and Gregory a Sotzing. "Rapid direct nanowriting of conductive polymer via electrochemical oxidative nanolithography." In: *Journal of the American Chemical Society* 126.31 (Aug. 2004), pp. 9476–7. ISSN: 0002-7863. DOI: 10.1021/ja047766+ (cit. on p. 156).

[20] By Jung-hyurk Lim and Chad A Mirkin. "Electrostatically Driven Dip-Pen Nanolithography." In: *Advanced Materials* 14.20 (2010), pp. 1474–1477 (cit. on pp. 156, 159, 163).

[21] Gerd Binnig and Heinrich Rohrer. "SCANNING TUNNELING MICROSCOPY - FROM BIRTH TO ADOLESCENCE." In: *Nobel Lecture* (1986) (cit. on p. 157).

[22] G Binnig, C F Quate, and Ch Gerber. "Atomic Force Microscope." In: *Physical Review Letters* 56.9 (1986), pp. 930–934 (cit. on p. 157).

[23] Kai-chih Chang et al. "Atomic force microscopy in biology and biomedicine." In: *Tzu Chi Medical Journal* 24.4 (2012), pp. 162–169. DOI: 10.1016/j.tcmj.2012.08.002 (cit. on p. 157).

[24] Brandon L Weeks, Mark W Vaughn, and James J Deyoreo. "Direct imaging of meniscus formation in atomic force microscopy using environmental scanning electron microscopy." In: *Langmuir : the ACS journal of surfaces and colloids* 21.18 (Aug. 2005), pp. 8096–8. DOI: 10.1021/la0512087 (cit. on p. 157).

[25] R. D. Piner et al. "Dip-Pen Nanolithography." In: *Science* 283.5402 (1999), pp. 661–663 (cit. on p. 157).

[26] Seunghun Hong, Jin Zhu, and Chad A Mirkin. "Multiple Ink Nanolithography : Toward a Multiple-Pen Nano-Plotter." In: *Science* 286 (1999), pp. 523–525 (cit. on p. 158).

[27] David S Ginger, Hua Zhang, and Chad A Mirkin. "The Evolution of Dip-Pen Nanolithography." In: *Angewandte Chemie International Edition* 43 (2004), pp. 30–45. DOI: 10.1002/anie.200300608 (cit. on p. 158).

[28] Hiroshi Nakashima et al. "Liquid Deposition Patterning of Conducting Polymer Ink onto Hard and Soft Flexible Substrates via Dip-Pen Nanolithography." In: *Langmuir* 28 (2012), pp. 804–811 (cit. on p. 158).

[29] E. Bellido et al. "Controlling the Number of Proteins with Dip-Pen Nanolithography." In: *Advanced Materials* 22 (2010), pp. 352–355 (cit. on p. 158).

[30] A. J. Senesi et al. "Agarose-Assisted Dip-pen Nanolithography of Oligonucleotides and Proteins." In: *ACS Nano* 3.8 (2009), pp. 2394–2402 (cit. on p. 158).

[31] Y. H. Shin et al. "Polymer-Coated Tips for Patterning of Viruses by Dip-pen Nanolithography." In: *Angewandte Chemie International Edition* 49 (2010), pp. 9689–9692 (cit. on p. 158).

[32] Minchul Yang et al. "Direct Writing of a Conducting Polymer with Molecular-Level Control of Physical Dimensions and Orientation." In: *Journal of the American Chemical Society* 128 (2006), pp. 6774–6775 (cit. on pp. 158, 163).

[33] Benjamin W Maynor et al. "Direct-Writing of Polymer Nanostructures : Poly (thiophene) Nanowires on Semiconducting and Insulating Surfaces." In: *Journal of the American Chemical Society* 124.4 (2002), pp. 2001–2002 (cit. on pp. 158, 163, 164).

[34] Lin Jiang, Xing Wang, and Lifeng Chi. "Nanoscaled surface patterning of conducting polymers." In: *Small (Weinheim an der Bergstrasse, Germany)* 7.10 (May 2011), pp. 1309–1321. DOI: 10.1002/smll.201002356 (cit. on p. 159).

[35] Tat'yana V Vernitskaya and Oleg N Efimov. "Polypyrrole: a conducting polymer; its synthesis, properties and applications." In: *Russian Chemical Reviews* 66.5 (May 1997), pp. 443–457. DOI: 10.1070/RC1997v066n05ABEH000261 (cit. on pp. 160, 165).

[36] Joonkyung Jang et al. "Self-assembly of ink molecules in dip-pen nanolithography : A diffusion model." In: *Journal of Chemical Physics* 115.6 (2001), pp. 2721–2729. DOI: 10.1063/1.1384550 (cit. on p. 162).

[37] Peter V Schwartz. "Molecular Transport from an Atomic Force Microscope Tip : A Comparative Study of Dip-Pen Nanolithography." In: *Langmuir : the ACS journal of surfaces and colloids* 18.100 (2002), pp. 4041–4046 (cit. on p. 162).

[38] Sergey Rozhok, Richard Piner, and Chad A Mirkin. "Dip-Pen Nanolithography : What Controls Ink Transport?" In: *Journal of Physical Chemistry B* 107 (2003), pp. 751–757 (cit. on p. 162).

[39] Alan G Macdiarmid. ""Synthetic metals": a novel rolefor organic polymers." In: *Current Applied Physics* 1 (2001), pp. 269–279 (cit. on pp. 164, 175).

[40] A Das et al. "Non-lithographic fabrication of PEDOT nano-wires between fixed Au electrodes." In: *Organic Electronics* 7 (2006), pp. 181–187. DOI: 10.1016/j.orgel.2005.12.006 (cit. on p. 165).

[41] Minhee Yun et al. "Electrochemically Grown Wires for Individually Addressable Sensor Arrays." In: *Nano Letters* 4.3 (Mar. 2004), pp. 419–422. DOI: 10.1021/nl035069u (cit. on p. 165).

[42] By Neil T Kemp et al. "Bridging the Gap : Polymer Nanowire Devices." In: *Advanced Materials* 19 (2007), pp. 2634–2638. DOI: 10.1002/adma.200602726 (cit. on p. 165).

[43] Maksudul M Alam et al. "Electrolyte-Gated Transistors Based on Conducting Polymer Nanowire Junction Arrays." In: *Journal of Physical Chemistry B* 109 (2005), pp. 12777–12784 (cit. on p. 165).

[44] Prem S Thapa et al. "Directional growth of metallic and polymeric nanowires." In: *Nanotechnology* 20 (2009), pp. 0–9. DOI: 10.1088/0957-4484/20/23/235307 (cit. on pp. 165, 173).

[45] Bhuvaneswari Kannan et al. "The electrochemical growth of conducting polymer nanowires." In: *Journal of Electroanalytical Chemistry* 669 (2012), pp. 82–89. DOI: 10.1016/j.jelechem.2012.01.022 (cit. on pp. 165, 173).

[46] Kumaran Ramanathan et al. "Individually Addressable Conducting Polymer Nanowires Array." In: *Nano Letters* 4.7 (July 2004), pp. 1237–1239. DOI: 10.1021/nl049477p (cit. on pp. 165, 169).

[47] Kumaran Ramanathan et al. "In Situ Fabrication of Single Poly (methyl pyrrole) Nanowire." In: *Electroanalysis* 19.7-8 (2007), pp. 793–797. DOI: 10.1002/elan.200603773 (cit. on p. 165).

[48] Minhee Yun et al. *Electrochemically grown single-nanowire sensors*. 2004. DOI: 10.1117/12.568948 (cit. on p. 165).

[49] Kumaran Ramanathan et al. "Bioaffinity sensing using biologically functionalized conducting-polymer nanowire." In: *Journal of the American Chemical Society* 127.2 (2005), pp. 496–497. DOI: 10.1021/ja044486l (cit. on p. 165).

[50] Innam Lee et al. "Highly sensitive single polyaniline nanowire biosensor for the detection of immunoglobulin G and myoglobin." In: *Biosensors and bioelectronics* 26.7 (Mar. 2011), pp. 3297–302. DOI: 10.1016/j.bios.2011.01.001 (cit. on p. 165).

[51] Thermo Scientific. *Chemical Compatibility Guide*. Tech. rep. Nalgene, Thermo Scientific (cit. on p. 167).

[52] Y Hu, A C To, and M Yun. "The controlled growth of single metallic and conducting polymer nanowires via gate-assisted electrochemical deposition." In: *Nanotechnology* 285605 (2009). DOI: 10.1088/0957-4484/20/28/285605 (cit. on p. 171).

[53] Prem S Thapa et al. "Directional growth of polypyrrole and polythiophene wires Directional growth of polypyrrole and polythiophene wires." In: *Applied Physics Letters* 033104.2009 (2014), pp. 10–13. DOI: 10.1063/1.3072611 (cit. on p. 174).

[54] Ryeo Yun Hwang et al. "Suppression of the loss of an electroactive dopant from polypyrrole by using a non-aqueous electrolyte of dopant-phobicity." In: *Journal of Electroanalytical Chemistry* 657.1-2 (July 2011), pp. 181–186. DOI: 10.1016/j.jelechem.2011.03.028 (cit. on p. 175).

[55] Petr Novák. "Limitations of polypyrrole synthesis in water and their causes." In: *Electrochimica Acta* 37.7 (June 1992), pp. 1227–1230. DOI: 10.1016/0013-4686(92)85060-X (cit. on p. 175).

[56] Chun-Guey Wu and Ching-Yuh Chen. "Chemical deposition of ordered conducting polypyrrole films on modified inorganic substrates." In: *Journal of Materials Chemistry* 7.8 (1997), pp. 1409–1413. DOI: 10.1039/a608365j (cit. on p. 175).

[57] Kwan Sik Jang, Hoosung Lee, and Bongjin Moon. "Synthesis and characterization of water soluble polypyrrole doped with functional dopants." In: *Synthetic Metals* 143 (2004), pp. 289–294. DOI: 10.1016/j.synthmet.2003.12.013 (cit. on p. 175).

[58] J G Park et al. "Non-linear I-V characteristics of polypyrrole micro-line synthesized using scanning probe microscope." In: *Current Applied Physics* 2 (2002), pp. 23–25 (cit. on p. 176).

6

GENERAL CONCLUSIONS

Although conducting polymers showed to be a promising alternative to conventional materials in biomedical devices, they are still far from being fully exploited and well integrated into functional devices. Patterning of conducting polymers with good spatial resolution is a key point for new generation of biomedical devices, as well as new device designs for obtaining better performances.

This thesis contributes at providing better understanding of the micro- and nanofabrication methodologies, appropriate for conducting polymers, together with novel functionalization strategies compatible with the construction of bioactive polymeric platforms that could be applied to areas such as biomolecule sensing and release.

In particular, a new on-surface biocatalytical procedure for the fabrication of conducting polypyrrole microelectrodes on insulating surfaces was developed, obtaining resolutions comparable to photolithography. This procedure showed to be compatible with the incorporation of bioactive compounds during the polymer synthesis, allowing to perform the fabrication in biological friendly environments. This bioactive polymer was tested under the controlled release of biotin, showing a good control on the release process.

Moreover, a novel electrochemical label-free DNA hybridization sensor for "Hepatitis C" virus sequences was developed based on azide-PEDOT electrodes. These polymeric electrodes allow the direct functionalization with acetylene-terminated DNA sequences, by the fast and robust "Click" reaction. This novel DNA post-functionalization strategy preserves DNA from denaturation during the polymerization process. DNA sensors fabricated in this way showed to be highly selective and sensitive, without the need of complex labelling or microfabrication processes, to achieve low limits of detection.

Finally, polymer structures at the nanoscale were achieved by two fabrication techniques, namely dip-pen nanolithography and electrochemical polymerization on template-assisted surfaces. Both techniques showed good control over

size and location of polymer nanowires, but the later provided better stability of the nanostructures. This work brings new results to the fabrication of single conducting polymer nanowires, resulting in ready-to-work systems, which might be integrated into routine devices.

Future perspectives of this work would be addressed to test conducting polymer nanowire-based devices into biomolecule sensing and release appliations, as the ones approached here.

7

RESUMEN EN CASTELLANO

INTRODUCCIÓN GENERAL

Aunque los polímeros conductores se presentan como una alternativa viable a los materiales convencionalmente usados en aplicaciones biomédicas, las técnicas de fabricación adaptadas a ellos y el aprovechamiento de sus propiedades están lejos de ser completos. Existen importantes limitaciones en la fabricación de micro y nano estructuras basadas en polímeros conductores, las cuales han demostrado ser de gran utilidad en el desarrollo de dispositivos biomédicos de última generación. Debido a la agresividad de las técnicas tradicionalmente usadas en microelectrónica, se hace necesaria la búsqueda de nuevas estrategias de fabricación adaptadas a polímeros conductores, así como de nuevos procesos que puedan mejorar el rendimiento de los dispositivos diseñados.

En esta tesis se abordan parte de estos problemas, aportando nuevos resultados a este campo.

En esta sección introductoria se describen las propiedades que hacen a los polímeros conductores tan atractivos en el campo de la biomedicina, así como los más relevantes ejemplos de aplicación. Un resumen de los principales resultados obtenidos en esta tesis se presenta en secciones posteriores.

Polímeros conductores en aplicaciones biomédicas

La mayor parte de los dispositivos biomédicos, como biosensores, dispositivos de liberación de fármacos y dispositivos implantables necesitan un buen interfaz dispositivo-biología. Sin embargo, los materiales que tradicionalmente han sido usados para estos fines (metales y semiconductores inorgánicos) han demostrado no ser suficientemente compatibles química y mecánicamente con sistemas biológicos [1]. Como alternativa a estos materiales convencionales, los

polímeros conductores ofrecen la posibilidad de manipular las propiedades eléctricas del material (con conductividades desde 10^{-12} hasta 10^{5} S/cm), mediante la variación de sus parámetros de síntesis, pueden conducir flujos de iones (de gran importancia para las comunicaciones con entes biológicos), son mecánicamente más compatibles con sistemas biológicos como células o tejidos y es sencillo incorporar a su estructura moléculas funcionales que puedan aumentar la biocompatibilidad del polímero, incrementando así su estabilidad y vida media [2, 3, 4].

Gracias a estas propiedades, los polímeros conductores han sido integrados en biosensores, por su capacidad de comportarse como matrices inmovilizadoras de moléculas funcionales y como transductores al mismo tiempo [5]. Las propiedades eléctricas, electroquímicas y ópticas de los polímeros conductores son sensibles a sucesos que ocurren en el entorno cerca de su superficie, como pueda ser un proceso de reconocimiento [6]. Además, se pueden funcionalizar por medio de múltiples técnicas, lo que permite incorporar biomoléculas a su estructura que impartan la selectividad necesaria para un sensor [7]. De este modo, los polímeros conductores han sido usados para detectar muchos tipos de analitos biológicos como proteínas, virus, oligonucleótidos, pequeñas biomoléculas, bacterias e incluso células [8].

También se ha demostrado que los polímeros conductores pueden desencadenar procesos biológicos como la adhesión, migración e incluso la diferenciación celular, por medio del estímulo eléctrico, o por medio de la liberación de biomoléculas que afecten a dichos procesos [9]. Un interesante ejemplo es el uso de sustratos de polipirrol para la estimulación eléctrica de neuronas, el cual ha demostrado mejorar la neuritogénesis in vitro, el primer paso en la diferenciación neuronal [10].

Además, la biocompatibilidad de algunos polímeros conductores ha demostrado ser útil para el desarrollo de dispositivos implantables, donde es prioritario preservar el entorno [6]. Un ejemplo de su aplicabilidad son las prótesis neuronales, como los implantes de oído. Tradicionalmente, estos implantes se han fabricado en forma de microelectrodos metálicos. Estos microelectrodos tienen una baja biocompatibilidad con el tejido neuronal, causando inflamación y tejido cicatrizal, lo que a medio plazo produce la pérdida de eficiencia del dispositivo [11]. En este ámbito, lo polímeros conductores han demostrado ser mecánicamente más respetuosos con el tejido neuronal, a la vez que buenos conductores [12, 13]. Más aún, la facilidad en la funcionalización de los polímeros, permite incorporar biomoléculas que mejoren la integración y la biocompatibilidad del

polímero con el tejido, alargando así la vida y funcionalidad de los dispositivos [14, 15].

Sin embargo, las nuevas tendencias en dispositivos implantables y biosensores necesitan de dispositivos más efectivos, con arrays de microelectrodos [5, 16, 17], para lo que las técnicas de fabricación de polímeros conductores no están preparadas. Los métodos de fabricación estandarizados para la industria microelectrónica, como la fotolitografía, no son aplicables a los polímeros conductores por producir daños térmicos en el polímero y ser incompatibles con las biomoléculas incorporadas en él [18]. Por tanto, el desarrollo de nuevas técnicas de fabricación a la micro- nanoescala para polímeros conductores, es uno de los mayores retos en este campo. Además, hay también un creciente interés en desarrollar métodos de fabricación más respetuosos medioambientalmente, no tóxicos, así como polímeros biodegradables, con nuevos diseños de funcionalización que permitan obtener mejores rendimientos, etc.

Esta tesis, con título "Conducting polymers for micro and nano electrodes. Application to biomolecule sensing and release", se han intentado resolver algunos de estos problemas, como la micro- y nanofabricación. También ha intentado abordar el desarrollo de nuevas plataformas poliméricas para aplicaciones en dispositivos biomédicos. Este trabajo contribuye a un mayor entendimiento de la fabricación de dispositivos biomédicos basados en polímeros conductores, abriendo el campo de aplicación de los polímeros en este ámbito.

7.1 MATERIALES Y MÉTODOS

Esta sección describe brevemente los materiales y métodos usados durante el desarrollo de esta tesis.

7.1.1 *Materiales*

En la sección referida a los materiales se distingue entre:

Los polímeros conductores empleados en este trabajo: polipirrol y azide-PEDOT.

Los sustratos sobre los que se han crecido los polímeros: obleas de Si/SiO_2, obleas de Si/SiO_2 con microelectrodos de oro y macroelectrodos cilíndricos de oro.

Y los agentes mediadores que han servido para fabricar patrones de polímero: monocapas autoensambladas de silanos como N-(3-Trimethoxysilylpropyl)pyrrole (silano-pirrol), perfluoropolyether-silyltriethoxy-terminated (silano-perfluoropol-

yether), (3-Aminopropyl)triethoxysilane (APTES) y Trichloro (1H,1H,2H,2H-perfluorooctyl)silane (FDTES). Poly(methyl methacrylate) (PMMA)se ha usado también para crear nanopatrones.

7.1.2 *Métodos*

Respecto a los métodos, se encuentran:

La polimerización, en sus dos estrategias abordadas: electroquímica y biocatalítica.

La preparación de sustratos sobre los que se crecen los polímeros, esto es, la fabricación de microelectrodos metálicos por medio de fotolitografía, grabado y depósito de materiales.

Los métodos de formación de patrones, con las técnicas de microcontact printing, dip pen, focused ion beam y electron beam lithography.

Y las técnicas de caracterización empleadas para estudiar los polímeros y los dispositivos desarrollados: microscopio atómico de fuerzas (AFM), microscopio electrónico de barrido (SEM), interferómetro de luz blanca (WLI), difracción de rayos X (XRD), microscopio electrónico de transmisión (TEM), espectroscopia fotoelectronica de rayos X (XPS), espectrometría de masas de iones secundarios por tiempo de vuelo (ToF-SIMS), espectroscopia infrarroja (IR), voltameria cíclica, voltametria diferencial de pulso, ángulo de contacto y cromatografía liquida acoplada a espectrometría de masas (HPLC-MS).

7.2 CAPAS DELGADAS Y MICROELECTRODOS DE POLIPIRROL PRODUCIDAS BIOCATALÍTICAMENTE, SOBRE SUPERFICIES AISLANTES

7.2.1 *Introducción*

En el campo de los dispositivos biomédicos hay una creciente demanda en el desarrollo de dispositivos formados por arrays de microlectrodos, que sean compatibles con los sistemas biológicos. Los polímeros conductores han demostrado ser mecánica y biológicamente compatibles con estos sistemas, en múltiples aplicaciones como en los dispositivos implantables [11]. Sin embargo, la fabricación de polímeros conductores a la micro escala no es compatible con los métodos estandarizados para materiales convencionales, puesto que degradan el polímero y los grupos funcionales que puedan contener. Por ello, técnicas de depósito directo de polímeros como el screen-printing, el inkjet printing, el termal-laser-

printing y la soft-lithography han sido abordadas, como alternativa para resolver este problema [19, 20, 21, 22, 23, 24, 25, 26, 27]. Aunque estas técnicas han demostrado su utilidad en el rango de la microescala, sufren de problemas en la adhesión a la superficie. Además, a veces necesitan de la manipulación química del polímero para aumentar su solubilidad, lo que acaba afectando a las propiedades del mismo. Como alternativa, la polimerización directa sobre superficie ha sido usada también. Así, es posible crecer electroquímicamente polímeros conductores, con buena adhesión y conductividad, pero sólo sobre superficies conductoras [28, 29]. O también sobre superficies aislantes de modo químico, aunque aquí los polímeros obtenidos son poco conductores y las condiciones de síntesis son demasiado agresivas para ser aplicadas en entornos biológicamente compatibles [30, 31]. Para superar estos problemas, recientemente ha surgido el método de polimerización biocatalítica. Esta polimerización se produce en medios acuosos, bajo condiciones muy suaves que permiten la convivencia con entes biológicos. También, se produce con alta selectividad y sin comprometer las propiedades eléctricas de los polímeros resultantes [32]. Los procesos de polimerizacion biocatalitica más frecuentes usan encimas como la lacasa y las peroxidasas, como la peroxidasa del rábano (HRP), la peroxidasa de la soja (SBP) y la peroxidasa de la palmera (PTP) [33, 34, 35]. Sin embargo la eficiencia de estas encimas respecto al pirrol es muy limitada debido al alto potencial de oxidación del pirrol. Para solucionar este problema, se ha demostrado que se pueden incorporar mediadores redox, que participen en la cadena de polimerizacion, completando así la reacción con el pirrol [36]. En concreto, este trabajo se centrará en el uso del HRP y el mediador redox 2,2'-azinobis(3-ethylbenzothiazoline-6-sulfonate) (ABTS) para la síntesis de polipirrol [37, 38].

El potencial de oxidación del pirrol está entre 0.8 V y 1.0 V y el de la enzima HRP es 0.7 V (potenciales referidos a electrodo Ag/AgCl) [35, 39], siendo esta una de las causas por las que el pirrol no es buen sustrato para la enzima. Sin embargo, ha sido demostrado que usando el mediador ABTS en la reacción, cuyo potencial de oxidación se sitúa entre 0.5 V y 1.0 V (vs. Ag/AgCl) [35], ésta se produce de modo eficiente [37, 38]. En este proceso, la enzima activada por medio de peróxido de hidrógeno, es capaz de oxidar dos moléculas de ABTS, que a su vez pueden oxidar sendos monómeros de pirrol desencadenando la reacción (Figura 7.1). Tras esta reacción, la enzima se reduce a su estado original, quedando de nuevo disponible para otra reacción.

Aunque este proceso ha demostrado crear capas de polipirrol en los contenedores de la reacción [38], nunca ha sido utilizado para crecer selectivamente

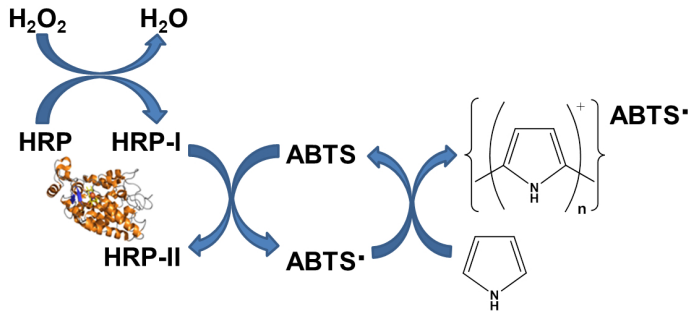

Figure 7.1: Esquema de la polimerización biocatalítica del polipirrol, usando la enzima HRP y el mediador redox ABTS.

capas de polipirrol. Por tanto, en esta sección describiremos la fabricación de microelectrodos de polipirrol, generados por método biocatalítico, usando la enzima HRP y el mediador redox ABTS. Caracterizaremos el polímero químicamente, estructuralmente y electroquímicamente. También demostraremos que tras un proceso de bio-funcionalizacion, el polímero sigue siendo electroactivo, ejemplificado por una prueba de concepto de liberación de fármacos. En ella, biotina atrapada en el polímero durante la síntesis, se liberará de modo controlado bajo estímulo eléctrico.

7.2.2 *Fabricación y caracterización de capas delgadas de polipirrol por método biocatalítico*

7.2.2.1 *Fabricación*

Capas delgadas de polipirrol fueron crecidas sobre superficies de SiO_2 con fines de caracterización. Para obtener una capa de polímero homogénea y bien adherida a la superficie se ha demostrado que el uso de silanos puede resultar eficiente [30]. En este caso, un silano con un terminal pirrol (silano-pirrol) se enlazó covalentemente a la superficie de óxido, para poder establecer un anclaje estable entre polímero y superficie. Así pues, superficies de SiO_2 fueron silanizadas por medio del método de fase vapor, con el silano-pirrol, para después ser polimerizadas. El proceso se describe a continuación:

Las superficies de SiO_2 fueron tratadas con piraña (7:3 (v/v) de H_2SO_4 concentrado y 30% H_2O_2) durante 15 minutos para crear grupos hidroxilos, necesarios en el proceso de silanización (Figura 7.2a).

Las superficies activadas fueron introducidas en un desecador con una gota de silano-pirrol puro y sometida a vacío durante 1 h (Figura 7.2b).

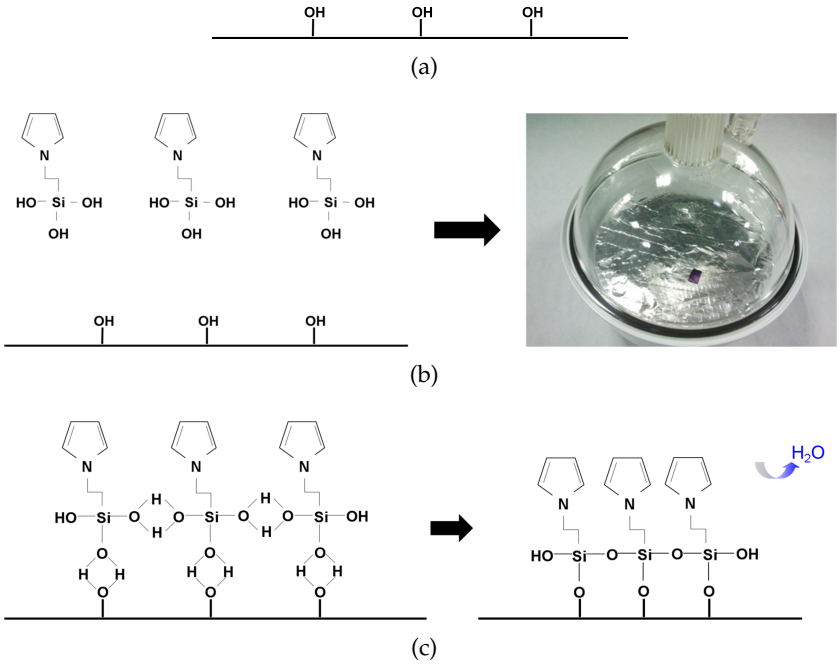

Figure 7.2: Silanizacion por fase vapor de superficies de SiO_2 con silano-pirrol. a) hidroxilación de SiO_2, b) depósito de silano por fase vapor and c) calentamiento.

Después, 1 h de calentamiento de la muestra a 80ºC fue necesaria para promover el enlace covalente O-Si-O (Figura 7.2c).

Tras el proceso de silanizacion, las muestras fueron introducidas en un reactor en el que la enzima, el pirrol y el mediador redox fueron añadidos. La reacción se desencadenó al añadir el peróxido de hidrogeno.* Finalmente, las muestras fueron lavadas con abundante agua y analizadas.

** Detalles de la polimerización:*
En 15 mL de buffer 4.0 pH (50 mM potassium biphtalate): 3.35 mmol pirrol, 0.123 mmol ABTS y 0.042 mmol EDTA.
Una cantidad 7.32 mg de HRP se disolvieron en 1.68 mL de buffer 7.0 pH (phosphate buffered saline, 10 x PBS).
3.35 mmol de H_2O_2.

7.2.2.2 *Caracterización*

Para investigar en detalle las características químicas de las capas de polipirrol crecidas en este trabajo, se usó la técnica de XPS. En la Figura 7.3, se muestra un espectro completo de una de las muestras de polipirrol en el que se pueden distinguir siete picos predominantes. Estos picos fueron identificados como carbono (C 1s), oxigeno (O 1s), silicio (Si 2s and Si 2p), nitrógeno (N 1s) y azufre (S 2s and S 2p). La señal del nitrógeno se asoció al pirrol, mientras que la señal

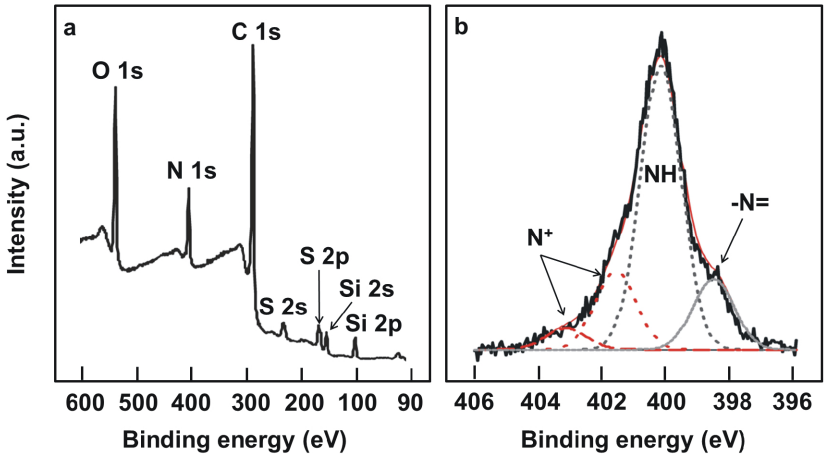

Figure 7.3: Análisis de XPS análisis de capas delgadas de polipirrol biocatalítico. a) Espectro completo de capa de polipirrol. b) Espectro de alta resolución del pico N 1s, mostrando las deconvoluciones.

de azufre demuestra la existencia del mediador ABTS, que actúa como dopante y permanece en la estructura polimérica [32, 38].

Si analizamos la señal de alta resolución del pico del nitrógeno (Figura 7.3), podemos extraer información adicional acerca de las propiedades del polímero. Las deconvoluciones de dicho pico, sugieren la existencia de tres estados diferentes de nitrógeno presentes en la muestra. La primera señal (-N= en 398.5 eV), correspondería al polipirrol oxidado, la segunda señal (NH en 400.1 eV), pertenecería al nitrógeno en estado de amina secundaria y la tercera, compuesta de dos picos (N+ en 401.6 y 403.1 eV), al nitrógeno cargado positivamente. Esta última señal representa el porcentaje de dopante presente en la muestra, que en este caso corresponde al el 28% del nitrógeno total de la muestra. Este valor está dentro de lo esperado para polipirrol idealmente dopado, donde el tanto por ciento de dopaje es del 25% [38].

También se analizó el grosor de las capas crecidas en función del tiempo. Para ello, se crecieron capas de polipirrol durante tiempos entre cinco minutos y dos horas. Tras el crecimiento, se realizó un proceso de lavado ultrasónico, en agua durante 5 minutos, para eliminar cualquier resto de polipirrol que no estuviera anclado fuertemente a la superficie de óxido. Las medidas de grosor, realizadas por AFM, revelaron que tras los primeros minutos de crecimiento, se formaban capas homogéneas de unos 30 nm de espesor, con independencia del tiempo de crecimiento. Esta limitación en el grosor de las capas fue atribuida a la perdida de cohesión del polímero a distancias superiores de 30 nm. Dicha cohesión po-

dría estar producida por la existencia del silano-pirrol, que obliga a ordenar las cadenas poliméricas de cierto modo durante los primeros nanómetros de espesor, y que va perdiéndose con la distancia a la superficie [40].

Por último se caracterizó el polímero electroquímicamente, mediante voltametría cíclica. Esta técnica ofrece una rápida visualización de los potenciales redox de las sustancias analizadas. En la Figura 7.4 observamos un voltamograma correspondiente a una capa delgada de polipirrol, entre -0.9 V y +0.9 V en PBS, a una velocidad de escaneo de 100m V/s. Aquí podemos identificar los picos anódico y catódico del polímero, situados a 0.45 V y -0.75 V respectivamente. Estos picos, como suele ocurrir en polímeros conductores, son anchos y poco pronunciados, pero reflejan la capacidad electroactiva del sistema [41].

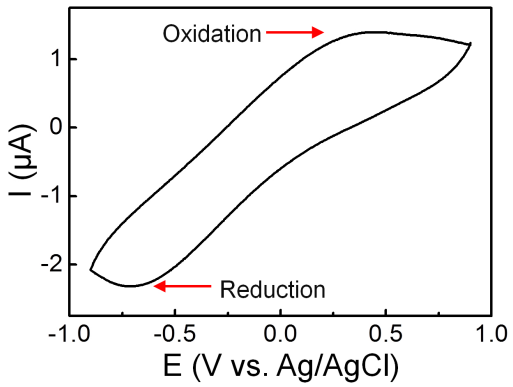

Figure 7.4: Voltamograma cíclico de capa de polipirrol biocatalítico.

7.2.3 *Fabricación y caracterización de microelectrodos de polipirrol por método biocatalítico*

La fabricación de arrays de microlectrodos de polipirrol está mostrada en la Figura 7.5a. Las dimensiones del microelectrodo se definieron introduciendo un patrón de un fluorosilano hidrofóbico (trichloro(1H, 1H, 2H, 2H-perfluoro octyl)silane) (FDTES) en la superficie de óxido, por medio de la técnica de microcontact printing. Este silano posee propiedades repelentes y anti adhesivas, que permitirán evitar el anclaje del polímero a la superficie [42]. En las zonas libres de fluorosilano, se depositó el silano-pirrol (método en fase vapor), promoviendo así un fuerte enlace del polímero en estas zonas. Después de la silanización, las superficies fueron polimerizadas durante 60 minutos, sonicadas y analizadas mediante SEM y ToF-SIMS (Figuras 7.5b y 7.5c).

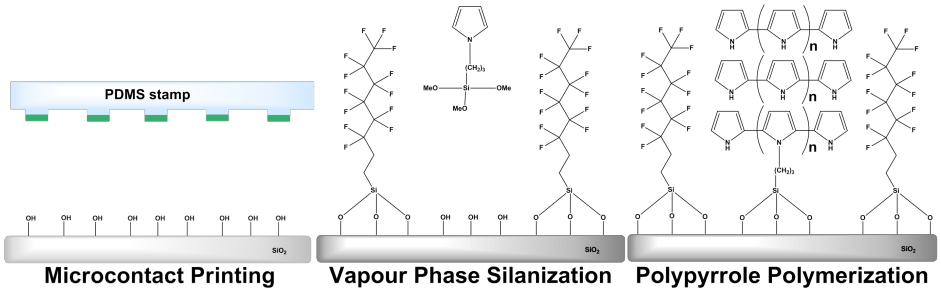

(a)

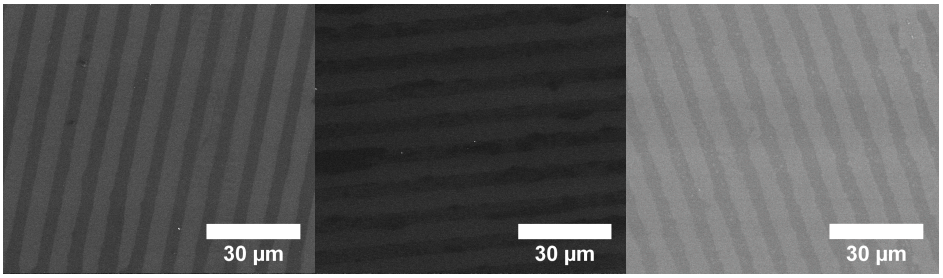

(b)

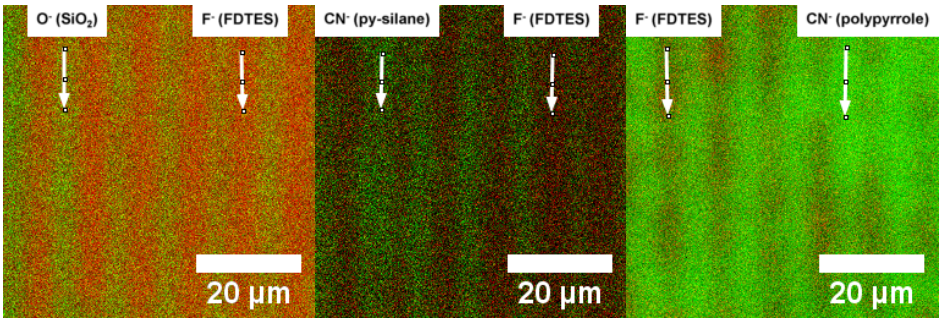

(c)

Figure 7.5: Fabricación de microelectrodos de polipirrol biocatalítico sobre superficies de óxiodo de silicio. a) Esquema del proceso. b) Imágenes de SEM a cada paso del proceso. c) Imágenes de ToF-SIMS a cada paso del proceso.

Las imágenes de SEM muestran como el patrón es conservado a lo largo del proceso de fabricación, habiendo conseguido una resolución de patrón de 5 µm, comparable a la capacidad de las técnicas fotolitográficas. Por otro lado, los resultados de ToF-SIMS, prueban la correcta distribución química sobre dicho patrón. En concreto, en la imagen correspondiente a la silanización con el flurosilano, se pueden observar franjas donde la presencia de iones de oxígeno (O^-, correspondiente al sustrato (SiO_2)) y de flúor (F^-, correspondiente al fluorosilano) están bien diferenciadas. En el paso siguiente (añadiendo el silano-pirrol), se puede observar como la alternancia de iones se da ahora en entre CN^-, correspondi-

ente al pirrol, y F^-, correspondiente al fluorosilano. Y por último, después de la polimerización se observan franjas de polímero (CN^-) y de silano (F^-).

7.2.4 *Funcionalización biológica de capas delgadas y microelectrodos de polipirrol crecidos de modo biocatalítico*

En este caso, capas y microelectrodos de polipirrol fueron fabricados, añadiendo biotina a la reacción de polimerización. De este modo, la biotina queda atrapada físicamente en la matriz polímerica, como quedó demostrado en los análisis realizados sobre capas delgadas por medio de XPS.

En la Figura 7.6, pueden observarse los espectros de alta resolución pertenecientes al azufre, de dos capas de polipirrol crecidas de modo biocatalítico, con y sin biotina. En este caso analizamos el azufre, puesto que es un elemento característico en la biotina.

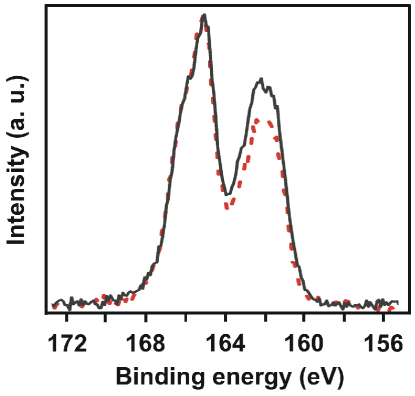

Figure 7.6: Espectros de alta resolución de XPS del azufre S 2p, correspondiente a una capa de polipirrol biocatalítico (línea roja de puntos) y una capa de polipirrol biocatalítico con biotina (línea negra sólida).

En estas muestras, como se ha mencionado anteriormente, se encuentran otras fuentes de azufre, como el mediador redox y la enzima, por lo que se evaluó la diferencia entre espectros para muestras con y sin biotina.

Para ambos casos se obtuvieron dos componentes centradas en 165.1 eV y 162.0 eV, respectivamente. El pico observado a 165 eV, correspondiente a especies oxidadas de azufre ($-SO_3H$), fue asociado al dopante ABTS, mientras que el pico a 162 eV, se asoció a la enzima HRP (C-S-C and C-SH) [43, 44, 45]. En ausencia de biotina, el ratio entre ambos picos resultó de 0.90, mientras que en presencia de biotina, éste aumentó hasta 1.14, sugiriendo la incorporación de biotina a la estructura.

Tras la confirmación de la correcta funcionalización del polímero con biotina, micorelectrodos con biotina fueron fabricados. Este proceso, resultó en estructuras como las mostradas en la Figura7.7.

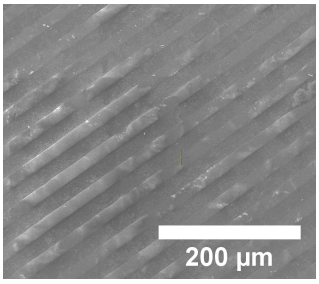

Figure 7.7: Imagen de SEM de microestructuras de polipirrol biocatalítico con presencia de biotina.

En esta imagen de SEM, se puede observar cómo la cohesión del polímero se ve afectada por la presencia de la biotina, lo que ha sido reportado anteriormente en otros trabajos [14]. Esto, fue atribuido al hecho de que la biotina, cargada negativamente durante el proceso de polimerización, actúe como dopante en la reacción, interfiriendo en el proceso de polimerización. Mediante el ajuste de los parámetros de revelado (tiempo de sonicación) los patrones fueron conservados.

7.2.5 *Aplicación: liberación controlada de biotina*

Ha sido demostrado que el salto electroquímico del polímero entre sus estados oxidado y reducido, produce la liberación de iones contenidos en su interior [46], lo que puede tener aplicaciones en dispositivos de liberación de fármacos.

Así pues, capas de polipirrol biocatalítico, crecidas en presencia de biotina, fueron sometidas a voltametría cíclica (CV) en PBS entre -0.9 V y +0.9 V, a una velocidad de escaneo de 100 mV/s. En el caso de la biotina y el polipirrol, cuando el polímero se reduce, la interacción electrostática entre los iones dopantes y el polímero desaparece, produciéndose una liberación al medio de dichos iones [47].

Tres experimentos fueron conducidos: uno en el que se aplicó voltametría cíclica a una capa de polipirrol con biotina durante 25 minutos, otro en el que se aplicó un potencial constante de oxidación de +0.9 V durante 25 minutos a otra capa con biotina y un último experimento en que no se aplicó estímulo eléctrico alguno sobre el polímero, pero se mantuvo en solución durante 25 minutos. Se extrajeron muestras de la solución de medida después del primer minuto de

experimento y cada 5 minutos hasta el final. Dichas muestras se analizaron por HPLC-MS, resultando en curvas de liberación de biotina con el tiempo, como las mostradas en la Figura 7.8.

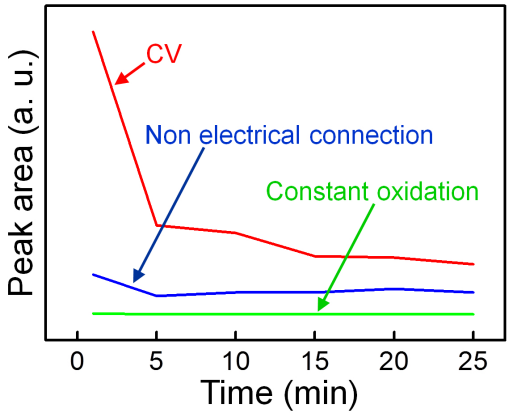

Figure 7.8: Resultados de HPLC-MS para la liberación de biotina. Gráfico de evolución del pico característico correspondiente al fragmento de la biotina m/z = 245.09, obtenido mediante el análisis de la solución de medida a diferentes tiempos, durante un proceso de reducción por CV (línea roja), un proceso de oxidación constante (línea verde) y sin aplicación de estímulo eléctrico (línea azul).

Los resultados muestran que bajo estimulación por voltametría cíclica, la mayor parte de la biotina atrapada en el polímero se libera durante los primeros 5 minutos. Por otro lado se observa un pequeño efecto de liberación cuando no hay estímulo eléctrico aplicado, producido por un intercambio iónico, cuando existe un gradiente de especies negativas entre la solución y el polímero [48]. Finalmente, cuando se aplica un potencial de oxidación constante, no se observa liberación significativa de biotina, ya que se incrementa la interacción electrostática entre polímero y biotina, impidiendo su liberación.

Estos resultados demuestran que tras el proceso de funcionalización con biotina, las capas de polipirrol generadas en este trabajo, siguen siendo electroactivas, liberando controladamente biotina al medio.

7.2.6 *Conclusiones*

Este trabajo introduce una nueva técnica biocatalítica en superficie, para la fabricación de microlectrodos de polipirrol sobre superficies aislantes, con resoluciones comparables a las de la litografía óptica. Esta es una técnica de microfabricación medioambientalmente respetuosa, que permite la incorporación de

biomoléculas durante el proceso de síntesis. Esta técnica ha demostrado retener la electroactividad del polímero después de los procesos de fabricación y funcionalización, como pudo ser observado mediante la liberación de biotina atrapada en la estructura, bajo estimulación eléctrica. Estas características podrían ser usadas en dispositivos de interacción con tejidos o células, mediante la liberación de fármacos o la estimulación eléctrica.

7.3 ELECTRODOS DE AZIDA-PEDOT. APLICACIÓN EN SENSORES DE ADN

7.3.1 *Introducción*

La detección específica y cuantitativa de secuencias de ADN es de gran importancia en el sector de la medicina, no sólo para diagnosticar enfermedades, sino también para desarrollar terapias efectivas [49, 50]. En este ámbito, los sensores de hibridación de ADN representan una alternativa atractiva a los métodos tradicionales de secuenciado, por ser simples, versátiles y útiles para el desarrollo de arrays de dispositivos [51, 52].

Los sensores de hibridación están generalmente compuestos por un elemento transductor, en el que una cadena simple de ADN, llamada prueba, se ancla. Este sistema se expone entonces a otra cadena simple de ADN, complementaria a la primera (diana), produciéndose la hibridación. Este proceso de reconocimiento (hibridación) genera una señal, que es traducida por el transductor a una señal directamente legible (Figura 7.9).

La calidad de un sensor se mide por su selectividad y su sensibilidad, las cuales dependen del diseño del dispositivo. La selectividad de un sensor de este tipo viene dada por la especificidad en el reconocimiento entre dos cadenas complementarias de ADN. Dicha especificidad en la interacción entre cadenas de ADN proviene de restricciones estéricas y de formación de puentes de hidrógeno entre bases purínicas (adenina o guanina) y pirimidínicas (timina o citosina) [53]. Esto es, el espacio interior de una doble hélice de ADN corresponde exactamente a una pareja purina-pirimidina, además adenina y timina forman dos puentes de hidrógeno, mientras que guanina y citosina forman tres puentes de hidrógeno, lo que determina inequívocamente la especificidad de la interacción entre las bases.

En cambio la sensibilidad viene dada por parámetros más técnicos como la matriz usada para la inmovilización de la prueba, la estrategia de inmovilización o el mecanismo de transducción. Así, es posible encontrar sensores de hibridación con estrategias de inmovilización variadas, como la simple adsorción en

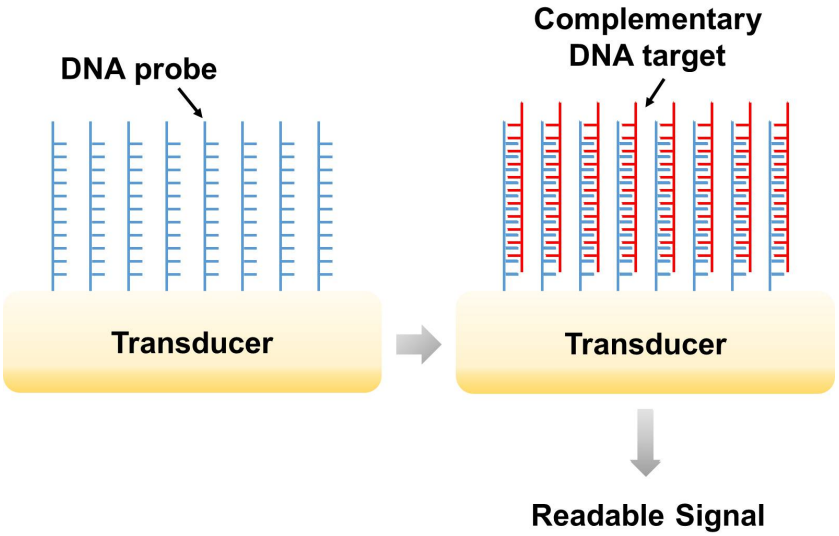

Figure 7.9: Esquema de un sensor de hibridación de ADN. Está compuesto de un elemento transductor, una capa de reconocimiento (DNA probe) y el analito a detectar (Complementary DNA target). Tras la hibridación una señal legible se obtiene del transductor.

la superficie, el enlace covalente o la interacción estreptavidina-biotina, etc [7]. Y basados en diferentes mecanismos de transducción como óptico, de masa o electroquímico [7, 54, 55, 56, 57]. En esta sección nos centraremos en el uso de sensores electroquímicos, por ser fiables, simples, rápidos, rentables y ser capaces de convertir directamente un proceso de hibridación en una señal eléctrica legible [7]. Diferentes técnicas se han empleado para monitorizar la hibridación de ADN, como amperometría, potenciometría, voltametría, cronoamperometria o espectroscopía electroquímica de impedancia [5, 58]. También se han desarrollado métodos indirectos de detección (de marcaje), en los que se usa un marcador electroquímico para detectar la hibridación. Ejemplos de estos marcadores son los indicadores redox (se anclan al ADN diana, enzimas, quantum dots) o los intercaladores redox (se intercalan en la doble hélice por interacción electrostática, iones complejos o marcadores orgánicos como el methylene blue), cuya detección evidencia la hibridación [59, 60, 61].

La detección mediante estas técnicas de marcaje ha demostrado ser muy sensible (rango nanomolar incluso femtomolar) y capaz de distinguir mutaciones de una sola base [62, 63]. Sin embargo, muchos de estos métodos pueden afectar al enlace con la secuencia de prueba, interfiriendo así en el proceso de re-

conocimiento. Además, estas técnicas necesitan tiempo de preparación, costes extraordinarios y no permiten detectar la hibridación en tiempo real.

Por el contrario existen también técnicas de detección directa (sin marcaje), en las que lo que se evalúa es la electroactividad de los ácidos nucleicos o los cambios producidos en las propiedades electrónicas del transductor tras el proceso de hibridación. Estas técnicas son más rápidas, no necesitan un tiempo adicional para hacer el marcaje y pueden ser usadas con independencia de la secuencia elegida [64].

Como se ha avanzado anteriormente, las técnicas de detección directa se basan o bien en la electroactividad de las bases nitrogenadas o en la electroactividad del transductor/sustrato del sensor. En el primer caso, se ha demostrado que la adenina y la guanina son las bases más electroactivas del ADN y son sus sendos picos de oxidación los que usualmente son evaluados para detectar su presencia [65, 66]. Sin embargo, esta técnica es muy controvertida y depende altamente de la secuencia elegida, así como de su contenido en guaninas y adeninas [7]. Por otro lado, respecto a la electroactividad del sustrato, los polímeros conductores han demostrado ser útiles por comportarse como matriz inmovilizadora de ADN y como transductor al mismo tiempo [5]. En particular, sus propiedades eléctricas, electroquímicas y ópticas son sensibles a sucesos que ocurren en el entorno cerca de su superficie, como pueda ser un proceso de hibridación [6]. Además, se pueden funcionalizar por medio de múltiples técnicas, permitiendo su uso en sensores de ADN sin marcaje [67].

En esta sección se describe la fabricación y prueba de un sensor de hibridación de ADN sin marcaje, basado en electrodos de poly(3,4-ethylenedioxythiophene) modificado con un grupo azida (azida-PEDOT). Estos electrodos de azida-PEDOT se fabricaron por medio de polimerización electroquímica sobre electrodos de oro, quedando directamente funcionalizados después del proceso de síntesis (parte de este trabajo fue desarrollado en colaboración con el instituto de química orgánica II y materiales avanzados de la universidad de Ulm, Alemania). Después, se usaron como plataformas para la inmovilización de secuencias de ADN modificadas con grupos acetileno por medio de la reacción "Click". Las secuencia inmovilizada en el polímero corrersponde a una secuencia de 21 bases complementaria al virus de la "Hepatitis C". Se comprobó la correcta inmovilización de la secuencia de prueba por diferentes técnicas como XPS, ToF-SIMS y voltametría diferencial de pulso. La hibridación de ADN se detectó por medio de voltametría diferencial de pulso, donde el cambio en la electroactividad del polímero se evaluó después del proceso de hibridación. Se evaluó la selectividad

del sensor de PEDOT por medio de su prueba con diferentes secuencias diana entre las que se encontraban la secuencia complementaria, una no complementaria y una secuencia con dos bases desaparejadas (a una concentración fija de 50 nM). También se evaluó la sensibilidad del sensor, probándolo a diferentes concentraciones de la secuencia complementaria desde 20 nM a 1 nM.

El sistema aquí presentado, representa una nueva herramienta para la preparación de sensores sin marcaje de hibridación de ADN, con gran potencial en el campo de la detección de enfermedades y mutaciones genéticas.

7.3.2 *Fabricación y caracterización de electrodos de azida-PEDOT*

7.3.2.1 *Fabricación*

Electrodos de oro fueron usados en un proceso estándar de crecimiento electroquímico de PEDOT, en una celda electroquímica de tres electrodos [68]. La electropolimeración se hizo bajo atmósfera de argón a temperatura ambiente usando diclorometano y tetrabutylamonium hexafluorophosphate como electrolito. Tras añadir a la celda electroquímica el monómero azida-EDOT, se inició un proceso de voltametria cíclica entre -1 V y 1.7 V (frente a un pseudo-electrodo de referencia de Ag/AgCl) a una velocidad de 100 mV/s. Se usó un contra-electrodo de platino. La Figura 7.10 muestra los voltamogramas correspondientes a la electropolimerización a partir del monómero azida-EDOT.

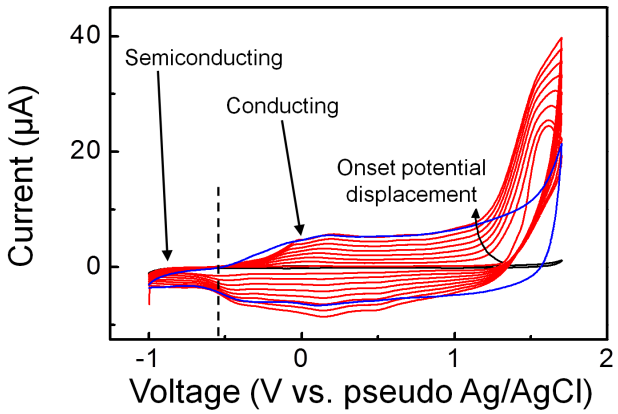

Figure 7.10: Comportamiento electroquímico en DCM y $TBAPF_6$. Línea negra: CV de electrodo limpio de oro en ausensia de monómero. Líneas rojas: CVs de azida-EDOT. Línea azul: CV de azida-PEDOT en ausencia de monómero.

El voltamograma negro representa el electrodo de oro en el electrolito sin la adición del monómero, mientras que los voltamogramas rojos representan los ciclos consecutivos de polimerización tras la adición del monómero. En azul se puede observar el voltamograma del electrodo de azida-PEDOT en diclorometano, en ausencia de monómero en la solución.

7.3.2.2 *Caracterización*

Ya que la técnica escogida para los experimentos de detección fue la voltametría diferencial de pulso, los electrodos de azida-PEDOT fueron caracterizados en Tris-HCl buffer por este método. La voltametría se realizó entre 0.3 V y 1.5 V a una velocidad de 100 mV/s. Los resultados mostraron que dos anchos picos de oxidación existían a valores aproximados de 0.8 V y 1.3 V, solapándose con los valores reportados en la literatura para la oxidación de la guanina y la adenina respectivamente (Figura 7.11). Por este motivo, los experimentos siguientes no evaluarán los picos de oxidación de dichas bases, sino que se centrarán en el estudio del carácter electroactivo de polímero bajo los sucesos de hibridación, entre 0.5 V y 1.0 V.

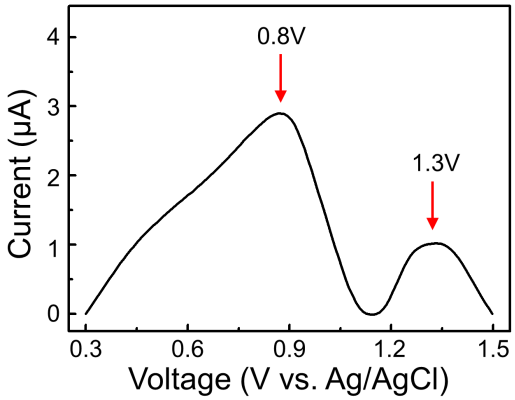

Figure 7.11: Voltametría diferencial de pulso de un electrodo de azida-PEDOT en Tris-HCl buffer. Los dos picos de oxidación marcados con flechas rojas, coinciden con los picos de oxidación para la guanina y la adenina.

7.3.3 *Inmovilización de secuencias de ADN del virus de la Hepatits C sobre electrodos de azida-PEDOT*

Los electrodos de azida-PEDOT fabricados aquí, permiten su directa funcionalización, mediante enlace covalente por la llamada química "Click". Para ello, secuencias complementarias al virus de la hepatitis C, fueron obtenidas (en colab-

oración con el Dr. Ramón Eritja, IQAC-CSIC, Barcelona) con un grupo acetileno, que permitió completar la reacción "Click" (Figura 7.12).

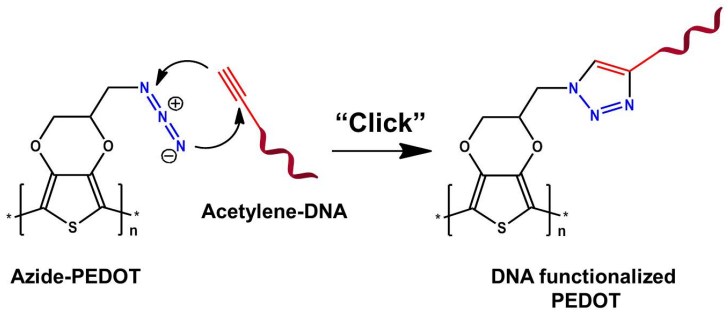

Figure 7.12: Esquema de la reacción "Click" entre el grupo azida del polímero y el grupo acetileno del ADN.

Dos espectros de alta resolución de XPS, correspondientes al nitrógeno presente en una muestra de azida-PEDOT y otra muestra de azida-PEDOT funcionalizada con aceileno-ADN fueron analizados. De estos resultados puede obtenerse un incremento y cambio en la distribución de los picos, atribuida al incremento de nitrógeno, aportado por las bases nitrogenadas de ADN y por la formación de triazoles cuando la reacción "Click" se completa.

De modo alternativo, se analizaron las mismas superficies por ToF-SIMS (Figura 7.13), obteniendo resultados similares.

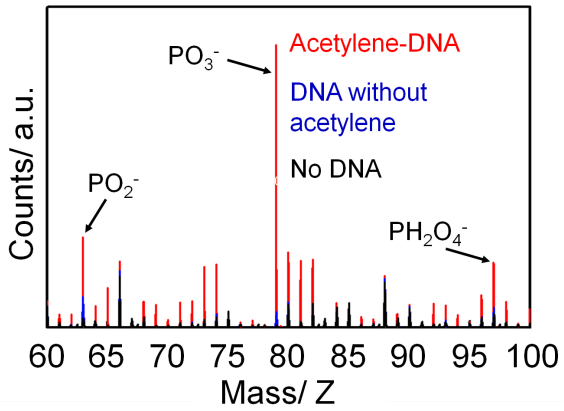

Figure 7.13: Espectros de ToF-SIMS de electrodos de azida-PEDOT incubados con diferentes soluciones de inmovilización. En negro, espectro correspondiente a un polímero incubado sin ADN. En azul espectro de un polímero incubado con AND sin acetileno. En rojo, polímero incubado con AND con acetileno.

Iones correspondientes a fragmentos de ADN se encontraron en cantidades significativas para muestras que fueron funcionalizadas con ADN, mientras que para las muestras control, dichas contribuciones fueron despreciables.

Finalmente, la funcionalización fue monitorizada por voltametría diferencial de pulso, como se muestra en la Figura 7.14. En dicha figura podemos observar como la electroactividad del polímero decrece cuando la muestra es funcionalizada con ADN (HCV-probe). Por el contrario, para polímeros en los que la reacción "Click" no ocurrió y por tanto no tienen ADN covalentemente anclado a la superficie, la electroactividad es mayor y bien diferenciada.

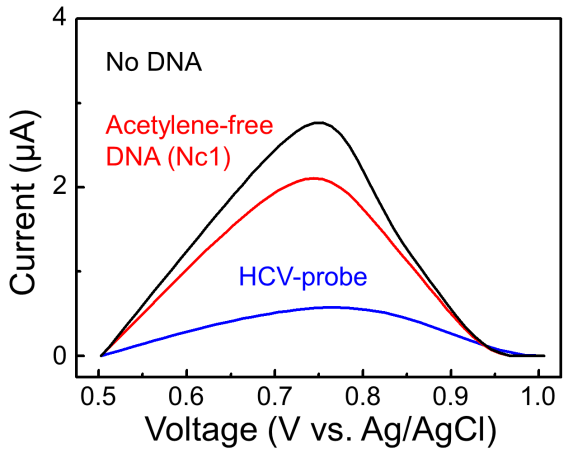

Figure 7.14: DPV de la reacción "Click". La muestra con ADN con acetileno (HCV-probe) es la única que experimenta una reducción abrupta de la electroactividad. Los controles, permanecen con alta electroactividad.

7.3.4 *Hibridación de secuencias diana sobre electrodos de azida-PEDOT funcionalizados con secuencias del virus de la Hepatitis C*

7.3.4.1 *Sensibilidad*

En estos experimentos se evaluó la respuesta electroquímica del polímero, funcionalizado con la cadena simple de ADN (ADN-prueba), a la hibridación con distintas concentraciones de ADN complementario (HCV-target). En la Figura 7.15 observamos como bajo la exposición del electrodo funcionalizado a las diferentes concentraciones, la electroactividad del polímero varía. A mayor concentración de ADN complementario, mayor resultó la perdida de electroactividad del polímero. Esto fue atribuido a la formación de puentes de hidrógeno en la superficie, lo que representa una barrera de potencial que dificulta el intercambio

iónico con el medio y por tanto la reducción en la electroactividad del polímero [69, 70, 71, 72].

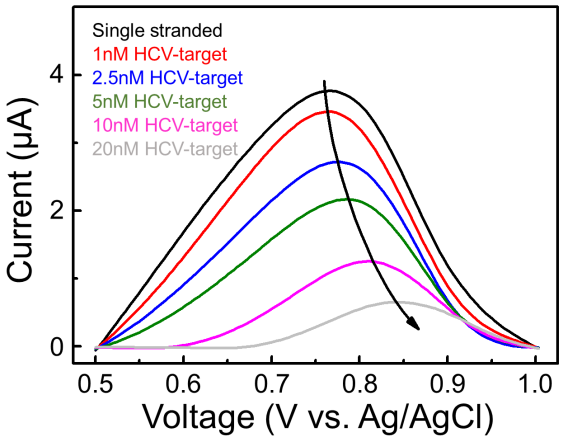

Figure 7.15: DPVs de electrodos de PEDOT funcionalizados con ADN, expuestos a diferentes concentraciones de ADN diana (entre 0 nM y 20 nM).

En la Figura 7.16, tenemos la recta de calibración correspondiente a estos experimentos de la que se pudo extraer el límite de detección del sistema, estimado en 0.13 nM. Este valor es comparable al obtenido en otros sensores electroquímicos de ADN, con una sensibilidad mejorada, gracias al uso de marcadores redox o sistemas miniaturizados [67].

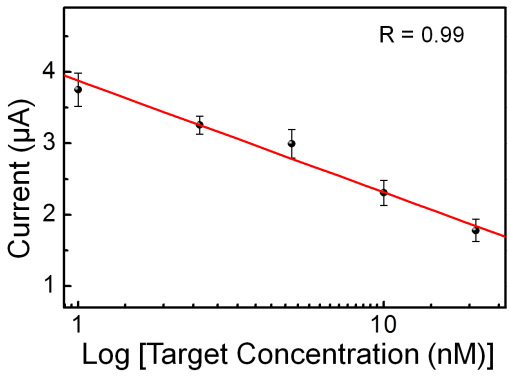

Figure 7.16: Recta de calibración para la señal de oxidación de los electrodos de PEDOT a diferentes concentraciones de ADN diana. La intensidad de corriente se representa frente al logaritmo de la concentración.

Además, la escasez de estudios publicados en relación a sensores de hibridación sin marcaje para la "Hepatitis C", hace especialmente importante la contribución de nuestro trabajo. Que nosotros sepamos, sólo existen dos trabajos

referentes a sensores de hibridación de "Hepatitis C" sin marcaje. Uno de ellos se basa en la detección directa de la oxidación de las bases de ADN. En él se obtuvo un límite de detección de 6.5 nM [73], similar al obtenido en otros sensores de hibridación del mismo tipo (basados en la oxidación de guaninas), pero muy superior al obtenido en nuestro trabajo. El otro estudio, reporta el uso de polypyrrole y se basa en la variación de electroactividad del polímero tras el proceso de hibridación [74]. Este sensor de polipirrol reporta límites de detección extremadamente bajos (10^{-21} M), pero hace uso de la miniaturización (mediante la fabricación de microelectrodos), para obtener dichos resultados. Además usa un monómero precursor modificado con la secuencia de prueba, lo que puede inducir la degradación de la prueba por acción de los potenciales eléctricos usados para la síntesis del polímero. Por el contrario, nuestro caso preserva la secuencia de prueba de la síntesis, puesto que la inmovilización se realiza en un proceso independiente ("Click"). Además, y a diferencia del trabajo basado en polipirrol, el tamaño de los electrodos usados en esta tesis es macro y no necesita de pasos adicionales de fotolitografía para obtener resultados en la nanoescala, compatibles con los rangos de detección de la "Hepatitis C" usados en análisis clínicos (1.5-2.0 µM) [75].

7.3.4.2 *Selectividad*

Después, se evaluó la respuesta del sensor a diferentes secuencias diana a la misma concentración (50 nM).

Las secuencias evaluadas consistieron en la secuencia complementaria, una secuencia no complementaria, una mezcla de dos secuencias no complementarias y la secuencia complementaria y una secuencia con dos bases desaparejadas. Los resultados, mostrados en la Figura 7.17 indicaron que todas las secuencias pudieron ser resueltas de los controles. Además la muestra consistente en una mezcla de no complementarios y la secuencia complementaria demostró el mismo carácter electroquímico que la muestra evaluada con la secuencia complementaria en solitario, lo que sugiere que el sensor desarrollado aquí, podría tener una potencial aplicación en muestras más complejas y reales.

7.3.5 *Conclusiones*

En esta sección se ha descrito la fabricación y prueba de un sensor de hibridación de ADN sin marcaje, basado en electrodos de poly(3,4-etilendioxitiofeno) modificado con un grupo azida (azida-PEDOT). Estos electrodos de azida-PEDOT se

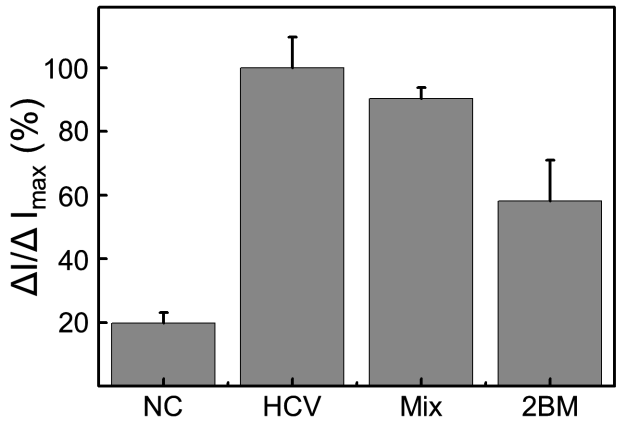

Figure 7.17: Selectividad del sensor de ADN. "NC" muestra la respuesta del sensor a la secuencia no complementaria. "HCV" muestra la respuesta del sensor a la secuencia complementaria (tomada como referencia 100%). "Mix" muestra la respuesta del sensor a una mezcla de secuencias no complementarias (Nc1, Nc2) y la secuencia complementaria. "2BM" muestra la respuesta del sensor a una secuencia con dos bases desaparejadas.

usaron como plataformas para la inmovilización de secuencias de ADN modificadas con grupos acetileno por medio de la reacción "Click". La hibridación de ADN se detectó por medio de voltametría diferencial de pulso (DPV), donde el cambio en la electroactividad del polímero se evaluó después del proceso de hibridación. Este sistema permitió distinguir entre diferentes secuencias a una misma concentración, probando su selectividad. Límites de detección por debajo del nM fueron obtenidos para secuencias complementarias, valores muy inferiores a los detectados en análisis clínicos comunes para la "Hepatitis C". Este sistema, no requirió de complicados procesos litográficos, ni marcajes para llegar a dichos límites de detección, lo que representa una mejora importante frente a los pocos trabajos reportados acerca de sensores sin marcaje para la "Hepatitis C".

7.4 FABRICACION DE DISPOSITIVOS DE NANOHILOS DE POLIPIRROL

7.4.1 *Introduccion*

Los nanohilos han demostrado ser muy útiles en diferentes aplicaciones, gracias a sus propiedades derivadas de su unidimensionalidad [76]. Desde sus primeras aplicaciones en electrónica, los nanohilos han sido usados mayormente como

parte de transistores de efecto campo (FET) [77, 78]. En estos dispositivos, la conducción a través del nanohilo (conectado a dos electrodos, source/drain) es manipulada por medio de un campo ejercido desde un tercer electrodo (gate) (Figura 7.18) [77]. En estos sistemas nanométricos, la influencia sobre la conducción del polímero es mucho mayor que en sistemas bidimensionales. Además, su alta razón superficie-volumen, sus propiedades ópticas, su sensibilidad a cambios en el entorno cercano a su superficie y sus excelentes propiedades mecánicas, hacen de los nanohilos, materiales especialmente útiles en aplicaciones optoelectrónicas, de cuidado medioambiental, en sensores químicos y biológicos, etc [2, 79, 80, 81, 82]. En aplicaciones biotecnológicas, el campo de los biosensores ha resultado ser uno de los que mayor provecho han obtenido de los nanohilos, con tiempos de detección y sensibilidades notablemente mejorados [83, 84]. Así, uno puede encontrar múltiples trabajos, donde los nanohilos han sido usados en la detección de importantes biomoléculas relacionadas con enfermedades comunes como la glucosa, o en la detección de secuencias específicas de ADN, virus y proteínas [85, 86, 87, 88].

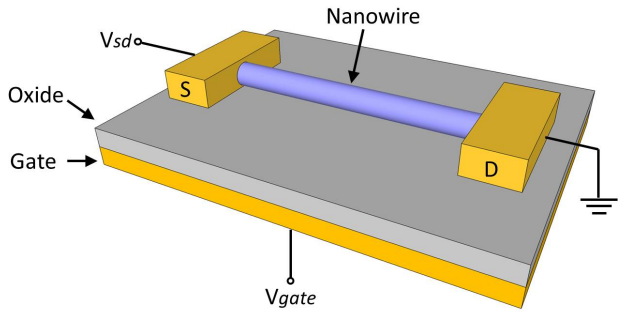

Figure 7.18: Transistor efecto campo basado en nanohilo. Un nanohilo conecta dos electrodos metálicos (source y drain) y reposa sobre una capa aislante que está sobre el electrodo gate, el cual ejerce un campo eléctrico sobre el nanohilo.

Polímeros conductores como el polipirrol, la polianilina o el politiofeno [2], aportan ventajas anteriormente mencionadas a estos fines, como pueden ser: la posibilidad de manipular sus propiedades eléctricas mediante acción sobre los parámetros de síntesis, las múltiples estrategias de funcionalización aplicables, su bajo coste, etc [31].

FETs basados en nanohilos de polímeros conductores pueden encontrarse en modo de arrays desordenados de nanohilos o en modo de dispositivos de un único nanohilo. El primer caso, ofrece una fácil fabricación del dispositivo, pero

carece de control en cuanto al número de nanohilos por dispositivo. Esto, produce diferentes resistencias de contacto para diferentes dispositivos, lo que es traducido en sistemas poco reproducibles [18]. Por el contrario, los dispositivos de un único nanohilo ofrecen un excelente entendimiento de las propiedades del dispositivo y del mecanismo de operación. También, ofrece la posibilidad de mejorar la resolución espacial del sistema mediante la fabricación de arrays ordenados de nanohilos [86, 89].

Sin embargo, la fabricación de dispositivos de un único nanohilo basada en polímeros conductores, sufre aún de serias limitaciones. Como explicado con anterioridad, los métodos litográficos desarrollados a la micro y nanoescala para materiales convencionales, no son compatibles con los polímeros conductores [18]. Hasta el momento, la técnica más usada para la fabricación de estos dispositivos, se basa en la fabricación de nanohilos en solución, para después dispersarlos sobre una superficie con electrodos y alinearlos por medio de campos magnéticos o eléctricos [90, 91]. Este proceso, requiere de muchos pasos y procesos de alineamiento para conseguir dispositivos de un único nanohilo, por lo que estrategias alternativas basadas en técnicas de barrido con sonda han sido también estudiadas (STM, AFM, DPN, etc.) [92, 93]. Últimamente, se han descrito también el uso de técnicas basadas en la directa electropolimerización de nanohilos entre electrodos metálicos, aunque aún es una técnica por optimizar, donde los parámetros experimentales influyen enormemente en los resultados obtenidos.

Así pues, aún no se disponen de técnicas para la fabricación de dispositivos de un único nanohilo de polímero conductor, que demuestren la habilidad de incorporar estos materiales en dispositivos funcionales de modo sencillo y estandarizado. Por ello, en esta sección se descibe la investigación de técnicas dirigidas a éste propósito, que permitan un mejor control y entendimiento de la fabricación de nanohilos de polímero conductor.

En este trabjo se estudiaron dos técnicas de fabricación de dispositivos de un único nanohilo de polímero conductor: la nanolitografia de dip-pen y la electropolimerizacion sobre superficies con plantillas. La técnica de dip pen se usó para depositar nanohilos sobre superficies de óxido de silicio, entre dos electrodos metálicos, para su uso como FETs en diferentes aplicaciones. Se optimizaron los parámetros de fabricación, obteniendo curvas que mostraban la dependencia del diámetro del nanohilo con la humedad y con la velocidad de deposición. Alternativamente, la electropolimerización añadió la capacidad de manipular el polímero químicamente, demostrado por el uso de varios electrolitos (fuente de

los iones dopantes), lo que se tradujo en dispositivos polméricos con diferentes conductividades.

7.4.2 *Nanohilos de polipirrol por medio de Dip-pen Naolithography*

Para el depósito de nanohilos de polipirrol sobre superficies de óxido de silicio, se usó la interacción electrostática entre "la tinta" (suspensión de polipirrol) y la superficie. Teniendo en cuenta que el polipirrol usado estaba dopado (cargado positivamente) [94], la superficie de óxido fue cargada negativamente para facilitar el transporte de "la tinta" desde la punta de dip pen a la superficie (Figura 7.19). Para ello, las superficies fueron tratadas con solución piraña durante 15 minutos, creando cargas negativas en su superficie.

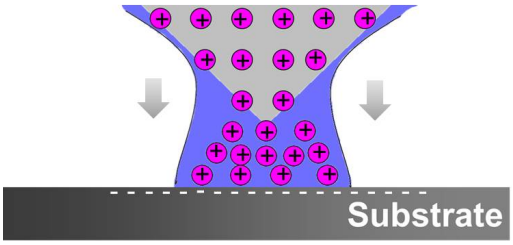

Figure 7.19: Fuerza electrostática para el depósito de polipirrole por DPN. La tinta de polímero está cargada positivamente y la superficie está cargada negativamente.

Los experimentos de dip pen fueron realizados a temperatura ambiente, a humedades relativas de 30%, 35% and 40%, y diferentes velocidades de escritura entre 0.1 µm/s y 2.0 µm/s (0.1, 0.3, 0.5, 0.7, 1, 1.5 and 2 µm/s). Las nanoestructuras resultantes fueron caracterizadas por lateral friction mode AFM, evaluando su diámetro. En la Figura 7.20 se muestra la dependencia en el diámetro del nanohilo con la humedad y con la velocidad de depósito.

De estos resultados podemos extraer principalmente dos conclusiones, que el diámetro decrece con la humedad y que decrece también con la velocidad de depósito, lo que coincide con los modelos reportados en la literatura [95, 96, 97]. De estos experimentos también podemos concluir que el menor diámetro obtenido para los nanohilos de polipirrol es de 101 ± 8 nm para un 35% de humedad relativa y una velocidad de depósito de 2.0 µm/s. Este es el menor valor reportado para nanohilos de polipirrol depositados por medio de DPN [93], sólo superado por otras técnicas basadas en DPN, pero más sofisticadas como el

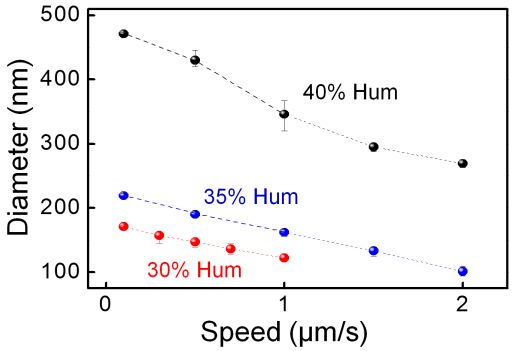

Figure 7.20: Dependencia del diametro de nanohilo de polipirrol con la humedad y la velocidad de depósito. En negro, resultados para humedades del 40%. En azul, resultados para humedades del 35%. En rojo, resultados para humedades 30%.

DPN térmico o electroquímico, donde los diámetros son ligeramente menores a 100 nm [98, 99].

Finalmente, para probar la capacidad de posicionar nanohilos entre electrodos metálicos y fabricar así un dispositivo, se depositaron nanohilos de polipirrole sobre superficies de óxido de silicio con contactos metálicos, resultando en dispositivos como el mostrado en la Figura 7.21. De este modo se demostró la capacidad de controlar dimensiones y localización de los nanohilos de polímero, por medio de esta técnica. Sin embargo, se encontraron problemas de adhesión de los nanohilos a la superficie. Además, mediante esta técnica no es posible manipular la estructura del polímero, por lo que se decidió estudiar otro método de fabricación alternativo, que salvara estos problemas y que permitiera un mayor control sobre las propiedades del dispositivo final.

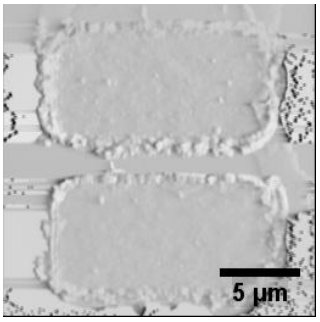

Figure 7.21: Imagen topográfica de AFM correspondiente a un nanohilo de polipirrol depositado entre electrodos metálicos. El nanohilo fue depositado a una humedad del 40% y una velocidad de depósito de 1µm/s. El diámetro del nanohilo fue de 339 nm.

7.4.3 *Nanohilos de polipirrol por medio de polimerización electroquímica entre superficies con plantillas*

Esta técnica se basa en la polimerización oxidativa común y el uso de superficies con plantillas que dirijan el crecimiento del polímero en forma de nanohilo [100, 101, 102, 103]. Para ello se fabricaron superficies en las que dos electrodos metálicos enfrentados estuvieran pasivados, excepto por un nanocanal que los conectase, como esquematizado en la Figura 7.22.

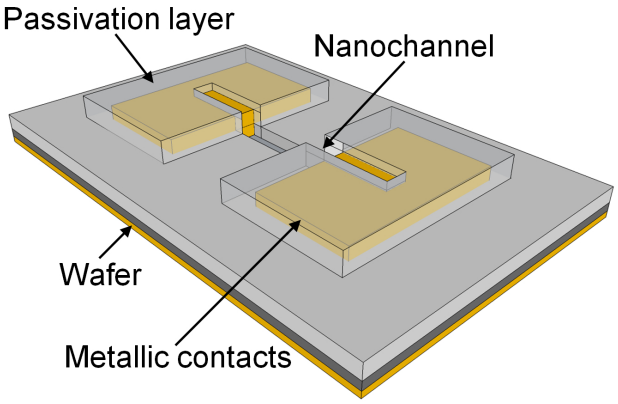

Figure 7.22: Esquema de superfice con plantilla. En él se puede observar el nanocanal abierto en la capa de pasivación, conectando los electrodos metálicos depositados sobre la oblea de óxido de silicio/silicio.

Para la fabricación de dicho nanocanal, se usó la técnica de e-beam. Los materiales empleados como pasivantes fueron PMMA y óxido de silicio. Los canales que se fabricaron tuvieron un ancho de 200 nm y 450 nm y los electrodos estuvieron separados por distancias de 15 µm y 5 µm.

Después de estudiar diferentes materiales de pasivación y condiciones experimentales, se llegó al establecimiento de unos parámetros óptimos para la fabricación de nanohilos de polipirrol. Estos parámetros consistieron en la aplicación de una corriente alternada entre los electrodos enfrentados de una magnitud de 1 µA, con una frecuencia de 0.5 kHz. Esto fue acompañado de la generación de un campo eléctrico perpendicular a la superficie de los electrodos, cuya función es la de confinar los monómeros oxidados en el nanocanal entre electrodos, como mostrado en la Figura 7.23. El potencial necesario para producir dicho campo fue de -1 V.

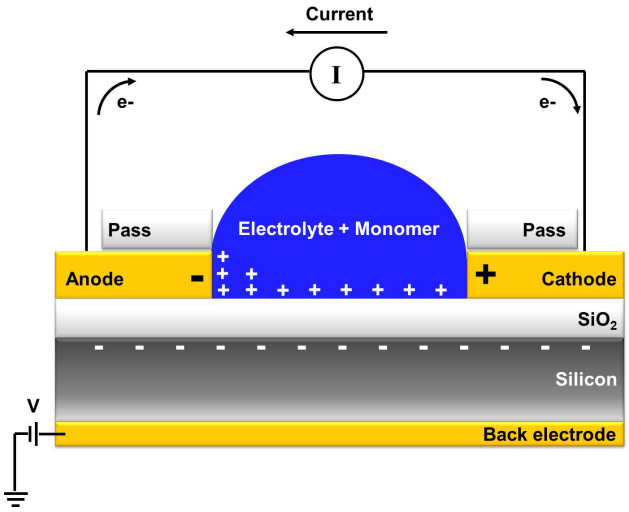

Figure 7.23: Esquema eléctrico usado en el proceso de electropolimerización. Una corriente es aplicada en el ánodo, iniciando la polimerización. Un campo perpendicular confina los monómeros oxidados en el nanocanal.

Por este método se consiguieron fabricar nanohilos de polipirrol en diferentes solventes (agua y acetonitrilo) con diferentes electrolitos (NaCl y $TBAPF_6$), como el nanohilo mostrado en la Figura 7.24a. Dichos nanohilos demostraron estar bien conectados con los electrodos metálicos (Figura 7.24b), resultando en dispositivos listos para usar en diferentes aplicaciones.

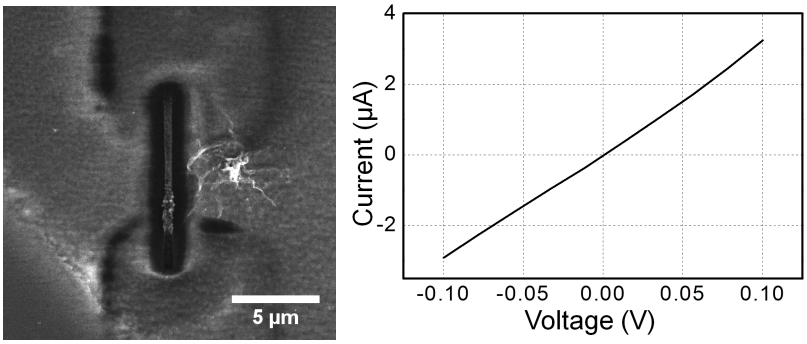

(a) (b)

Figure 7.24: Nanohilo de polipirrol (450 nm de diámetro) crecido en un nanocanal de PMMA. a) Imagen de SEM del nanohilo. b) Curva I-V del nanohilo.

Así pues, mediante la variación del solvente y electrolito, se obtuvieron diferentes valores para la conductividad del sistema (de 7 S/cm para nanohilos crecidos en agua y cloruro de sodio y de 45 S/cm para nanohilos crecidos en ace-

tonitrilo con tetrabutilammonium hexafluorophosphate), lo que confirma que la variación de los parámetros de síntesis influencia las propiedades del dispositivo final. Además, dichos valores superan lo reportado en el caso de disolventes acuosos y están dentro del rango de lo esperado para disolventes orgánicos [104, 105].

7.4.4 *Conclusiones*

Aquí se discute la fabricación de nanohilos de polipirrol para el desarrollo de dispositivos FET. Se investigaron dos técnicas: la nanolitografia de dip-pen y la electropolimerizacion sobre superficies con plantillas. La técnica de dip-pen demostró ser útil en la deposición de nanohilos de polipirrol con un buen control sobre las dimensiones y la localización del polímero. Por otro lado, la electropolimerización añadió la capacidad de manipular el polímero químicamente, lo que se tradujo en dispositivos polméricos con diferentes propiedades físicas.

7.5 CONCLUSIONES GENERALES

En esta tesis se han investigado nuevas técnicas de fabricación y de funcionalización de polímeros conductores, poniendo un especial interés en su aplicación biomédica.

Una nueva técnica de fabricación de microestructuras de polipirrol por método biocatalítico sobre superficies aislantes ha sido desarrollada con resoluciones comparables a las de la litografía óptica. Dicha técnica es compatible con la incorporación de biomoléculas durante el proceso de síntesis, lo que garantiza su utilización en entornos biológicos. Esto fue demostrado mediante la incorporación de biotina durante el proceso de polimerización y su posterior liberación, mediante estimulo eléctrico.

También se ha desarrollado un nuevo sensor de ADN sin marcaje basado en electrodos de azida-PEDOT, para la detección de secuencias basadas en la "Hepatitis C". Estos electrodos, permiten la directa y covalente funcionalización con secuencias de ADN, modificadas con grupos acetileno, por medio de la química "Click". La hibridación fue detectada mediante la evaluación de la electroactividad del polímero tras el suceso de reconocimiento. Esta novedosa modalidad de sensores demostró ser selectiva y sensible, siendo capaz de detectar secuencias complementarias en el rango nM, sin necesidad de marcajes, ni complejas técnicas de microfabricación.

Finalmente, se estudiaron dos técnicas de fabricación de nanohilos de polímero conductor: nanolitografía de dip-pen y electropolimerización sobre superficies con plantillas. Estos estudios proveen al incompleto campo de la fabricación de nanoestructuras de polímeros conductores de resultados adicionales, que amplían el campo de aplicación de dichos materiales.

7.6 REFERENCIAS

[1] Laura Poole-Warren et al. "Development of bioactive conducting polymers for neural interfaces." In: *Expert review of medical devices* 7.1 (Jan. 2010), pp. 35–49 (cit. on p. 185).

[2] Carlos M. Hangarter et al. "Conducting polymer nanowires for chemiresistive and FET-based bio/chemical sensors." In: *Journal of Materials Chemistry* 20.16 (2010), p. 3131 (cit. on pp. 186, 208).

[3] Róisín M Owens and George G Malliaras. "Organic Electronics at the Interface with Biology." In: *MRS Bulletin* 35.June (2010), pp. 449–456 (cit. on p. 186).

[4] Catalina Vallejo-Giraldo, Adriona Kelly, and Manus J P Biggs. "Biofunctionalisation pf electrically conducting polymers." In: *Drug Discovery Today* 19.1 (2014), pp. 88–94 (cit. on p. 186).

[5] Hui Peng et al. "Conducting polymers for electrochemical DNA sensing." In: *Biomaterials* 30.11 (Apr. 2009), pp. 2132–48 (cit. on pp. 186, 187, 199, 200).

[6] G.G. Adeloju, S.B., Wallace. "Conducting Polymers and the Bioanalytical Sciences : New Tools for Biomolecular Communications: A Review." In: *The Analyst* I.June (1996) (cit. on pp. 186, 200).

[7] M I Pividori, A Merkoçi, and S Alegret. "Electrochemical genosensor design : immobilisation of oligonucleotides onto transducer surfaces and detection methods." In: *Biosensors and bioelectronics* 15 (2000), pp. 291–303 (cit. on pp. 186, 199, 200).

[8] Khalil Arshak et al. "Conducting Polymers and Their Applications to Biosensors: Emphasizing on Foodborne Pathogen Detection." In: *IEEE Sensors Journal* 9.12 (2009), pp. 1942–1951 (cit. on p. 186).

[9] Leandro Forciniti et al. "Schwann cell response on polypyrrole substrates upon electrical stimulation." In: *Acta Biomaterialia* 10.6 (2014), pp. 2423–2433 (cit. on p. 186).

[10] Robert L. Anger et al. "Stimulation of neurite outgrowth using an electrically conducting polymer." In: *Proceedings of the National Academy of Sciences* 94.August (1997), pp. 8948–8953 (cit. on p. 186).

[11] Vadim S Polikov, Patrick a Tresco, and William M Reichert. "Response of brain tissue to chronically implanted neural electrodes." In: *Journal of neuroscience methods* 148.1 (Oct. 2005), pp. 1–18 (cit. on pp. 186, 188).

[12] Manrico Fabretto et al. "High conductivity PEDOT resulting from glycol/oxidant complex and glycol/polymer intercalation during vacuum vapour phase polymerisation." In: *Polymer* 52.8 (Apr. 2011), pp. 1725–1730 (cit. on p. 186).

[13] Kwanghee Lee et al. "Metallic transport in polyaniline." In: *Nature* 441.7089 (May 2006), pp. 65–68 (cit. on p. 186).

[14] Brianna C Thompson et al. "Optimising the incorporation and release of a neurotrophic factor using conducting polypyrrole." In: *Journal of controlled release: official journal of the Controlled Release Society* 116.3 (Dec. 2006), pp. 285–294 (cit. on pp. 187, 196).

[15] D H Szarowski et al. "Brain responses to micro-machined silicon devices." In: *Brain Research* 983 (2003), pp. 23–35 (cit. on p. 187).

[16] Uta Reich et al. "Differential fine-tuning of cochlear implant material-cell interactions by femtosecond laser microstructuring." In: *Journal of biomedical materials research. Part B, Applied biomaterials* 87.1 (2008), pp. 146–153 (cit. on p. 187).

[17] Mikhail a Lebedev and Miguel a L Nicolelis. "Brain-machine interfaces: past, present and future." In: *Trends in neurosciences* 29.9 (2006), pp. 536–546 (cit. on p. 187).

[18] Hyeonseok Yoon et al. "A novel sensor platform based on aptamer-conjugated polypyrrole nanotubes for label-free electrochemical protein detection." In: *Chembiochem: a European journal of chemical biology* 9.4 (Mar. 2008), pp. 634–41 (cit. on pp. 187, 209).

[19] Francis Garnier et al. "All-Polymer Field-Effect Transistor Realized by Printing Techniques." In: *Science* 265 (1994), p. 1684 (cit. on p. 189).

[20] Sunappan Vasudivan. "Fine line screen printed electrodes for polymer microfluidics." In: *2010 12th Electronics Packaging Technology Conference* (Dec. 2010), pp. 89–93 (cit. on p. 189).

[21] Ken Gilleo. "POLYMER THICK FILM TECHNOLOGY." In: *Pollution Prevention Review* (1996), pp. 65–74 (cit. on p. 189).

[22] T. R. Hebner et al. "Ink-jet printing of doped polymers for organic light emitting devices." In: *Applied Physics Letters* 72.5 (1998), p. 519 (cit. on p. 189).

[23] Yang Yang et al. "Organic / polymeric electroluminescent devices processed by hybrid ink-jet printing." In: *Journal of Materials Science: Materials in Electronics Journal of Materials Science: Materials in Electronics* 1 (2000), pp. 89–96 (cit. on p. 189).

[24] Jun Xu, Chengmei Zhong, and Chun Fu. "Novel method for printing high-quality metal wires." In: *SPIE* (2007) (cit. on p. 189).

[25] Graciela B. Blanchet et al. "Large area, high resolution, dry printing of conducting polymers for organic electronics." In: *Applied Physics Letters* 82.3 (2003), p. 463 (cit. on p. 189).

[26] J R Sheats et al. "Patterning of Polymer Light-Emitting Diodes with Soft Lithography." In: *Advanced Materials* 12 (2000), pp. 269–273 (cit. on p. 189).

[27] Tobias Kaufmann and Bart Jan Ravoo. "Stamps, inks and substrates: polymers in microcontact printing." In: *Polymer Chemistry* 1.4 (2010), p. 371 (cit. on p. 189).

[28] Sarah M Richardson-Burns et al. "Polymerization of the conducting polymer poly(3,4-ethylenedioxythiophene) (PEDOT) around living neural cells." In: *Biomaterials* 28.8 (Mar. 2007), pp. 1539–52 (cit. on p. 189).

[29] Luigi Sasso et al. "Doped overoxidized polypyrrole microelectrodes as sensors for the detection of dopamine released from cell populations." In: *The Analyst* 138.13 (July 2013), pp. 3651–9 (cit. on p. 189).

[30] Gyoujin Cho and Daniel T Glatzhoferc. "Enhanced adhesion of polypyrrole film through a novel grafting method." In: *Journal of Materials Chemistry* 9 (1999), pp. 345–347 (cit. on pp. 189, 190).

[31] Rajeswari Ravichandran et al. "Applications of conducting polymers and their issues in biomedical engineering." In: *Journal of the Royal Society, Interface / the Royal Society* 7 Suppl 5 (Oct. 2010), S559–79 (cit. on pp. 189, 208).

[32] Hyun-Kon Song and G Tayhas R Palmore. "Conductive polypyrrole via enzyme catalysis." In: *The journal of physical chemistry B* 109.41 (Oct. 2005), pp. 19278–19287 (cit. on pp. 189, 192).

[33] Yong Hwan Kim et al. "Polymerization of cardanol using soybean peroxidase and its potential application as anti-biofilm coating material." In: *Biotechnology letters* 25.18 (Sept. 2003), pp. 1521–4 (cit. on p. 189).

[34] H. B Dunford. *Peroxidases in Chemistry and Biology*. Ed. by J. Everse and M. B. Grisham. 1991, pp. 1–24 (cit. on p. 189).

[35] Ryan Bouldin et al. "Enzymatic Synthesis of Electrically Conducting Polymers." In: *American Chemical Society* X.Symposium series (2010), pp. 315–341 (cit. on p. 189).

[36] G V Otrokhov et al. "Biocatalytic synthesis of conducting polymers and prospects for its application." In: *Biochemistry. Biokhimiya* 78.13 (Dec. 2013), pp. 1539–53 (cit. on p. 189).

[37] Yulia N. Kupriyanovich et al. "Peroxidase-catalysed synthesis of electroconductive polypyrrole." In: *Mendeleev Communications* 18.1 (Jan. 2008), pp. 56–58 (cit. on p. 189).

[38] R Cruz-Silva et al. "Biocatalytic synthesis of polypyrrole powder, colloids, and films using horseradish peroxidase." In: *Journal of colloid and interface science* 328.2 (Dec. 2008), pp. 263–269 (cit. on pp. 189, 192).

[39] Jalal Arjomandi and Rudolf Holze. "Spectroelectrochemistry of conducting polypyrrole and poly(pyrrole-cyclodextrin) prepared in aqueous and nonaqueous solvents." In: *Journal of Solid State Electrochemistry* 11.8 (Jan. 2007), pp. 1093–1100 (cit. on p. 189).

[40] Chun-Guey Wu and Ching-Yuh Chen. "Chemical deposition of ordered conducting polypyrrole films on modified inorganic substrates." In: *Journal of Materials Chemistry* 7.8 (1997), pp. 1409–1413 (cit. on p. 193).

[41] Germà Garcia-Belmonte et al. "Doping-induced broadening of the hole density-of-states in conducting polymers." In: *Electrochimica Acta* 55.21 (2010), pp. 6123–6127 (cit. on p. 193).

[42] Sunil Kwon et al. "Patterning of polypyrrole using a fluoropolymer as an adsorption-protecting molecule." In: *Applied Surface Science* 257.1 (Oct. 2010), pp. 165–171 (cit. on p. 193).

[43] A. Ramanavicius et al. "Redox enzyme - glucose oxidase - initiated synthesis of polypyrrole." In: *Synthetic Metals* 156.5-6 (Mar. 2006), pp. 409–413 (cit. on p. 195).

[44] X. Cui et al. "Biocatalytic Generation of Ppy-Enzyme-CNT Nanocomposite: From Network Assembly to Film Growth." In: *Journal of Physical Chemistry C* 111.5 (Feb. 2007), pp. 2025–2031 (cit. on p. 195).

[45] Youngnam Cho and Richard Ben Borgens. "Biotin-doped porous polypyrrole films for electrically controlled nanoparticle release." In: *Langmuir; the ACS journal of surfaces and colloids* 27.10 (May 2011), pp. 6316–22 (cit. on p. 195).

[46] P. M. Paul M. George et al. "Electrically Controlled Drug Delivery from Biotin-Doped Conductive Polypyrrole." In: *Advanced Materials* 18.5 (Mar. 2006), pp. 577–581 (cit. on p. 196).

[47] Reecha Wadhwa et al. "Electrochemically controlled release of dexamethasone from conducting polymer polypyrrole coated electrode." In: *Journal of controlled release : official journal of the Controlled Release Society* 110.3 (Feb. 2006), pp. 531–41 (cit. on p. 196).

[48] Ryeo Yun Hwang et al. "Suppression of the loss of an electroactive dopant from polypyrrole by using a non-aqueous electrolyte of dopant-phobicity." In: *Journal of Electroanalytical Chemistry* 657.1-2 (July 2011), pp. 181–186. DOI: 10.1016/j.jelechem.2011.03.028 (cit. on p. 197).

[49] Susan R Mikkelsen. "Electrochemical Biosensors for DNA Sequence Detection." In: *Electroanalysis* 8 (1996), pp. 15–19 (cit. on p. 198).

[50] Minhaz Uddin Ahmed and Mosharraf Hossain. "Electrochemical Biosensors for Medical and Food Applications." In: *Electroanalysis* (2008), pp. 616–626 (cit. on p. 198).

[51] R B Wallace et al. "The use of synthetic oligodeoxyribonucleotides to phi chi 174 DNA: the effect of single base pair mismatch." In: *Nucleic acids research* 9.4 (1981), p. 879 (cit. on p. 198).

[52] A N N Caviani Pease et al. "Light-generated oligonucleotide arrays for rapid DNA sequence analysis." In: *Proceedings of the National Academy of Sciences* 91.May (1994), pp. 5022–5026 (cit. on p. 198).

[53] James D Watson and Francis H Crick. "Molecular Structure of Nucleic Acids." In: *Nature* (1953), p. 4356 (cit. on p. 198).

[54] Hui Peng et al. "DNA Hybridization Detection with Blue Luminescent Quantum Dots and Dye-labeled Single-stranded DNA." In: *Journal of the American Chemical Society* c (2007), pp. 3048–3049 (cit. on p. 199).

[55] T Livache et al. "Polypyrrole electrospotting for the construction of oligonucleotide arrays compatible with surface plasmon resonance hybridization detection." In: *Synthetic metals* 121 (2001), pp. 1443–1444 (cit. on p. 199).

[56] Naomi Flowers Campbell, Jeffrey A Evans, and Newton C Fawcett. "Detection of Poly(U) hybridization using Azido modified Poly (A) coated piezoelectric crystals." In: *Biochemical and Biophysical Research Communications* 196 (1993), pp. 563–858 (cit. on p. 199).

[57] Jungyul Sakong, Heesu Roh, and Yongrae Roh. "Surface Acoustic Wave DNA Sensor with Micro-Fluidic Channels Surface Acoustic Wave DNA Sensor with Micro-Fluidic Channels." In: *The Japan Journal of Applied Physics* 46 (2007), pp. 4729–4733 (cit. on p. 199).

[58] Tae-young Lee and Yoon-bo Shim. "Direct DNA Hybridization Detection Based on the Oligonucleotide-Functionalized Conductive." In: *Analytical chemistry* 73.22 (2001), pp. 5629–5632 (cit. on p. 199).

[59] Ningning Zhu et al. "Electrochemically fabricated polyaniline nanowire-modified electrode for voltammetric detection of DNA hybridization." In: *Electrochimica Acta* 51.18 (May 2006), pp. 3758–3762 (cit. on p. 199).

[60] Kelly M Millan and Susan R Mikkelsen. "Sequence-Selective Biosensor for DNA Based on Electroactive Hybridization Indicators." In: *Analytical chemistry* (1993), pp. 2317–2323 (cit. on p. 199).

[61] Adam B Steel, Tonya M Herne, and Michael J Tarlov. "Electrochemical Quantitation of DNA Immobilized on Gold." In: *Analytical chemistry* 70.22 (1998), pp. 4670–4677 (cit. on p. 199).

[62] Yanli Zhang et al. "Electrochemical DNA Biosensor Based on the Proximity-Dependent Surface Hybridization Assay." In: *Analytical chemistry* 81.5 (2009), pp. 1982–1987 (cit. on p. 199).

[63] Boon Ping Ting et al. "A DNA biosensor based on the detection of doxorubicin-conjugated Ag nanoparticle labels using solid-state voltammetry." In: *Biosensors and bioelectronics* 25 (2009), pp. 282–287 (cit. on p. 199).

[64] Nai-ying Wu et al. "Direct electrochemical sensor for label-free DNA detection based on zero current potentiometry." In: *Biosensors and Bioelectronic* 39.1 (2013), pp. 210–214 (cit. on p. 200).

[65] Burcu Meric et al. "Indicator-Free Electrochemical DNA Biosensor Based on Adenine and Guanine Signals." In: *Electroanalysis* 14.18 (2002), pp. 1245–1250 (cit. on p. 200).

[66] Arzum Erdem et al. "Rigid carbon composites: a new transducing material for label-free electrochemical genosensing." In: *Journal of Electroanalytical Chemistry* 567.1 (June 2004), pp. 29–37 (cit. on p. 200).

[67] Bhuvaneswari Kannan et al. "High-sensitivity, label-free DNA sensors using electrochemically active conducting polymers." In: *Analytical chemistry* 83.9 (May 2011), pp. 3415–21. DOI: 10.1021/ac1033243 (cit. on pp. 200, 205).

[68] Hang-Beom Bu et al. "Click-functionalization of conducting poly (3,4 - ethylenedioxythiophene) (PEDOT)." In: *Chemical communications (Cambridge, England)* 11 (Mar. 2008), pp. 1320–2 (cit. on p. 201).

[69] Peter Bäuerle and Andreas Emge. "Specific Recognition of Nucleobase-Functionalized Polythiophenes." In: *Advanced Materials* 10.4 (Mar. 1998), pp. 324–330 (cit. on p. 205).

[70] Hafsa Korri-Youssoufi and Bouchra Makrouf. "Electrochemical biosensing of DNA hybridization by ferrocenyl groups functionalized polypyrrole." In: *Analytica Chimica Acta* 469.1 (Sept. 2002), pp. 85–92 (cit. on p. 205).

[71] Junhoe Cha et al. "DNA hybridization electrochemical sensor using conducting polymer." In: *Biosensors and Bioelectronics* 18.10 (Sept. 2003), pp. 1241–1247 (cit. on p. 205).

[72] Aude-Emmanuelle Navarro et al. "Characterization of PEDOT film functionalized with a series of automated synthesis ferrocenyl-containing oligonucleotides." In: *Tetrahedron* 61.16 (Apr. 2005), pp. 3947–3952 (cit. on p. 205).

[73] M. H. H Pournaghi-Azar, F. Ahour, and M. S. S Hejazi. "Differential Pulse Voltammetric Detection of Hepatitis C Virus 1a Oligonucleotide Chain by a Label-Free Electrochemical DNA Hybridization Biosensor Using Consensus Sequence of Hepatitis C Virus 1a Probe on the Pencil Graphite Electrode." In: *Electroanalysis* 21.16 (Aug. 2009), pp. 1822–1828 (cit. on p. 206).

[74] Carla dos Santos Riccardi et al. "Label-free DNA detection of hepatitis C virus based on modified conducting polypyrrole films at microelectrodes and atomic force microscopy tip-integrated electrodes." In: *Analytical chemistry* 80.1 (Jan. 2008), pp. 237–45 (cit. on p. 206).

[75] Shuna Liu et al. "Electrochemical detection of hepatitis C virus based on site-specific DNA cleavage of BamHI endonuclease." In: *Chem. Commun.* 13 (2009), pp. 1635–1637 (cit. on p. 206).

[76] Hiroyuki Sakaki. "Scattering Suppression and High-Mobility Effect of Size-Quantized Electrons in Ultrafine Semiconductor Wire Structures." In: *Japanese Journal of Applied Physics* 19.12 (1980), pp. L735–L738 (cit. on p. 207).

[77] Neil P Dasgupta et al. "25Th Anniversary Article: Semiconductor Nanowires–Synthesis, Characterization, and Applications." In: *Advanced materials (Deerfield Beach, Fla.)* 26.14 (Apr. 2014), pp. 2137–84 (cit. on p. 208).

[78] Yi Cui et al. "High Performance Silicon Nanowire Field Effect Transistors." In: *Nano Letters* 3.2 (Feb. 2003), pp. 149–152 (cit. on p. 208).

[79] Hyesung Park et al. "Graphene Cathode-Based ZnO Nanowire Hybrid Solar Cells." In: *Nano Letters* 13.1 (2013), pp. 233–239 (cit. on p. 208).

[80] David T Schoen et al. "High Speed Water Sterilization Using One-Dimensional Nanostructures." In: *Nano Letters* 10.9 (2010), pp. 3628–3632 (cit. on p. 208).

[81] Wenjun Dong et al. "Multifunctional Nanowire Bioscaffolds on Titanium." In: *Chemistry of Materials* 19.18 (2007), pp. 4454–4459 (cit. on p. 208).

[82] Matt Law et al. "Nanoribbon Waveguides for Subwavelength Photonics Integration." In: *Science* 305.5688 (Aug. 2004), pp. 1269–1273 (cit. on p. 208).

[83] P. R. Nair and M. a. Alam. "Performance limits of nanobiosensors." In: *Applied Physics Letters* 88.23 (2006), p. 233120 (cit. on p. 208).

[84] Guo-Jun Zhang et al. "Silicon nanowire biosensor for highly sensitive and rapid detection of Dengue virus." In: *Sensors and Actuators B-chemical* 146.1 (2010), pp. 138–144 (cit. on p. 208).

[85] Fernando Patolsky et al. "Electrical detection of single viruses." In: *Proceedings of the National Academy of Sciences of the United States of America* 101.39 (Sept. 2004), pp. 14017–14022 (cit. on p. 208).

[86] Gengfeng Zheng et al. "Multiplexed electrical detection of cancer markers with nanowire sensor arrays." In: *Nat Biotech* 23.10 (Oct. 2005), pp. 1294–1301 (cit. on pp. 208, 209).

[87] Guo-Jun Zhang et al. "Highly sensitive measurements of PNA-DNA hybridization using oxide-etched silicon nanowire biosensors." In: *Biosensors and Bioelectronics* 23.11 (2008), pp. 1701–1707 (cit. on p. 208).

[88] Ruomeng Yu et al. "Enhanced Performance of a ZnO Nanowire-Based Self-Powered Glucose Sensor by Piezotronic Effect." In: *Advanced functional materials* (2013), pp. 1–7 (cit. on p. 208).

[89] Innam Lee et al. "Highly sensitive single polyaniline nanowire biosensor for the detection of immunoglobulin G and myoglobin." In: *Biosensors and bioelectronics* 26.7 (Mar. 2011), pp. 3297–302 (cit. on p. 209).

[90] Jeong In Lee et al. "Highly Aligned Ultrahigh Density Arrays of Conducting Polymer Nanorods using Block Copolymer Templates 2008." In: *Nano letters* 8 (2008), pp. 23–25 (cit. on p. 209).

[91] Yaping Dan et al. "Gas Sensing Properties of Single Conducting Polymer Nanowires and the Effect of Temperature." In: *Nanotechnology* 20 (2009), p. 434014 (cit. on p. 209).

[92] Sung-Yeon Jang, Manuel Marquez, and Gregory a Sotzing. "Rapid direct nanowriting of conductive polymer via electrochemical oxidative nanolithography." In: *Journal of the American Chemical Society* 126.31 (Aug. 2004), pp. 9476–7. ISSN: 0002-7863. DOI: 10.1021/ja047766+ (cit. on p. 209).

[93] By Jung-hyurk Lim and Chad A Mirkin. "Electrostatically Driven Dip-Pen Nanolithography." In: *Advanced Materials* 14.20 (2010), pp. 1474–1477 (cit. on pp. 209, 210).

[94] Tat'yana V Vernitskaya and Oleg N Efimov. "Polypyrrole: a conducting polymer; its synthesis, properties and applications." In: *Russian Chemical Reviews* 66.5 (May 1997), pp. 443–457 (cit. on p. 210).

[95] Joonkyung Jang et al. "Self-assembly of ink molecules in dip-pen nanolithography : A diffusion model." In: *Journal of Chemical Physics* 115.6 (2001), pp. 2721–2729 (cit. on p. 210).

[96] Peter V Schwartz. "Molecular Transport from an Atomic Force Microscope Tip: A Comparative Study of Dip-Pen Nanolithography." In: *Langmuir: the ACS journal of surfaces and colloids* 18.100 (2002), pp. 4041–4046 (cit. on p. 210).

[97] Sergey Rozhok, Richard Piner, and Chad A Mirkin. "Dip-Pen Nanolithography: What Controls Ink Transport?" In: *Journal of Physical Chemistry B* 107 (2003), pp. 751–757 (cit. on p. 210).

[98] Minchul Yang et al. "Direct Writing of a Conducting Polymer with Molecular-Level Control of Physical Dimensions and Orientation." In: *Journal of the American Chemical Society* 128 (2006), pp. 6774–6775 (cit. on p. 211).

[99] Benjamin W Maynor et al. "Direct-Writing of Polymer Nanostructures: Poly (thiophene) Nanowires on Semiconducting and Insulating Surfaces." In: *Journal of the American Chemical Society* 124.4 (2002), pp. 2001–2002 (cit. on p. 211).

[100] Kumaran Ramanathan et al. "Individually Addressable Conducting Polymer Nanowires Array." In: *Nano Letters* 4.7 (July 2004), pp. 1237–1239 (cit. on p. 212).

[101] Minhee Yun et al. "Electrochemically Grown Single Nanowire Sensors." In: *SPI, Journal of optical engineering* 100 (2004) (cit. on p. 212).

[102] Kumaran Ramanathan et al. "In Situ Fabrication of Single Poly (methyl pyrrole) Nanowire." In: *Electroanalysis* 19.7-8 (2007), pp. 793–797 (cit. on p. 212).

[103] Minhee Yun et al. "Electrochemically Grown Wires for Individually Addressable Sensor Arrays." In: *Nano Letters* 4.3 (Mar. 2004), pp. 419–422 (cit. on p. 212).

[104] Prem S Thapa et al. "Directional growth of polypyrrole and polythiophene wires Directional growth of polypyrrole and polythiophene wires." In: *Applied Physics Letters* 033104.2009 (2014), pp. 10–13 (cit. on p. 214).

[105] J G Park et al. "Non-linear I-V characteristics of polypyrrole micro-line synthesized using scanning probe microscope." In: *Current Applied Physics* 2 (2002), pp. 23–25 (cit. on p. 214).

A

FABRICATION OF AZIDE-PEDOT MICROWIRE-BASED DEVICES

It is demonstrated that by reducing the size of a sensor's electrode, many benefits can be obtained regarding the device performance. By using microelectrodes, faster double-layer charging can be achieved, poorly ionic conducting solvents can be used and high mass-transfer ratios can be obtained. Additionally, small volume samples can be investigated and an improvement of the spatial resolution of the sensor is possible, which benefits the development of multiplexed sensors [1, 2]. This appendix describes the miniaturization process of the sensor developed in chapter 4, based on Azide-PEDOT electrodes. After the fabrication process was developed, the microwire-based systems were characterized, resulting in ready-to-use devices to perform the detection of DNA hybridization events in further investigations. In this case, the rod-like electrodes used in chapter 4 to perform the electrochemical polymerization of Azide-EDOT monomers, were substituted by opposite microelectrodes deposited on a Si/SiO_2 substrate. Similarly to the fabrication process conducted in chapter 2, microelectrodes consisting on 10 nm of a titanium adhesion layer and 70 nm of gold were deposited by evaporation on Si/SiO_2 wafers with the help of direct write laser lithography (DWL).

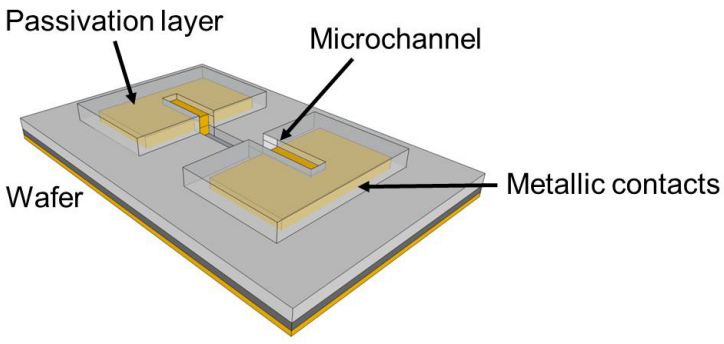

Figure A.1: Schematics of the two opposite-electrode chip for microwire fabrication.

The two opposite microelectrodes were separated by a distance of 5 µm and later were coated by a passivation layer of SiO_2. Microchannels of 2 µm width were opened on the SiO_2 surface between electrodes by applying e-beam lithography and resulted in the configuration schematized in Figure A.1.

Then, the substrates were diced in pieces containing just two opposite electrodes and they were stuck on polyvinyl chloride (PVC) substrates, with large printed copper electrodes (Figure A.2).

Figure A.2: Images of a two opposite-electrode chip and a PVC substrate with copper electrodes.

To achieve a good electrical connection with the external copper electrodes, the large electrical pads of the microelectrodes were soldered to the printed electrodes. Subsequently, the whole system was passivated with teflon tape, containing a 2 mm circular openings that exposed the microchannel area to the polymerization solution (Figure A.3). This eluded the interference of the external contacts and solderings with the solution. The configuration employed here was designed to avoid the use of drop-sized electrochemical cells, where the evaporation of the solvent would represent an important limitation.

Then, cyclic voltammetry was applied on the couple of opposite electrodes, using both microelectrodes as working electrodes. 100 mM tetrabutylammonium hexafluorophosphate ($TBAPF_6$) and 1.5 mM Azide-EDOT monomer were dissolved in 5 mL dichloromethane and used as polymerization solution under argon atmosphere at room temperature. 2 scans between -1 V and +1.7 V at 100 mV/s, versus an Ag/AgCl pseudoreference (used for organic solvents, see chapter 4), were performed to obtain microwire-based devices, as the ones observed in Figure A.4. An external platinum counter electrode was used.

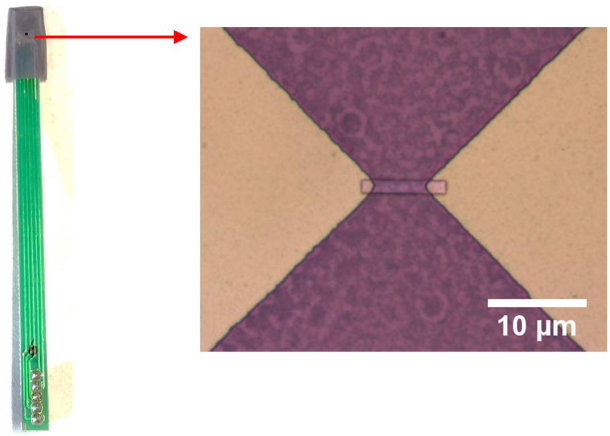

Figure A.3: Image of a Teflon passivated two opposite-electrode chip, mounted on a PVC substrate. Inset corresponds to a microscope image of the central part of the chip between electrodes.

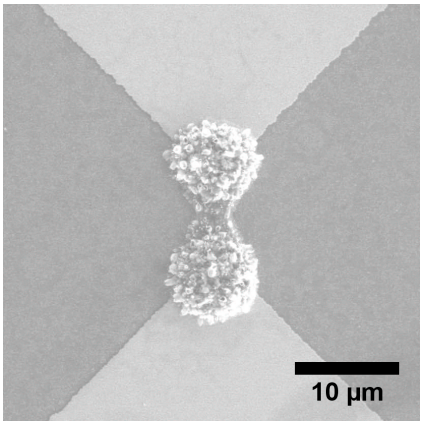

Figure A.4: SEM image of an azide-PEDOT microwire of 6 µm averaged diameter.

The Azide-PEDOT microwires showed a tapered body from the electrode proximities, which was attributed to the use of cyclic voltammetry on both electrodes at the same time. When the cyclic potential is applied, the Azide-EDOT monomers are oxidized to radical cations, keeping a high concentration of radicals near the working electrodes (the two opposite electrodes) that gradually decrease away, due to the diffusion of the ions [3]. Since the electron transfer is much faster than the diffusion process, there is a competition between the formation of ions and the migration away from the electrode, which produces an accumulation of polymer at the electrodes, distorting the straight shape of the wire.

Microwires of sizes between 4 and 6 µm in averaged diameter were obtained, with good ohmic contact with the metallic electrodes as evidenced by the I-V characteristics shown in Figure A.5.

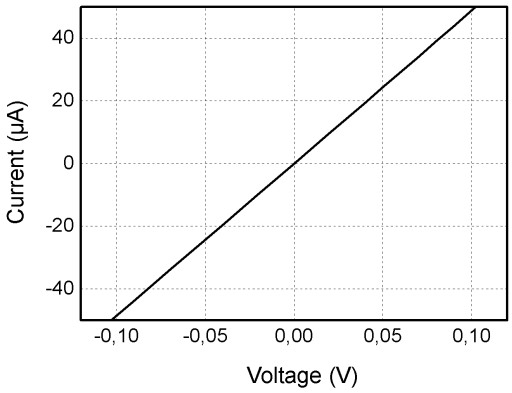

Figure A.5: I-V characteristics of an azide-PEDOT microwire.

Conductivities between 1 and 8 S/cm, depending on their geometry, were calculated by Equation A.1. σ is the conductivity, R the measured resistance, A the area of the microwire's cross section and l de separation between contacts.

$$\sigma = \frac{l}{AxR} \tag{A.1}$$

These conductivity values are in good agreement with the conductivity expressed by other PEDOT micro- and nanowires reported in litterature [3, 4, 5, 6]. This fabrication route provides microwire-based devices, readily functionalized in a single step fabrication process, which permits the direct reaction with acetylene-modified molecules. This represents a fundamental improvement for further applications, as for instance in the development DNA hybridization microsensors, extending the work performed in chapter 4 of this thesis. Further investigations in this direction will be directed to the application of these ready-to-work Azide-PEDOT microwire-based devices in DNA hybridization sensors.

REFERENCES

[1] Cynthia G Zoski. *Handbook of Electrochemistry*. 2007, pp. 1–935 (cit. on p. 227).

[2] Bhuvaneswari Kannan et al. "High-sensitivity, label-free DNA sensors using electrochemically active conducting polymers." In: *Analytical chemistry* 83.9 (May 2011), pp. 3415–21 (cit. on p. 227).

[3] Hong Xie, Shyh-Chyang Luo, and Hsiao-Hua Yu. "Electric-field-assisted growth of functionalized poly(3,4-ethylenedioxythiophene) nanowires for label-free protein detection." In: *Small (Weinheim an der Bergstrasse, Germany)* 5.22 (Nov. 2009), pp. 2611–7 (cit. on pp. 229, 230).

[4] Prem S Thapa et al. "Directional growth of polypyrrole and polythiophene wires Directional growth of polypyrrole and polythiophene wires." In: *Applied Physics Letters* 033104.2009 (2014), pp. 10–13 (cit. on p. 230).

[5] A Das et al. "Non-lithographic fabrication of PEDOT nano-wires between fixed Au electrodes." In: *Organic Electronics* 7 (2006), pp. 181–187 (cit. on p. 230).

[6] Bhuvaneswari Kannan et al. "The electrochemical growth of conducting polymer nanowires." In: *Journal of Electroanalytical Chemistry* 669 (2012), pp. 82–89 (cit. on p. 230).

B

FABRICATION OF NANOPATTERNS BY ELECTRON-SENSITIVE SILANES

Self-assembly monolayers (SAMs) acting as electron-beam (EBL) resists have been shown to be very useful for the development of nanopatterns in the biomedical field [1, 2, 3]. The fabrication of such nanopatterns has shown to bring important improvements as a higher spatial resolution, the capability of using small volume samples and a higher detection sensitivity like in the case of sensors [2]. Traditional polymeric electron-beam resists have shown to limit the resolution of the lithographic process due to their excessive thickness, which increases the effects of scattering and the proximity effect. On the contrary, self-assembly monolayers, with few nanometers of thickness, have been used to reduce the feature size down to 5 nm [4]. Aliphatic and aromatic SAMs have been employed on different surfaces as positive and negative resists, respectively. For aliphatic SAMs the e-beam radiation causes desorption of the monolayer and on aromatic SAMs the electron beam crosslinks the neighboring aromatic moieties, increasing their etching resistance [4]. Therefore, by employing the electron radiation with SAMs, chemical patterns can be created over a wide variety of surfaces, with nanometer resolution.

This appendix describes the fabrication of Trichloro(1H,1H,2H,2H-perfluorooctyl)silane (FDTES) nanopatterns by electron-beam lithography, on silicon oxide (SiO_2) surfaces. Moreover, it was demonstrated that FDTES acts as a good protection layer against wet chemical etching, preserving the SiO_2 surface of the areas that were not exposed to the electron beam. Characterization of the nanopatterns was performed by scanning electron microscopy (SEM) and atomic force microscopy (AFM). This nanopatterned surfaces will be used in future works for the development of polymer nanostructures.

For the fabrication of nanopatterns, FDTES monolayers were deposited on SiO_2 surfaces by the vapor phase deposition method [5]. This is a relatively cheap and straightforward technique that limits the concentration of alkoxysilanes on

the surface, favoring homogeneous silane formation, although the formation of multilayers is not avoided. To prevent the formation of silane multilayers, more sophisticated silanization techniques, such as chemical vapor deposition (CVD) would be preferred [6]. However, it requires expensive CVD growth chambers in a clean room environment, which was beyond our possibilities during these preliminary experiments.

Therefore, fresh SiO_2 surfaces were treated with "piranha" solution (7:3 (v/v) of concentrated H_2SO_4 and 30% H_2O_2) for 30 minutes, to obtain high density of terminal hydroxyl groups and proceed with a silanization process. Then, a drop of FDTES and the activated SiO_2 surfaces were placed inside a dissecator on which vacuum was applied (vapor phase method) for 1 hour. The process was followed by an annealing step of 1 h at 80°C, required to promote covalent Si-O-Si bonds between the surface and the silane compound.

Afterwards, substrates were sonicated for 10 minutes in ethanol to remove any not attached silane compound and subjected to the electron beam radiation. Lines of 200 nm of width separated 5 µm were patterned by e-beam at doses of 250 $\mu As/cm^2$. A chemical etching process was conducted after electron beam exposure, testing the resistance of the non-affected silane regions. The pattern was treated with a hydrofluoric acid solution (Buffered Oxide Etch, BOE 7:1 (HF : NH_4F = 12.5 : 87.5%, from MicroChemicals GmbH.) for 10 s. The process is schematized in Figure B.1.

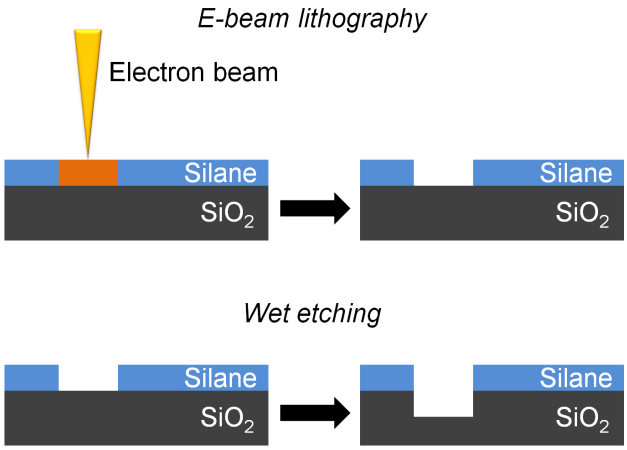

Figure B.1: Nanopattern fabrication process. First, silanized surfaces were exposed to electron radiation, resulting in desorption of the silane. Then, a wet (chemical) etching was applied on the surfaces to create nanochannels on the SiO_2 surface.

Figure B.2a shows SEM images of a SiO_2 surface after the nanopatterning process. In the first image one can observe that large areas can be patterned by the method described here in a uniform way. Moreover, lines between 200 and 250 nm of width separated 5 µm were obtained after the etching process, which were slightly wider than the lines initially designed.

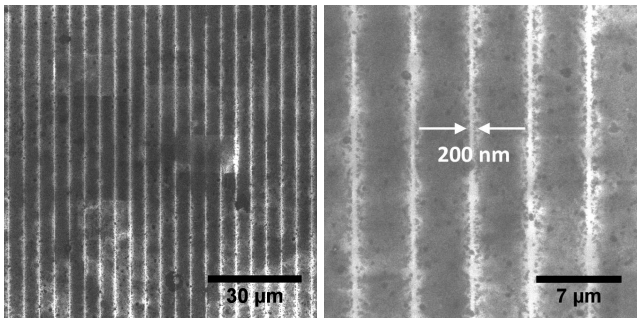

(a) (b)

Figure B.2: SEM images of a nanopatterned SiO_2 surface. Nanochannels between 200 and 250 nm in width were obtained.

This discrepancy in the width of the channel could arise from an excessive etching time, which over etched the initial lithography, or from the use of non-fully optimized e-beam conditions. To characterize in detail these patterns and to elucidate the reason for the oversize in the channels, AFM studies were conducted (Figure B.3).

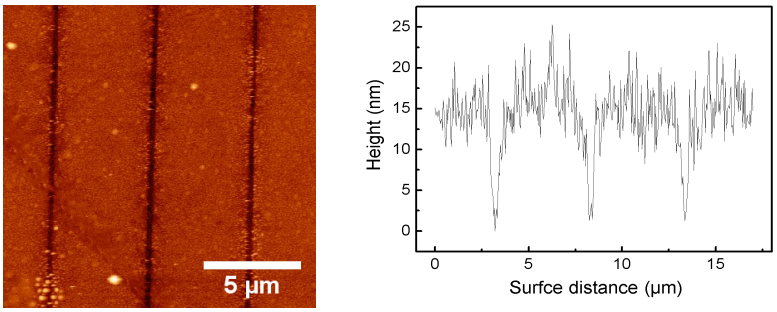

(a) (b)

Figure B.3: AFM image and profile of a nanopatterned SiO_2 surface. Nanochannels with 10 to 15 nm in depth were obtained.

AFM showed that the FDTES silane areas, not exposed to the electron beam, remained unaffected by the etching process, which confirms that FDTES is a good

mask for preserving the surface underneath, against etching processes of this nature. Moreover, it revealed that depths between 10 and 15 nm were etched away after 10 seconds of etching treatment, which indicates that the discrepancy in the width of the channel cannot account for an etching effect but instead should come from a non-optimized e-beam process. Therefore, to achieve accurate nanopatterns special care should be taken regarding the e-beam process.

These preliminary results, although need further optimization, reveal the potential of the method described here for the fabrication of highly homogeneous nanopatterns, which have the capability of being chemically tunable by means of functional groups, providing not only physical but also chemical patterns.

REFERENCES

[1] Raghavendra Palankar et al. "Fabrication of Quantum Dot Microarrays Using Electron Beam Lithography for Applications in Analyte Sensing and Cellular Dynamics." In: *ACS Nano* 7.5 (2013), pp. 4617–4628 (cit. on p. 233).

[2] Guo-jun Zhang et al. "Patterning of DNA nanostructures on silicon surface by electron beam lithography of self-assembled monolayer." In: *Chemical communications (Cambridge, England)* (2004), pp. 786–787 (cit. on p. 233).

[3] Guo-Jun Zhang et al. "Nanoscale patterning of protein using electron beam lithography of organosilane self-assembled monolayers." In: *Small (Weinheim an der Bergstrasse, Germany)* 1.8-9 (2005), pp. 833–837 (cit. on p. 233).

[4] Paula M Mendes and Jon A Preece. "Precision chemical engineering : integrating nanolithography and nanoassembly." In: *Current Opinion in Colloid and Interface Science* 9 (2004), pp. 236–248 (cit. on p. 233).

[5] C M Halliwell and a E Cass. "A factorial analysis of silanization conditions for the immobilization of oligonucleotides on glass surfaces." In: *Analytical chemistry* 73.11 (June 2001), pp. 2476–83 (cit. on p. 233).

[6] Gaurav Saini et al. "Two-silane chemical vapor deposition treatment of polymer (nylon) and oxide surfaces that yields hydrophobic (and superhydrophobic), abrasion-resistant thin films." In: *Journal of Vacuum Science and Technology A: Vacuum, Surfaces, and Films* 26.5 (2008), p. 1224 (cit. on p. 234).